

FAULT TOLERANT SLIDING MODE CONTROL SCHEMES WITH AEROSPACE APPLICATIONS

Thesis submitted for the degree of
Doctor of Philosophy
at the University of Leicester

by

Halim Alwi B.Eng., Leicester

Control and Instrumentation Research Group
Department of Engineering
University of Leicester

February 2008

Abstract

FAULT TOLERANT SLIDING MODE CONTROL SCHEMES WITH AEROSPACE APPLICATIONS

Halim Alwi

The thesis concerns the theoretical development and implementation of sliding mode schemes for fault tolerant control. The theoretical ideas developed in the thesis have been applied to aerospace systems. In particular, actuator and sensor fault tolerant control schemes have been developed for a high fidelity full nonlinear model of a Boeing 747 aircraft which is a widely researched testbed in the open literature. A key development in this thesis considers sliding mode control allocation schemes for fault tolerant control based on integral action and a model reference framework. Unlike many control allocation schemes in the literature, one of the main contributions of this thesis is the use of actuator effectiveness levels to redistribute the control signals to the remaining healthy actuators when faults/failures occur. A rigorous stability analysis and design procedure is developed from a theoretical perspective for this scheme. A fixed control allocation structure is also rigorously analyzed in the situation when information on actuator effectiveness level is not available. The proposed scheme shows that faults and even certain total actuator failures can be handled directly without reconfiguring the controller. A design of an adaptive gain for the nonlinear component of the sliding mode controller for handling faults is also described. The later chapters of the thesis present the results obtained from real time hardware implementations of the controllers on the 6-DOF SIMONA flight simulator at Delft University of Technology as part of the GARTEUR AG16 programme. The schemes have been evaluated by experienced pilots and the results have shown good performance in both nominal and failure scenarios. A reconstruction of the Bijlmermeer ELAL 1862 scenario on SIMONA using one of the controllers shows that a safe flight and landing is possible with significant reduction in pilot workload when compared with the classical controller.

Acknowledgments

To my supervisor Dr. Christopher Edwards;

to my parents, siblings and in-laws;

to my friends and colleagues at the University of Leicester, especially the past and present members of the Control and Instrumentation Research Group & Embedded Systems Laboratory;

to the members of GARTEUR AG16, especially Olaf Stroosma at the International Research Institute for Simulation, Motion & Navigation (SIMONA) and Prof. J.A. Mulder at the Control and Simulation Division, Faculty of Aerospace Engineering, Delft University of Technology;

to my dearest friends Dr. Nai One Lai & Dr. Devaraj Ayavoo;

and finally, special acknowledgment to my loving wife, Nor Mazuita Noor Azizuddin.

This research was supported by an EPSRC grant GR/S70876 and ORSAS.

Halim Alwi

6th February 2008

1744hrs

Contents

Acknowledgments	i
1 Introduction	1
1.1 Motivation for fault tolerant control systems	3
1.2 Challenges in the field of FTC and FDI	5
1.3 Thesis Structure and Contributions	6
2 Fault Tolerant Control and Fault Detection and Isolation	9
2.1 Faults and failures	9
2.1.1 Definition	9
2.1.2 Type of faults and failures	10
2.2 Fault tolerant control: general overview	12
2.3 Criteria for fault tolerant control: Redundancy	14
2.4 How fault tolerance is achieved	16
2.4.1 Adaptation (Model reference adaptive control and self tuning control)	17
2.4.2 Switching or blending	20
2.4.3 Scheduling	23
2.4.4 Prediction	25
2.4.5 Control signal redistribution	26
2.4.6 Robust control (\mathcal{H}_∞ control)	30
2.5 Fault Detection and Isolation	31

2.5.1	Classification of FDI	31
2.6	Comparisons of different FDI designs	34
2.6.1	Model-based	34
2.6.2	Non Model-based	38
2.6.3	New emerging FDI methods	39
2.7	Conclusions	40
3	Sliding Mode Control	41
3.1	Introduction	41
3.1.1	Regular form	42
3.1.2	Properties of the sliding mode	44
3.2	A simple example: pendulum	45
3.2.1	Simulations and results	47
3.2.2	A practical control law	49
3.3	Unit vector approach	51
3.3.1	Analysis of stability for the closed-loop system	53
3.3.2	The unit vector pseudo sliding term	54
3.4	Design of sliding surface (hyperplane)	54
3.4.1	Quadratic Minimization	55
3.5	Design of controller for tracking requirement	57
3.5.1	Integral action approach	57
3.5.2	Model reference approach	60
3.6	Sliding mode in the field of FTC	62
3.6.1	Robustness against actuator faults	62
3.6.2	Actuator failures	62
3.7	SMC on a large civil passenger aircraft	63
3.8	Conclusions	64

4	Fault Tolerant Control Applied to a Large Civil Aircraft	65
4.1	Introduction	65
4.2	Actuator fault tolerant control	66
4.2.1	Sliding Mode Controller Design	68
4.2.2	The sliding mode hyperplane design.	73
4.3	Simulation Results	75
4.3.1	Fault-Free Simulations	77
4.3.2	Changes in effectiveness gain	77
4.3.3	Total elevator failure simulations	80
4.3.4	Total elevator failure simulations with wind and gust	80
4.3.5	Combined loss of effectiveness and total elevator failure	80
4.4	Conclusions	87
5	Sliding Mode Fault Reconstruction and Sensor Fault Tolerant Control	88
5.1	Introduction	88
5.2	Sliding Mode observers for FDI	89
5.3	A typical sliding mode observer	90
5.4	The Edwards-Spurgeon observer for fault reconstruction	92
5.4.1	Reconstruction of input faults	92
5.4.2	Reconstruction of output faults	93
5.5	Sensor fault tolerant controller closed-loop analysis	94
5.5.1	Preliminaries	94
5.5.2	closed-loop analysis	97
5.6	A Robust sensor fault reconstruction scheme for the B747	98
5.7	Sensor Fault Tolerant Control Simulation Results	102
5.7.1	Fault-free simulation	102
5.7.2	Fault simulations: FDI switched off	102

5.7.3	Fault simulation: FDI switched on	104
5.7.4	Fault simulations with sensor noise	105
5.7.5	Threshold selection	105
5.8	Conclusions	106
6	Fault Tolerant Control Using Sliding Modes with On-line Control Allocation	107
6.1	Introduction	107
6.2	Controller Design	108
6.2.1	Problem Formulation	109
6.2.2	Stability analysis	114
6.2.3	Sliding Mode Control laws	115
6.3	The effect of non-perfect fault reconstruction	117
6.4	Sliding mode design issues	120
6.5	ADMIRE simulations	121
6.5.1	Controller design	121
6.5.2	Actuator fault estimation using a sliding mode observer	123
6.5.3	ADMIRE: simulation results	124
6.6	Conclusions	127
7	SIMONA Implementation Results	128
7.1	Introduction	128
7.2	Test facilities (SIMONA)	129
7.2.1	The SIMONA research simulator	129
7.2.2	Benchmark V2.2 - FTLAB747 V6.5/7.1/2006b	130
7.3	Controller Design	130
7.3.1	Lateral Controller Design	134
7.3.2	Longitudinal Controller Design	135
7.4	SIMONA Implementations	136

7.5	Results	138
7.5.1	No fault	138
7.5.2	Actuator effectiveness	140
7.5.3	Stabilizer runaway	140
7.5.4	Elevator jam with offset	140
7.5.5	Aileron jam with offset	143
7.5.6	Rudder missing	143
7.5.7	Rudder runaway	143
7.6	Conclusions	147
8	Model Reference Sliding Mode FTC	148
8.1	Introduction	148
8.2	Controller Design	149
8.3	On-line Control Allocation	150
8.3.1	Stability analysis	153
8.3.2	A Sliding Mode Control Law	154
8.4	Fixed Control Allocation	157
8.4.1	A Sliding Mode Control Law	159
8.5	Adaptive Reference Model	163
8.6	ADMIRE simulations: on-line control allocation	163
8.6.1	Controller design	163
8.6.2	Actuator fault estimation using least square method	165
8.6.3	Simulation results	166
8.7	ADMIRE simulations: fixed control allocation	167
8.7.1	Controller design	167
8.7.2	Simulation results	168
8.8	Conclusions	170

9	GARTEUR AG16 Case Study: ELAL Flight 1862 Bijlmermeer Incident	171
9.1	Introduction	171
9.2	ELAL flight 1862: the incident	172
9.3	ELAL flight 1862: aircraft damage analysis	175
9.3.1	ELAL flight 1862: controllability and performance of the damage aircraft	177
9.4	Controller design	179
9.4.1	Lateral Controller Design	180
9.4.2	Longitudinal Controller Design	182
9.5	SIMONA implementation	184
9.5.1	ILS landing	184
9.6	SIMONA flight simulator results with experienced pilots	186
9.6.1	Classical Controller	188
9.6.2	SMC controller	191
9.7	Conclusions	197
10	Conclusions and Future Work	198
10.1	Conclusions	198
10.2	Future work	200
	Nomenclature and Abbreviations	201
	Author's Biography	203
	List of publications	204
	Bibliography	205

Chapter 1

Introduction

From Watt's centrifugal governor [78] shown in Figure 1.1 devised to control the speed of steam engines, control system methodologies have evolved from simple mechanical feedback structures, into sophisticated and advanced electronic devices for controlling high performance and highly unstable systems which optimize the cost and control effort. The last five decades have seen the emergence of multivariable and robust control ideas [18, 139, 177, 186, 243] to increase the practical performance capabilities and at the same time ensure stability in the face of modeling uncertainty and robustness to noise and disturbances. Some of these control methodologies, for example the "three term" PID (Proportion, Integral and Derivative) controller [20] and Kalman filters [192, 218], have found success in industry with a wide range of applications. Other control methodologies have not so readily been accepted by industry.

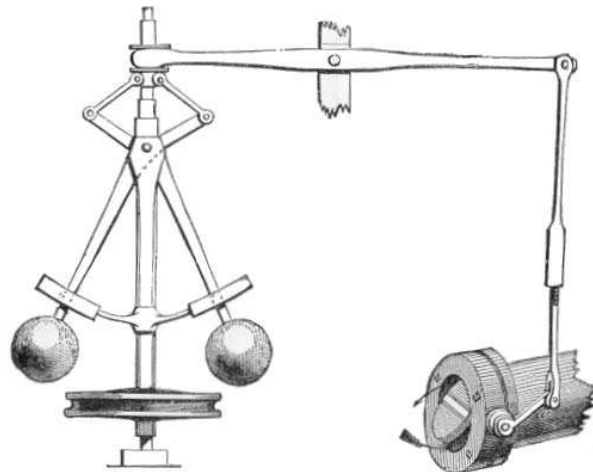


Figure 1.1: Watt's centrifugal governor (Figure from [178])

Some of the control methods that have received a good deal of attention in the last couple of decades are robust and adaptive control. This is motivated by the need to optimize the performance of safety critical systems such as aircraft, chemical plants and nuclear power plants, which require the control systems to deal with wide changes in the operating conditions of the plant. However some unexpected scenarios or unusual events in the system mean the designed controller is sometimes simply 'overwhelmed' and a loss of performance and stability might occur. Examples of these unexpected scenarios are faults, failures or system 'damage', which

are typically not considered in the controller design process.

The problem of achieving some level of performance and stability in the case when these unexpected scenarios occur, especially for safety critical systems (e.g. chemical and nuclear power plants) and expensive autonomous systems (e.g. satellites and underwater remote operating vehicles (ROV)) requires a different control strategy rather than just having a robust or adaptive controller (which only guarantees stability and performance for perturbations in the nominal plant). An example of a system which requires such a control strategy is the problem of increasing the survivability of an aircraft when an unexpected problem (such as faults or failures to the actuators/sensors or structural damage) occurs during a flight. In such a situation the aircraft requires some ‘emergency’ strategy to allow the pilot to safely land the aircraft. This challenge has motivated a control strategy widely known in the literature as *fault tolerant control* (FTC).

Many different control paradigms have been applied to the problem of FTC. Examples of some of the existing control approaches can be found in Table 1.1. Table 1.2 shows different systems that FTC has been applied to. In this thesis, the advantages of FTC will be demonstrated on aircraft systems as an example of a safety critical plant.

Design approaches	references
Model reference adaptive control (MRAC)	[112, 114, 187, 240]
Adaptive control	[22, 62, 114, 114]
Multiple model switching and tuning (MMST)	[19, 33, 42, 84, 85, 103, 119, 159, 160, 208]
Interactive multiple model (IMM)	[120, 137, 174, 230, 238]
Gain scheduling	[134]
Linear parameter varying systems (LPV)	[23, 80, 146, 149, 176, 182, 183, 225]
Model predictive control (MPC)	[140–142, 180]
Pseudo-inverse method (PIM)	[81, 102, 151, 166, 230]
Control allocation (CA)	[31, 34, 39–41, 58, 64, 70, 95, 98, 103, 181, 191]
Dynamic Inversion (DI)	[108, 109, 115, 138, 203, 204]
Robust control e.g. H_∞	[142, 186]
Sliding mode control (SMC)	[67, 98, 210]

Table 1.1: An example of existing approaches in FTC (adapted from [239])

Applications	references
Aircraft	[23, 42–46, 80, 149, 187, 189, 208, 208]
Spacecraft	[83, 108, 113]
Automotive	[87, 124]
Engine & propulsion control	[44, 125, 163, 208]
Chemical/petrochemical plants	[140]
Robots	[161]

Table 1.2: An example of applications of FTC & FDI (adapted from [239])

1.1 Motivation for fault tolerant control systems

The safety of aircraft passengers has been and will continue to be an important issue in the commercial aviation industry. Figures 1.2 and 1.3 represent some recent civil aviation safety statistics. Although the number of flights has doubled since 1980, the number of fatal accidents has been maintained over the years, and in fact decreased during the period from 1999-2003 [4]. This is contributed to by many factors, such as the stringent safety measures imposed on the aircraft and the implementation of important safety technology. Furthermore all pilots undergo extensive training to help them to react to unforeseen difficulties which may arise during a flight.



Figure 1.2: Number of flights and fatal accidents (Figure from [4])

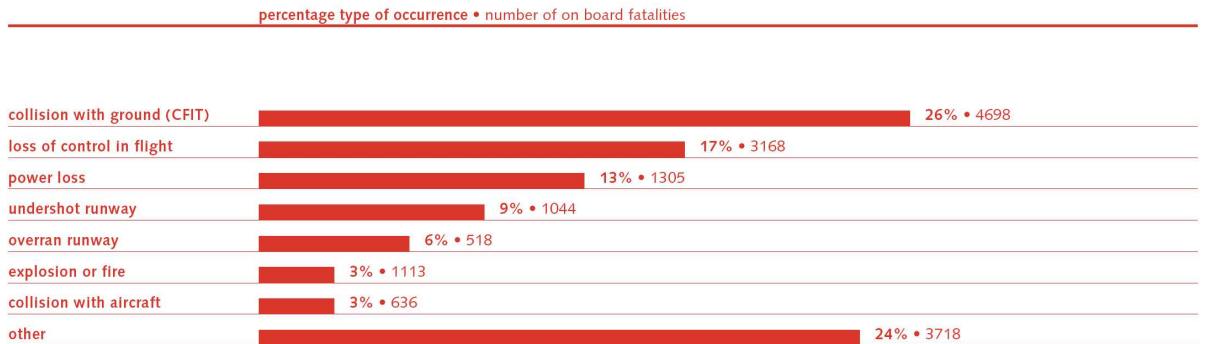


Figure 1.3: Type of occurrences and fatalities (Figure from [4])

Figure 1.3 shows that ‘controlled flight into terrain’ (CFIT) and ‘loss of control in flight’ are the two most important occurrences and involve the most fatalities [4]. Loss of control during flight is one of the motivating factors for fault tolerant control: the idea being, to increase the ‘flyability’ of aircraft in the event of faults, failures or airframe damage. Learning from previous incidents, where pilots successfully landed crippled aircraft – such as Flight 232 in Sioux City, Iowa 1989¹, the Kalita Air freighter in Detroit, Michigan, October 2004 (Figure 1.5)² and the DHL freighter incident in Baghdad, November 2003 (Figure 1.4)³ – suggest that in many cases, the damaged or faulty aircraft is still ‘flyable’, controllable and some level of performance still can be achieved, sufficient to allow the pilot to safely land the aircraft.

¹Flight 232 suffered tail engine failure that caused the total loss of hydraulics [42, 84].

²The freighter shed engine No. 1, but the crew managed to land safely without any casualties.

³The DHL A300B4 was hit by a missile on its left wing and lost all hydraulics, but still landed safely [42].



Figure 1.4: DHL A300B4 emergency landing after being hit by missile in Baghdad, 2003.



Figure 1.5: Kalita Air emergency landing after losing one engine, 2004.

It has been argued that with pilot skill and a fault tolerant control system, several accidents could have been avoided. For example, a recent report [44, 208] described a NASA experiment in which by clever manipulation of thrust (in the event of total hydraulic loss), it was possible to land the ‘crippled’ plane. Pilot reviews and comments after the flight test indicate that fault tolerant control did help the pilot to control the crippled plane when compared to pilot control alone [44, 208]. Although the work by NASA on propulsion controlled aircraft successfully handles total hydraulic loss, it is not sufficient to solve the general problem of fault tolerant control for aircraft; especially when other control surfaces are still functional or when dealing with structural damage and aerodynamic change (which for example occurred in the ELAL flight 1862 which is also known as the Bijlmermeer incident [2]) or when dealing with control surface jams or runaways (such as occurred in flight 427, near Aliquippa, Pennsylvania in 1994 [3]).

Consider the situation in which during a manoeuvre, the pilot suspects that there is something wrong when the aircraft starts to handle in an abnormal way. What has gone wrong? What can the pilot do? These are important questions that need to be answered. The question regarding what has gone wrong requires detection of the ‘fault’ and location of the source – this is the motivation for the field of fault detection and isolation (FDI) [50]. The answer to what the pilot can do in this situation relates to the area of fault tolerant control (FTC) [114, 239]. One of the objectives of this thesis is to look at how sliding mode techniques [67, 210] can be applied in terms of fault tolerant control to achieve stability and recover some performance when a fault or failure occurs.

1.2 Challenges in the field of FTC and FDI

Recent developments in FTC and FDI have seen the application of sliding mode ideas [67, 210] by some researchers. This is due to the inherent robustness properties of sliding modes to a certain class of uncertainty, including its ability to directly handle actuator faults without requiring the fault to be detected and without requiring controller reconfiguration.

Despite its robustness property in handling actuator faults, (as with most other controllers) sliding mode control (SMC) cannot handle total actuator failures. Some of the current research in solving this problem has assumed that exact replication of the failed actuator is available [55]. However this is only applicable to a few over actuated systems. In most over actuated systems such as large transport aircraft, actuator redundancy is available, but mostly not in the form of an exact replication of the primary actuators or control surfaces. Therefore the challenge is to find a way that sliding modes can deal with total actuator failure.

There is very limited literature on the application of SMC to aerospace systems. Most of the applications of SMC in the literature consider fast high performance aircraft; for example, tailless aircraft [185, 219]. It is rare (in the author’s opinion) to find literature describing SMC applied to large transport aircraft – especially for FTC purposes. One of the reasons for this is probably the scepticism among research engineers and the control community regarding the ‘chattering problem’ associated with an ideal sliding motion and the ‘myth’ that sliding modes require high computational power to be implemented in real aircraft. Therefore, one of the motivations of this thesis is to show that SMC can be applied to a large transport aircraft

system without high computational power and with no ‘chattering’. The challenge is also to show that it can be a powerful and robust tool for handling faults or failures in aircraft systems.

One reason why a large transport aircraft is used as an example throughout the thesis is the availability of the FTLAB747 model, which is one of the most accurate mathematical models of an aircraft system in the literature, with aerodynamic coefficients obtained from NASA [91, 92] through flight tests and wind tunnel testing. It has been used by many researchers (see for example Marcos *et al.* [149], Ganguli *et al.* [80], Szaszi *et al.* [199], Maciejowski & Jones [141] and Aravena *et al.* [19]). Although there exist models in the literatures (such as ADMIRE [75]) which comprise full order nonlinear equations, the FTLAB747 is the only model in the literature (as far as the author is aware) which replicates a real failure condition, and it was used in the independent investigation of the ELAL flight 1862 (Bijlmermeer incident) in 1992 [188] using the real flight recorded data. Therefore the FTLAB747 model represents a realistic test bed for the fault tolerant control schemes developed in this thesis. The flight 1862 (Bijlmermeer incident) scenario, available in FTLAB747, has also become one of the ultimate goals of this thesis: to show that SMC can be used as a fault tolerant strategy to enable a pilot to safely land the aircraft.

1.3 Thesis Structure and Contributions

This thesis is arranged in the following manner:

Chapter 2 begins with the definition of the terms fault and failure and briefly discusses the different types of faults and failures which can occur on actuators and sensors with specific aircraft examples. The chapter introduces the concept of fault tolerant control and gives a general overview of the different FTC and FDI research fields. Some general classifications on the different FTC and FDI strategies are also presented. The main concepts and strategies behind some of the FTC and FDI schemes in the literature, as well as their advantages and drawbacks, are also discussed.

Chapter 3 gives a brief introduction to the concept of sliding mode control and examines its properties. This chapter also highlights the benefits of sliding modes when applied in the fields of FTC and FDI. The basic design process and technical analysis is undertaken based on a simple pendulum example to introduce the concept. The unit vector approach for multi-input systems, sliding surface design and tracking requirements (integral action and model reference based tracking) are also discussed. Chapter 3 ends with some discussions on the benefits and motivation for sliding mode control in the field of FTC and FDI – especially for aircraft systems.

Chapter 4 presents a new sliding mode control scheme for reconfigurable control of a large civil transport aircraft. The controller is based around a state-feedback sliding mode scheme where the nonlinear unit vector term is allowed to adaptively increase when the onset of a fault is detected. In comparison to other fault tolerant controllers which have been previously implemented on this model, the controller proposed in this thesis is simple and yet is shown to work across the entire ‘up and away’ flight envelope. Excellent rejection of a certain class of actuator faults is shown by this scheme. However the proposed controller cannot directly cope with total failure of an actuator. This issue is also explored in this chapter. A range of realistic

fault scenarios are considered and the results of simulations using the full nonlinear aircraft model are presented. The main contribution of this chapter is the development of an adaptive gain for the nonlinear unit vector term which ‘compensates’ for the effects of faults, and the design of the sliding surface based on LMI formulations which takes into consideration the effect of uncertainty and the effect of changing the redundant control surfaces in the event of total actuator failure. A version of this chapter has appeared in [7] and [8]. The developments in this chapter form the basis of a paper [13] accepted for publication in the *IEEE Transactions on Control Systems Technology*.

Chapter 5 proposes a sensor fault tolerant control scheme for a large civil aircraft. It is based on the application of a robust method for sensor fault reconstruction using sliding mode ideas. The contribution lies in the application of the sensor fault reconstruction scheme to correct the corrupted measured signals before they are used in the controller calculations and therefore the controller does not need to be reconfigured to adapt to sensor faults. A further contribution is the analysis of the effect of imperfect fault reconstruction signals on the performance and stability of the closed-loop system. The results of this chapter appear in [8] and [9]. The developments in this chapter also form part of a paper [13] accepted for publication in the *IEEE Transactions on Control Systems Technology*.

Chapter 6 proposes an on-line sliding mode control allocation scheme for fault tolerant control. The effectiveness level of the actuators is used by the control allocation scheme to redistribute the control signals to the remaining actuators when a fault or failure occurs. The chapter provides an analysis of the sliding mode control allocation scheme and determines the nonlinear gain required to maintain sliding. The on-line sliding mode control allocation scheme shows that faults and even certain total actuator failures can be handled directly without reconfiguring the controller. The main contribution of this chapter is a novel sliding mode control allocation scheme and the associated stability analysis – including the effect of the use of imperfect actuator effectiveness estimates. The combination of SMC with CA is a new extension of existing theory. Another major contribution is the use of the actuator effectiveness levels to redistribute the control signals to the remaining control surfaces in the event of faults and failures. The theoretical developments in this chapter have been accepted for publication in *Automatica*. An early version of this chapter appears in [10], and the implementation results on the full nonlinear B747 aircraft appear in [11].

Chapter 7 considers the implementation of the sliding mode allocation schemes from Chapter 6 on the SIMONA research flight simulator at Delft University of Technology, the Netherlands, configured to represent the B747 aircraft. As in the previous chapter, the schemes allow redistribution of the control signals to the remaining functioning actuators when a fault or failure occurs. Here the controller from Chapter 6 is implemented in ‘C’ and runs on the ‘flight control’ computer associated with SIMONA. Real time implementation issues are discussed and a range of fault scenarios from the GARTEUR AG16 benchmark are tested and discussed. The main contribution of this chapter is the application and implementation of the controller, proposed in Chapter 6, on the SIMONA flight simulator. The results from rigorous simulator flight tests indicate that the controller can run in real-time without chattering problems or high computational power requirements. Results from this chapter appear in [15]. A version of this chapter has been accepted for publication in *AIAA Journal of Guidance, Control and Dynamics*.

Chapter 8 describes an adaptive model reference sliding mode fault tolerant control scheme with on-line control allocation. As in Chapter 6, the control allocation scheme uses the effectiveness level of the actuators to redistribute the control signals to the remaining actuators when a fault or failure occurs. Meanwhile, the adaptive non-linear gain and reference model provide on-line tuning for the controller. This chapter provides a rigorous stability analysis for the proposed model reference scheme. The scheme has been implemented on a linearization of the ADMIRE aircraft model to convey the ideas associated with the proposed scheme and shows that various faults and even total actuator failures can be handled. The contributions of this chapter include the incorporation of a model-reference tracking framework within the proposed SMC and CA controller from Chapter 6. A further contribution is a rigorous stability analysis in the absence of an FDI unit (i.e. a fixed CA strategy) and the incorporation of an adaptive nonlinear unit vector term. Results from this chapter appear in [12].

Chapter 9 presents the ELAL flight 1862 (Bijlmermeer incident) scenario which is one of the case studies of the GARTEUR AG16. The results presented in this chapter represent the outcome of the ‘flight testing’ campaign and the GARTEUR AG16 final workshop at Delft University of Technology in November 2007. This was an open meeting aimed at the general public. The results represent the successful real-time implementation of a SMC controller on the SIMONA 6-DOF flight simulator with experienced test pilots flying and evaluating the controller. The simulator tests conducted by the pilots included individual control surface failure scenarios (e.g. jammed actuator with an offset or runaway) and in particular the actual flight 1862 scenario (Bijlmermeer incident). The application of the proposed controller from Chapter 8 under the assumption that no information about the aircraft’s damage is available, coupled with automatic landing using the ILS is, in the author’s opinion, probably the most realistic and rigorously tested controller used in FTC studies on the ELAL flight 1862 incident. Results from this chapter appear in [14].

Finally Chapter 10 provides conclusions based on the work done in this thesis – especially the successful combination of CA with SMC in order to handle total actuator failures in systems with redundancy. This chapter also highlights and discusses possible areas of future research.

Chapter 2

Fault Tolerant Control and Fault Detection and Isolation

When a fault occurs in a system, the main problem to be addressed is to diagnose what fault has occurred, and then decide how to deal with it. The problem of detecting a fault, finding the source/location and then taking appropriate action is the basis of fault tolerant control.

In this chapter, an introduction and discussions on fault tolerant control (FTC) and fault detection and isolation (FDI) will be presented. The chapter will start with some definitions and will describe different types of faults and failures on actuators and sensors. Later, different types of fault tolerant controllers and FDI schemes will be presented. In the discussions in this chapter, the emphasis is on FTC and FDI for *aircraft applications*.

2.1 Faults and failures

First, the terms fault and failure need to be defined. The definition provided in this thesis is in compliance with the definitions given by the IFAC SAFEPROCESS technical committee (as given in [107]) which were developed to set a standard [50] in this area in order to avoid confusion among researchers. This will also enable the strategy of fault tolerant control (FTC) to be specified in terms of faults and/or failures later in the chapter.

2.1.1 Definition

Tubb and Omerdic [207] (similar to the definition in [50, 107]) define:

fault: an undesired change in a system parameter that degrades performance: a fault may not represent a component failure.

failure: a catastrophic or complete breakdown of a component or function (to be contrasted with a fault which may be a tolerable malfunction).

In other words, a failure is a condition which is much more severe than a fault. When a fault occurs on an actuator for example, the actuator is still usable but may have a slower response or become less effective. But when a failure occurs, a totally different actuator is needed to be able to produce the same desired effect.

2.1.2 Type of faults and failures

An actuator fault is normally represented in the literature as a decrease in the actuator's effectiveness. Faults that develop in a linear system associated with the actuators can be represented by an equation

$$\dot{x}(t) = Ax(t) + Bu(t) - BKu(t) \quad (2.1)$$

with $x(t) \in \mathbb{R}^n$, $u(t) \in \mathbb{R}^m$ and $K = \text{diag}(k_1, \dots, k_m)$ where the k_i are scalars satisfying $0 \leq k_i \leq 1$. These scalars model a decrease in the effectiveness of a particular actuator. If $k_i = 0$, the i th actuator is working perfectly whereas if $k_i > 0$, a fault is present, and if $k_i = 1$ the actuator has failed completely. Mathematically, the difference between faults and failures is therefore clearly seen.

Remark: The representation of actuator faults/failures in Equation (2.1) represents a *reduction in the effectiveness* of a particular actuator via the diagonal structure of K . This representation is used by many other researchers such as [32,81,112,119,205,240,242]. Posing the faults/failures as in (2.1), makes the stability analysis and FDI integration much simpler. Other representations of actuator faults/failures can be found in [214,238].

Actuator faults are the most commonly considered by FTC researchers e.g. [73,242]. In aircraft systems, there are a few distinct types of actuator failures, the three most common are shown in Figure 2.1(b). *Lock failure* is a failure condition when an actuator becomes stuck and immovable. This might be caused by a mechanical jam, due to lack of lubrication for example. This type of failure is considered in [51,73,80,85,240] and occurs in documented incidents such as flight 1080 (Lockheed L-1011, San Diego, 1977) [42] (where one of the horizontal stabilizers jammed in the full trailing edge-up position) and flight 96 (DC-10, Windsor, Ontario, 1972) [42] (where the rudder jammed with an offset).

Float failure is a failure condition when the control surface moves freely without providing any moment to the aircraft. An example of a float failure is the loss of hydraulic fluid in the elevator's actuator causing it to move freely in the direction of angle of attack and therefore cannot produce any effective moment in the pitch axis. Examples of researchers considering float type failures are [45,73,80] and it occurred in incidents such as Flight 123 (B-747, Japan, 1985) and DHL A300B4 (A300, Baghdad, 2003) [42] where a total loss of hydraulics occurred.

One of the most catastrophic types of failure is *runaway/hardover*. A runaway control surface will move at its maximum rate limit until it reaches its maximum position limit or its blowdown limit¹. For example, a rudder runaway can occur when there is an electronic component failure which causes a (wrong) large signal to be sent to the actuators causing the rudder to be deflected at its maximum rate to its maximum deflection at low speed (or its blowdown limit at high speed). This type of failure is considered in [190] and occurs in incidents such as Flight 85 (B-747, Anchorage, Alaska, 2002) [42] (which suffered a lower rudder runaway to full left deflection, causing the airplane to roll excessively) and flight 427 (B-737, Near Aliquippa, Pennsylvania,

¹A blowdown limit is an aerodynamic limit of the control surface deflection at a specified speed which overpowers the movement of the actuator. The blowdown limits might not be the maximum physical deflection of the control surface— any deflection above the blowdown limit can cause structural damage [195] as it imposes the maximum physical and structural limit the control surface and the surrounding structure can have.

1994) [3] (which suffered from a rudder runaway to its blowdown limits).

Note that the above faults and failures are related to the aircraft's control surfaces. In terms of the linear control system described in Equation (2.1), this only effects the B matrix of the linear system. Another type of fault that occurs in aircraft, is *structural damage*. Structural damage may change the operating conditions of the aircraft (from its nominal conditions) due to changes in the aerodynamic coefficients of the aircraft or a change in the centre of gravity. Therefore in terms of linear control systems, the A matrix will also be perturbed. Mathematically, this can be represented as [112]

$$\dot{x}(t) = (A + \Delta A)x(t) + (B + \Delta B)u(t) + \xi(x, u, t) \quad (2.2)$$

Where ΔA and ΔB represent the changes in the A and B matrices and $\xi(x, u, t) \in \mathbb{R}^n$ represents additional changes, not included in ΔA and ΔB , i.e. added uncertainty or a mismatch between the nominal plant and the damaged plant. Examples of failures that cause structural damage are wing battle damage [33], detachment of control surfaces, for example the rudder (flight 961, A310, Varadero, Cuba, 2005) [6] or engines (flight 1862, B-747, Amsterdam, 1992) [188], or detachments of some body parts of the aircraft e.g. the vertical fin/stabilizer (Flight 123, B-747, Japan, 1985) [42, 84] and (flight 587, A300, New York, 2001) [42], wing (DHL A300B4, A300, Baghdad, 2003) [42], fuselage skin or cargo doors (flight 981, DC-10, Paris, 1974) [42].

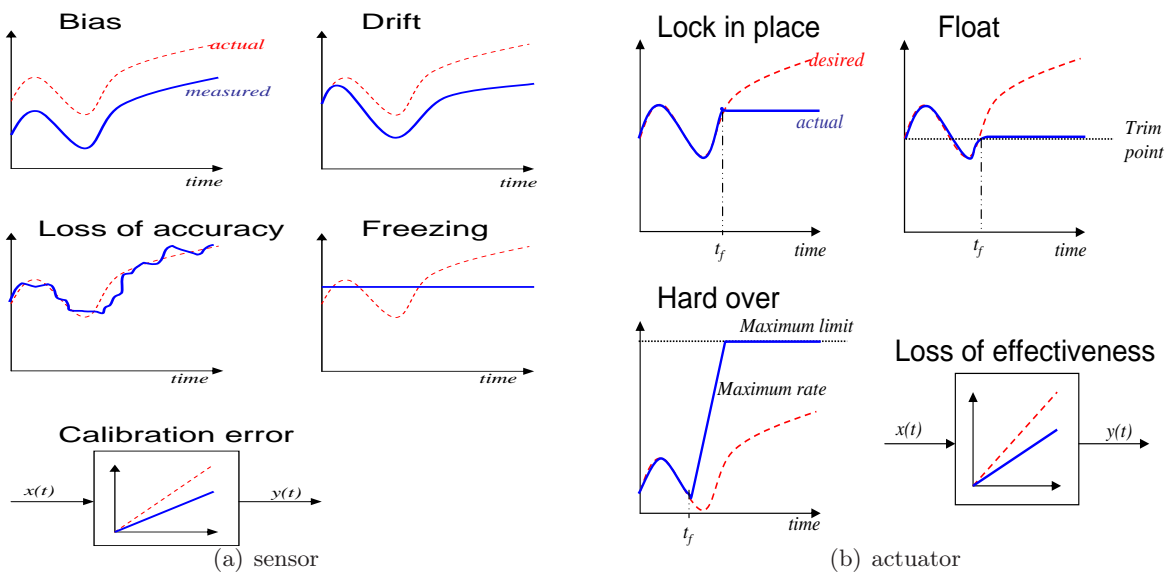


Figure 2.1: Type of fault and failures on sensor and actuator (adapted from [32])

Figure 2.1(a) describes some typical sensor faults in aircraft. Bias is a constant offset/error between the actual and measured signals. Sensor drift is a condition whereby the measurement errors increase over time (and might be due to loss of sensitivity of the sensor). Loss of accuracy occurs when the measurements never reflect the true values of the states. Freezing of sensor signals indicate that the sensor provides a constant value instead of the true value. Finally calibration error is a wrong representation of the actual physical meaning of the states from the electrical or electronic signals that come out from the sensor unit itself². Sensor faults/failures

²Sensors, most of the time, provide measurements in terms of current or voltage and therefore require transformation to represent the actual physical meaning of the states or measured signals.

can occur due to malfunctions in the components in the sensor unit, loose mounting of the sensors and loss of accuracy due to wear and tear. An example of an incident resulting from sensor failures occurred in flight 124 (B-777, Perth, 2005) [5] which caused flight control upset and contributed to the violent behaviour of the aircraft which required the auto pilot and navigation unit to be switched off.

It is interesting to mention that faults/failures can also be categorized in terms of time i.e. abrupt (quickly varying) and incipient (slowly varying) [200]. Abrupt faults/failures exhibit a sudden and unexpected change and are usually easily noticed by the pilot. An example of an abrupt failure is an actuator jam, or a jam with offset and hard-over. Incipient faults are more subtle and the effect is not so obvious. However, incipient faults if left unattended for a long period of time might degrade the required performance of the system and might lead to abrupt and catastrophic failures. Incipient faults can be caused by operational wear and tear as the effect is negligible at the beginning but becomes gradually worse before it fails abruptly.

2.2 Fault tolerant control: general overview

In the literature, most of the motivation and research work in fault tolerant control involves solving problems encountered in safety critical systems such as aircraft. Applications can also be found in other systems, for example robots [136], space systems [206] and underwater remotely operated vehicles (ROV) [161].

Patton in [166] stated that, ‘... *Research into fault tolerant control is largely motivated by the control problems encountered in aircraft system design. The goal is to provide a “self-repairing” capability to enable the pilot to land the aircraft safely in the event of serious fault ...*’

While Zhang and Jiang [239] define ‘... *fault tolerant control systems (FTCS) are control systems that possess the ability to accommodate system component failures automatically. They are capable of maintaining overall system stability and acceptable performance in the event of such failure. FTCS were also known as self-repairing, reconfigurable, restructurable, or self designing control systems ...*’

FTC is a complex combination of three major research fields [166], FDI, robust control, and reconfigurable control (see Figure 2.2). Patton [166] also discussed the relationship between these fields of research. In summary the interconnection between the fields are shown in Figure 2.3. For a typical FTC scheme, when a fault/failure occurs either in an actuator or sensor, the FDI scheme will detect and locate the source of the fault. This information is then passed to a mechanism to initiate reconfiguration. The reconfigurable controller will try to adapt to the fault, therefore providing stability and some level of performance. Both the FDI and reconfigurable controller need to be robust against uncertainty and disturbance.

Robust control relates closely to passive fault tolerant control systems (PFTCS) [166]. The controller is designed to be robust against disturbances and uncertainty during the design stage. This enables the controller to counteract the effect of a fault without requiring reconfiguration or FDI. For some robust methodologies, its fault tolerant capability is limited, i.e. total actuator failure cannot be handled directly. An example of a robust control strategy is \mathcal{H}_∞ where the effect of uncertainty is minimized during the design stage [186].

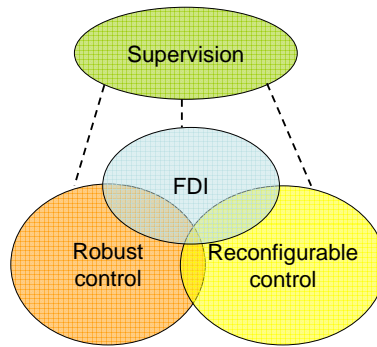


Figure 2.2: Scattered areas of fault tolerant control research (adapted from [166])

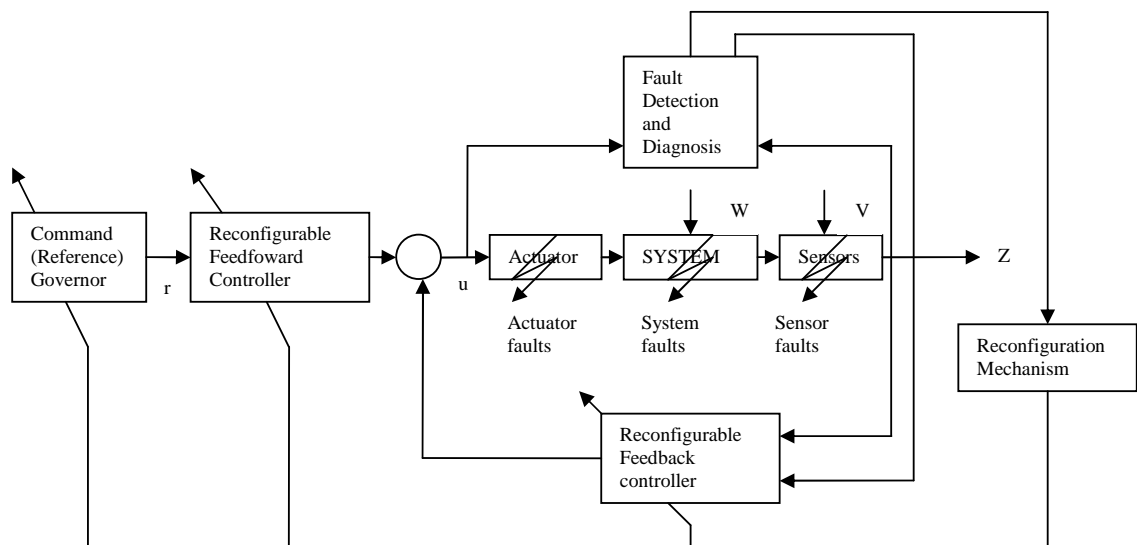


Figure 2.3: General structure of active fault tolerant control systems (AFTCS) (adapted from [239])

Some widely referred to survey materials on FTC and FDI are:

- Reconfigurable control and FTC: [102, 114, 142, 166, 239, 241].
- FDI: [50, 107].

and more recent publications (books and edited monographs) such as [27, 28, 47, 143] in the field of FTC and [105, 106] for FDI. There is increasing literature on FTC, reconfigurable control and FDI but the above are the most widely cited.

Zhang & Jiang [239] gives a good bibliographical review of reconfigurable fault tolerant control systems. The paper also proposes a classification of reconfiguration methods which is based on a few categories (the mathematical tools used, the design approach used, the way of achieving reconfiguration, e.t.c). It also provides a bibliographical classification based on the design approaches and the different applications, discussing open problems and current research topics in active fault tolerant control systems (AFTCS).

Zhang & Jiang [239] and Patton [166], classify FTC into 2 major groups (see Figure 2.4): passive fault tolerant control systems (PFTCS) and active fault tolerant control systems (AFTCS). In passive fault tolerant control systems, the controller is designed to be *robust against faults* and

uncertainty. Therefore when a fault occurs, the controller should be able to maintain stability of the system with an acceptable degradation in performance. PFTCS does not require FDI and does not require controller reconfiguration or adaptation.

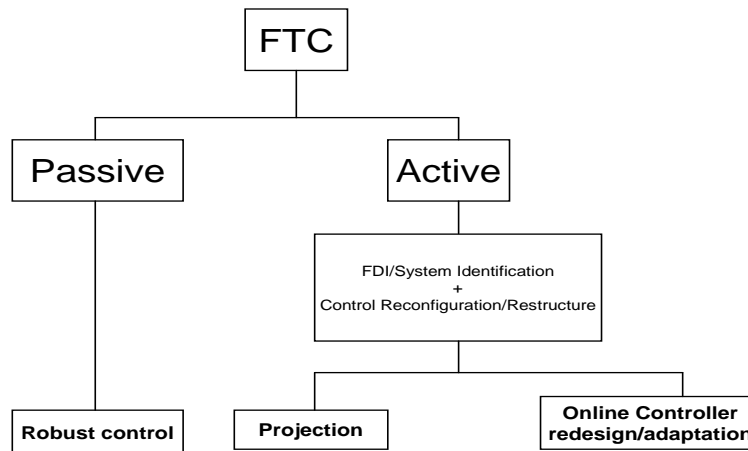


Figure 2.4: Classification of FTC by [166]

AFTCS on the other hand ‘... reacts to system component failures actively by reconfiguring control actions so that stability and acceptable performance of the entire system can be maintained ...’ [239]. Therefore most AFTCS require FDI to provide the fault or failure information so that reconfiguration can be done.

Other key sources of literature on reconfigurable control are [102] and [114]. The report [102], give some insight into many methods used for reconfigurable control for flight applications, while [114] gives a survey on reconfiguration methods used specifically for FTC in flight control applications. In [114], different types of FTC strategy are presented and Table 2.1 gives in a compact way, a brief comparison of the FTC methods and compares each method’s capability, advantages and disadvantages [114]. Note that in Table 2.1, ‘fault model’ refers to the assumption that the faulty system is available and used in the design process. Actuator constraints refers to the ability of the controller to handle actuator limits.

2.3 Criteria for fault tolerant control: Redundancy

Flight 232 DC-10 in Sioux City, Iowa 1989 (which suffered a tail engine failure that caused the total loss of hydraulics) [42, 84], the Kalita Air freighter in Detroit, Michigan, October 2004 (where engine No: 1 was shed but the crew managed to land safely without any casualties) and the DHL A300B4, Baghdad, November 2003 (which was hit by a missile on its left wing and lost all hydraulics, but still landed safely using only the engines) [42], represent some examples of successful landings using clever manipulation of the remaining functional redundant control surfaces. Here it can be seen that one of the main factors that enabled safe landing after faults/failures is the clever manipulation of the redundant control surfaces to achieve the desired level of acceptable degraded performance. In the event of an emergency due to faults/failures, pilots will use all the available resources to help in a safe landing.

Redundancy can be categorized into two types; direct and analytical. In direct redundancy, actual physical hardware redundancy is available. In terms of sensors redundancy, two or

Method	Actuator Failures	Structural Failures	Robust	Adaptive	FDI	Fault Model Assumed	Actuator Constraints	Linear Model	Nonlinear Model
Multiple model switching and tuning (MMST)		•		•	•			•	
Interactive multiple model (IMM)		•		•	•		◦	•	
Propulsion controlled aircraft (PCA)	•		◦			•		•	•
Control allocation (CA)	•					•	◦	•	
Feedback linearization	•	•		•	•				•
Sliding mode control (SMC)	◦ ^a	•	• ^b				•		•
Eigenstructure assignment (EA)		•				•		•	
Pseudo inverse method (PIM)		•				•		•	
Model reference adaptive control (MRAC)		•		•	•			•	
Model predictive control (MPC)	•	•	◦	◦	•	•	•	•	•

• means that the method has the property

◦ implies that an author suggested that the approach could be modified to incorporate the property [114]

Table 2.1: Current FTC methods comparison.

^aSMC can handle partial loss of effectiveness of actuator but not complete loss

^bSMC assumes robust control can handle all forms of structural failures

three sensors that measure the same state is called double and triple redundancy. In normal operation, only one sensor is sufficient, however, two or three sensors are required to ensure reliable measurements in the case of faults. A voting system is a typical way to decide which channels are working correctly and which are faulty. This hardware redundancy concept can also be extended to the actuators.

In terms of analytical redundancy, instead of having two or three sensors that measure the same signal, an observer that provides an estimation of the signals of interest provide analytical redundancy. There is no actual hardware implemented, instead some algorithm or mathematical model or observer runs in the flight control computer. This is desirable in many systems especially in aircraft and unmanned air vehicles (UAVs) since, analytical redundancy eliminates the requirements for extra hardware therefore reducing weight and cost.

The development of new safety critical systems such as the re-entry vehicle [108, 109] allows the possibility of building in redundancy during the design process [166]. For many systems, however, the challenge is to use the existing available sensors and actuators to deal with faults/failures. In large transport aircraft, redundancy is already available in abundance. Even though it is not meant for the purpose of FTC, the use of these extra control surfaces provide the possibility of them being used to obtain the same desired effect as using the original control surface e.g. horizontal stabilizers can be used if elevators fail.

In large passenger transport aircraft, sensors are mostly triple redundant [36, 37]. In view of the aerospace industry's attempts to reduce the 'carbon footprint' left by aircraft, many manufacturers have tried to reduce the consumption of fuel by designing high efficiency engines and by reducing weight and therefore reducing the number of hardware redundancies, replacing them with analytical ones i.e. using observers to estimate the aircraft states. This is also beneficial in the development of cheap, robust and maintenance-free UAVs. Due to the low production cost, there is no requirement for repair, and instead, the whole unit is replaced.

In aircraft, a control surface, for example the rudder, can have three different hydraulic actuators running from three separate lines to three independent hydraulic pumps [37]. This means, most control surfaces will have triple redundancy. In terms of the control surface itself, there exist secondary control surfaces that can be used in an emergency or in an unconventional way to achieve the same effect as the primary control surface (see Figure 2.5). In large passenger transport aircraft for example, the spoilers which are typically deployed to reduce speed, can also be used differentially to create roll which normally is achieved by using ailerons; also engines can be used differentially to create yaw, which is typically achieved by using the rudder; and finally the horizontal stabilizer (see Figure 2.5) which is normally used to set the angle of attack, can also replace elevators for pitch movement.

2.4 How fault tolerance is achieved

In this thesis, Figure 2.6 gives a general overview based on how the FTC is achieved. The top level of the tree diagram is based on the one proposed in [166]. The lower level of the tree diagram is based on the different approaches for achieving FTC as discussed above.

Passive FTC is usually based on robust control ideas and therefore robustly handles faults/failures

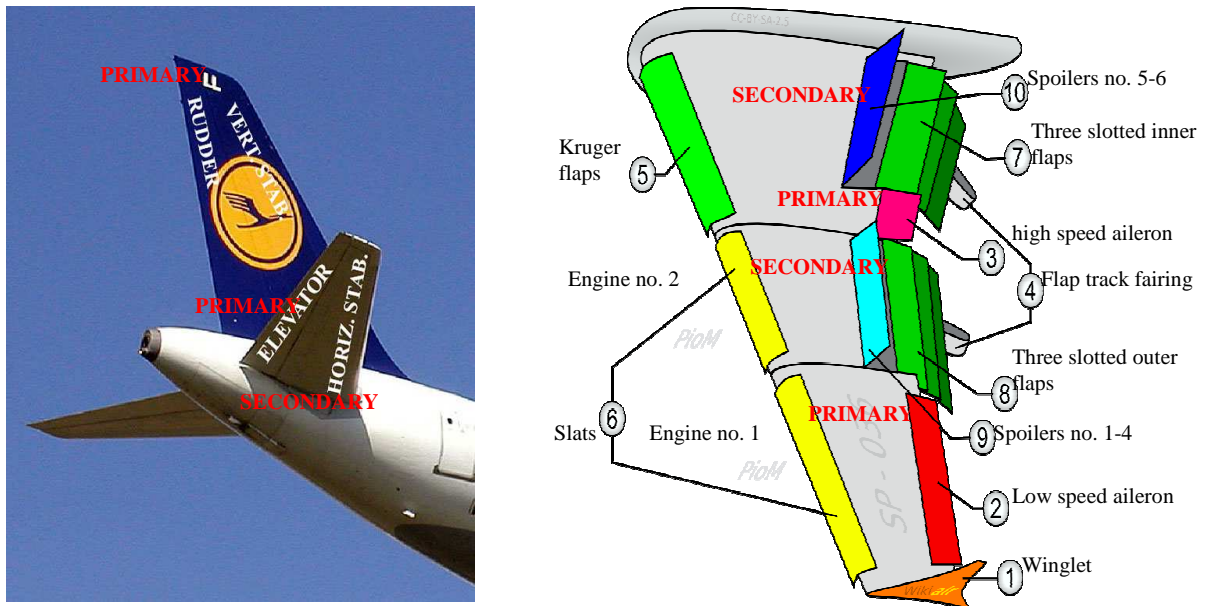


Figure 2.5: Large transport aircraft: typical control surfaces

without requiring any information from any FDI scheme. Active FTC (AFTC) in general requires some information on the faults/failures that occur and therefore generally some sort of FDI is required. AFTC can be divided into two sub groups: projection type FTC; and online reconfiguration/adaptation. In projection based FTC, the controller is designed for all possible faults/failures that might occur in the system. The projected controller will only be activated when a specific designed for fault/failure occurs. Projection based FTC is subdivided into three categories which are model switching or blending, scheduling and prediction. AFTC is based on reconfiguration or adaptation online. Here, two further subcomponents have been proposed: FTC which is achieved through adaptive control; and FTC which can be achieved through redistributing the control signals (control allocation).

Some discussion on the different FTC strategies is provided in the following subsections.

2.4.1 Adaptation (Model reference adaptive control and self tuning control)

One way of dealing with changes in the system (including faults/failures) is by adapting the controller. Motivated by the design of autopilots for high performance aircraft in the 1950s, adaptive control was proposed as a way of dealing with a wide range of flight conditions [187]. Adaptive control is used in order to automatically adjust the controller parameters to achieve the desired performance. There are two approaches in adaptive control which are direct and indirect adaptation [22, 62, 114]. In indirect adaptation, there are two stages in designing the controller. First, the system parameters need to be estimated. In the case of linear systems, the matrix pair (A, B) needs to be estimated due to changes in the operating conditions e.g. faults/failures. The next step in the indirect adaptation approach is to use this information to design the controller. In the direct adaptation approach, the controller is designed directly without estimating the system parameters.

Examples of controller design in adaptive control are model reference adaptive control (MRAC) and self tuning control (STC) [187]. In self tuning control, online parameter estimation is

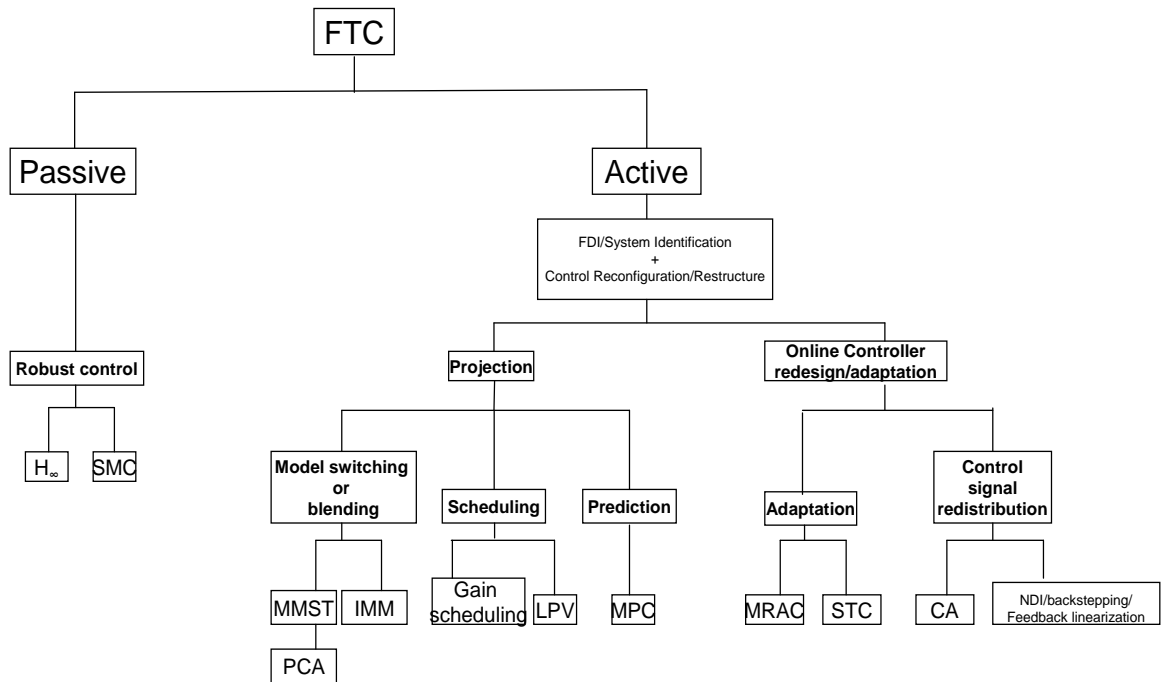


Figure 2.6: Classification of FTC - how FTC is achieved

required for the controller adaptation. Meanwhile, in the MRAC, the unknown parameters are not perfectly estimated, but rather are tuned and adjusted so that the output of the plant follows the desired closed-loop performance (the output of the reference model) by making the tracking error converge to zero. Figures 2.7–2.8 show the differences in structure between MRAC and STC.

The idea of tuning a controller is quite popular especially when there are no requirements for the structure of the controller to be changed. This is indeed one of the components of multiple model switching and tuning (MMST) control. In MMST, when the system is at an operating condition, a predefined model and controller will be chosen and the structure of the controller will remain unchanged near that operating condition. During this period, tuning the controller parameters may help to achieve better performance compared to a fixed controller. In MRAC, the idea is to use the classical model reference approach and combine it with an adaptive scheme so that the system has the ability to handle changes in the system.

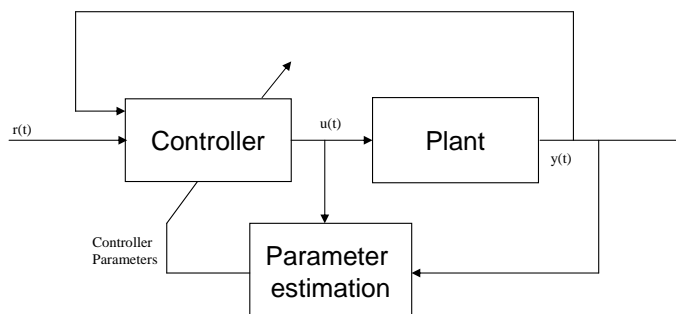


Figure 2.7: A self tuning control system

Figure 2.8 shows the typical structure of a MRAC scheme. It contains the reference model, the adaptation law and the adaptive controller [187]. The plant is assumed to have a fixed

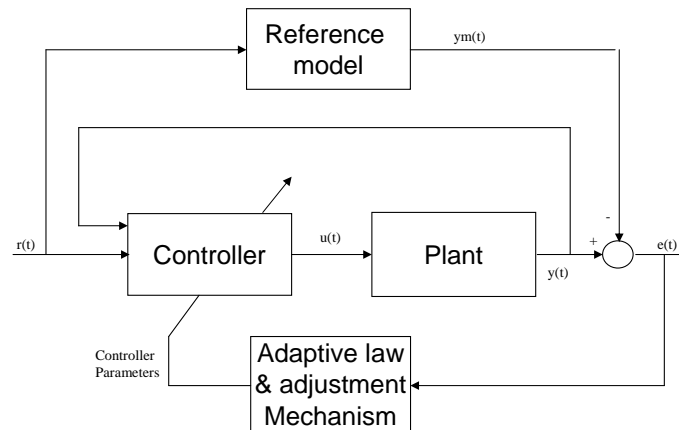


Figure 2.8: A model reference adaptive control system

structure but the parameters are unknown. The reference model is typically the ideal closed-loop response to the external command signals. Most performance specifications are given in the time domain e.g. rise time, damping ratio and decoupling effects. These can be represented in terms of an ideal transfer function response, which become the reference signals the closed-loop system must follow for tracking purposes. The controller is parameterized by adjustable parameters to allow the controller to adapt to changes in the system and for the output of the plant to track the desired performance.

One major difference between the MMST and IMM (interacting multiple model) – which will be discussed in the next subsection – compared to MRAC is that, the reference model provides the desired closed-loop performance which the controller forces the system to follow, and it takes the input from reference signals. Meanwhile, in MMST and IMM, a bank of open loop models or a blend of open loop models are used instead. The MMST and IMM schemes use these open loop models to identify the correct one to be used for the current operating conditions, therefore activating the associated predetermined controller. Therefore in general, the MRAC scheme closed-loop model has a fixed structure with adaptive/tunable parameters.³

Even though there is the possibility of changing the reference model and probably the controller in the face of significant damage or ‘hard’ faults/failures, the MRAC and STC schemes alone do not have the capability to do this [114]. Therefore a combination of the MRAC and STC schemes with other reconfiguration methods such as a bank of controllers i.e MMST and IMM is required to handle major changes in the system. In fact, the ideas employed in adaptive control, such as model reference following and parameter tuning can also be found in other reconfigurable and FTC control methods [114]. In the field of FTC, [56, 64, 112, 240] are examples of research which uses adaptive control to handle faults/failures.

³unless a secondary reference model is supplied which has a slower defined response and is used in the event of faults/failures to ensure a safe degraded level of performance [112, 240] without jeopardizing the stability of the system.

2.4.2 Switching or blending

Bank of controllers: multiple model switching and tuning (MMST)

The idea of using multiple models for reconfigurable control was introduced in the early 1990s [160]. Multiple model schemes have been motivated by the problem of coping with changes in operating conditions and varying flight envelopes. Most early classical control methods were based on linear methods, and multiple model schemes seem an ideal extension to solve the problem of changing operating conditions.

When implementing on a real system, usually linear controllers need to adapt to changes in operating conditions since the controller is only guaranteed to be stable near the linearization condition. Therefore using multiple model schemes is one way to ensure that the controller can be designed so that stability and performance can be guaranteed for a wide flight envelope.

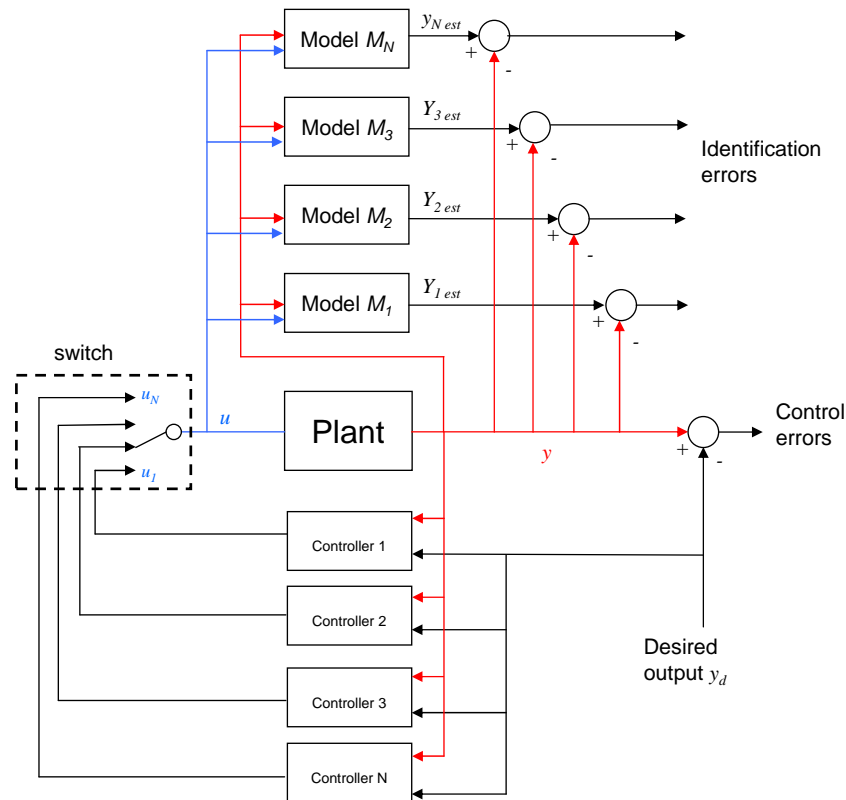


Figure 2.9: SMMST control strategy (adapted from [160])

From an FTC point of view, the ‘bank’ of controllers acts as a backup and are only activated when faults for which the controller is designed occur. This method depends on the robustness of the FDI to provide the correct information on the type and location of the faults/failures to enable the correct controller to be switched on. The ‘bank’ of models must contain all the possible faults and failure modes. An FDI scheme can be created by comparing the current plant states and the outputs of all models in the bank [33] (Figure 2.9). Roughly speaking, the model with the smallest error is the nearest model to the actual plant and therefore its associated controller can be switched on. More elaborate descriptions of the switching rule are available in [159, 160]. These papers discuss the stability of the switching schemes as well as the performance after a switch has occurred.

One way of designing the controller is using eigenstructure assignment and the multi-model approach improves the robustness (page 31 in [142]). Figure 2.9 shows that for a chosen operating condition, a single model and controller will be chosen based on the error between the current system and the predesigned model. Once a model and its respective controller is chosen, an adaptive method can be employed to fine tune the controller gains. Other controller methods such as model predictive control (MPC) have also been considered for designing multiple controllers [85]. In [160], a review of the most recent development in MMST has been presented.

The advantage of this method lies in the application of well known linear control design methodologies and the guarantee of stability upon deployment of the correct controller. The speed of the fault detection is also fast [114]. Even though this method is based on well known linear control methods, implementation can be tedious. To handle all possible types of faults and failures means that the number of models and controllers that need to be designed and tuned is enormous. The switching between models and controllers sometimes introduces undesired transients. Therefore bumpless transfer methods [48, 66] are sometimes needed to reduce the effect. Another disadvantage is that some faults that occur are not predicted. For example, in several flight incidents, unthinkable failures have occurred e.g. the Bijlmermeer incident in Amsterdam [189], where two engines detached from the right wing and caused unpredictable effects on the aerodynamics of the aircraft due to the damaged airframe. One disadvantage of this method is the dependency on the robustness of the FDI to identify the correct model and controller pair to be activated. Another disadvantage highlighted in [114], is the schemes inability to handle multiple faults/failures. The survey in [114], gives a brief introduction to MMST. More detailed descriptions can be found in [159, 160]. The application of multiple model ideas in terms of FTC for aircraft systems can be found in [33, 85] and recently in [19].

Propulsion controlled aircraft (PCA): a successful implementation of MMST on real aircraft

The incident in Sioux city in 1999 and more recently in Baghdad in 2003 [42] showed remarkable recoveries using only engine thrust after a major loss of hydraulics to all control surfaces. One unlucky incident with a similar failure of the hydraulics was flight 123 in Japan [84]. Learning from these past incidents, it is clearly possible that, using only the engines, a safe approach and landing can be achieved. After the incident in Sioux city, the National Transportation Safety Board (NTSB) recommended and encouraged the development of backup flight controllers to be used in such emergency situations [208]. NASA Dryden led by F.W. Burcham and C.G. Fullerton took up the challenge and conceived, developed and tested the first propulsion controlled aircraft system [208]. Impressive simulator and actual flight test results were obtained during the project. Tests were done on many types of aircraft ranging from fighter jets (F15 [208]) to large transport aircraft (DC11 and the B747 [43–46, 208]).

Based on one particular type of failure, the PCA scheme is considered as a MMST by [114]. Tests using the PCA scheme system and its variant by NASA Dryden have been done on a real aircraft. The PCA scheme has shown its airworthiness during these flight tests. Even though the PCA considers one of the most catastrophic types of failure, it is not sufficient to solve general FTC problems [114]. In the case of airframe damage, loss of engines (as occurred in the

ELAL flight 1862 Bijlmeer incident [189]) and indeed the partial loss of the hydraulic systems, PCA might not be suitable.

NASA reports on PCA can be found in [42–46, 208, 208]. Other papers such as [93, 103] also consider propulsion control strategies. Both papers use a different type of controller design to the MMST and in [103] an adaptive neural network with control allocation is used instead.

Interacting multiple model (IMM)

Even though MMST can be used to tackle the problem of varying operating conditions, in some cases, to obtain a linear model that exactly matches the varying plant is hard to achieve; since hundreds (if not thousands) of linear models and controllers are needed to match every possible flight condition including faults/failures. Therefore, an interaction between linear models can be used. The idea is to obtain a few linear models based on a few carefully chosen flight conditions and to design multiple linear controllers at these selected operating conditions (or faults/failures). When the operating conditions change (or faults/failures occur), an estimated plant output or control input is obtained by blending the predetermined models. This can be seen in Figure 2.10.

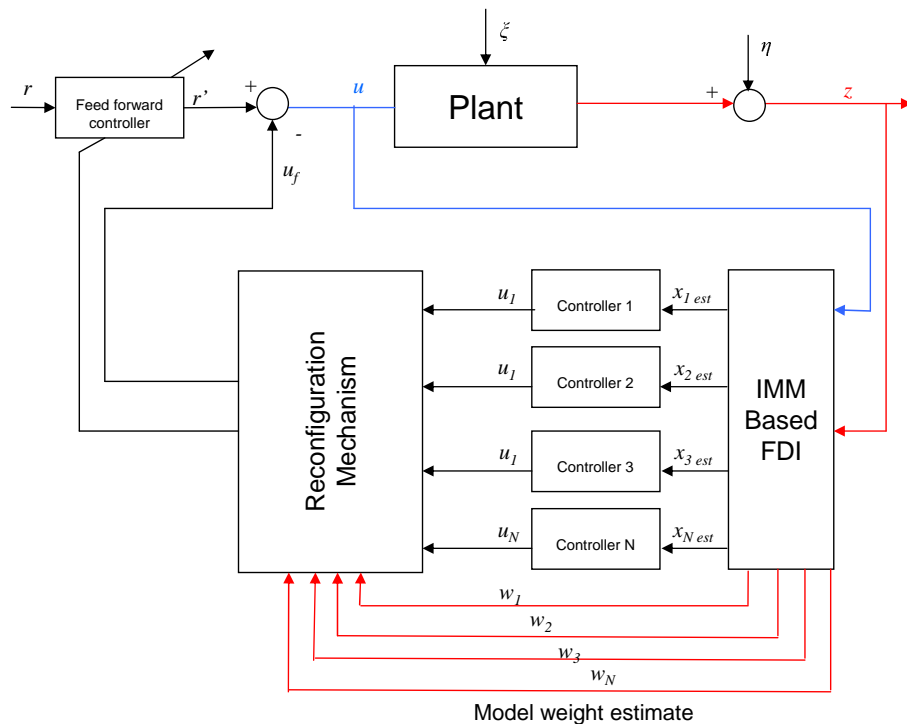


Figure 2.10: IMM control strategy (adapted from [238])

The control strategy in IMM schemes is first for the IMM estimator to detect and isolate the faults/failures by obtaining an estimate of the plant output from a blend of predefined linear models and to provide a probability weight for the controller reconfiguration. The main assumption used in IMM is that every possible flight condition including faults/failures can be modeled as a convex combination of the predetermined linear models. The second step is to obtain a control signal based on a blend of predefined controllers [238] or online control law calculations using the probability weight provided by the IMM estimator.

In the first step of the IMM scheme, [238] and [174] proposed the use of a bank of Kalman filters to calculate the probability of the individual faults/failures. This probability is also used as weighted average of each predefined linear model to estimate the state of the plant. In the second step, a bank of controllers is predesigned based on the anticipated/projected faults/failures that might occur [174,238]. The idea is that, during faults/failures, the eigenvalues of the closed-loop system need to be as close as possible to the nominal no fault conditions. The reconfiguration of the controller comes from the online use of the probability weighted average to determine the blending ratio for the control input from the predefined/projected controllers when a fault or failure occurs [174,238]. This approach is similar to the MMST scheme in the sense that if the exact or anticipated faults/failures occur, the probability weight will be unity and the rest of the models and controllers will have no contribution to the state estimate and input signals to the plant.

In [238], it has been shown that system faults⁴ can be handled. In comparison to the MMST, the IMM has the ability to cope with non anticipated faults/failures [174,238]. One problem of IMM schemes is finding the right balance of blending/probability weights to get the best model match. IMM is also heavily dependent on the FDI scheme to correctly identify the faults/failures.

Details on IMM schemes can be found in [120]. In [238], an integrated IMM approach is discussed where both FDI and FTC are integrated. The application of IMM to an Eagle-Eye UAV can be found in [174].

2.4.3 Scheduling

Gain scheduling

In the survey paper [134], gain scheduling is linked to the ‘divide and conquer’ design procedure. This procedure aims to solve nonlinear control problems by decomposing the nonlinear system into a family of linear systems and designing a linear controller for each one of them [134]. Based on this definition, MMST and IMM are particular types of gain scheduling. The term gain scheduling also refers to the scheduling of linear models and its associated controllers either by parameters or states, in order to deal with nonlinear control problems resulting from a change in the operating conditions and flight envelope. Another type of gain scheduling is the linear parameter varying (LPV) control method [134] described in the next subsection.

Gain scheduling is also based on precalculated control laws. In some flight conditions, there is no requirement for the controller structure to be changed. Only the gains of the controller need to be changed according to the flight conditions or the severity of the faults/failures. The tuning is not done adaptively, instead, predefined gains are chosen for specific flight conditions or specific parameters. This can be presented in the form of a simple logic switch between two gains, or more commonly through the use of lookup tables or curve fitting [23].

One of the advantages of gain scheduling is that it is easily understood and implemented. However, in some cases, the faults/failures are so significant that the structure of the nominal controllers simply cannot cope. In this case, gain scheduling is insufficient and controller

⁴In terms of linear methods, system faults are the ones that affect the A matrix i.e. airframe or wing damage.

reconfiguration is required. A recent survey on gain scheduling developments can be found in [134].

Linear parameter varying(LPV)

Linear parameter varying (LPV) control design is closely related to gain scheduling [134]. It is motivated by the lack of performance and stability proofs for classical gain scheduling [23, 80]. LPV is also motivated by the problem of obtaining and designing multiple models and controllers, which is tedious for a large flight envelope.

The idea in LPV is to obtain smooth semi-linear models that can vary or be scheduled using a parameter like altitude and/or speed so that the LPV model will mimic the actual nonlinear plant. Here instead of choosing a combination of predefined linear models, the models change parametrically. The LPV model has the structure of a linear system with A, B, C matrices, but each matrix can be changed based on the chosen parameter. An LPV system can be represented by [80]

$$\dot{x}(t) = A(p)x(t) + B(p)u(t) \quad (2.3)$$

$$y(t) = C(p)x(t) + D(p)u(t) \quad (2.4)$$

where p is the varying parameter e.g. speed or altitude. If p is a constant, then the LPV system becomes a linear time invariant (LTI) system [80]. Methods for obtaining LPV models are discussed in [23]. The first method corresponds to the rearrangement and transformation of the nonlinear system into a quasi-LPV system where it has the structure of a linear system, but where the components of these matrices vary depending on some common variables [23, 146]. The second method is based on a parameterized family of Jacobian linearizations. The collection of the linear models is parameterized by one or two variables associated with the linearization point. The results are polynomially fitted state space matrices which are continuous throughout the operating conditions [23, 146].

After the LPV models have been obtained, the controller can be designed. In comparison to the classical gain scheduling methods where the gains are interpolations of predesigned controller gains, the LPV controllers are dependent on the parametric changes in the system. Lyapunov methods have been used to design LPV controllers [23, 225]. Alternatively ‘small gain theorem’ based methods [23] have also been used. In the field of FTC, LPV ideas have been used for dealing with actuator faults/failures [80]. LPV observers have also been considered for FDI to generate residual signals for the fault detection of actuator and sensor faults [149].

LPV provides some guarantees of stability and performance when compared to classical gain scheduling. Nonlinear controller methods can be used for the simplified LPV model. This means that compared to the MMST and IMM methods, controllers do not need to be designed for all linearization points.

Some general papers on LPV are [23, 225]. In the field of FTC, papers such as [80, 149] represent some of the research work in this area. Both of these papers have considered a LPV approach for dealing with faults/failures in the B747 model. The most recent LPV papers in the field of FTC are [176, 182, 183].

2.4.4 Prediction

Model predictive control (MPC)

Unlike many other control paradigms which came from the academic community, the development of predictive control/model predictive control (MPC) was initiated in the process industry. This is due to the fact that the concept and the mathematical description is easy to understand by most control engineers in industry. Therefore it is no surprise that (other than classical PID control), MPC is the most widely used and implemented method in the process control industry [140].

The original idea for MPC is to allow the production process to run as close as possible to the process limits (i.e. physical and safety) without violating any of the limits, in order to maximize production and therefore profit. The main benefit of MPC is in the handling of limits and constraints. This is the main motivation for the study of MPC for flight control and especially FTC. Examples of MPC in the field of flight control and FTC can be found in [141,142] respectively. During faults/failures, especially to the actuators, the remaining actuators will be driven to their limits [141]. Here, MPC naturally has the ability to handle the actuator limits by including these limits in the optimization process which is used to obtain the control signals. Structural damage can also be handled in MPC by modifying the internal/reference model [141].

Roughly speaking MPC is an iterative control algorithm based on optimal control. The iteration can be summarized as follows: at the current time, the current plant states are sampled and a cost minimizing strategy (using on-line optimal control and taking into account the system constraints) is computed for a relatively short time horizon into the future. The objective is to obtain predicted state trajectories in the future using the current states and the computed control signals. Only the first control signal from the optimization is applied to the real actuators. Then the states are sampled again and the calculations are repeated. MPC is also known as receding horizon control [140,142]. Figure (2.11) below provides some insight into the structure of MPC.

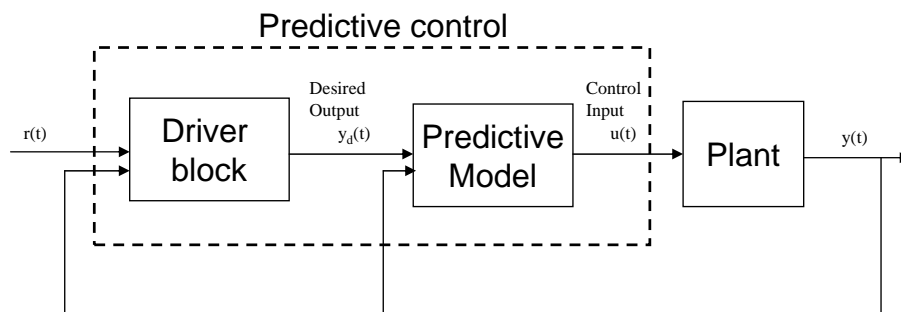


Figure 2.11: Predictive control strategy (adapted from [180])

Here, the driver block/reference model generates the desired output based on the physical feasibility and desired dynamics. The predictive model block generates the control signals that force the output of the plant to follow the desired outputs using previous inputs and outputs of the plant [180]. The optimization can be solved using quadratic programming or fast linear programming algorithms [140].

MPC in its most powerful form requires an on-line solution to the constrained optimization problem [140]. However, with the current state of computer technology, on-line optimization is still hard to achieve for systems requiring fast responses – such as aircraft. As in most FTC strategies, MPC is dependent on reliable FDI to provide information on the faulty system. In the case of actuator faults, the behaviour of the faulty actuator is needed from the FDI scheme so that a new constraint can be included in the optimization process. In terms of tuning for flight control systems, there is still a lack of guidance in assisting the design process [142], which typically requires trial and error and experience. The major benefit of MPC is that it can handle actuator constraints and this has provided motivation for the study of MPC in flight control and FTC [142].

2.4.5 Control signal redistribution

Pseudo inverse method

The idea of the pseudo inverse method (PIM) is to design a controller such that the poles of the system subject to a fault/failure condition will be as close as possible to the nominal closed-loop poles. The following equations give insight into the PIM method. Consider a linear system given by

$$\dot{x}(t) = Ax(t) + Bu(t) \quad (2.5)$$

Assume that a state feedback gain K has been design, and the control law is defined as

$$u(t) = Kx(t) \quad (2.6)$$

and therefore the closed-loop system is given by

$$\dot{x}(t) = (A + BK)x(t) \quad (2.7)$$

During faults/failures, the closed-loop faulty system can be represented by

$$\dot{x}_f(t) = (A_f + B_f K_f)x_f(t) \quad (2.8)$$

The idea is to obtain a K_f so that the faulty system closed-loop performance will be as close as possible to the nominal (2.7) one. Since the objective is to obtain $x_f(t) = x(t)$, a necessary condition is to ensure

$$(A + BK) = (A_f + B_f K_f)$$

and therefore

$$K_f = B_f^\dagger (A - A_f + BK)$$

where B_f^\dagger is the pseudo inverse of B_f . The plant matrices A and B and the gain K is assumed to be known a priori. The faulty system (A_f, B_f) can be obtained from online system identification or from FDI: then in principle, K_f can be obtained online. For a non square B_f matrix, the pseudo inverse of B_f provides some degrees of freedom. In [151], this degree of freedom from the pseudo inverse B_f^\dagger was used to redistribute the control commands in order to improve the closed-loop system stability [166].

Even though the concept given above is quite simple and easy to understand, the PIM has several drawbacks which hindered its further progress. As argued in [102, 114, 166, 230], one of the main drawbacks is the lack of stability analysis. The other drawbacks highlighted by [166] and [230] are associated with the assumption that the state measurements are always available. Meanwhile [230] highlights the problem of lack of robustness when the system pair (A_f, B_f) from the system identification is not perfectly known.

Some suggestions are given in [81, 102, 166] for improving the PIM method. In [81], the concept of modifying the PIM (MPIM) is discussed. It is based on the combination of PIM with the theory of robust stability of systems with structured uncertainty [102, 166]. In [102], a bank of pre-computed K_f matrices, which ensure a stable closed-loop system for all possible faults, was suggested. In [230], a robust ‘control mixer’ which relates to the IMM method was proposed. It is also interesting to point out the resemblance between the PIM approach and model following methods [166], where the closed-loop system is forced to follow pre-specified desired closed-loop dynamics.

Control allocation

Early ideas of control allocation are discussed in [166]. In its early development, the idea of redistributing the control signals to the remaining healthy actuators was called ‘restructuring’ [166]. An early example is given in [101], where a ‘restructuring controller’ utilizing a ‘control mixer concept’ is used to redistribute the control signals. Due to some drawbacks, the restructuring type of controller was not explored in the 90’s. It has re-emerged in recent years as control allocation partly because of the development of high performance, highly redundant aircraft (such as [34, 39, 184, 219]) and improvements in computational power (which is necessary in order to solve on-line optimization problems [26, 31, 63, 70, 115]).

Control allocation (CA) has the capability to redistribute the control command signals to the actuators especially during faults/failures. Even though PIM and CA seem to be identical in the sense that both employ a pseudo inverse which provides some design freedom, one major difference between CA and PIM is that in CA, the controller is designed based on a ‘virtual control’ signal and the CA will map the virtual control to the actual control demand to the actuators. The benefit here is that the controller design is independent of the CA unit. Therefore, CA can be used in conjunction with any other controller design paradigm such as LQR or \mathcal{H}_∞ control. Papers such as [95, 181] represent some of the recent work done in this area.

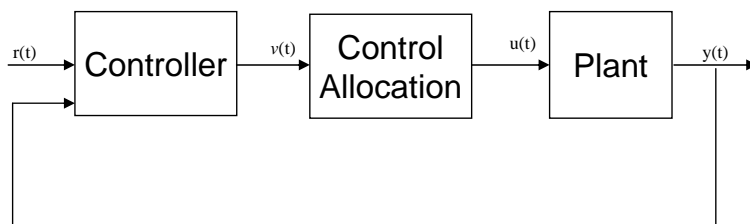


Figure 2.12: Control allocation strategy

CA has the capability to manage the actuator redundancy that exists in passenger aircraft [37] and modern fighter aircraft [75]. Not only is CA beneficial for FTC (see for example [40, 58]),

it has also been used for different control strategies i.e. optimally using the actuators to reduce drag and increase efficiency. There is extensive literature on CA which discusses different algorithms, approaches and applications: [70] discusses two (broadly) linked approaches (linear and quadratic programming) based on finding the ‘best solution’ to a system of linear equations. The work in [95] compares control allocation with optimal control design for distributing the control effort amongst redundant actuators. The authors in [41] demonstrate that feedback control systems with redundant actuators can be reduced to a feedback control system without redundancy using a special case of CA known as ‘daisy chaining’. In this approach, a subset of the actuators, regarded as the primary actuators are used first, then secondary actuators are used if the primary actuators reach saturation. Other CA approaches which take into account actuator limits (using constrained optimization) are discussed in [31, 34], while [94] discusses frequency weighted CA.

CA occurs naturally with nonlinear methods like feedback linearization and backstepping [26, 94, 184, 185]. It is based on separating the control law from the control allocation task (see Figure 2.12). This is done by designing a controller to provide a ‘virtual control’ which will be mapped to the actual control signals sent to the actuators. Consider an overactuated system such as a passenger aircraft [37] or modern fighter aircraft [75] represented by a linear system

$$\dot{x} = Ax + B_u u \quad (2.9)$$

where B_u can be factorized such that

$$B_u = B_\nu B$$

Therefore, the linear system in (2.9) becomes

$$\dot{x} = Ax + B_\nu \nu$$

where ν is the ‘virtual control’ defined by

$$\nu := Bu$$

For a given ν , the control signal $u(t)$ is recovered as

$$u = B^\dagger \nu$$

where $B^\dagger = WB^T(BWB^T)^{-1}$ is a right pseudo inverse of B . The weight matrix W is design freedom which distributes the control signals to each available actuator.

In most of the literature, the weight $W = I$ [181] (i.e. equal control signal distribution among all actuators) is typically chosen. In some cases (such as finding the control signal distribution that reduces drag and fuel consumption), a different choice of weighting matrix W can be employed. In a constrained optimization problem, the weight W can be chosen to achieve the desired performance taking into consideration actuator constraints [70].

The work in [40, 58] uses CA as a means for FTC. The benefits of CA is that the controller structure does not have to be reconfigured in the case of faults and it can deal directly with

total actuator failures without requiring reconfiguration/accommodation: the CA scheme automatically redistributes the control signal. As in MPC, another major benefit of CA is that actuator limitations can be handled by including the actuator constraint in the optimization process.

One of the drawbacks of CA is that, for linear systems, the pure factorization $B_u = B_\nu B$ is a very strong requirement and therefore approximations $B_u \approx B_\nu B$ have been made [40, 58, 95, 98]. In the case of optimal control surface deflection, linear or quadratic programming is required. This is quite difficult to achieve online in real time due to the requirements of high computational power during the optimization process. There are only a few reported examples in the literature which have successfully implemented control allocation in real time (see for example [58]).

Examples of the application of CA are given in [39, 191], while papers such as [64, 95, 103, 181, 185, 214] consider CA as an FTC strategy.

Dynamic inversion

A major attraction of dynamic inversion (DI) is its ability to naturally handle changes of operating condition. This capability has motivated researchers such as [108, 109] to consider DI for control of the space re-entry vehicle. This vehicle has extreme and wide operating conditions which vary from supersonic speed during re-entry and subsonic regions during the glide back to the runway.

The idea of DI can be shown by considering a linear system

$$\dot{x} = Ax + Bu$$

By rearranging the equation with respect to $u(t)$, as in [203], the control law can be represented by

$$u = B^{-1}(\dot{x}_d - Ax)$$

where \dot{x}_d is the predetermined desired closed-loop reference demand. In [108], dynamic inversion is described as ‘... a controller synthesis technique by which existing deficient, or undesirable, dynamics are cancelled and replaced by desirable dynamics. Cancellation and replacement are achieved through careful algebraic selection of the feedback function. For this reason, this methodology is also called feedback linearization ...’. Figure 2.13 below shows an example of the overall nonlinear dynamic inversion controller interconnections on the re-entry vehicle.

The main assumption in DI is that the plant dynamics are assumed to be perfectly modeled and therefore can be cancelled exactly. In practice this assumption is not realistic. In dealing with this issue, [108, 175] suggested the use of robust control methods such as \mathcal{H}_∞ and μ -synthesis as outer loop control to minimize or suppress undesired behaviour due to plant uncertainties which cause imperfect plant dynamic cancellation. Other control methods such as neural networks [103] also have been proposed in the literature.

The benefit of DI is that it does not require (or requires only small amounts of) gain scheduling to work in a wide range of operating conditions. DI also has a natural control allocation capability and therefore has the ability to redistribute the control signal in the case of faults or

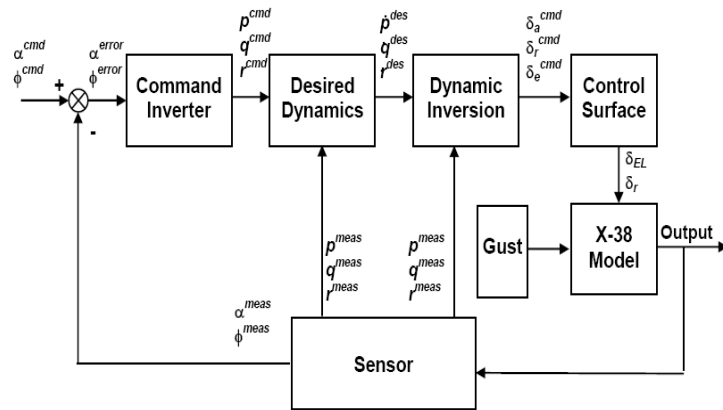


Figure 2.13: Dynamic inversion strategy (adapted from [108])

failures [115].

Despite these advantages, there are some issues with regard to DI. Firstly, nonlinear dynamic inversion (NDI) assumes full-state feedback. This is not an issue in modern aircraft, civil [37] or advanced military aircraft [75], but full state measurement is not always available for many other systems. DI also requires a deep understanding and knowledge of the plant in order to be able to cancel the plant dynamics perfectly. In reality, this is quite impractical. Currently, this limits its usage and requires a robust outer-loop controller [108].

In terms of FTC for flight control, papers such as [73, 103, 108, 109] and more recently [115] describe the potential of dynamic inversion for dealing with faults/failures. In [73] dynamic inversion with adaptive robust control (ARC) has been discussed. It is based on the work in [231] where a combination of SMC and adaptive control is conceived and called ARC. The controllers have been tested for several types of faults/failures such as loss of effectiveness, float and hard-over failures on the control surfaces. In terms of FTC on large civil passenger aircraft, [103] has provided some insight on the application of dynamic inversion with online learning neural networks. More recently, [115] considered dynamic inversion and uses explicitly the inherent control allocation properties to handle actuator failures. In [115], the change in the aircraft aerodynamic coefficients due to faults/failures and structural damage is estimated using on-line using parameter identification (called the two step method [138]) in order to obtain ‘perfect’ inversion of the nonlinear plant.

2.4.6 Robust control (\mathcal{H}_∞ control)

\mathcal{H}_∞ is a robust control methodology and therefore can be considered as a passive fault tolerant control scheme. \mathcal{H}_∞ is one of the most developed methods for multivariable control [142], with many applications ranging from industrial process control to aircraft control problems. Most robust control approaches do not require any information on faults and therefore work in nominal as well as in faulty conditions. The ability to deal with faults depends on the predesigned controller which is based on minimizing the effect of uncertainty or disturbances on the system [142]. The first step in \mathcal{H}_∞ control design is to decide the type and structure of the uncertainty to be considered. It is argued that this process is somewhat difficult and requires some insight into the plant (page 65 in [142]). The most general type of unstructured

uncertainty is based on normalized coprime factor representations. The second method is to choose frequency dependent weights based on some performance specifications and then to solve an optimization problem. Some well studied \mathcal{H}_∞ controller design techniques are \mathcal{H}_∞ mixed sensitivity, μ -synthesis and \mathcal{H}_∞ loop shaping [186].

One disadvantage of \mathcal{H}_∞ is the fact that in some cases, the controller is conservative in the nominal conditions in order to guarantee stability in the event of faults, and the performance in the nominal condition is sometimes sacrificed for robustness. Another drawback is that the final controller is usually of a higher order than the system. In some cases model reduction is required to truncate the order of the controller (page 339 [142]). In the field of FTC, papers like [148] and the chapters in [142] describe some of the research that has been done in the area of flight control.

2.5 Fault Detection and Isolation

In active FTC, FDI plays a vital role to provide information on faults/failures in the system and to enable appropriate reconfiguration to take place. Therefore the main function of FDI is to detect a fault or failure and to find its location so that corrective action can be made to eliminate or minimize the effect on the overall system performance [200].

The IFAC technical committee, as stated in [107], defines:

- *fault detection*: determination of the faults present in a system and the time of detection
- *fault isolation*: determination of the kind, location and time of detection of a fault
- *fault identification*: determination of the size and time-variant behaviour of a fault

The interconnection of FDI with FTC is discussed in [166, 239, 241]. For most AFTC systems, the robustness of the FDI has a strong effect on the robustness of the FTC and this is discussed in [166, 237, 241]. In [50, 200], a few methods ensuring robustness of the FDI have been discussed such as eigenstructure assignment, parity equations, unknown input observers, frequency domain methods and careful selection of thresholds.

An important aspect in FDI is redundancy. As mentioned in Section 2.3, redundancy can be either in the form of hardware or analytical redundancy. Since the appearance of drive and fly by wire technology, there has been an increase in analytical redundancy. In analytical redundancy methods, the measured signals are compared to a mathematical model. The benefit of using analytical redundancy is clear: there is no need for redundant hardware to be installed, therefore reducing weight and cost. This is very useful for energy and weight critical systems such as satellites and spacecraft.

2.5.1 Classification of FDI

There are many classifications of FDI in the literature [50, 107]. One obvious classification is model and non-model based FDI. In this thesis the emphasis will be on model based FDI. In view of the overall fault tolerant strategy, model based FDI schemes are grouped based on

their capabilities into two major categories; FDI using residual schemes and FDI which has the capability to estimate the faults.

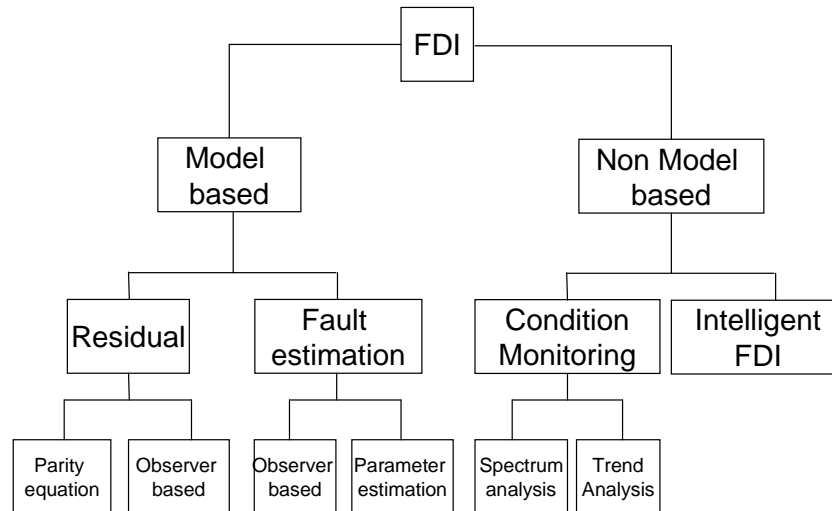


Figure 2.14: FDI classification

Figure 2.14 above represents a possible classification for FDI. The model based residual classification is obtained from [50].

Condition monitoring

Condition monitoring is one of the traditional methods used widely in industry. It is important as early detection of faults in components such as bearings enables preventive maintenance to be done therefore reducing downtime. Condition monitoring is very popular in production processes (such as computer chip or electronic component production lines) and non-safety critical systems. Condition monitoring mostly depends on the statistical properties of the measurements (i.e. structural vibrations) taken from specific points on the equipment and spectral analysis such as fast fourier transform (FFT) or trend analysis such as MTTF (mean time to failure) and MTBF (mean time between failures) [1]. These analysis tools provide information on the ‘health’ condition of components, and faults can be detected when selected thresholds have been violated [222] or some familiar fault trend appears in the analyzed data. The analysis from the condition monitoring allows advanced planning of maintenance routines. One drawback of most condition monitoring methods is the slow and tedious process of data collection, and interpretation of the data. It also has a limited capability for FTC, as usually faults can only be detected off line because it depends on data collected during plant operation and how the data is interpreted. Here, good experience or good maintenance history provides data for trend analysis to detect faults or failures. Condition monitoring also suffers from variations in terms of changing operating conditions. Sometimes this means that it is difficult to differentiate between faults or operation related disturbance. Another drawback in condition monitoring is that a single fault can cause multiple alarms and sometimes causes anomalies in the collected data for other units. This gives difficulties in locating the original source of the faults/failures.

Recent examples of condition monitoring and trend analysis can be found in [221–223] which

monitors the health of helicopter components – especially the rotor blade assembly.

Residual based FDI

In residual based FDI, signals from a mathematical model and hardware measurements are compared and the filtered difference forms a residual signal [50]. In nominal fault-free conditions, the residuals should be zero, and nonzero when faults/failures occur. This residual signal sometimes is applied with a threshold to avoid false alarms from disturbances or uncertainty. When the residual signal exceeds the threshold, a fault is said to occur. Usually in residual generation, a fault is detected and its location identified, but there is no further information on the fault.

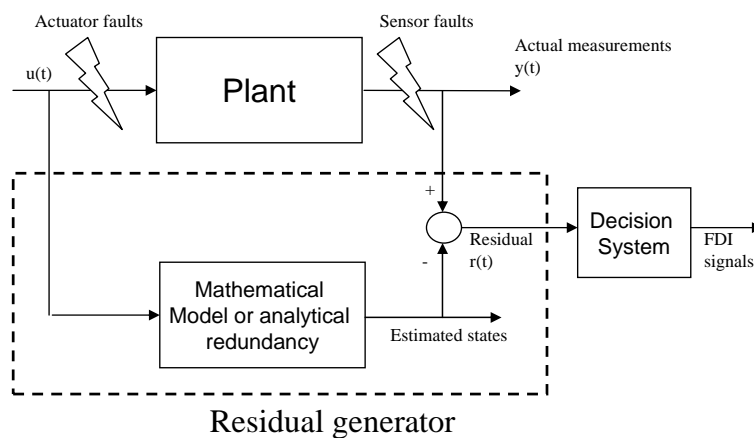


Figure 2.15: residual based FDI

A good deal of research has been done on residual based FDI using different methods for various applications. In particular, [50] provides an excellent discussion on model based residual FDI schemes covering all aspects including basic principles and robustness issues. Other recent literature which uses residual based FDI with specific application to aircraft systems is, Szaszi *et al* [198], Marcos *et al* [149]. In the area of sliding mode observer based residual FDI, Yang & Saif [229] and Floquet *et al* [74] represent some of the examples of work available in the literature.

There are many benefits of using residual based FDI. Most residual based FDI systems are easy to understand and implement, with many mature topic areas and examples of applications in the literature. For many systems, detection and isolation of the fault is sufficient to trigger the reconfiguration for FTC. For example multiple model controllers will switch on a particular controller when the designated failure occurs to the actuators or sensors based on the information about the location of the fault. However, for some FTC schemes, detecting and isolating the faults is not sufficient. Some FTC schemes requires further information about the nature and behaviour of the fault.

Fault identification/estimation/reconstruction FDI

This is one step further than the residual based FDI, but is mostly specific to certain types of reconfigurable/FTC controllers.

Some FTC controllers such as the methods proposed in [227, 237, 242], require estimates of the actuator efficiency to allow the FTC controller to tolerate the faults/failures. In terms of sensor fault FTC, if the sensor fault can be estimated/reconstructed, this information can be used directly to correct the corrupted sensor measurements before they are used by the controller. This avoids reconfiguring or restructuring the controller to be tolerant to sensor faults. This is one aspect that will be considered in the later chapters of this thesis.

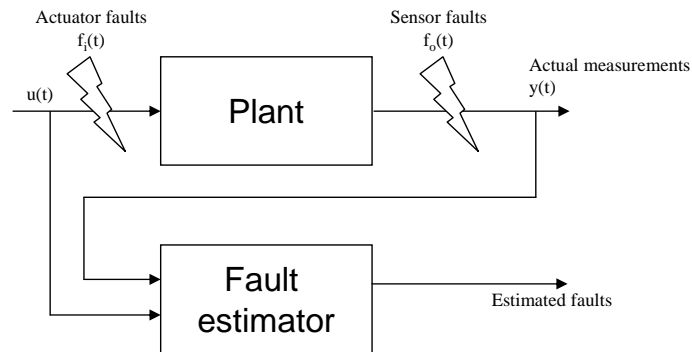


Figure 2.16: fault estimation based FDI

2.6 Comparisons of different FDI designs

In this section, some of the recent popular methods of FDI for flight control will be discussed. The idea is to give some flavour in terms of the concepts, advantages and disadvantages of the methods.

2.6.1 Model-based

Below are discussions on some methods of model-based FDI with aircraft applications in the literature.

Kalman filter

The Kalman filter is probably one of the most well known and used methodologies in industry. Conceived in the 60's by Rudolf Kalman and made famous by its application in the NASA Apollo space program, the Kalman filter has found applications in many engineering systems (e.g. navigation, tracking targets such as aircraft and missiles using radar) as well as other fields such as economics.

A Kalman filter as summarized in [126], is an optimal estimator based on indirect, inaccurate and uncertain observations. It is recursive so that new measurements can be processed as they arrive. If all noise is Gaussian, the Kalman filter minimizes the mean square error of the estimated parameters and therefore is optimal. Since its famous application in the Apollo space program, the Kalman filter has continued to be popular especially in industry for these reasons: (a) Kalman filters provide fairly accurate results in most application due to its optimality and structure. (b) Kalman filters have a recursive form and are suitable for online real time digital processing and it is easy to formulate and implement.

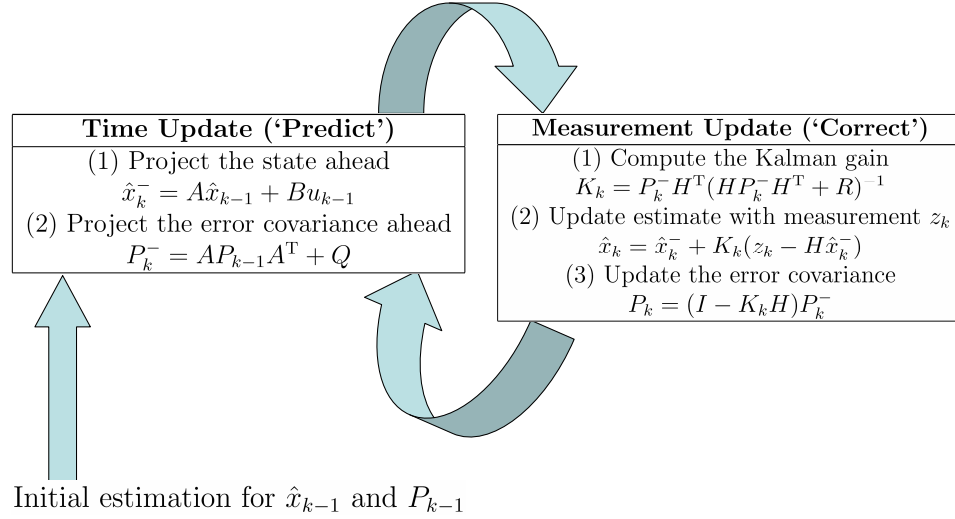


Figure 2.17: Kalman filtering (adapted from [218])

The idea behind the Kalman filter is described in Figure 2.17 [218], where (A, B, H) represents a linear system triple (in discrete time) of the form

$$x_k = Ax_{k-1} + Bu_{k-1} + w \quad (2.10)$$

$$z_k = Hx_k + v \quad (2.11)$$

where the random variables w and v represent process and measurement noise respectively, while Q and R are process noise covariance and measurement noise covariance respectively. The Kalman filter cycle starts with the initial estimate of \hat{x}_{k-1} and the error covariance P_{k-1} . The time update block projects the current state and error covariance estimate ahead in time (this capability of future projection is the attraction in the field of Economics). The measurement update block calculates the Kalman gain K_k using the projected error covariance P_k^- and uses it to adjust the projected state estimate \hat{x}_k using the actual measurement z_k from (2.11) at the current time. The error covariance P_k is also updated using the Kalman gain K_k . Then the cycle continues as the current \hat{x}_k and P_k are used to project the future state estimate ahead of the current time i.e. at time $k + 1$.

Due to its wide usage in industry and its popularity among academics, it is no surprise that Kalman filters are also used for fault diagnosis. Basic Kalman filters act as an observer and therefore can be used to detect faults or failures by creating residual signals from comparing the actual and the estimated outputs. The basic concept of the Kalman filter has been upgraded to enable many applications, such as the Extended Kalman filter for nonlinear systems analysis and nonlinear system FDI [135] and for parameter estimation [82, 87] in which parameters to be estimated are incorporated into the formulation as augmented states. Often this introduces bi-linearities which can be overcome by the use of Extended Kalman Filters.

The Kalman filter can also be composed into a bank of Kalman filters [127, 128] or interacting multiple model Kalman filters (IMM-KF) [174, 238] in order to create a residual which can be used for fault detection. The IMM-KF uses the same IMM as used for controller reconfiguration which was discussed in Section 2.4.2. The Kalman filter also has been combined with the receding horizon (predictive control) method as shown in [131], which has the potential for

fault diagnosis in a system.

Another variant called the two stage Kalman filter [121, 122] has the ability not only to detect and isolate faults, it also has the ability to estimate the effectiveness levels of the actuators [110, 226, 227, 237]. This capability is a bonus for the FTC schemes which depend on the effectiveness level of the actuator for reconfiguration [183, 242].

The early papers by Kalman, on Kalman filtering can be found in [117, 118] whilst the most cited books and references are [21, 150, 192].

\mathcal{H}_∞ based FDI

Using the same principles as for designing \mathcal{H}_∞ controllers, an observer can be designed by applying the \mathcal{H}_∞ filtering technique as a residual based FDI scheme [149]. The idea is to allow the residual to be sensitive only to faults and robust against disturbances, modeling errors and noise [149]. This can be done by selecting the observer gains (using LMI formulations for example) which minimize the \mathcal{H}_∞ norm between the uncertainty and the residual signal.

Fault detection filters using the \mathcal{H}_∞ filtering technique as a residual based FDI is one of the most popular and mature FDI schemes in the literature [100] with many applications in industry including aerospace [148, 149, 198]. Apart from the \mathcal{H}_∞ optimization technique, other frequency domain design approaches for model based FDI e.g. μ synthesis are also discussed in [50] and [77].

Applications of \mathcal{H}_∞ for robust detection of faults can be found in [148, 149]. Both papers are based on an application to the B747 aircraft [147]. In [148] an integrated design of both controller and observer is considered. The integrated design proposed in [149] gives some insight on designing a controller that is not only robust against actuator faults but also considers the robustness properties of the FDI in the design of the controller.

Parameter estimation based FDI

Parameter estimation is quite synonymous with controllers such as nonlinear dynamic inversion and some other nonlinear based controllers. Parameter estimation schemes provide a means of updating the system's parameters online in real time and for controller reconfiguration. Parameter estimation is one of many methodologies which has been applied to aircraft. Aircraft contain many coefficients (especially aerodynamic coefficients) which change, based on the operating conditions. These parameters are typically pre-estimated offline through wind tunnel and flight test before being used for modeling or control design. However, during faults/failures (especially structural damage, such as wing damage or missing fuselage/skin), no accurate pre-estimate is available and therefore these aerodynamic coefficients need to be obtained online.

Examples of parameter estimation methods appear in [82, 87] which uses Kalman filters, and [53, 138] which uses the two step method. In the two step method (TSM), the original state-parameter estimation problem is decomposed into a state estimation one and a subsequent linear parameter identification sub problem [53, 156]. In [156], the main focus is given to the first step of the TSM which is often referred to as 'flight path reconstruction'. Other sources of information on parameter estimation of aircraft systems can be found in [144, 145, 157, 162, 213].

Early papers on FDI using parameter estimation can be found in [104]. In [87], parameter estimation based on an extended Kalman filter is used for FDI in an automotive engine. One of the most recent papers for aircraft FDI is [115]. This paper proposes the use of online parameter estimation provided by the two step method [138] (which identifies and estimates the current aircraft parameters which change due to structural damage). Here, not only are the changes to the aerodynamic coefficients used to detect faults/failures in the system, they are also used as part of the reconfiguration to achieve fault tolerance.

In most parameter estimation methods, in order to get good estimates, it may be necessary to introduce perturbation signals to make sure that all the plant's modes are sufficiently excited [166]. For this reason, most parameter estimation methods work best in the presence of wind and gusts. However, in many practical applications, it is hard and not advisable to apply additional perturbation signals, especially when faults/failures or structural damage has occurred in the system.

Multiple model & Interacting multiple model based FDI

In multiple model based FDI, a bank of models with anticipated faults/failures is created. The output from this bank of models can be compared with the actual plant output to create residual error signals [33] (see Figure 2.9). Here the model with the smallest error is the model which best represents the current faults/failures in the system. Therefore the faults/failures can be detected and isolated and the associated controller that handles the faults/failures is activated. The drawback of multiple model based FDI, is that it is quite tedious (and impossible) to include all possible fault models into the bank of anticipated faults models. Therefore one solution is to use the interacting multiple model. In Interacting multiple model based reconfigurable control (see Figure 2.10), an FDI scheme which provides the estimate of the model weights is required. Researchers such as [238] and [174] have proposed the use of a bank of Kalman filters to calculate these weights in terms of the probability of the individual faults/failures. Other methods such as the one proposed in [90] use convex combinations of predefined limited models. The model weight itself provides the fault detection and some sort of identification especially for partial faults [89]. This method can also be used for detecting structural damage. The scheme suffers from the same drawbacks as the multiple model approach, in particular in terms of computational burden, as some of the model weight estimates require online optimization routines.

Parity equation based FDI

A paragraph in [50] best described the parity based FDI approach '*... The basic idea of the parity relation approach is to provide a proper check of the parity (consistency) of the measurements of the monitored system ... The term 'parity; was first used in connection with digital logic systems and computer software reliability to enable 'parity checks' to be performed for error checking. In the fault diagnosis field, it has similar meaning in the context of providing an indicator for the presence of a fault (or error) in system components ...*'

Redundancies in a system can be used for inconsistency (parity) checking in the measurements

and subsequently for sensor FDI e.g. by using a voting system. This method is slightly different to observer based FDI, as the redundancies (hardware and analytical) are compared directly amongst each other and between the actual system in order to check for inconsistency e.g. by using residuals. No observers are required for parity based FDI.

The following description, also adapted from [50], illustrates the basic concept. Consider a system with redundant sensors where the measurement equations can be represented by

$$y(k) = Cx(k) + f(k) + \xi(k)$$

where $y(k) \in \mathbb{R}^q$ is a measurement vector, $x(k) \in \mathbb{R}^n$ is the state vector, and $f(k)$ is the vector of sensor faults, $\xi(k)$ is a noise vector. If there are more sensors than variables to be measured, then $q > n$ and $\text{rank}(C) = n$. The vector $y(k)$ can be combined into a linearly independent parity equation to generate a parity vector (residual) by choice of a matrix $V \in \mathbb{R}^q$

$$r(k) = Vy(k)$$

where $C \in \mathbb{R}^{1 \times q}$ is chosen such that $VC = 0$. When this condition is satisfied, the parity residual can be written as

$$r(k) = \underbrace{\begin{bmatrix} v_1 & v_2 & \dots & v_q \end{bmatrix}}_V \underbrace{\begin{bmatrix} f_1(k) + \xi_1(k) \\ f_2(k) + \xi_2(k) \\ \dots \\ f_q(k) + \xi_q(k) \end{bmatrix}}_{f(k) + \xi(k)} \quad (2.12)$$

In the above equation, the parity vector only contains faults and uncertainty information, and is independent of the state $x(k)$. In terms of design and implementation, parity equations are simpler than observer-based approaches [105] especially for isolating sensor faults. However, parity equation based FDI provides less design flexibility compared to that of observer based FDI [50].

Examples of parity based FDI for aircraft systems can be found in [105, 116, 167].

2.6.2 Non Model-based

Intelligent FDI

One of the main issues associated with model based designs is the availability and quality of the model. Errors resulting from imperfect or inaccurate models will affect the performance of the fault diagnosis scheme [168, 170]. The use of robust model based methods usually results in a design which is too conservative and insensitive to faults, too complicated or limited to certain classes of uncertainty [168]. Since the late 90's there has been an increase in research on non model-based FDI methods – especially those utilizing artificial intelligence and ‘soft computing’ approaches such as neural networks, and fuzzy logic (see for example [29, 129, 130, 169, 171, 224]).

In [168], a combination of numerical (quantitative) and symbolic (qualitative) knowledge of the system in a single framework has been proposed. The idea was inspired by earlier work which

uses observers for residual generation and fuzzy logic for decision making. The underlying concept is to structure the neural network in a fuzzy logic format which allows residual generation (through the rapid and correct training of the neural network to model the nonlinear dynamics of the system) and evaluation and diagnosis of the fault (through the fuzzy logic). In [130], neuro-fuzzy modeling and diagnosis is considered with the addition of an adaptive threshold in the fault detection scheme, to achieve some level of robustness.

One of the benefits of using the intelligent approach, especially neural networks for FDI is its ability to model any nonlinear function [168]. In terms of FDI, neural networks have ‘black box’ characteristics and therefore the ability to learn from ‘examples’ and ‘training’, requiring little or no a-priori information and knowledge of the system’s structure [168]. Two major drawbacks of conventional neural networks are highlighted in [168]: namely, heuristic knowledge from an experienced expert cannot easily be incorporated, and the ‘black box’ characteristic means that its internal behavior cannot be easily understood. Another drawback of neural networks is the lack of understanding of its internal behavior, causing clearance problems – especially for aircraft systems.

Examples of recent research work can be found in [153, 173, 224] while application examples can be found in [17, 49, 154, 209, 235]. Finally, examples of an intelligent approach for FDI in aircraft systems appear in papers such as [16, 193] and the references therein.

2.6.3 New emerging FDI methods

In recent years, some new and unconventional methods for detecting faults or failures have emerged in the literature especially for applications of aircraft systems. Examples of these methods are LPV based FDI and residual generation using high fidelity models. Details are as follows:

LPV based FDI is motivated by the problem of coping with a wide range of operating conditions. As in the design of FTC controllers (in Section 2.4.3), the FDI is based on linear parameter varying models. It has been claimed that even though there are various FDI approaches for LTI, LTV and bilinear systems, there are only a few available methods for LPV systems [30]. Therefore the focus of the work in [30] was to introduce FDI based schemes for LPV systems using an extension of the approach called the fundamental problem of residual generation. Other recent researchers in [199] and [88] have looked into FDI for LPV systems. FDI based on the LPV system has inherent performance and stability guarantees for the overall operating conditions compared to multiple model or gain schedule based FDI. Even though it seems that LPV based FDI has high potential, especially for aircraft systems, there is still limited source literature.

Some systems are well known, and almost exact nonlinear high fidelity models can be obtained from first principles. Systems such as aircraft are well understood and represents one of the most studied systems with all the aerodynamic coefficients of the aircraft obtained through extensive laboratory, wind tunnel and actual flight tests. High fidelity model such as the B747 [91, 147, 189, 190, 212] and Admire [75] have been created from first principles. The B747 model has even been validated using flight recorder data in the study of the Bijlmermeer incident in Amsterdam [189]. The output states from these high fidelity models can be compared to

the actual measurements and residual signals can be generated. A fault can be declared once the residual signal exceeds some predetermined threshold. This method is explicitly considered in [19]. One of the advantages of using high fidelity models is that it ensures a fast fault detection time and is quite robust. However, only well known systems can be used. It also requires high computational power to enable this to be implemented in real time due to the complexity of the high fidelity nonlinear model.

2.7 Conclusions

This chapter has presented a brief introduction and motivation to the field of FTC and FDI. These include definitions of terms regularly used in FTC and FDI such as faults and failures. This chapter also briefly discussed the type of faults and failures to actuators and sensors and a discussion on redundancy and its importance to FTC and FDI. The different methods of FTC were discussed based on how the fault tolerance is achieved, ranging from robust control to control signal redistribution. Different methods for FDI were also discussed.

Chapter 3

Sliding Mode Control

Sliding mode control was conceived in the USSR in the 50's and spread into the west in the 70's. Sliding mode control (SMC) is a nonlinear type of control and a special case of Variable structure control. It is a robust control methodology. The controller design is quite unique compared to any other controller design methods since the performance of the controller depends on the design of the sliding surface and not the state tracking directly. The idea is to force the trajectory of the states towards the sliding surface and once reached, the states are forced to remain on that surface [67, 210]. Sliding mode control has an inherent robustness property to a certain type of uncertainty which makes SMC a strong candidate for passive FTC when handling actuator faults. The work by Hess & Wells [98] argues that SMC has the potential to become an alternative to reconfigurable control and has the ability to maintain the required performance without requiring FDI. In the previous chapter, Table 2.1, indicates that SMC is categorized as a robust control methodology and has the ability to handle structural damage and actuator faults without reconfiguring.

The objective of this chapter is to introduce the concept of sliding modes and to examine its properties, in order to highlight its benefits in the fields of FTC and FDI. Many of the concepts in this chapter are closely based on the book by Edwards and Spurgeon [67]. An analysis is undertaken based on a simple pendulum example to introduce the concept of SMC.

3.1 Introduction

There are two stages for designing SMC controllers. First to be designed is the sliding surface. Only then the control law can be designed so that sliding is achieved and then, is maintained on the surface. Once sliding occurs, robustness to a certain type of uncertainty is guaranteed and the system behaves as a reduced order motion independent of the control. The performance of the controller depends on the choice of the sliding surface. A typical sliding mode control law consists of linear and nonlinear components. The nonlinear control law drives the states towards the sliding surface and once on the surface, the linear control law becomes more dominant than the nonlinear one. The nonlinear part of the control law determines the robustness property of the controller. This will be discussed in detail in the next sections.

3.1.1 Regular form

In order to explain the concept of sliding mode and its properties conveniently, the system need to be transformed into a suitable canonical form. Consider the following linear time invariant (LTI) system:

$$\dot{x}(t) = Ax(t) + Bu(t) \quad (3.1)$$

where $A \in \mathbb{R}^{n \times n}$, $B \in \mathbb{R}^{n \times m}$ with $1 \leq m \leq n$. Assume $\text{rank}(B) = m$ (i.e. matrix B is full rank) and the pair (A, B) is controllable [67, 210]. Since $\text{rank}(B) = m$, there exists an invertible (and orthogonal) matrix $T_r \in \mathbb{R}^{n \times n}$ such that

$$T_r B = \begin{bmatrix} 0 \\ B_2 \end{bmatrix} \quad (3.2)$$

where $B_2 \in \mathbb{R}^{m \times m}$ and is nonsingular [67]. The orthogonal matrix T_r can be computed using ‘QR’ decomposition: details can be found in [67]. After the coordinate transformation $x(t) \leftrightarrow T_r x(t)$, the states can be partitioned as

$$x(t) = \begin{bmatrix} x_1(t) \\ x_2(t) \end{bmatrix} \quad (3.3)$$

where $x_1(t) \in \mathbb{R}^{n-m}$ and $x_2(t) \in \mathbb{R}^m$, so that (in the new coordinates), Equation (3.1) can be written as

$$\begin{bmatrix} \dot{x}_1(t) \\ \dot{x}_2(t) \end{bmatrix} = \begin{bmatrix} A_{11} & A_{12} \\ A_{21} & A_{22} \end{bmatrix} \begin{bmatrix} x_1(t) \\ x_2(t) \end{bmatrix} + \begin{bmatrix} 0 \\ B_2 \end{bmatrix} u(t) \quad (3.4)$$

This representation is referred to as ‘regular form’ [67]. Define a linear combination of the states to be

$$s(t) = Sx(t) \quad (3.5)$$

where $S \in \mathbb{R}^{m \times n}$ is full rank and let \mathcal{S} be the hyperplane defined by

$$\mathcal{S} = \{x \in \mathbb{R}^n : Sx(t) = 0\} \quad (3.6)$$

Equation (3.5) is called the ‘switching function’ [67]. The matrix S can be partitioned into

$$S = \begin{bmatrix} S_1 & S_2 \end{bmatrix} \quad (3.7)$$

where $S_2 \in \mathbb{R}^{m \times m}$ and $S_1 \in \mathbb{R}^{(n-m) \times m}$. By choice, let S be chosen so that $\det(S_2) \neq 0$. During sliding, $Sx(t) = 0$ for all $t > t_s$, where t_s is the time when sliding commences, therefore

$$Sx(t) = S_1 x_1(t) + S_2 x_2(t) = 0 \Rightarrow x_2(t) = - \underbrace{S_2^{-1} S_1}_{M} x_1(t) \quad (3.8)$$

Equation (3.8) implies that once $x_1(t)$ is known, the states $x_2(t)$ are completely determined. Therefore only the $\dot{x}_1(t)$ (top) partition from (3.4) needs to be considered. Partitioning (3.4) gives

$$\dot{x}_1(t) = A_{11} x_1(t) + A_{12} x_2(t) \quad (3.9)$$

and then substituting for $x_2(t)$ from Equation (3.8) into (3.9) yields the following reduced order system

$$\dot{x}_1(t) = (A_{11} - A_{12}M)x_1(t) \quad (3.10)$$

where $M = S_2^{-1}S_1$. The choice of surface \mathcal{S} from (3.6) clearly affects the dynamics in (3.10) through the design of M in (3.8). *By analogy to the ‘classical’ state feedback theory, it can be seen that this is the same as the problem of finding the state feedback matrix M for the system in (3.9) where the $x_2(t)$ plays the role of the ‘control’ signal.*

The stability (and performance) of the system in (3.10) depends on the fictitious reduced order pair (A_{11}, A_{12}) . Thus the design of M depends on the controllability (or otherwise) of the pair (A_{11}, A_{12}) . Proposition 3.3 in [67] states that the matrix pair (A_{11}, A_{12}) is controllable, if and only if the pair (A, B) is controllable. In other words, if the original system is controllable, M can be designed using a ‘classical’ state feedback method, and once M is obtained, the surface \mathcal{S} can also be obtained.

The overall problem of designing a sliding mode controller can be viewed as one of

- designing the matrix S to achieve the required performance and stable dynamics for the closed-loop sliding mode system;
- designing a control law to ensure that the sliding surface is reached and subsequently maintained

This design procedure is unique and differentiates SMC from other ‘classical’ design methods. Any ‘classical’ state feedback method can be used to compute M , and then the matrix S can be obtained as

$$S = \begin{bmatrix} S_2M & S_2 \end{bmatrix} \quad (3.11)$$

The nonsingular matrix S_2 can be chosen arbitrarily, but for ease of computation, often it is chosen as $S_2 = I_m$. The following ‘classical’ approaches can be adopted to obtain the matrix M (and subsequently S – details are given in [67]).

1. quadratic minimization [60, 211] – this will be discussed later in Section 3.4.1;
2. robust eigenstructure assignment [61];
3. direct eigenstructure assignment [60].

Recent approaches for the design of S which are based on Linear Matrix Inequality (LMI) methods appear in Edwards [65] and Choi [52].

Note that the control law $u(t)$ is not designed to directly specify any desired dynamics for the closed-loop system, but rather to ensure that the sliding surface is reached and motion on \mathcal{S} is maintained. In the sliding mode literature, $u(t)$ is said to be designed in order for the *reachability condition* to be satisfied [67]. The reachability condition specifies that the *trajectory of the system states must always point towards the sliding surface*. For the case of a single input system, this can be expressed as

$$\begin{aligned} \lim_{s \rightarrow 0^+} \dot{s} &< 0 \\ \lim_{s \rightarrow 0^-} \dot{s} &> 0 \end{aligned} \quad (3.12)$$

or more compactly as

$$s\dot{s} < 0 \quad (3.13)$$

near $s(t) = Sx(t) = 0$. This is often referred to as the reachability condition [67, 210]. A more strict reachability condition to ensure that the control law $u(t)$ is designed so that the sliding surface is reached despite the presence of uncertainty and in *finite time* is given by

$$s\dot{s} \leq -\eta|s| \quad (3.14)$$

where η is a positive design scalar. Equation (3.14) is called the ' η -reachability condition' [67].

Remarks:

1. Notice S_2 has no direct effect on the dynamics of the sliding motion. In equations (3.8) and (3.11), S_2 acts only as a scaling factor for the switching function.
2. In the above analysis, during an ideal sliding mode, the closed-loop system which governs the sliding motion given in Equation (3.10) is of a reduced order.
3. For multivariable systems, the natural extension of (3.14) is

$$s^T \dot{s} \leq -\eta \|s\| \quad (3.15)$$

where again η is a positive scalar.

3.1.2 Properties of the sliding mode

The following is a summary of the properties of the system in a sliding mode. Whilst sliding:

1. the system behaves as a reduced order motion which (apparently) does not depend on the control signal $u(t)$;
2. there are $n - m$ states that determine the dynamics of the closed-loop system;
3. the closed-loop sliding motion depends only on the choice of the sliding surface;
4. the poles of the sliding motion are given by the invariant zeros of the system triple (A, B, S) [67, 69].

A fifth property (which is probably the most important for FTC in terms of handling actuator faults) is discussed next. Consider the uncertain linear system

$$\dot{x}(t) = Ax(t) + Bu(t) + D\xi(t, x) \quad (3.16)$$

where $D \in \mathbb{R}^{n \times l}$ is known but the function $\xi : \mathbb{R}_+ \times \mathbb{R}^n \rightarrow \mathbb{R}^l$ is unknown and represents the uncertainty. During sliding,

$$s(t) = \dot{s}(t) = 0 \quad (3.17)$$

which implies

$$\dot{s}(t) = S\dot{x}(t) = S(Ax(t) + Bu(t) + D\xi(t, x)) = 0 \quad (3.18)$$

rearranging the equation with respect to $u(t)$ gives

$$u_{eq}(t) = -(SB)^{-1}(SAx(t) + SD\xi(t, x)) \quad (3.19)$$

The quantity $u_{eq}(t)$ is the so-called ‘*equivalent control*’ and is the theoretical average value the control signal must take to maintain a sliding motion on \mathcal{S} [67]. Substituting $u_{eq}(t)$ into the system in (3.16) yields

$$\dot{x}(t) = (I_n - B(SB)^{-1}S)Ax(t) + \underbrace{(I_n - B(SB)^{-1}S)D}_{P_s}\xi(t, x) \quad (3.20)$$

It is easy to verify that the matrix P_s satisfies

$$SP_s = P_sB = 0 \quad (3.21)$$

If $\mathcal{R}(D) \subset \mathcal{R}(B)$, then write $D = BR$ for some $R \in \mathbb{R}^{m \times l}$. Therefore

$$\dot{x}(t) = P_sAx(t) + P_sBR\xi(t, x) \quad (3.22)$$

and since $P_sB = 0$

$$\dot{x}(t) = P_sAx(t) \quad (3.23)$$

Here it can be seen that during the ideal sliding motion, the uncertainty (the signal $\xi(t, x)$) does not affect the reduced order sliding motion. The condition $\mathcal{R}(D) \subset \mathcal{R}(B)$ means the uncertainty is ‘**matched**’. In [67], ‘... any uncertainty which can be expressed as in Equation (3.16) where $\mathcal{R}(D) \subset \mathcal{R}(B)$, is described as **matched uncertainty**. Any uncertainty which does not lie within the range space of the input distribution matrix is described as *unmatched uncertainty* ...’

3.2 A simple example: pendulum

This section will apply the above methods to a simple pendulum example to give some insight into the design of SMC systems and the characteristics of the sliding motion. Consider a typical pendulum, consisting of a (weightless) shaft and a mass which is driven by a motor (torque) at the point of suspension. The objective is to design a sliding mode controller so that the pendulum will return to its vertically downwards equilibrium point when the pendulum is left to swing from a near-equilibrium initial condition. The closed-loop dynamics are chosen to have a settling time of less than 3 seconds, with no (or small) overshoot on the pendulum angular displacement.

Consider the following pendulum system (taken from page 34 & 171 in [78]):

The dynamic equation is given by:

$$T_c - mgl\sin\theta = I\ddot{\theta} \quad (3.24)$$

where θ represents the angular displacement from the vertical, T_c is the applied torque, m is the

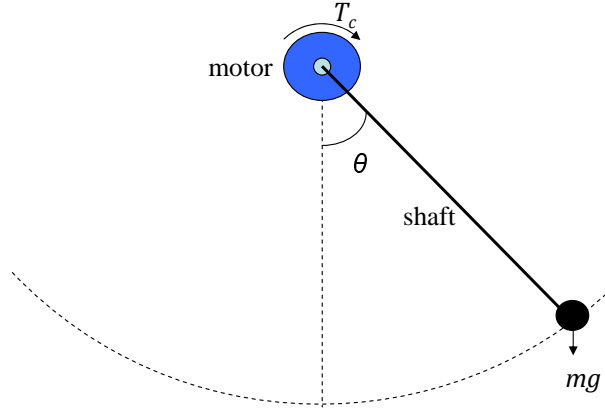


Figure 3.1: Schematic of a pendulum

mass, g is gravitational acceleration, l is the length of the shaft. Here it is assumed that $l = 1\text{m}$, $m = 0.2\text{kg}$, $g = 9.82\text{m/s}^2$. Linearizing Equation (3.24) about the vertically down equilibrium position yields the following state space model:

$$\begin{bmatrix} \dot{x}_1(t) \\ \dot{x}_2(t) \end{bmatrix} = \begin{bmatrix} 0 & 1 \\ -9.82 & 0 \end{bmatrix} \begin{bmatrix} x_1(t) \\ x_2(t) \end{bmatrix} + \begin{bmatrix} 0 \\ 5 \end{bmatrix} u(t) \quad (3.25)$$

where the states $(x_1(t), x_2(t))$ represent $(\theta, \dot{\theta})$ which are angular displacement and angular velocity respectively. Note that the B matrix has only one nonzero contribution in the bottom row of the matrix and is in regular form as in (3.4). For other systems, state similarity transformations using an orthogonal transformation matrix T_r as in (3.2) can be employed to achieve this form [67].

The first step is to design the sliding surface matrix S . During an ideal sliding motion, $s(t) = Sx(t) = 0$ and from (3.8)

$$x_2(t) = -Mx_1(t) \quad (3.26)$$

where $x_1(t), x_2(t)$ and M (as defined in (3.11)) are scalars. Substituting (3.26) into the top of Equation (3.25), it follows that the reduced order sliding motion is given by

$$\dot{x}_1(t) = x_2(t) = -Mx_1(t) \quad (3.27)$$

and the solution is $x_1(t) = x_1(t_s)e^{-Mt}$ where t_s is the time at which sliding occurs. If $M = 2$, this gives a design with a settling time less than 3 sec as required. From (3.11), choosing $S_2 = 1$ gives

$$S = \begin{bmatrix} 2 & 1 \end{bmatrix} \quad (3.28)$$

Now a control law $u(t)$ needs to be developed to satisfies the reachability condition.

Consider the following control law

$$u(t) = -(SB)^{-1}(SAx(t) + \eta \text{sgn}(s)) = \underbrace{-(SB)^{-1}SAx(t)}_{u_{eq}(t)} - (SB)^{-1}\eta \text{sgn}(s) \quad (3.29)$$

where η is a positive scalar and $\text{sgn}(\cdot)$ represents the signum function. It follows that

$$\dot{s}(t) = S\dot{x}(t) = S(Ax(t) + Bu(t)) \quad (3.30)$$

Substituting (3.29) into the above yields

$$\dot{s}(t) = SAx(t) - (SB)(SB)^{-1}(SAx(t) + \eta \text{sgn}(s)) \quad (3.31)$$

$$= -\eta \text{sgn}(s) \quad (3.32)$$

Consequently

$$s\dot{s} = s(-\eta \text{sgn}(s)) = -\eta |s|$$

Therefore the chosen control law $u(t)$ satisfies the η -reachability condition in (3.15). Using the matrix S obtained from the design in (3.28), and letting $\eta = 1$ the following control law is obtained from (3.29)

$$u(t) = \begin{bmatrix} 1.9640 & -0.4 \end{bmatrix} x - 0.2 \text{sgn}(s) \quad (3.33)$$

Remark: The term $u_{eq}(t) = -(SB)^{-1}SAx(t)$ is called the nominal ‘*equivalent control*’. It can be viewed as the control law required to maintain the ideal sliding motion. However, it does not induce a sliding motion – the switching term $\text{sgn}(s)$ is needed to induce the sliding motion.

3.2.1 Simulations and results

The following simulations were done with an initial condition of 1deg for the initial pendulum deflection angle θ . Figure 3.2 shows the results for the simulation and includes the states (angular velocity and deflection angle), the phase portrait, the input torque and the switching function $s(t)$. The deflection angle shows that the design requirement of a settling time less than 3 sec with little or no overshoot is met. Since this particular example is a 2nd order system, its possible to do a phase portrait [187] analysis. The phase portrait shows the stability of the system since the trajectories end up at the origin. Since in this example $A_{11} = 0$ and $A_{12} = 1$, the reduced order sliding motion is governed by (3.27) and therefore the sliding surface design problem corresponds to the problem of finding a suitable gradient in the phase portrait. Here the sliding surface is indicated by the line with gradient $M = -2$.

Define

$$\mathcal{L} := \{(x_1, x_2) : x_2 = -2x_1\} \quad (3.34)$$

to represent the sliding surface (line). Edwards and Spurgeon [67] best describe what happens during the sliding motion as: ‘...high frequency switching between the two different control structures will take place as the system trajectories repeatedly cross the line \mathcal{L} . This high frequency motion (associated with $\text{sgn}(s) = 1$ and $\text{sgn}(s) = -1$) is described as chattering. If infinite frequency switching were possible, the motion would be confined to the line \mathcal{L} . The motion when confined to the line \mathcal{L} behaves like a first order decay and the trajectories will slide along the line \mathcal{L} to the origin. Such behaviour is describe as an ideal sliding mode or an ideal sliding motion and the line \mathcal{L} is termed the sliding surface...’.

It is interesting to point out that the trajectory of the phase portrait can be classified into

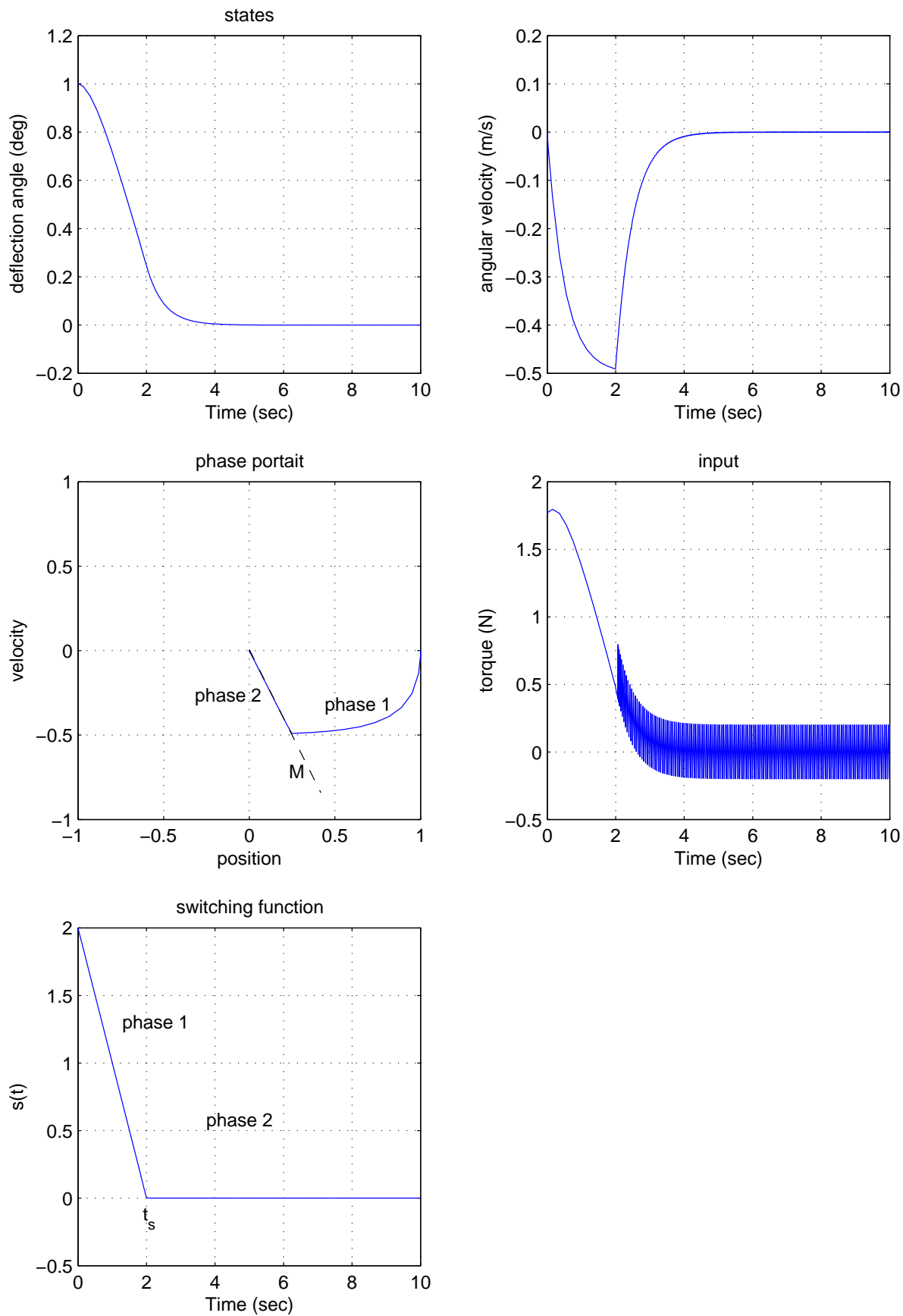


Figure 3.2: simulation results for the pendulum

Phase 1 and 2. Phase 1 starts from the initial conditions. Due to the reachability conditions being met by the control law $u(t)$, sliding is induced and the trajectories move towards the sliding surface. Once the sliding surface is reached, Phase 2 begins and the trajectory ‘slides’ along the surface towards the origin.

Even though the phase portrait shows the ‘sliding’ trajectory moving towards the origin, it does not, however, give any indication at which time sliding occurs (t_s). This information is available from the switching function plot. The plot shows that the sliding surface is reached in 2 seconds.

Note that the systems closed-loop poles $\lambda(A - B(SB)^{-1}SA)$ are $\{0, -2\}$. The pole at -2 is obtained from the choice of M and the other pole is zero. Generally, for an n th order system with m inputs, the reduced order system during sliding has $n - m$ states and so will have $n - m$ nonzero closed-loop poles. The remaining m poles lie at the origin.

The input plot shows that the control action is highly discontinuous. This control law is not desirable for most systems due to the wear and tear that would occur on the mechanical components and to the actuators. It is therefore desirable for this discontinuity to be reduced or smoothed. A more practical control law design is introduced in the next section.

3.2.2 A practical control law

Consider the following control law:

$$u(t) = -(SB)^{-1}(SA - \Phi S)x(t) - \rho(SB)^{-1} \frac{s}{(|s| + \delta)} \quad (3.35)$$

where Φ is a negative scalar. The quantity δ is a small positive scalar and the positive scalar ρ depends on the magnitude of the uncertainty. Note the difference between the controller in Equation (3.35) and (3.29) is the introduction of the Φ term and the approximation of the $sgn(s)$ term.

Using the same design of S as in the example in Section 3.2 and choose $\Phi = -6$. Let the design parameter $\rho = 1$ and $\delta = 0.001$. Therefore, the control law in Equation (3.35) becomes

$$u = \begin{bmatrix} -0.4360 & -1.6 \end{bmatrix} x - 0.2 \frac{s}{(|s| + \delta)}$$

Figure 3.3 shows the results of the simulation. Since the choice of S is from the previous design, the objective of having a setting time of less than 3 second with little or no overshoot is also met with this controller. The phase portrait looks similar to the one in Figure 3.2. The difference is mainly in the input and switching function plots. The input plot shows no chattering, or high frequency switching, and a smooth signal is obtained. This is because of the approximation of $sgn(s)$ by the continuous term given by $\frac{s}{(|s| + \delta)}$ (see Figure 3.4). The δ term is chosen as a compromise between an ideal sliding motion and chattering. A smaller δ will give an ideal sliding motion but with high chattering; larger δ will give less chattering but a trajectory close to the sliding surface rather than remaining on it. Figure 3.3 also shows that the extra degree of freedom Φ , has been used to determine how fast the sliding surface is attained. In Section 3.2 $\Phi = 0$, now $\Phi = -6$ has been chosen, and the difference between the previous controller

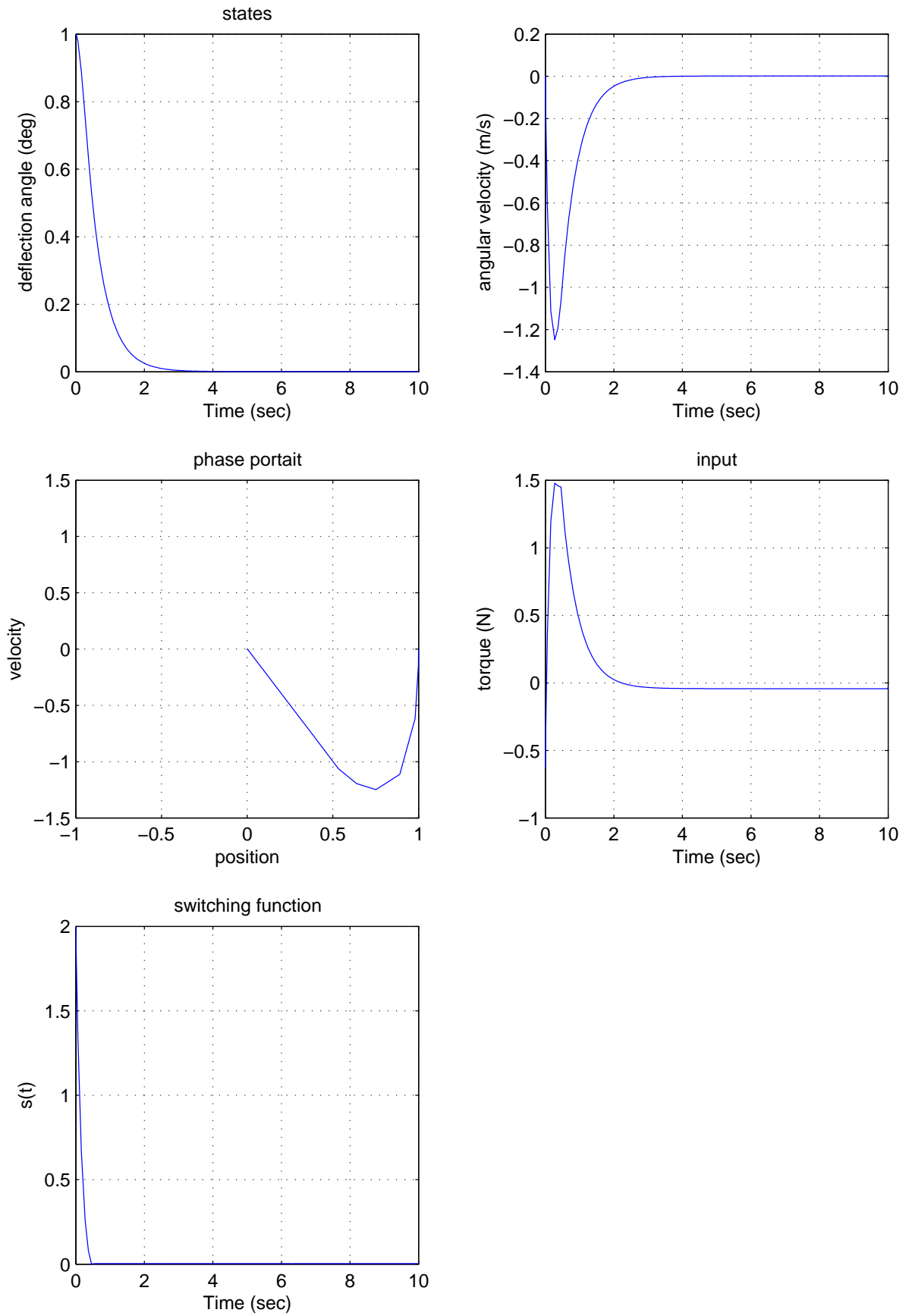


Figure 3.3: pendulum practical controller: simulation results

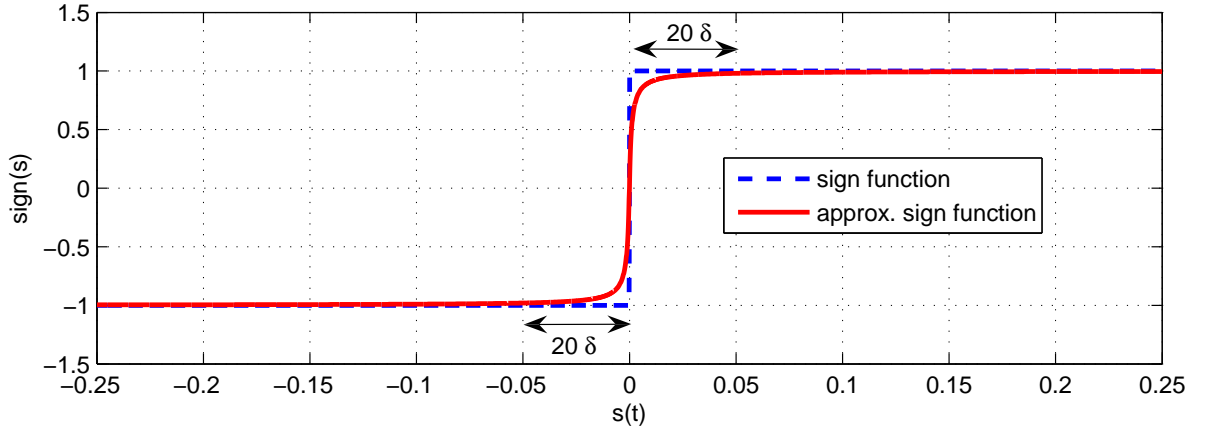


Figure 3.4: An approximation of the signum function [67]

design and the practical controller design can be seen in Figure 3.3. Sliding is now obtained in 0.46 secs whilst the previous design took almost 2 secs.

3.3 Unit vector approach

In the previous section, a practical design of controller for a pendulum system was introduced. The pendulum system represented a single input system. The most convenient control structure for multivariable systems from a sliding mode perspective is the ‘unit vector’ control structure by Ryan and Corless [179]. This method will form the basis for the controller designs in this thesis.

Consider a system with a matched uncertainty

$$\dot{x}(t) = Ax(t) + Bu(t) + f_m(t, x, u) \quad (3.36)$$

where $f_m(t, x, u) : \mathbb{R} \times \mathbb{R}^n \times \mathbb{R}^m \rightarrow \mathcal{R}(B)$ is unknown but bounded and satisfies

$$\|f_m(t, x, u)\| \leq k\|u(t)\| + \alpha(t, x) \quad (3.37)$$

As in Section 3.1.1, there exists an orthogonal transformation so that the system above can be transformed into the following ‘regular form’:

$$\begin{bmatrix} \dot{x}_1(t) \\ \dot{x}_2(t) \end{bmatrix} = \begin{bmatrix} A_{11} & A_{12} \\ A_{21} & A_{22} \end{bmatrix} \begin{bmatrix} x_1(t) \\ x_2(t) \end{bmatrix} + \begin{bmatrix} 0 \\ B_2 \end{bmatrix} u(t) + \begin{bmatrix} 0 \\ I \end{bmatrix} \bar{f}_m(t, x, u) \quad (3.38)$$

where \bar{f}_m is a projection of f_m in the regular form coordinates. Therefore

$$\|\bar{f}_m(t, x, u)\| \leq k\|u(t)\| + \alpha(t, x) \quad (3.39)$$

since the Euclidean norm of $f_m(t, x, u)$ is preserved by the orthogonal transformation.

In regular form the switching function $s(t)$ can be written as:

$$s(t) = \begin{bmatrix} S_1 & S_2 \end{bmatrix} \begin{bmatrix} x_1(t) \\ x_2(t) \end{bmatrix} = S_2 \begin{bmatrix} M & I_m \end{bmatrix} \begin{bmatrix} x_1(t) \\ x_2(t) \end{bmatrix} \quad (3.40)$$

The choice of $S_2 \in \mathbb{R}^{m \times m}$ is arbitrary but here it is chosen so that

$$S_2 B_2 = \Lambda \quad (3.41)$$

where Λ is a nonsingular diagonal matrix. Define another coordinate transformation so that the system can be partitioned into:

$$\begin{bmatrix} x_1(t) \\ s(t) \end{bmatrix} = T_s \begin{bmatrix} x_1(t) \\ x_2(t) \end{bmatrix} \quad (3.42)$$

where the transformation matrix T_s is given by:

$$T_s = \begin{bmatrix} I & 0 \\ S_1 & S_2 \end{bmatrix} \quad (3.43)$$

Then the system in (3.38) can be written as:

$$\begin{bmatrix} \dot{x}_1(t) \\ \dot{s}(t) \end{bmatrix} = \begin{bmatrix} \bar{A}_{11} & A_{12} \\ \bar{A}_{21} & \bar{A}_{22} \end{bmatrix} \begin{bmatrix} x_1(t) \\ s(t) \end{bmatrix} + \begin{bmatrix} 0 \\ \Lambda \end{bmatrix} u(t) + \begin{bmatrix} 0 \\ S_2 \end{bmatrix} \bar{f}_m(t, x, u) \quad (3.44)$$

where $\bar{A}_{11} = A_{11} - A_{12}M$, $\bar{A}_{21} = M\bar{A}_{11} + A_{21} - A_{22}M$ and $\bar{A}_{22} = MA_{12} + A_{22}$. The Ryan & Corless [179] control law comprises linear and nonlinear components given by

$$u(t) = u_l(t) + u_n(t) \quad (3.45)$$

The linear component is defined as

$$u_l(t) = \Lambda^{-1}(-S_2\bar{A}_{21}x_1(t) - (S_2\bar{A}_{22}S_2^{-1} - \Phi)s(t)) \quad (3.46)$$

where $\Phi \in \mathbb{R}^{m \times m}$ is any stable design matrix and the nonlinear component is defined as

$$u_n = -\rho(t, x)\Lambda^{-1} \frac{P_2 s}{\|P_2 s\|} \quad (3.47)$$

where $P_2 \in \mathbb{R}^{m \times m}$ is a symmetric positive definite matrix satisfying the Lyapunov equation

$$P_2\Phi + \Phi^T P_2 = -I_m \quad (3.48)$$

The scalar function ρ depends on the magnitude of uncertainty and is any function satisfying:

$$\rho(t, x) \geq \frac{\|S_2\|(k\|u_l\| + \alpha(t, x)) + \eta}{(1 - k\|B_2^{-1}\|)} \quad (3.49)$$

where η is a positive scalar and k is a known constant with $k < \sqrt{\lambda_{\min}(B^T B)}$. In other words ρ must be greater than the magnitude of the uncertainty in Equation (3.37).

Remark: In the above analysis, the uncertainty is assumed to be matched. The inclusion of unmatched uncertainty to the above analysis can be found in [67].

3.3.1 Analysis of stability for the closed-loop system

The problem of determining the stability of the closed-loop system under the influence of matched uncertainty becomes the problem of ensuring that sliding occurs despite the presence of uncertainty. This is due to the fact that when the controller induces an ideal sliding motion, the closed-loop system is stable by design. This section will show that the unit vector controller from (3.45) will still induce sliding in the presence of uncertainty.

Substituting the control law in (3.45) into the partitioned system (3.44) gives the following:

$$\dot{x}_1(t) = \bar{A}_{11}x_1(t) + A_{12}S_2^{-1}s(t) \quad (3.50)$$

$$\dot{s}(t) = \Phi s(t) - \rho(t, x) \frac{P_2 s}{\|P_2 s\|} + S_2 \bar{f}_m(t, x, u) \quad (3.51)$$

Consider a Lyapunov function $V(s) = s^T P_2 s$. Differentiating the Lyapunov function yields:

$$\begin{aligned} \dot{V} &= \dot{s}^T P_2 s + s^T P_2 \dot{s} \\ &= (\Phi s - \rho \frac{P_2 s}{\|P_2 s\|} + S_2 \bar{f}_m)^T P_2 s + s^T P_2 (\Phi s - \rho \frac{P_2 s}{\|P_2 s\|} + S_2 \bar{f}_m) \\ &= s^T (\Phi^T P_2 + P_2 \Phi) s - 2\rho \frac{1}{\|P_2 s\|} (s^T P_2 P_2 s) + 2s^T P_2 S_2 \bar{f}_m \\ &= -s^T s - 2\rho \|P_2 s\| + 2s^T P_2 S_2 \bar{f}_m \end{aligned} \quad (3.52)$$

since $s^T P_2 P_2 s = \|P_2 s\|^2$ and $\Phi^T P_2 + P_2 \Phi = -I$. Since $\|s^T P_2 S_2 \bar{f}_m\| < \|P_2 s\| \|S_2\| \|\bar{f}_m\|$ from the Cauchy-Schwarz inequality

$$\dot{V} \leq -\|s\|^2 - 2\|P_2 s\|(\rho - \|S_2\| \|\bar{f}_m\|) \quad (3.53)$$

The idea is to represent ρ in (3.53) in terms of the uncertainty \bar{f}_m using the definition of ρ given in (3.49). From (3.45) and (3.47) and using the triangle inequality property of norms

$$\|u(t)\| \leq \|u_l(t)\| + \|u_n(t)\| \leq \|u_l(t)\| + \rho \|\Lambda^{-1}\| \quad (3.54)$$

Equation (3.49) can be written as

$$\rho(t, x)(1 - k\|B_2^{-1}\|) \geq \|S_2\|(k\|u_l\| + \alpha(t, x)) + \eta \quad (3.55)$$

Rearranging this equation yields

$$\begin{aligned} \rho(t, x) &\geq \|S_2\|(k\|u_l\| + \alpha(t, x)) + \eta + \rho k\|B_2^{-1}\| \\ &\geq \|S_2\|(k\|u_l\| + \rho k\|\Lambda^{-1}\| + \alpha(t, x)) + \eta \end{aligned} \quad (3.56)$$

Using (3.54) and (3.37), the above can be written as

$$\rho(t, x) \geq \|S_2\|(k\|u\| + \alpha(t, x)) + \eta \geq \|S_2\|\bar{f}_m + \eta \quad (3.57)$$

Substitute (3.57) into (3.53) yields

$$\dot{V} \leq -\|s\|^2 - 2\|P_2s\| (\|S_2\|\|\bar{f}_m\| + \eta) + 2\|P_2s\| \|S_2\|\bar{f}_m \quad (3.58)$$

$$\leq -\|s\|^2 - 2\eta\|P_2s\| \quad (3.59)$$

The above shows that the controller in the form (3.45), induces ideal sliding in the presence of matched uncertainty.

3.3.2 The unit vector pseudo sliding term

In achieving this ideal sliding motion, discontinuous infinite frequency switching or chattering occurs. This is undesirable for some practical systems, especially for mechanical systems with actuators prone to wear and tear. It is therefore required that this discontinuity is ‘smoothed’ and an approximation to ideal sliding (sometimes called ‘*pseudo sliding*’) is achieved. Here the states of the system are only required to stay close to the sliding surface instead of on it. However, the total robustness property (invariance) to the matched uncertainty is no longer guaranteed. On the other hand, if the approximation is close enough to the actual discontinuous term, a good approximation to ideal sliding can still be achieved. Therefore, there is a trade off between robustness and reducing the chattering effect.

There are several methods used to achieve ‘pseudo sliding’; but the one that will be used in this thesis is based on a method called ‘*fractional approximation*’ (or sigmoidal approximation) [67]. This is similar to the one in Figure 3.4. Other approximation methods are discussed in [67], including the boundary layer approach and power law interpolation. The nonlinear term of control law in Equation (3.35) is given by

$$u_n = -\rho(SB)^{-1} \left(\frac{P_2s}{\|P_2s\| + \delta} \right) \quad (3.60)$$

where $\delta > 0$ is a small positive scalar which determines the quality of the approximation. A very small δ will give a better approximation to the actual discontinuous function $\text{sgn}(s)$; but to reduce chattering, a larger δ is needed. A small δ will ensure the state’s trajectory will remain close to the sliding surface, but the control action may have chattering. A larger δ will ensure that the chattering effect is reduced but the trajectory usually evolves further away from the sliding surface.

Other approaches to mitigate the chattering problem apart from the ‘pseudo sliding’ have been proposed; see for example [25, 54, 79, 234] which uses supertwisting or higher order sliding mode control.

3.4 Design of sliding surface (hyperplane)

So far the above sections have discussed the design of the control law. In the following section, the design of the switching surface, namely the matrix S in the switching function $s(t) = Sx(t)$, is discussed. The next sections describe a design method for S from Chapter 4 in [67]. This is based on the modified classical LQR design problem. This sliding surface design approach will

be used extensively in this thesis.

3.4.1 Quadratic Minimization

Consider a linear system given by

$$\dot{x}(t) = Ax(t) + Bu(t) \quad (3.61)$$

with an ‘error’ signal

$$w(t) = Cx(t) + Du(t) \quad (3.62)$$

The linear quadratic regulator (LQR) problem is to find the control input $u(t)$ which minimizes the ‘energy’ cost function

$$J = \int_0^{\infty} (w^T w) dt \quad (3.63)$$

In other words, finding the minimum (optimum) control input (effort) to produce the desired performance. Arguing as in Boyd *et al* [35], assume that $D^T D$ is invertible and $D^T C = 0$, then, substituting Equation (3.62) into (3.63) yields:

$$J = \int_0^{\infty} (x^T C^T C x + u^T D^T D u) dt \quad (3.64)$$

Let $C^T C = Q$ and $D^T D = R$, then

$$J = \int_0^{\infty} (x^T Q x + u^T R u) dt \quad (3.65)$$

It is well known the optimal $u(t)$ is given by $u(t) = Kx(t)$ where

$$K = -R^{-1} B^T P \quad (3.66)$$

and P is the unique s.p.d. matrix which satisfies

$$A^T P + P A - P B R^{-1} B^T P + Q = 0 \quad (3.67)$$

In designing the sliding surface, the control input is not considered explicitly [211]. The minimization problem for sliding mode control becomes one of minimizing

$$J = \frac{1}{2} \int_{t_s}^{\infty} (x^T Q x) dt \quad (3.68)$$

where t_s indicates the start of sliding. Consider a coordinate transformation $z(t) = T_r x(t)$ so that the system in (3.61) is in regular form as in Section 3.1.1. In regular form, the matrix Q can be written as:

$$T_r Q T_r^T = \begin{bmatrix} Q_{11} & Q_{12} \\ Q_{21} & Q_{22} \end{bmatrix} \quad (3.69)$$

where $Q_{21} = Q_{12}^T$. Therefore, in regular form, the LQR problem can be written as:

$$J = \frac{1}{2} \int_{t_s}^{\infty} (z_1^T Q_{11} z_1 + 2z_1^T Q_{12} z_2 + z_2^T Q_{22} z_2) dt \quad (3.70)$$

Equation (3.70) does not have the form of the state feedback LQR in Equation (3.65). Utkin & Young [211] proposed factorizing the last two term of Equation (3.70) yielding

$$2z_1^T Q_{12} z_2 + z_2^T Q_{22} z_2 = (z_2 + Q_{22}^{-1} Q_{21} z_1)^T Q_{22} (z_2 + Q_{22}^{-1} Q_{21} z_1) - z_1^T (Q_{21}^T Q_{22} Q_{21}) z_1 \quad (3.71)$$

Using (3.71), Equation (3.70) can be written as

$$J = \frac{1}{2} \int_{t_s}^{\infty} (z_1^T (Q_{11} - Q_{12} Q_{21}^T Q_{22}^{-1} Q_{21}) z_1 + (z_2 + Q_{22}^{-1} Q_{21} z_1)^T Q_{22} (z_2 + Q_{22}^{-1} Q_{21} z_1)) dt \quad (3.72)$$

Define

$$\hat{Q} = Q_{11} - Q_{12} Q_{21}^T Q_{22}^{-1} Q_{21} \quad (3.73)$$

and a pseudo control as

$$v = z_2 + Q_{22}^{-1} Q_{21} z_1 \quad (3.74)$$

Then Equation (3.72) can be written as

$$J = \frac{1}{2} \int_{t_s}^{\infty} (z_1^T \hat{Q} z_1 + v^T Q_{22} v) dt \quad (3.75)$$

This minimization is associated with the dynamical system in Equation (3.9) which is given by:

$$\dot{z}_1 = A_{11} z_1 + A_{12} z_2 \quad (3.76)$$

Eliminating the z_2 term in (3.76) by using Equation (3.74), the system in (3.76) becomes

$$\dot{z}_1 = \hat{A}_{11} z_1 + A_{12} v \quad (3.77)$$

where $\hat{A} = A_{11} - A_{12} Q_{22}^{-1} Q_{21}^T$. The ‘optimal control law’ is

$$v = -(Q_{22}^{-1} A_{12}^T P_1) z_1 \quad (3.78)$$

where P_1 satisfies

$$\hat{A}^T P_1 + P_1 \hat{A} - P_1 A_{12} Q_{22}^{-1} A_{12}^T P_1 + \hat{Q} = 0 \quad (3.79)$$

Recall that during sliding, $s(t) = 0$ and therefore

$$z_2 = -M z_1 \quad (3.80)$$

the manipulations resulting from solving for z_2 from Equation (3.74) and (3.78) yield

$$z_2 = -Q_{22}^{-1} (A_{12}^T P_1 + Q_{21}) z_1 \quad (3.81)$$

and therefore the matrix M is defined as

$$M = Q_{22}^{-1}(A_{12}^T P_1 + Q_{21}) \quad (3.82)$$

Once the matrix M has been obtained, matrix S can be calculated using (3.11) where S_2 can be arbitrarily chosen. In this thesis S_2 will typically be designed so that $S_2 B_2 = I_m$.

3.5 Design of controller for tracking requirement

The control law discussions in this chapter has so far only considered state regulation i.e. the control law has been designed so that the system trajectory returns to the equilibrium point once perturbed. In this section, a tracking requirement will be discussed. In [67], two methods are discussed in detail; tracking using integral action and a model reference approach.

3.5.1 Integral action approach

Consider a nominal linear system that is in regular form given by:

$$\dot{x}(t) = Ax(t) + Bu(t) \quad (3.83)$$

where $A \in \mathbb{R}^{n \times n}$ and $B \in \mathbb{R}^{n \times m}$. In addition, identify some controlled outputs as

$$y(t) = Cx(t) \quad (3.84)$$

where $y(t) \in \mathbb{R}^m$. Consider additional states $x_r(t) \in \mathbb{R}^m$ defined as:

$$\dot{x}_r(t) = r(t) - Cx(t) \quad (3.85)$$

where $r(t)$ is the ‘filtered’ reference signal given by

$$\dot{r}(t) = \Gamma(r(t) - R(t)) \quad (3.86)$$

where $\Gamma \in \mathbb{R}^{m \times m}$ is a stable design matrix and R is a constant demand vector. The signal R represents step changes in demand (a piecewise constant demand) which is not differentiable at certain time instants. Equation (3.86) represents a low pass filtered version of the signal R and so (3.86) can be viewed in the classical terms as a pre-filtering of the demand signal which removes ‘derivative kick’. It is argued in Section 7.4.2 in [67] that Γ represents a useful design parameter for tailoring the closed-loop response to demand changes. The analysis of the augmented tracking system is described below.

Augment the nominal system with the new additional states x_r to obtain

$$\tilde{x} = \begin{bmatrix} x_r \\ x \end{bmatrix} \quad (3.87)$$

Now the augmented system can be written as

$$\begin{bmatrix} \dot{x}_r \\ \dot{x} \end{bmatrix} = \begin{bmatrix} 0 & -C \\ 0 & A \end{bmatrix} \begin{bmatrix} x_r \\ r \end{bmatrix} + \begin{bmatrix} 0 \\ B \end{bmatrix} u + \begin{bmatrix} I_p \\ 0 \end{bmatrix} r \quad (3.88)$$

Since the pair (A, B) is assumed to be in regular form, the state \tilde{x} can be partitioned as

$$\tilde{x} = \begin{bmatrix} \tilde{x}_1 \\ \tilde{x}_2 \end{bmatrix} \quad (3.89)$$

where $\tilde{x}_1 \in \mathbb{R}^n$ and $\tilde{x}_2 \in \mathbb{R}^m$. In the new partition, the system can be written as:

$$\begin{bmatrix} \dot{x}_1 \\ \dot{x}_2 \end{bmatrix} = \begin{bmatrix} \tilde{A}_{11} & \tilde{A}_{12} \\ \tilde{A}_{21} & \tilde{A}_{22} \end{bmatrix} \begin{bmatrix} x_1 \\ x_2 \end{bmatrix} + \begin{bmatrix} 0 \\ B_2 \end{bmatrix} u + \begin{bmatrix} B_r \\ 0 \end{bmatrix} r \quad (3.90)$$

where the augmented and partitioned system matrix is given by

$$\tilde{A} = \begin{bmatrix} \tilde{A}_{11} & \tilde{A}_{12} \\ \tilde{A}_{21} & \tilde{A}_{22} \end{bmatrix} \cong \left[\begin{array}{cc|c} 0 & -C_1 & -C_2 \\ 0 & A_{11} & A_{12} \\ \hline 0 & A_{21} & A_{22} \end{array} \right] \quad (3.91)$$

and

$$B_r = \begin{bmatrix} I_m \\ 0 \end{bmatrix} \quad (3.92)$$

In expression (3.91), the matrix $[C_1 \ C_2]$ is a partition of the output distribution matrix C . The objective is to design a sliding surface of the form

$$\mathcal{S} = \{\tilde{x} \in \mathbb{R}^{n+m} : S\tilde{x} = 0\} \quad (3.93)$$

where $S \in \mathbb{R}^{m \times (n+m)}$ is designed to meet performance specifications for the closed-loop reduced order system. The matrix S can be partitioned as

$$S = \begin{bmatrix} \xrightarrow{n} & \xrightarrow{m} \\ S_1 & S_2 \end{bmatrix} \quad (3.94)$$

and assume that $\Lambda = S_2 B_2$ is a nonsingular diagonal design matrix. During an ideal sliding motion the reduced order system is governed by the top partition of Equation (3.90), which is

$$\dot{\tilde{x}}_1 = \tilde{A}_{11}\tilde{x}_1 + \tilde{A}_{12}\tilde{x}_2 + B_r r \quad (3.95)$$

During the sliding motion $s(t) = 0$, and therefore

$$S_1\tilde{x}_1(t) + S_2\tilde{x}_2(t) = 0 \quad (3.96)$$

and

$$\tilde{x}_2(t) = -M\tilde{x}_1 \quad (3.97)$$

where $M = S_2^{-1}S_1$. Substituting (3.97) into the top partition of (3.90) yields the following:

$$\dot{\tilde{x}}_1 = (\tilde{A}_{11} - \tilde{A}_{12}M)\tilde{x}_1 + B_r r \quad (3.98)$$

The design of the hyperplane is determined by the controllability of the pair $(\tilde{A}_{11}, \tilde{A}_{12})$. Edwards & Spurgeon in [67] prove that if the system triple (A, B, C) is completely controllable and has no invariant zeros at the origin, then the pair $(\tilde{A}_{11}, \tilde{A}_{12})$ is completely controllable. Details can be found in [67].

If the above condition is satisfied, then the design methods described in Section 3.4.1 can be used for the augmented system above. The unit vector approach described earlier will be applied to the augmented system above. First transform system using the coordinate change associated with the matrix

$$T_s = \begin{bmatrix} I_n & 0 \\ S_1 & S_2 \end{bmatrix} \quad (3.99)$$

The augmented and partitioned states become

$$\begin{bmatrix} \tilde{x}_1 \\ s \end{bmatrix} = T_s \begin{bmatrix} \tilde{x}_1 \\ \tilde{x}_2 \end{bmatrix} \quad (3.100)$$

and the augmented system can be written as

$$\begin{bmatrix} \dot{\tilde{x}}_1 \\ \dot{s} \end{bmatrix} = \begin{bmatrix} \bar{A}_{11} & \bar{A}_{12} \\ S_2 \bar{A}_{21} & S_2 \bar{A}_{22} S_2^{-1} \end{bmatrix} \begin{bmatrix} \tilde{x}_1 \\ s \end{bmatrix} + \begin{bmatrix} 0 \\ \Lambda \end{bmatrix} u + \begin{bmatrix} B_r \\ S_1 B_r \end{bmatrix} r \quad (3.101)$$

where $\bar{A}_{11} = \tilde{A}_{11} - \tilde{A}_{12}M$, $\bar{A}_{21} = M\tilde{A}_{11} + \tilde{A}_{21} - A_{22}M$, $\bar{A}_{22} = M\tilde{A}_{12} + A_{22}$, and $\bar{A}_{12} = \tilde{A}_{12}S_2^{-1}$. As in Section 3.3, the proposed controller will have the form $u(t) = u_l(t) + u_n(t)$ where

$$u_l = \Lambda^{-1}(-S_2 \bar{A}_{21} \tilde{x}_1 + (\Phi - S_2 \bar{A}_{22} S_2^{-1})s - S_1 B_r r) \quad (3.102)$$

and

$$u_n = \begin{cases} -\rho \Lambda^{-1} \frac{\bar{P}_2 s}{\|\bar{P}_2 s\|} & \text{if } s \neq 0 \\ 0 & \text{otherwise} \end{cases} \quad (3.103)$$

where \bar{P}_2 is a s.p.d. matrix satisfying

$$\bar{P}_2 \Phi + \Phi^T \bar{P}_2 = -I \quad (3.104)$$

and $\Phi \in \mathbb{R}^{m \times m}$ is any stable design matrix. Edwards & Spurgeon [67] argue in the original coordinates, Equation (3.102) can be written as

$$u_l = L\tilde{x} + L_r r \quad (3.105)$$

where

$$L = -\Lambda^{-1}(S\tilde{A} - \Phi S) \quad (3.106)$$

$$L_r = -\Lambda^{-1}S_1 B_r \quad (3.107)$$

In the next section, a model reference approach for tracking control is discussed briefly.

3.5.2 Model reference approach

In the model reference approach, the idea is to compare the output of the nominal plant with an ideal model [24,155,232,233,245]. The information obtained from the tracking error between the nominal plant output and the ideal model is taken as the state variable for design purposes.

Consider a nominal plant given by

$$\dot{x} = Ax + Bu \quad (3.108)$$

and suppose the ideal model is given by

$$\dot{x}_m = A_m x_m + B_m r \quad (3.109)$$

where $r \in \mathbb{R}^r$ is an input vector representing the reference signal. Define the tracking error as

$$e = x - x_m \quad (3.110)$$

During perfect tracking, $e = 0$. The objective of the model reference method is to design a controller so that the tracking error will be zero, and therefore the nominal plant is said to have perfect tracking. Suppose the reference model pair (A_m, B_m) is obtained from ‘controller gains’ G and F through the following equation:

$$A_m = A + BF \quad (3.111)$$

and

$$B_m = BG \quad (3.112)$$

Mudge & Patton [155], propose a controller structure

$$u = u_{smc} + Fx + Gr \quad (3.113)$$

where u_{smc} is a sliding mode controller based on e . Consider taking the derivative of the error given in (3.110), which yields

$$\dot{e} = \dot{x} - \dot{x}_m = Ax - A_m x_m + Bu - B_m r \quad (3.114)$$

Adding and subtracting $A_m x$ to Equation (3.114) gives

$$\dot{e} = A_m e + (A - A_m)x + Bu - B_m r \quad (3.115)$$

Based on Equation (3.115), a controller can be designed to eliminate the x and r term on the right hand side of the equation. First define an error switching function

$$s(e) = Se(t) \quad (3.116)$$

which correspond to the following hyperplane

$$\mathcal{S}_e = \{e \in \mathbb{R}^n : Se = 0\} \quad (3.117)$$

Therefore during an ideal sliding motion,

$$s(e) = Se(t) = 0 \quad (3.118)$$

Differentiating this equation and substituting from Equation (3.115) yields the following;

$$\dot{s}(e) = S\dot{e}(t) = S(A_m e + (A - A_m)x + Bu - B_m r) = 0 \quad (3.119)$$

Assuming that SB is nonsingular, Edwards and Spurgeon [67] propose the equivalent control

$$u_{eq} = -(SB)^{-1}S(A_m e + (A - A_m)x - B_m r) \quad (3.120)$$

The reduced order system is given by

$$\dot{e} = (I - B(SB)^{-1}S)(A_m e - (A - A_m)x - B_m r) \quad (3.121)$$

Substituting equations (3.111) and (3.112) in the above yields

$$\dot{s}(e) = (I - B(SB)^{-1}S)(A_m e + BFx - BGr) \quad (3.122)$$

Using a similar argument to that in Section 3.1.2, the last two terms in the right hand side of the above equation can be viewed as matched uncertainty. During the ideal sliding motion Equation (3.122) reduces to

$$\dot{s}(e) = (I - B(SB)^{-1}S)A_m e \quad (3.123)$$

If the pair (A_m, B) is controllable, then a hyperplane matrix S can be designed using any of the previously introduced methods for S , to make the tracking error $e \rightarrow 0$ as $t \rightarrow \infty$.

Edwards and Spurgeon [67] propose a controller of the form in (3.113) where

$$u_{smc}(e) = u_l + u_n \quad (3.124)$$

and where

$$u_l = -(SB)^{-1}(SA_m - \Phi S)e \quad (3.125)$$

and

$$u_n = -\rho(SB)^{-1} \frac{P_2 s}{\|P_2 s\|} \quad \text{for } s(t) \neq 0 \quad (3.126)$$

where $P_2 \in \mathbb{R}^{m \times m}$ satisfies

$$P_2 \Phi + \Phi^T P_2 = -I_m \quad (3.127)$$

The scalar ρ depends on the magnitude of the uncertainty, and $\Phi \in \mathbb{R}^{m \times m}$ is a stable design matrix.

3.6 Sliding mode in the field of FTC

From the earlier introductory sections of this chapter, it is clear that there are some inherent benefits of SMC for FTC. The following subsection will highlight some of these advantages in terms of FTC.

3.6.1 Robustness against actuator faults

As discussed in Section 3.1.2, during sliding, the trajectory of the closed-loop system is independent of the control input signal $u(t)$, and therefore any uncertainty that occurs in these control input channels does not have any effect on the sliding motion and does not affect the system performance provided sliding can still be maintained. If as in (2.1), actuator faults in a linear system can be represented by

$$\dot{x} = Ax + Bu + \underbrace{(-BK)}_D \underbrace{u(t)}_{\xi(t,u,x)} \quad (3.128)$$

where $K = \text{diag}(k_1, \dots, k_m)$ and the k_i are scalars satisfying $0 \leq k_i \leq 1$. This representation of the actuator fault (nearly) fits the definition for matched uncertainty given in Section 3.1.2 (see equation (3.16)). When $k_i = 0$ the actuator is said to be working perfectly and when $k_i > 0$ some degree of fault is present in the actuator. When $k_i = 1$ this means that the actuator has failed completely. This will be dealt with separately since sliding mode controllers cannot deal directly with total actuator failures. (Although this will be dealt with later in the thesis). Provided that the nonlinear gain $\rho(\cdot)$ is large enough to overcome the effect of matched uncertainty, sliding will always be guaranteed even in the presence of faults.

The robustness properties of sliding modes against actuator faults make it a suitable candidate for FTC. A few researchers [98, 184, 185, 214, 219] have already studied the potential of sliding mode control in the field of reconfigurable control and FTC. For example Hess & Wells [98] suggested that sliding mode control has the potential to become an alternative to reconfigurable control due to its robustness properties.

3.6.2 Actuator failures

Despite its ability of handling actuator faults without require reconfiguring, as pointed out in [114], it cannot deal directly with total actuator failures. During total actuator failures, some sort of reconfiguration or accommodation is needed to enable the actuator failures to be handled by SMC. This is one motivation for works in the later chapter of this thesis.

In some systems, exact duplication of redundant actuators is available. This is considered in [55]. In this situation, the sliding mode controller can deal with total failures by simply channeling the control signals to the duplicate actuators without changing or reconfiguring the controller. This is simple in terms of designing the controller, since the same sliding mode controller output will be able to be used by many actuators. This is however restricted to systems with redundant actuators which are an exact duplicate of the original. In many real

systems, this exact duplication is simply not available. Thus, other tools are required by sliding mode schemes to deal with total actuator failures.

This raises the question of whether some other tools can be combined with sliding mode control to deal with total actuator failures? One potential candidate from the list of FTC methods in Chapter 2 is CA. This will be one facet of the research in this thesis and will be discussed in the later chapters. In safety critical systems such as large passenger transport aircraft, there already exist available redundancies. Learning from previous flight incidents and safe landings under extreme fault and failure conditions, these redundancies can be used unconventionally. This redundancy can be managed in a good way by CA to achieve many objectives including reducing drag and fuel consumption. In the case of an actuator fault/failure, CA has the ability to redistribute the control signals to the remaining functional actuators.

Even better, a combination of the robustness properties of SMC and the control reallocation capability of CA allows, in layman's terms, the possibility of simple and robust controllers that deal with faults and failures without reconfiguration. This allows a single controller to work for almost all conditions. The strategy, the methods, and the theory on how SMC can deal directly with actuator failures is one of the main contributions of this thesis.

3.7 SMC on a large civil passenger aircraft

In terms of improving the safety of large passenger aircraft, there is already significant literature investigating FTC e.g. [37, 80, 141, 148, 244]; not to mention the successful NASA work on propulsion controlled aircraft (PCA) which includes a successful flight test. Apart from [37], all these papers describe work on the same high fidelity nonlinear model of a B747 aircraft based on software called FTLAB747 [147, 189, 190]. In [80], an LPV controller is proposed for FTC, however, only longitudinal control is considered. Marcos & Balas [148] looked into robust integrated controller design and diagnosis for the longitudinal axis. The work in [244] considered both longitudinal and lateral control, but is only applied on the linear model of the aircraft. In [93] an integrated propulsion controlled aircraft has been proposed using a modified version of the FTLAB747 software. However this paper considers thrust vectoring¹ which is currently not available in any large passenger transport aircraft. (Although thrust vectoring is currently available in advanced fighter aircraft such as Saab JAS 39 'Gripen' [75] and Sukhoi Su-30MKM).

Sliding mode methods have been applied to high performance prototype aircraft such as the tailless aircraft [185, 219] where redundant actuators have been purposely built into the aircraft for performance and fault tolerance reasons. Researchers in [181] use SMC on a similar aircraft but not using the validated FTLAB747 high fidelity model. This is one of the motivations behind the research in this thesis; the challenge is for sliding mode methods to exploit all actuators available in the large passenger transport aircraft to achieve fault tolerance especially when total actuator failures occur.

¹Thrust vectoring refers to the capability of the nozzle of the jet engine to be directed at any angle. Typically most jet engine nozzle fixed and not movable.

3.8 Conclusions

In this chapter, the concept and the design process for sliding mode ideas have been presented using a simple pendulum example. The properties of sliding modes, especially robustness against matched uncertainty, have been presented. Some approaches for the design of the sliding surface (for closed-loop performance) and the control law (to ensure sliding is reached and maintained) have been presented. Modifications of the control law for tracking requirements (integral action and model reference based tracking) have also been discussed. Finally, some advantages and drawbacks of sliding mode control and how it can be applied for FTC, especially on large civil aircraft, have also been discussed. These ideas will be explored in the remainder of the thesis.

Chapter 4

Fault Tolerant Control Applied to a Large Civil Aircraft

In the last chapter, some ideas and benefits of using sliding mode schemes for fault tolerant control were discussed. In this chapter the benefit of using SMC, especially when handling actuator faults will be demonstrated using a realistic high fidelity nonlinear aircraft model. New ideas for the switching surface design and the control law are proposed. A simple idea of how SMC can handle total actuator failures is presented based on a specific example of aircraft longitudinal control adapted from [80].

4.1 Introduction

In this chapter, sliding mode schemes for FTC are developed and applied to an aircraft system. The aircraft system is a high fidelity model of a Boeing 747 which has been used by other researchers as a test bed for their developments: see for example [80, 141, 147–149]. The design of the sliding mode switching surface for the controller uses a new idea building on previous work from the sliding mode literature. A novel adaptive gain is used in the nonlinear part of the control law which reacts to the occurrence of a fault and attempts to keep the switching function as close as possible to zero, thus trying to maintain nominal tracking performance. If the total failure of an actuator is detected a switch is made to a ‘back-up’ control surface but the linear component of the control law remains unchanged. This controller is then tested in a number of different actuator fault scenarios. In comparison to the work of Hess & Wells [98] and Shtessel *et al.* [185] the novelty of the work in this chapter is the design of the sliding hyperplane which minimizes the effect of unmatched uncertainty on the sliding motion arising from actuator failures, and the development of a simple adaptive scheme for the nonlinear unit vector scaling gain.

The FTLAB747 software running under MATLAB¹ has been developed for the study of fault tolerant control and FDI schemes. It represents a ‘real world’ model of a B747-100/200 aircraft, where the technical data and the underlying differential equations have been obtained from NASA [91, 92]. The software was originally initiated at Delft University of Technology by van

¹®MATHWORKS trademark

der Linden (Delft University Aircraft Simulation and Analysis Tool, DASMAT) [212] and Smaili (Flight Lab 747, FTLAB747) [189], and later developed and enhanced for use in terms of fault detection and fault tolerant control by Marcos & Balas [147] (FTLAB747 V6.1/V6.5). The high fidelity nonlinear model has 77 states incorporating rigid body variables, sensors, actuators and aero-engine dynamics. All the control surfaces and engine dynamics are modeled with realistic position limits and rate limits. The specific aerodynamic coefficients are taken from [92], which have been obtained from extensive wind tunnel experiments, simulations and test flights. The capabilities of this software as a realistic platform to test FTC and FDI schemes is demonstrated by its subsequent use by many researchers (see for example Marcos *et al* [149], Ganguli *et al* [80] and Maciejowski & Jones [141]).

4.2 Actuator fault tolerant control

This section will concentrate on the design of a fault tolerant controller to handle actuator faults. Consider the n th order linear time invariant system with m inputs subject to uncertainty given by

$$\dot{x}_p(t) = A_p x_p(t) + B_p u(t) - B_p K(t) u(t) + M_p \xi(t, x_p) \quad (4.1)$$

where $A_p \in \mathbb{R}^{n \times n}$, $B_p \in \mathbb{R}^{n \times m}$ and $M_p \in \mathbb{R}^{n \times q}$. As in (2.1), the matrix $K(t) = \text{diag}(k_1(t), \dots, k_m(t))$ is comprised of scalar functions $k_i(t)$ which satisfy $0 \leq k_i(t) < 1$. These model a decrease in effectiveness of a particular actuator: so if $k_i(t) = 0$, the i th actuator is working perfectly whereas if $k_i(t) > 0$, some level of fault is present. Since by assumption $k_i(t) < 1$, this excludes the possibility of the actuators failing completely (although this issue will be addressed in detail separately later in the chapter). Without loss of generality it can be assumed that the input distribution matrix B_p has full rank and the pair (A_p, B_p) is controllable. The function $\xi(t, x_p)$ is assumed to be unknown but bounded and represents uncertainty in the system. Here, it is assumed to satisfy

$$\|\xi(t, x_p)\| < \mathbf{C}_1 \|x_p(t)\| + \mathbf{C}_2 \quad (4.2)$$

where \mathbf{C}_1 and \mathbf{C}_2 are known constants. This uncertainty structure has been considered in Section 3.6 in [67]. Only longitudinal control is considered: all lateral and directional states have been set to trim values. This is similar to the scenario considered in [80]. The controller is designed for an ‘up and away’ [80] flight envelope and the main objective is to obtain good tracking of flight path angle (FPA) and true airspeed (V_{tas}). The nominal (fault-free) sliding mode controller has first been designed using a linear model obtained from FTLAB747. The linearization has been obtained around an operating condition of 300,000 Kg, 184 m/s true airspeed, and an altitude of 4000m at half maximum thrust. The result is a 6th order model associated with pitch rate q , true airspeed V_{tas} , angle of attack α , pitch angle θ , altitude h_e and horizontal position along the earth x -axis x_e . For design purposes, only the first four states have been retained and the four individual engine thrusts have been aggregated to produce a single control input. The two other inputs represent elevator deflection and horizontal stabilizer deflection. In the following state-space representation, the three inputs have been individually scaled which results in a

system and input distribution matrix pair (A_p, B_p) with

$$A_p = \begin{bmatrix} -0.6803 & 0.0002 & -1.0490 & 0 \\ -0.1463 & -0.0062 & -4.6726 & -9.7942 \\ 1.0050 & -0.0006 & -0.5717 & 0 \\ 1 & 0 & 0 & 0 \end{bmatrix} \quad (4.3)$$

$$B_p = \begin{bmatrix} -1.5539 & 0.0154 \\ 0 & 1.3287 \\ -0.0398 & -0.0007 \\ 0 & 0 \end{bmatrix}, \quad b_s = \begin{bmatrix} -1.5760 \\ 0 \\ -0.0398 \\ 0 \end{bmatrix} \quad (4.4)$$

where the states represent pitch rate (rad/s), true airspeed (m/s), angle of attack (rad) and pitch angle (rad) respectively. The inputs associated with B_p are elevator deflection (rad) and total thrust (N) (scaled by 10^5), and b_s is the distribution matrix associated with the horizontal stabilizer.

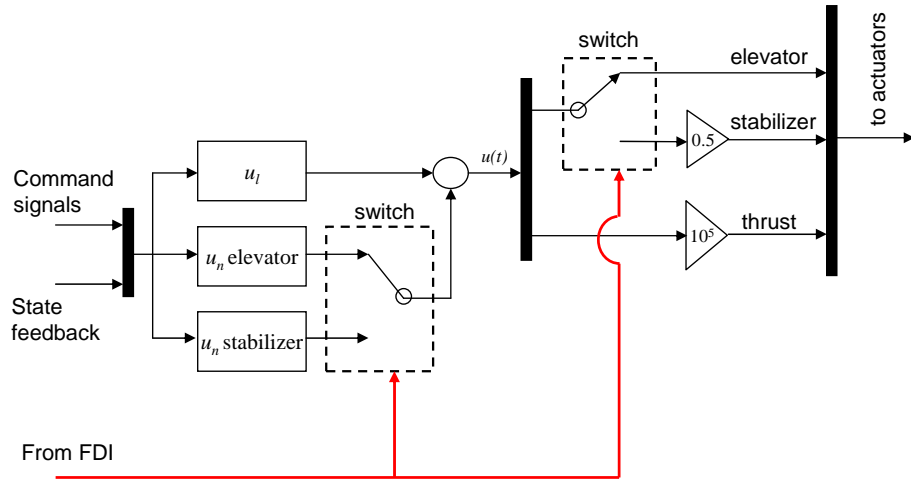


Figure 4.1: controller interconnection

During normal operation, the aircraft would be controlled using the thrust and elevator, however in the event of an elevator failure, the horizontal stabilizer can be used as ‘back-up’ (see Figure 4.1). In this situation b_s will be used to replace the first column of B_p when the ‘back-up’ controller is activated (this will be discussed later). When implementing the controller on the nonlinear model a simple gain block (10^5 for thrust and 0.5 for horizontal stabilizer [80]) is used to recover the signal sent to the actuator (see Figure 4.1). The controlled output distribution matrix is

$$C_c = \begin{bmatrix} 0 & 0 & -1 & 1 \\ 0 & 1 & 0 & 0 \end{bmatrix} \quad (4.5)$$

which represents flight-path angle (FPA)² and true airspeed (V_{tas}). This linear model will be used to design the controller scheme which will be described in the sections which follow.

²Flight-path angle is the difference between pitch angle and angle of attack [38].

4.2.1 Sliding Mode Controller Design

Integral action (as discussed in Section 3.5.1) will be included to add a tracking facility for the two controlled outputs FPA and V_{tas} . The uncertain faulty system from (4.1) has been augmented with integral action states $x_d \in \mathbb{R}^m$ satisfying

$$\dot{x}_d(t) = y_c(t) - C_c x_p(t) \quad (4.6)$$

where the differentiable signal $y_c(t)$ satisfies

$$\dot{y}_c(t) = \Gamma (y_c(t) - Y_d) \quad (4.7)$$

with $\Gamma \in \mathbb{R}^{m \times m}$ a stable design matrix and Y_d a constant demand vector. Augmenting the states from (4.1) with the integral action states and defining $x = \text{col}(x_d, x_p)$ it follows

$$\dot{x}(t) = Ax(t) + Bu(t) + B_d y_c(t) - BK(t)u(t) + M\xi(t, x) \quad (4.8)$$

where

$$A = \begin{bmatrix} 0 & -C_c \\ 0 & A_p \end{bmatrix}, \quad B = \begin{bmatrix} 0 \\ B_p \end{bmatrix}, \quad B_d = \begin{bmatrix} I_m \\ 0 \end{bmatrix}, \quad M = \begin{bmatrix} 0 \\ M_p \end{bmatrix} \quad (4.9)$$

Since the pair (A_p, B_p) is controllable, if (A_p, B_p, C_c) does not have any invariant zeros at the origin, then (A, B) is controllable [67]. For the later analysis, define an augmented version of b_s from (4.4) as

$$B_s = \begin{bmatrix} 0 \\ b_s \end{bmatrix} \quad (4.10)$$

Although B_s does not directly appear in Equation (4.8), it represents the distribution matrix associated with Equation (4.8) when the horizontal stabilizer is employed as a ‘back-up’ control surface if a total failure in the elevator occurs. Define a switching function

$$s(t) = Sx(t) \quad (4.11)$$

as a linear combination of the states, where $S \in \mathbb{R}^{m \times (n+m)}$ is full rank. If a control law can be developed which forces the closed-loop trajectories onto the surface $s(t) = 0$ in finite time (despite faults) and constrains the states to remain there, then an ideal sliding motion is said to have been attained. Suppose the matrix S is designed so that the square matrix SB is nonsingular (in practice this is easily accomplished since B is full rank and S is a free parameter). Then, as discussed in Section 3.5.1, the ideal sliding motion is given by

$$\begin{aligned} \dot{x}(t) &= (I_{(n+m)} - B(SB)^{-1}S)Ax(t) + (I_{(n+m)} - B(SB)^{-1}S)M\xi(t, x) \\ &\quad + (I_{(n+m)} - B(SB)^{-1}S)B_d y_c(t) \end{aligned} \quad (4.12)$$

for all $t \geq t_s$ and $Sx(t_s) = 0$. It can be seen from Equation (4.12) that the sliding motion is a control independent free motion which depends on the choice of sliding surface. If $M_p \in \mathcal{R}(B_p)$ i.e. M_p belongs to the range-space of the matrix B_p then $(I_{(n+m)} - B(SB)^{-1}S)M = 0$ and the sliding motion is independent of the uncertainty. Several approaches have been proposed

in the literature for the design of the matrix S including quadratic minimization (as discussed in Section 3.4.1), eigenvalue placement, eigenstructure assignment and LMI methods (see for example Chapter 4 in [67] and [65]). Furthermore, without loss of generality, the surface can always be designed so that $SB = I_m$.

The proposed control law comprises two components; a linear component to stabilize the nominal linear system; and a discontinuous component. Specifically

$$u(t) = u_l(t) + u_n(t) \quad (4.13)$$

where the linear component is given by

$$u_l(t) = \underbrace{-(SB)^{-1}(SA - \Phi S)}_L x(t) - \underbrace{(SB)^{-1}SB_d}_{L_d} y_c(t) \quad (4.14)$$

where $\Phi \in \mathbb{R}^{m \times m}$ is any stable design matrix and u_n is a discontinuous component which is a function of s .

In this chapter, the choice of the nonlinear term $u_n(t)$ is facilitated by the choice of S for which $SB = I_m$, which effectively decouples the components of the sliding surface and associates with each a particular control input. Componentwise, the proposed control structure has the form

$$u_i(t) = u_{l_i}(t) - (\rho_i(t) + \eta_i)\text{sign}(s_i(t)), \quad i = 1 \dots m \quad (4.15)$$

where the η_i are positive constants³, $u_{l_i}(t)$ is the i th component of $u_l(t)$, $s_i(t)$ is the i th component of $s(t) = Sx(t)$. It is easy to see from (4.14) that $u_{l_i}(t)$ is bounded by $|u_{l_i}(t)| < l_1\|x(t)\| + l_2$ where l_1 and l_2 are known positive constants. The gains $\rho_i(\cdot)$ in each of the control channels are defined as

$$\rho_i(t) = r_i(t)(\bar{r}_{(i,1)}\|x(t)\| + \bar{r}_{(i,2)}) \quad (4.16)$$

where

$$\bar{r}_{(i,1)} := (l_1 + \|S_i M\|_{\mathbf{C}_1}), \quad \bar{r}_{(i,2)} := (l_2 + \|S_i M\|_{\mathbf{C}_2}) \quad (4.17)$$

and the constants \mathbf{C}_1 and \mathbf{C}_2 are from (4.2). The variables $r_i(t)$ are adaptive gains which vary according to

$$\dot{r}_i(t) = \alpha_i \left(\bar{r}_{(i,1)}\|x(t)\| + \bar{r}_{(i,2)} \right) D_\epsilon(|s_i(t)|) - \beta_i r_i(t), \quad r_i(0) = 0 \quad (4.18)$$

where the α_i and β_i are positive design constants. The function $D_\epsilon : \mathbb{R} \mapsto \mathbb{R}$ is the nonlinear function

$$D_\epsilon(s) = \begin{cases} 0 & \text{if } |s| < \epsilon \\ s & \text{otherwise} \end{cases} \quad (4.19)$$

where ϵ is a positive scalar. (This function is also considered in [228]). Here, ϵ is set to be small and helps define a boundary layer about the surface $\mathcal{S} = \{x(t) : Sx(t) = 0\}$ inside which an acceptably close approximation to ideal sliding takes place. Provided the states evolve with time

³The η_i could be chosen as functions of the state, large enough to bound the uncertainty in the fault-free case when $K(t) = 0$.

inside the boundary layer, no adaptation of the switching gains takes place. If a fault occurs, which starts to make the sliding motion degrade so that the states evolve outside the boundary layer i.e. $|s_i(t)| > \epsilon$, then the dynamic coefficients $r_i(t)$ increase in magnitude (according to (4.18)) to force the states back into the boundary layer around the sliding surface.

Remark: In a fault-free situation it is not necessary and indeed is not advisable to have a large gain on the switched term – therefore ideally the term $\rho(\cdot)$ should adapt to the onset of a fault and react accordingly. This adaptation scheme differs from the one in [220] and is more akin to the scheme from [228].

The choice of the design parameters η_i , α_i , β_i and ϵ depends on the closed-loop performance specifications and requires some design iteration. In general, the η_i need to be chosen as the nominal (no fault) gains for the nonlinear component of the control law (4.15) to ensure that sliding occurs in the fault-free system. The parameter ϵ is chosen to be small to form a boundary layer about \mathcal{S} , but not too small to cause ‘false alarms’ and unnecessary increases in $\rho_i(t)$. Thus ϵ dictates how sensitive the adaptive gains $r_i(t)$ are to changes in $s(t)$. The gain α_i dictates the rate at which $r_i(t)$ increases in reaction to faults: a large value for α_i indicates a fast increase of $r_i(t)$. On the other hand β_i dictates the rate at which $r_i(t)$ decreases to the nominal gain η_i when the fault has been rectified. A relationship between ϵ , η_i , α_i and β_i will be determined in the proof of the proposition which follows. The choice of these design parameters will be discussed further in §4.3. The following lemma shows the gain functions are bounded and motion inside a boundary layer around \mathcal{S} is obtained.

Proposition 1 *Consider the potentially faulty augmented system represented by (4.8) with the control law in (4.15); then each of the components $r_i(t)$ remain bounded and the switching states $s(t)$ enter a boundary layer around \mathcal{S} in finite time.*

Proof: Consider $\bar{k} = \max\{k_1(t) \dots k_m(t)\}$. Notice that by assumption $\bar{k} < 1$. From the decoupled structure which results from $SB = I_m$, it follows that

$$\dot{s}_i = -\phi_i s_i - (1 - k_i(t))(\rho_i(t) + \eta_i) \text{sign}(s_i) - k_i(t)u_i(t) + S_i M \xi(t, x) \quad (4.20)$$

where it has been assumed that $\Phi = \text{diag}(-\phi_1, \dots, -\phi_m)$ and the ϕ_i are positive scalars. Therefore

$$s_i \dot{s}_i \leq -\phi_i s_i^2 - (1 - \bar{k})(\rho_i(t) + \eta_i)|s_i| + s_i(S_i M \xi(t, x) - k_i(t)u_i(t)) \quad (4.21)$$

Using (4.17) and the fact that $\bar{k} = 1 - (1 - \bar{k})$, then by construction

$$\begin{aligned} |(S_i M \xi(t, x) - k_i(t)u_i(t))| &\leq |S_i M \xi(t, x)| + \bar{k}|u_i(t)| \\ &\leq (\bar{r}_{(i,1)}\|x(t)\| + \bar{r}_{(i,2)}) - (1 - \bar{k})|u_i(t)| \quad \text{for } i = 1 \dots m \end{aligned} \quad (4.22)$$

since from (4.2), $\|\xi(t, x)\| < \mathbf{C}_1\|x(t)\| + \mathbf{C}_2$. Define a scalar

$$\zeta := 1/(1 - \bar{k}) > 0 \quad (4.23)$$

and a component Lyapunov function

$$V_i = \frac{1}{2} \left\{ s_i^2 + \frac{1}{\alpha_i} (1 - \bar{k}) (r_i(t) - \zeta)^2 \right\} \quad (4.24)$$

where α_i is the positive scalar from (4.18). Clearly $V_i(\cdot)$ is positive definite with respect to s_i , the adaptive gain errors $r_i(t) - \zeta$, and is radially unbounded. Taking derivatives

$$\dot{V}_i = s_i \dot{s}_i + \frac{1}{\alpha_i} (1 - \bar{k}) (r_i(t) - \zeta) \dot{r}_i(t) \quad (4.25)$$

then substituting from (4.16), (4.18), (4.21) and (4.22) into the above and using the fact that $(1 - \bar{k})\zeta = 1$, it follows

$$\begin{aligned} \dot{V}_i \leq & -\phi_i s_i^2 - |s_i| (1 - \bar{k}) (\eta_i + |u_i(t)|) - |s_i| (1 - \bar{k}) (\bar{r}_{(i,1)} \|x(t)\| + \bar{r}_{(i,2)}) (r_i(t) - \zeta) \\ & + \frac{1}{\alpha_i} (1 - \bar{k}) (r_i(t) - \zeta) \left(\alpha_i (\bar{r}_{(i,1)} \|x(t)\| + \bar{r}_{(i,2)}) D_\epsilon(|s_i(t)|) - \beta_i r_i(t) \right) \end{aligned} \quad (4.26)$$

If $|s_i| > \epsilon$ then $D_\epsilon(|s_i|) = |s_i|$ and so substituting in (4.26) and simplifying terms yields

$$\dot{V}_i \leq -\phi_i s_i^2 - |s_i| (1 - \bar{k}) (\eta_i + |u_i(t)|) - \frac{\beta_i}{\alpha_i} (1 - \bar{k}) (r_i(t) - \zeta) r_i(t) \quad (4.27)$$

Notice by construction $\bar{k} < 1$ and $r_i(t) \geq 0$. Further manipulation of (4.27) and using (4.23) yields

$$\dot{V}_i \leq -\phi_i s_i^2 - |s_i| (1 - \bar{k}) (\eta_i + |u_i(t)|) - \frac{\beta_i}{\alpha_i} (1 - \bar{k}) \left(\frac{1}{2} \zeta - r_i(t) \right)^2 + \frac{\beta_i}{4\alpha_i(1 - \bar{k})} \quad (4.28)$$

since expanding the quadratic term on the right-hand side of (4.28) gives (4.27). If $|s_i| > \epsilon$, then $|s_i|(1 - \bar{k})\eta_i \geq (1 - \bar{k})\epsilon\eta_i$. The quantities $\epsilon, \eta_i, \alpha_i$ and β_i are design parameters and so if they are chosen to satisfy

$$(1 - \bar{k})\epsilon\eta_i \geq \frac{\beta_i}{4\alpha_i(1 - \bar{k})} \quad (4.29)$$

then

$$\dot{V}_i \leq -\phi_i s_i^2 - |s_i| (1 - \bar{k}) |u_i(t)| - \frac{\beta_i}{\alpha_i} (1 - \bar{k}) \left(\frac{1}{2} \zeta - r_i(t) \right)^2 \leq 0 \quad (4.30)$$

If $|s_i| < \epsilon$ then $D_\epsilon(|s_i|) = 0$ and so substituting in (4.26) and simplifying terms yields

$$\begin{aligned} \dot{V}_i \leq & -\phi_i s_i^2 - |s_i| (1 - \bar{k}) (\eta_i + |u_i(t)|) - |s_i| (1 - \bar{k}) (\bar{r}_{(i,1)} \|x(t)\| + \bar{r}_{(i,2)}) (r_i(t) - \zeta) \\ & - \frac{\beta_i}{\alpha_i} (1 - \bar{k}) (r_i(t) - \zeta) r_i(t) \end{aligned} \quad (4.31)$$

Notice again by construction $\bar{k} < 1$ and $r_i(t) \geq 0$ and therefore for $|s_i| < \epsilon$ and $r_i(t) > \zeta$, it follows $\dot{V}_i < 0$. Define a rectangle in \mathbb{R}^2 as

$$\mathcal{R}_i = \{(s_i, r_i) \mid |s_i| \leq \epsilon, 0 \leq r_i \leq \zeta\} \quad (4.32)$$

Also define $\mathcal{R}_+ = \{(s_i, r_i) \mid r_i \geq 0\}$. By construction of the adaptive gains, $r_i(t) \geq 0$ for all time and so the trajectory of $(s_i(t), r_i(t)) \in \mathcal{R}_+$ for all time, and so outside $\mathcal{R}_i \cap \mathcal{R}_+ = \mathcal{R}_i$, from (4.28) and (4.31), the derivative of the Lyapunov function $\dot{V}_i < 0$. Let $\mathcal{V}_{r,i}$ denote the truncated ellipsoid

$$\mathcal{V}_{r,i} = \{(s_i, r_i) \mid V_i(s_i, r_i) \leq r\} \cap \mathcal{R}_+$$

where $V_i(\cdot)$ is defined in (4.24). Because \mathcal{R}_i in (4.32) is a compact set, \exists a unique $r_{i,0} > 0$ s.t. $r_{i,0} = \min\{r \in \mathbb{R}_+ \mid \mathcal{R}_i \subset \mathcal{V}_{r,i}\}$ and in fact $r_{i,0} = \frac{1}{2}(\epsilon^2 + \frac{\zeta}{\alpha_i})$.

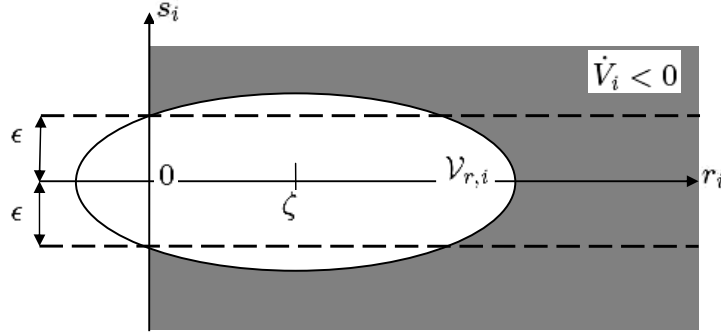


Figure 4.2: Level set of the Lyapunov functions V_i

As shown in Figure 4.2, since $\mathcal{R}_i \subset \mathcal{V}_{r_{i,0}}$, it follows outside $\mathcal{V}_{r_{i,0}}$ the derivative of the Lyapunov function $\dot{V}_i < 0$ and so $\mathcal{V}_{r_{i,0}}$ is an invariant set which is entered in finite time t_0 . Since $\mathcal{V}_{r_{i,0}}$ is entered in finite time, $V_i(s_i, r_i) \leq r_{i,0}$ for all $t > t_0$ which implies $|s_i| \leq \sqrt{2r_{i,0}}$ for all time $t > t_0$, and hence s_i enters and remains in a boundary layer of size $\sqrt{2r_{i,0}}$ around the ideal sliding surface \mathcal{S} . ■

From the arguments above, for an appropriate choice of α_i , β_i and ϵ , close approximation to ideal sliding can be maintained even in the presence of faults. The reduced order sliding motion is then governed by (4.12). The motion depends on the uncertainty, but using arguments similar to those in §3.6 in [67], for a small enough \mathbf{C}_1 , ultimate boundedness of the states $x(t)$ can be proved.

Remarks:

- If $\epsilon = 0$ and $\beta_i = 0$ then ideal sliding can be guaranteed since it follows from (4.27) that the Lyapunov derivative $\dot{V}_i(s) \leq -\phi_i s_i^2 - |s_i|(1 - \bar{k})(\eta_i + |u_i(t)|)$. This means ideal sliding can be attained and maintained in finite time. However this adaptive scheme has disadvantages in practice since the gains $r_i(t)$ may become unbounded in the presence of noise [220].
- The adaptive gains act as a measure of severity of the actuator fault. Once the adaptive gain $\rho_i(t)$ from (4.16) exceeds a predetermined maximum value $\rho_{max,i}$, a very severe fault or failure can be declared and a ‘backup’ control strategy can be initiated if required.
- From (4.23), as $\bar{k} \rightarrow 1$, ζ becomes infinitely large. In the case of total failure ($k_i(t)=1 \Rightarrow \bar{k}=1$), an alternative control strategy must be employed.

4.2.2 The sliding mode hyperplane design.

The first step in sliding mode controller design is the selection of the sliding surface matrix S . One methodology is the quadratic cost function approach which was discussed in Section 3.4.1. In this chapter, a novel modification of this approach is considered to take into account the occurrence of failures. The design approach adopted here is described specifically for the aircraft system. However, its underlying philosophy is generic and could be adopted in other systems.

First consider the problem of designing a sliding surface matrix S for the nominal linear system associated with (4.24). Assume there are no faults (i.e. $K(t) = 0$) and there is no reference demand ($y_c(t) = 0$)⁴. Also for the purpose of design, ignore the uncertainty term. For this nominal linear system, as discussed previously in Section 3.4.1, consider the problem of minimizing the quadratic performance index

$$J = \frac{1}{2} \int_{t_s}^{\infty} x(t)^T Q x(t) dt \quad (4.33)$$

where Q is a symmetric positive definite (s.p.d) matrix and t_s is the time at which the sliding motion commences. Define a change of coordinates given by

$$z(t) = T_r x(t) \quad (4.34)$$

where T_r is an orthogonal matrix, so that the system in (4.8) is in regular form: i.e

$$T_r A T_r^T = \begin{bmatrix} A_{11} & A_{12} \\ A_{21} & A_{22} \end{bmatrix} \quad T_r B = \begin{bmatrix} 0 \\ B_2 \end{bmatrix}$$

where $A_{11} \in \mathbb{R}^{n \times n}$, $B_2 \in \mathbb{R}^{m \times m}$. Also assume that, (in regular form) the matrix $T_r Q T_r^T$ associated with equation (4.33) has a block diagonal structure so that $T_r Q T_r^T = \text{diag}(Q_1^T Q_1, Q_2^T Q_2)$ where $Q_1^T Q_1 = 0$ and the matrix $Q_2^T Q_2 \in \mathbb{R}^{m \times m}$ is nonsingular. It follows that

$$J = \frac{1}{2} \int_{t_s}^{\infty} z_1(t)^T Q_1^T Q_1 z_1(t) + z_2(t)^T Q_2^T Q_2 z_2(t) dt \quad (4.35)$$

where $z = \text{col}(z_1, z_2)$ with $z_1 \in \mathbb{R}^n$. Because of the assumption of regular form, under nominal fault-free operation, the differential equation constraint (4.8), whilst sliding, may be written as

$$\dot{z}_1(t) = A_{11} z_1(t) + A_{12} z_2(t) \quad (4.36)$$

where the ‘virtual control’ z_2 satisfies

$$\mathcal{K} z_1 + z_2 = 0 \quad (4.37)$$

Here Equation (4.37) represents the hyperplane equation $Sx = 0$ for $S T_r^T = S_2 [\mathcal{K} \quad I_m]$, where $S_2 \in \mathbb{R}^{m \times m}$ and is nonsingular. Substituting for z_2 from (4.37) in (4.36) gives an autonomous reduced order sliding motion. The matrix \mathcal{K} must be chosen to make $(A_{11} - A_{12} \mathcal{K})$ stable. This

⁴Although as argued in §7.3.3 in [67] since $y_c(t) \rightarrow Y_d$ the effect of the demand signal can be removed by a change of coordinates which considers the system states relative to their steady state values.

is always possible since (A_{11}, A_{12}) is controllable if (A, B) is controllable. As argued in [35] the optimal cost is given by $J = z_1(t_s)^T P_c z_1(t_s)$ where P_c is the symmetric positive definite solution to the Riccati equation

$$P_c A_{11} + A_{11}^T P_c - P_c A_{12} (Q_2^T Q_2)^{-1} A_{12}^T P_c + Q_1^T Q_1 = 0 \quad (4.38)$$

where $z_1(t_s)$ is the value of the state component z_1 at the time at which sliding occurs and the optimal choice of $\mathcal{K} = (Q_2^T Q_2)^{-1} A_{12}^T P_c$. This problem can be posed as an LMI optimization: Minimize $\text{trace}(X^{-1})$ subject to

$$\begin{bmatrix} A_{11}X + XA_{11}^T - A_{12}N - N^T A_{12}^T & (Q_1X - Q_2N)^T \\ Q_1X - Q_2N & -I \end{bmatrix} < 0, \quad X > 0 \quad (4.39)$$

where $N := \mathcal{K}X$. As argued on page 114 in [35], any solution to (4.39) satisfies $X^{-1} \geq P_c$. Consequently $\text{trace}(X^{-1}) \geq \text{trace}(P_c)$ and hence the minimization process results in $X^{-1} = P_c$.

In the ‘back-up’ case, the input distribution matrix is perturbed by the change in actuator. Now the new input distribution matrix \tilde{B} (say) is formed from replacing the first column from B in (4.9) associated with the elevator, with B_s in (4.10) which is associated with the horizontal stabilizer. In the regular form coordinates

$$T_r \tilde{B} = \begin{bmatrix} B_1 \\ B_2 R \end{bmatrix}$$

where $B_1 \in \mathbb{R}^{n \times m}$ and $R \in \mathbb{R}^{m \times m}$. Provided a sliding motion can be maintained with the new actuator set, in the regular form coordinates, then the uncertain reduced order motion can be represented as

$$\dot{z}_1(t) = (A_{11} - A_{12}\mathcal{K})z_1(t) + M_1\xi + B_1 u_{eq}(t) \quad (4.40)$$

instead of (4.36) and (4.37), where $u_{eq}(t)$ is the equivalent control signal necessary to maintain a sliding motion on \mathcal{S} and M_1 represents the top n rows of $T_r M$ i.e. the un-matched uncertainty distribution matrix in the regular form coordinates. The signal $u_{eq}(t)$ will be a function of the states z_1 and will include the effects of any additional mismatched disturbances resulting from the failure (such as turning moments generated from stuck actuators). The objective is to minimize the effect of $u_{eq}(t)$ on the nominal performance of the system in Equation (4.40) in an \mathcal{L}_2 sense [123]. Under the constraint that a common Lyapunov function for both the quadratic cost problem and the \mathcal{L}_2 gain problem is sought, from the Bounded Real Lemma [35], the \mathcal{L}_2 gain between $u_{eq}(t)$ and z_1 is less than γ if

$$\begin{bmatrix} A_{11}X + XA_{11}^T - A_{12}N - N^T A_{12}^T & [B_1 \ M_1] & X \\ [B_1 \ M_1]^T & -\gamma I & 0 \\ X & 0 & -\gamma I \end{bmatrix} < 0 \quad (4.41)$$

The overall optimization problem used here is: Minimize $(a_1 \text{trace}(Z) + a_2 \gamma)$ subject to

$$\begin{bmatrix} -Z & I_n \\ I_n & -X \end{bmatrix} < 0 \quad (4.42)$$

in addition to (4.39) and (4.41). The matrix variable Z is a ‘slack variable’ which satisfies $Z > X^{-1}$ and so $\text{trace}(Z)$ bounds $\text{trace}(X^{-1})$. Here a_1 and a_2 are positive scalars which determine the relative weighting between the quadratic cost and \mathcal{L}_2 problem. This represents a convex optimization problem in terms of X, Z, N and γ and can be solved using standard LMI packages. The matrix which determines the hyperplane is computed as $\mathcal{K} = NX^{-1}$ and finally (in the original coordinates), the matrix

$$S = S_2 \begin{bmatrix} \mathcal{K} & I_m \end{bmatrix} T_r \quad (4.43)$$

The nonsingular matrix S_2 is then chosen to ensure $SB = I_m$. Although the development above is specific to the B747 backup stabilizer scenario, the approach is more flexible and could be used in more general situations.

4.3 Simulation Results

This subsection describes the actuator fault tolerant controller designed for the B747-100/200 aircraft. The controller is designed for longitudinal axis control in the ‘up and away’ flight envelope [80]. The main objective is to obtain tracking of flight path angle (FPA) and true air speed V_{tas} . The settling time when there is no fault/failure should be approximately 20sec for FPA and 45sec for V_{tas} . If a fault/failure occurs, the tracking requirement is 30sec for FPA with no difference in the V_{tas} tracking. These specifications are adopted from [80].

The weighting matrix for the hyperplane design has been chosen as

$$T_r Q T_r^T = \begin{bmatrix} 0.5 & 0 & 0 & 0 & 0 & 0 \\ 0 & 0.5 & 0 & 0 & 0 & 0 \\ 0 & 0 & 2 & -1 & 0 & 0 \\ 0 & 0 & -1 & 1 & 0 & 0 \\ 0 & 0 & 0 & 0 & 5 & 0 \\ 0 & 0 & 0 & 0 & 0 & 20 \end{bmatrix} \quad (4.44)$$

The last two elements of $T_r Q T_r^T$ multiply the z_2 term in (4.35) and thus weight the ‘virtual control’ term. Thus, by analogy to a more typical LQR framework, they affect the speed of response of the closed-loop system. The last state is weighted heavily to reduce the gains in the engine channels. The first two terms in (4.44) are associated with the integral action states and are less heavily weighted. The non-diagonal term in (4.44) arises from the fact that flight path angle is the quantity of interest. In the following design, the parameters $a_1 = a_2 = 1$. Here an equal weight on the quadratic cost performance and the \mathcal{L}_2 robustness has been chosen to represent the equal importance of the nominal (no fault) performance and robustness when a total actuator failure occurs. In this example, the choice of a_2 is not crucial because the degree of mismatch between B and \tilde{B} , represented by $\|B_1\|$, is small. The LMI optimization software gives a unique solution for \mathcal{K} in (4.43). This results in

$$S = \begin{bmatrix} 0.2163 & -0.0013 & -0.6524 & 0.0077 & 0.3471 & -0.9034 \\ -0.0000 & -0.1192 & 0.0000 & 0.7526 & -0.0005 & -0.0000 \end{bmatrix}$$

where the original sliding surface matrix S obtained from the optimization software (4.43) has been scaled using S_2 in order that $SB = I_2$. The poles associated with the reduced order sliding motion are $\{-0.6786, -0.3566 \pm 0.3802i, -0.1584\}$. From Equation (4.14) the stable matrix has been chosen as $\Phi = -I_2$ which gives faster poles than those associated with the reduced order sliding motion. This results in (from Equation (4.14))

$$L = \begin{bmatrix} -0.2163 & 0.0013 & 0.7643 & -0.0086 & -1.0891 & 1.1956 \\ 0.0000 & 0.1192 & 0.1107 & -0.8672 & -3.8542 & 7.3710 \end{bmatrix}, \quad L_d = \begin{bmatrix} -0.2163 & 0.0013 \\ 0.0000 & 0.1192 \end{bmatrix}$$

The pre-filter matrix from (4.7) has been designed to be

$$\Gamma = \begin{bmatrix} -0.2400 & 0 \\ 0 & -0.1250 \end{bmatrix}$$

This may be viewed as representing the ideal response in the FPA and the V_{tas} channels. Again the FPA response is faster than the V_{tas} response. In the simulations the discontinuity in the nonlinear control term has been smoothed, as in Section 3.2.2, by using a sigmoidal approximation where the fixed scalar $\delta = 0.01$. This removes the discontinuity and introduces a further degree of tuning to accommodate the actuator rate limits, especially during actuator fault or failure conditions. The initial fixed gains for the ‘back-up’ controller (using the horizontal stabilizer) are given by $\rho_{s,1} = 0.4$ and $\rho_{s,2} = 0.05$. Here the smoothing parameter is chosen as $\delta_s = 0.1$. The larger value of δ_s is used to accommodate the smaller positional movement and lower rate limits of the horizontal stabilizer. In this chapter, only the gains in the elevator channel are allowed to adapt: the gains associated with the thrust channel are fixed. When employing the adaptive gain for the controller from (4.15), it was found for this particular example the $\bar{r}_{(i,1)}(t)$ in (4.17) have no significant effect on the closed-loop performance and so $l_1 = \mathbf{C}_1 = 0$ was chosen and therefore $\bar{r}_{(i,1)}(t) \equiv 0$. The parameters, l_2 and \mathbf{C}_2 have been chosen as $l_2 = 0.5$ and $\mathbf{C}_2 = 0.9117$ and therefore $\bar{r}_{(i,2)}(t) \equiv 1$. The upper and lower limits for $\rho_1(t)$ have been chosen as $\rho_{max,1} = 5$ and $\rho_{min,1} = \eta_1 = 0.2$ respectively. Here $\eta_1 = 0.2$ is chosen to be larger than the uncertainty in the no fault condition. The choice of $\rho_{max,1}$ dictates how fast a severe or total failure can be detected. Here, $\rho_{max,1}$ has been chosen large enough to compensate for the worse case fault on the elevator (before the switch to stabilizer is activated) at a 70% decrease in effectiveness. The adaptation parameters are $\alpha_1 = 600$ and $\beta_1 = 0.02$ and the tolerance $\epsilon = 0.0005$. Appropriate values for α_1 , β_1 and ϵ involve some design iteration. The parameter ϵ was chosen to be able to tolerate the variation in $s(t)$ due to normal changes in flight conditions but small enough to enable the adaptive gain to be sensitive to deviations from zero in the switch term s_1 when a fault or severe disturbance occurs. The term α_1 dictates the rate at which $\rho(t)$ increases and reacts to the faults. Here, it needs to be large to enable small changes in s_1 to cause significant changes in the gain so that the control system reacts quickly to the onset of a fault. From (4.29), $(1 - \bar{k})\epsilon\eta_i = 3.0 \times 10^{-5}$ and $\beta_i/(4\alpha_i(1 - \bar{k})) = 2.78 \times 10^{-5}$ and therefore the condition in Proposition 1 is satisfied.

The simulations presented in this chapter are all based on the *full non-linear model*. For the ‘up and away’ flight condition, the elevator is used to track FPA demands. As in the work of Ganguli *et al* [80], this chapter only considers faults/failures to the elevator.

4.3.1 Fault-Free Simulations

In this section, simulations are presented for the nominal controller design as described in Section 4.3. The simulation covers the entire ‘up and away’ flight region, from an altitude of 4000m with a velocity of 184m/s, to the end of the region at an altitude of 8500m and with a velocity of 280m/s. A series of 3 degree FPA and 10m/s V_{tas} commands are issued during the simulation to take the aircraft through the entire envelope. Figures 4.3(a),4.3(c),4.3(d) show the results associated with the controller designed for the elevator and thrust, whilst Figure 4.3(b) shows the performance with the horizontal stabilizer as the control surface (together with thrust). In these responses the adaptive gain in each channel has been fixed throughout the simulation. Figure 4.3 shows that both the controllers are able to maintain satisfactory tracking performance (using elevator or horizontal stabilizer) over the range of the ‘up and away’ flight region even though these conditions become increasingly far away from the designed condition. This indicates the robustness of the single fixed sliding mode controller.

4.3.2 Changes in effectiveness gain

This section shows how the controller with an adaptive gain $\rho(t)$ as defined in Section 4.2.1 copes with different percentages of faults as modeled in (4.1). This section also demonstrates the fault detection capability of the controller. The simulations have been conducted at an altitude of 4000m and a V_{tas} of 184m/s with a 3 degree of FPA (0.5-30sec) step change and a 20m/s V_{tas} step change at 55sec as command signals. The ‘effectiveness gain’ has been implemented as a simple but unknown (as far as the controller is concerned) gain between the output of the controller block and the actuator dynamics. These simple tests indicate the effect of a loss of efficiency of the elevator due to damage or faults. Figure 4.4 shows comparisons of the adaptive gain controller with $k_1 = 0, 0.5, 0.6, 0.7, 0.7, 0.8, 0.9$ (which indicate 0, 50, 60, 70, 80, 90 percent failure, respectively). It can be seen that there is a slight variation in FPA tracking and no visible difference in V_{tas} tracking. Overall FPA tracking is still possible (although with some degradation in performance) even at a 90% fault. This indicates that the adaptive gain controller is robust and has the ability to maintain good tracking even for severe faults. Looking at the signal s_1 (the switching signal associated with the elevator channel) in Figure 4.4(c), its value is still relatively close to zero even when the percentage of fault increases. The adaptive gain signal shows that at 70% failure, the gain reaches the maximum allowable set gain ($\rho_{max,1}=5$). At this point it would be possible for a warning signal to be sent to the pilot or an automatic change to the ‘back-up’ controller could be initiated. Notice that even though the nominal adaptive gain controller is still able to maintain stability up to 90% failure, early failure detection is more desirable to provide advanced warning and to avoid potentially irrecoverable instability.

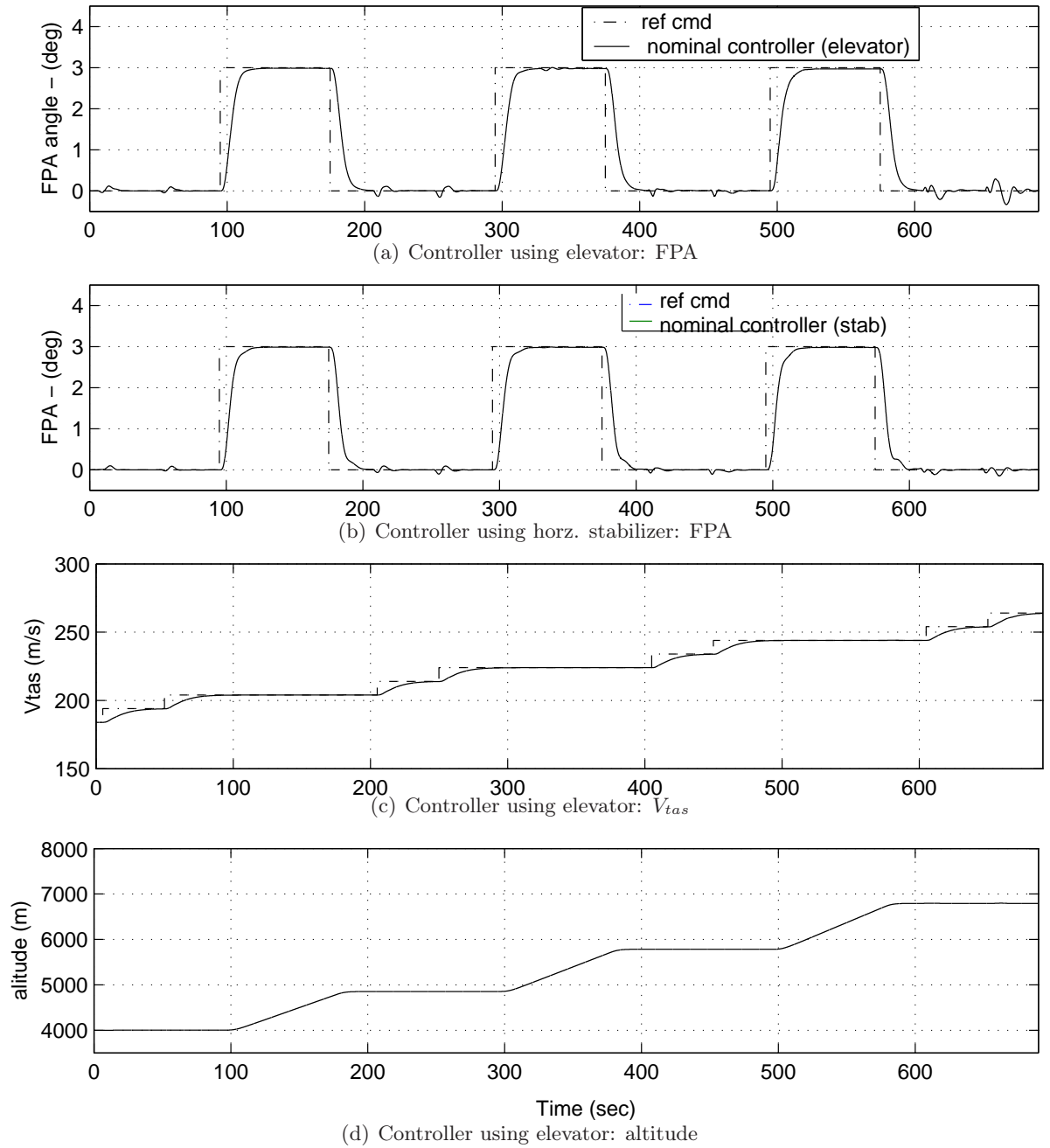


Figure 4.3: Nominal fault-free performance

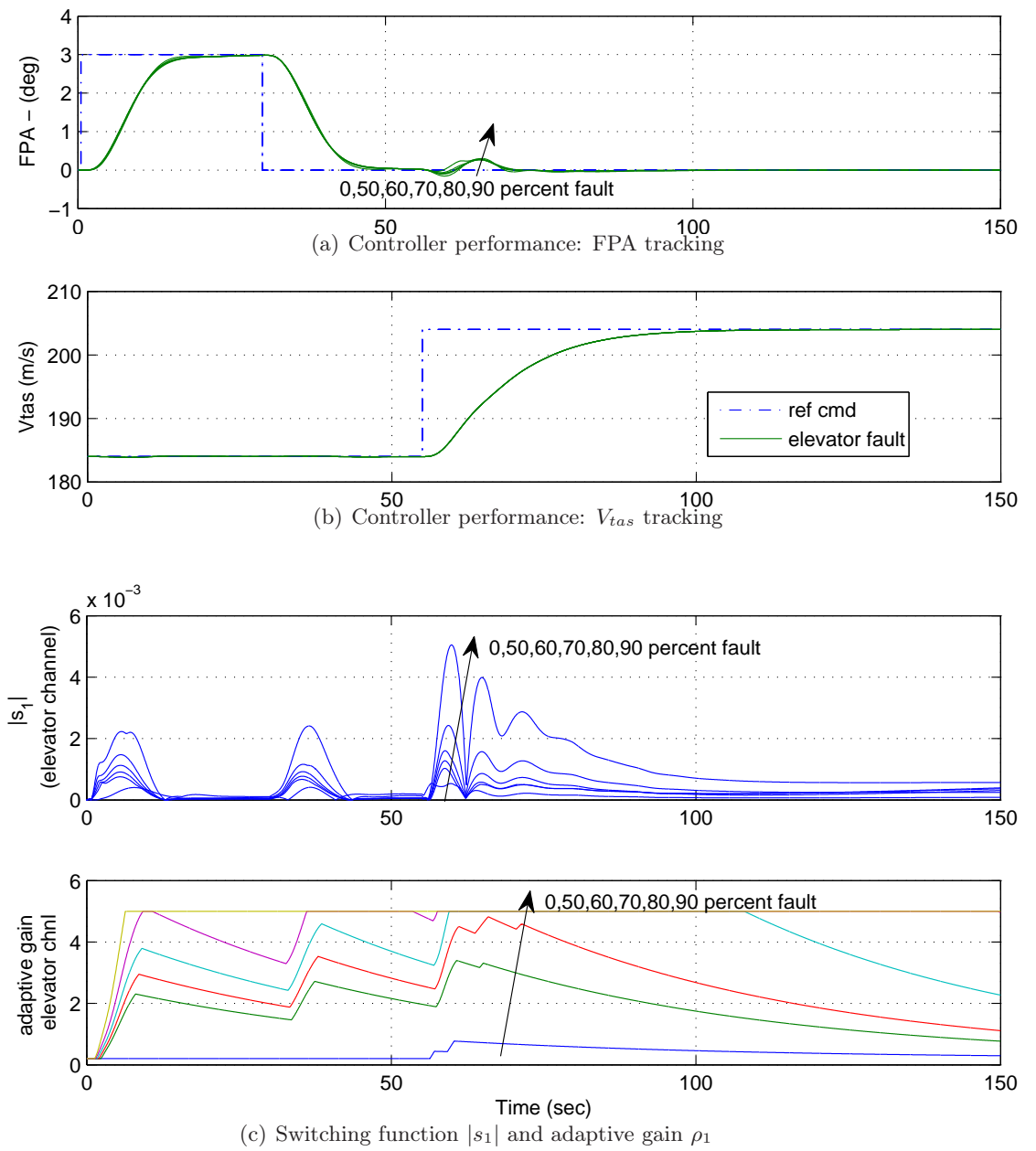


Figure 4.4: Responses of different effectiveness gain

4.3.3 Total elevator failure simulations

This section shows the results of nonlinear simulations when the elevator develops floating and/or lock type actuator failures. These simulate total failure of the elevator and therefore require stabilization of the aircraft using the ‘back-up’ controller (which uses the horizontal stabilizer). A similar flight scenario to previous test is considered. The failure is set to occur during the climb (pitch up) manoeuvre at 10sec for both failure scenarios. To simulate a floating actuator type of failure, the elevator signal is replaced with the angle of attack [80]. This simulates the ineffectiveness of the elevator to provide a moment and therefore the aircraft is unable to perform a pitch manoeuvre. Figure 4.5(a) shows that FPA tracking performance is slightly degraded and the response is slower. Figure 4.5(c) shows that the failure is detected at 11.38 sec when the adaptive gain reaches its maximum set value. Some peaks can be seen in the horizontal stabilizer signal (Figure 4.5(b)) after activation due to the sudden change of control signal, but this stabilizes after a few seconds. *Once the controller is switched to the horizontal stabilizer, that surface is used for the remainder of the simulation.* Overall performance is satisfactorily maintained after detection of the failure and after the change to the ‘back-up’ controller. To simulate lock failures, the elevator position is held at its value at 10sec. Fig 4.6(a) shows that, as before, the FPA tracking is slightly degraded. Failure is detected at 13.45 sec (Figure 4.6(c)) and the horizontal stabilizer is activated (Figure 4.6(b)). A high peak occurs in the horizontal stabilizer signal but disappears after a few seconds (Figure 4.6(b)). Overall tracking performance is maintained.

4.3.4 Total elevator failure simulations with wind and gust

The same set of flight conditions and tests as above has been repeated in the presence of nonzero wind and gust (turbulence) conditions. The nonzero wind condition is set to approximate the wind profile at the time of the crash for EL-AL flight 1862 which is $-11, -12, 0$ (m/s) for the u, v, w wind axis respectively [147]. The turbulence parameter is set as white noise with a variance of 1 [147]. Figures 4.7 and 4.8 show the simulation results for float and lock type failures with wind and turbulence disturbances. As in the previous test, all the plots show that the controller has been able to maintain stability and tracking performance even in the presence of disturbances.

4.3.5 Combined loss of effectiveness and total elevator failure

The simulations have been conducted at an altitude of 4000m and a V_{tas} of 184m/s. The reference command requests a change in flight path angle of 3 deg for 20 sec followed by a 20 m/s change in speed over a period of 45 sec (in 2 steps). The command sequence for the FPA demand is then reversed after 250 sec so that the aircraft is returned to (approximately) the initial flight conditions. These simple tests indicate the effect of a loss of efficiency of the elevator due to damage or faults.

Figures 4.9 and 4.10 show the results of nonlinear simulations for various fault conditions: a nominal (no fault) period for the first 150sec, followed by degradation of the elevator effectiveness (150-260sec) and finally total failure (260-400sec). From 150-260sec, as shown in Figure

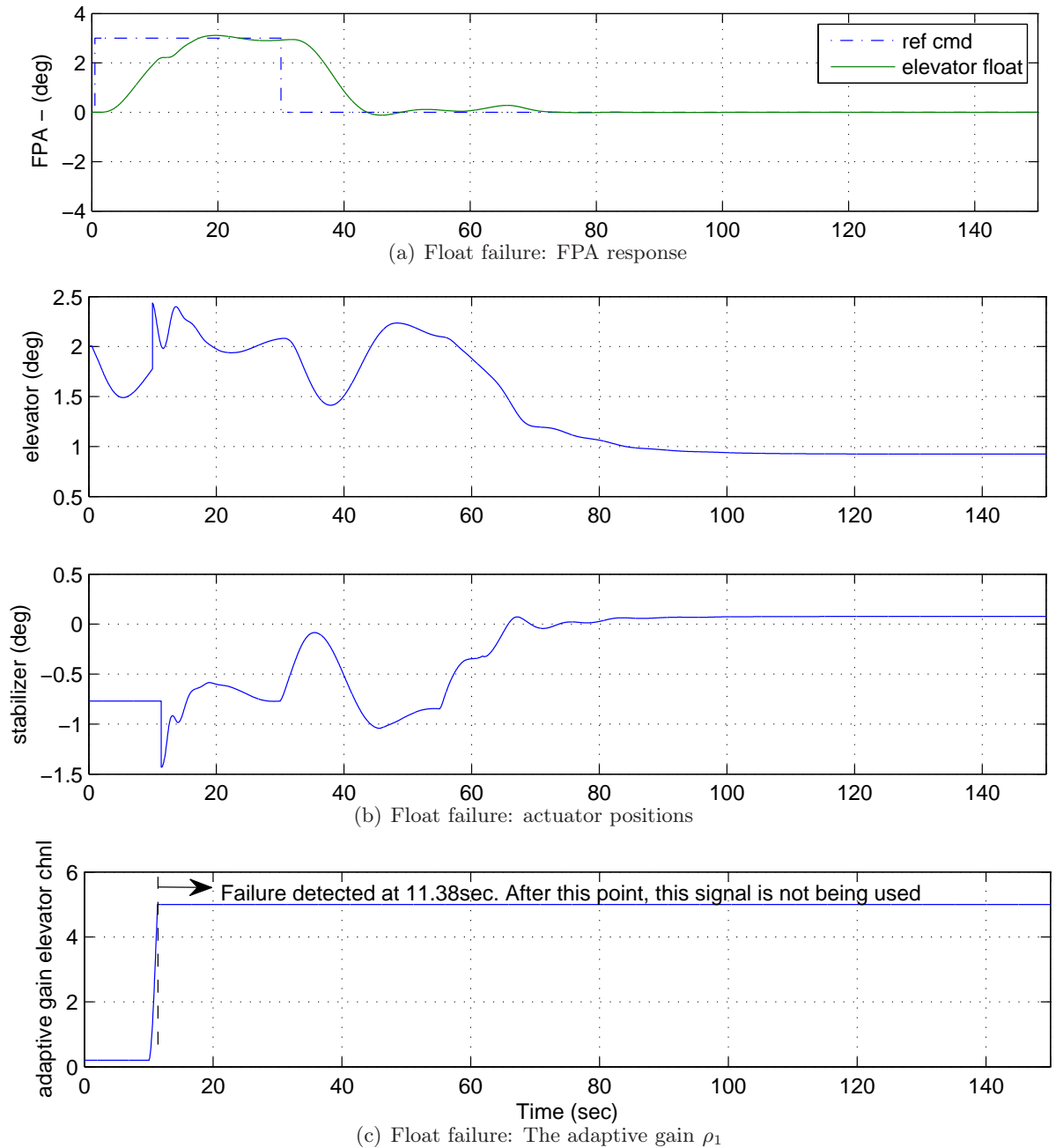


Figure 4.5: Responses of float failure

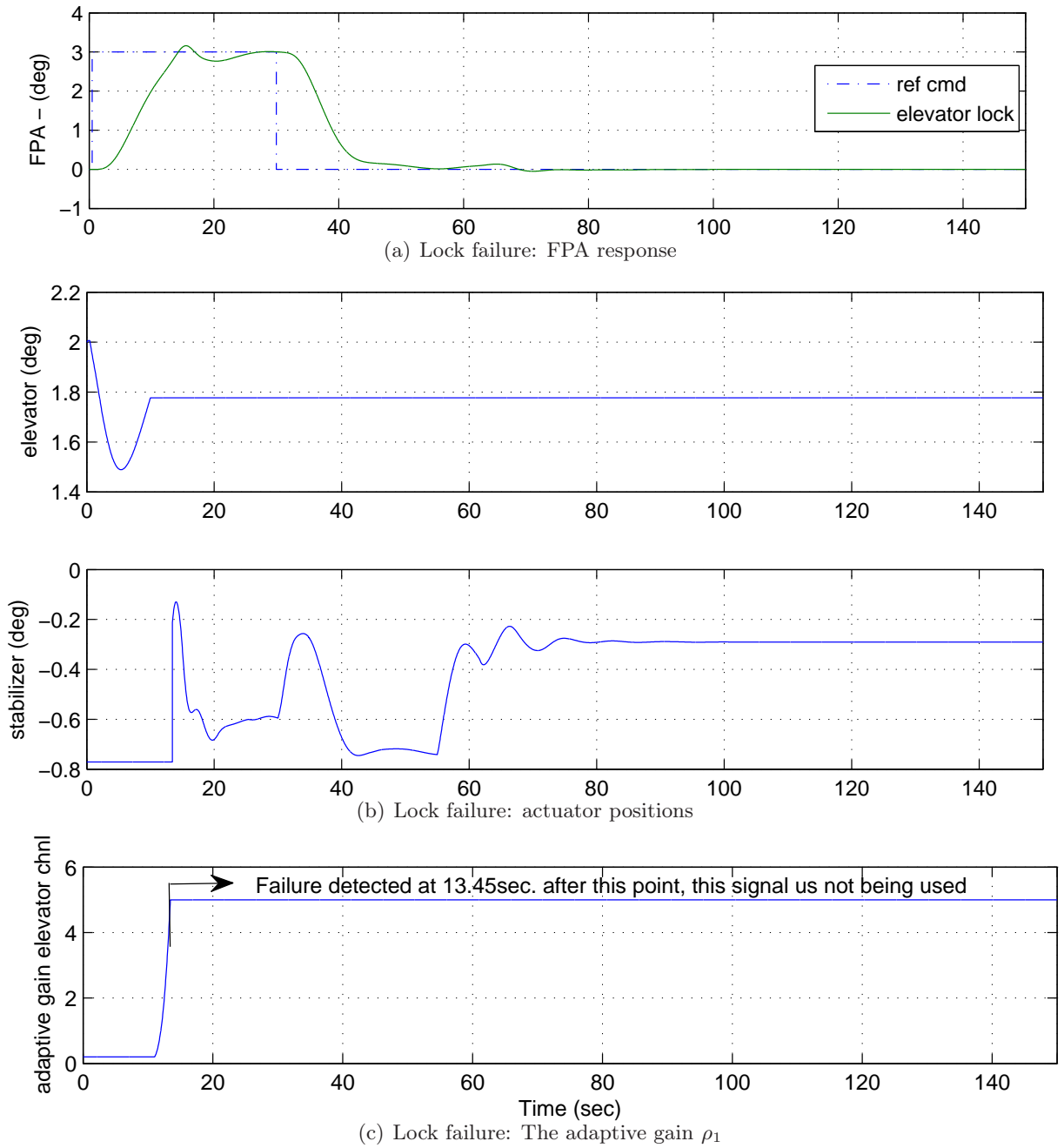


Figure 4.6: Responses of lock failure

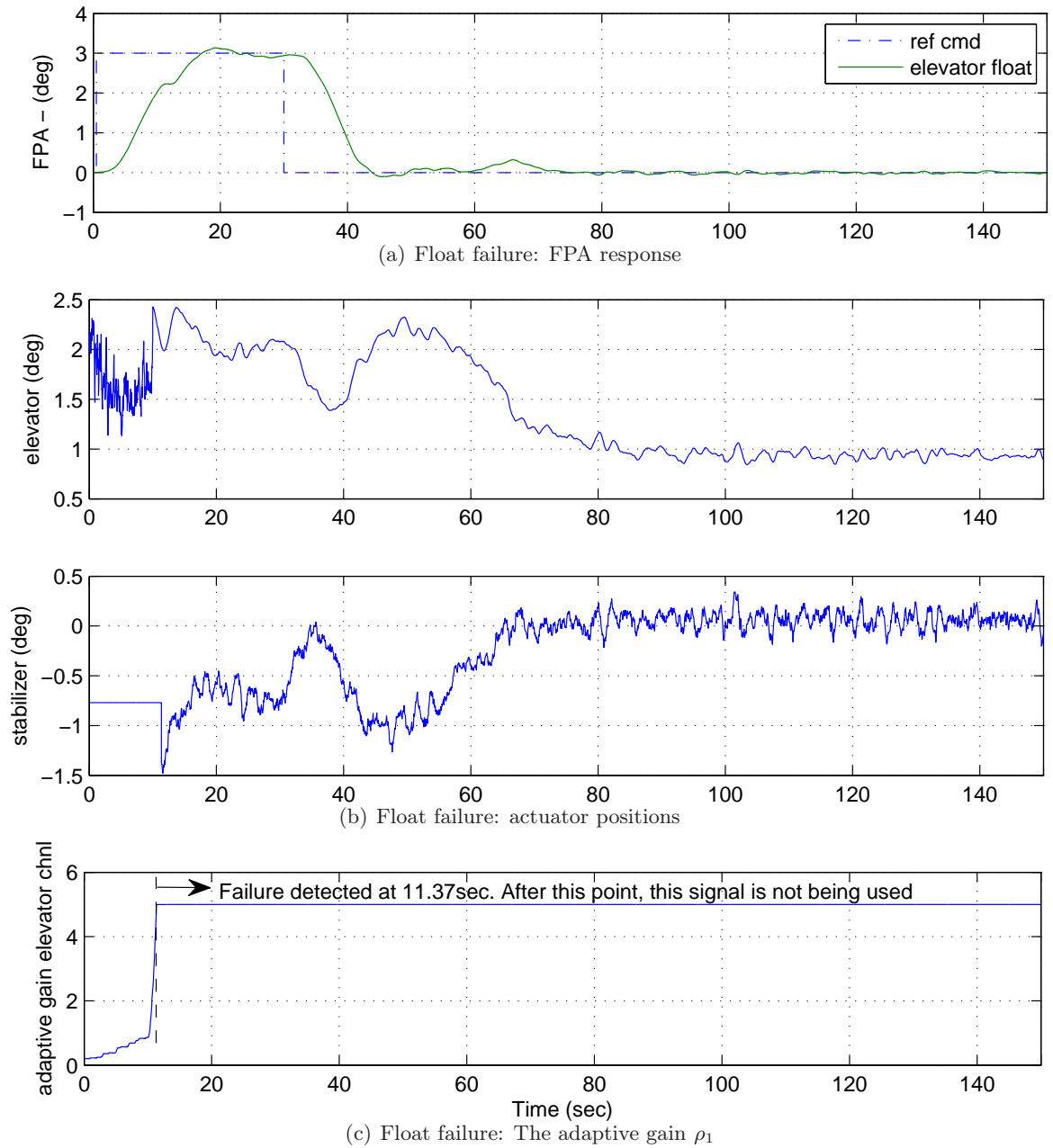


Figure 4.7: Responses of float failure with wind & gust disturbances

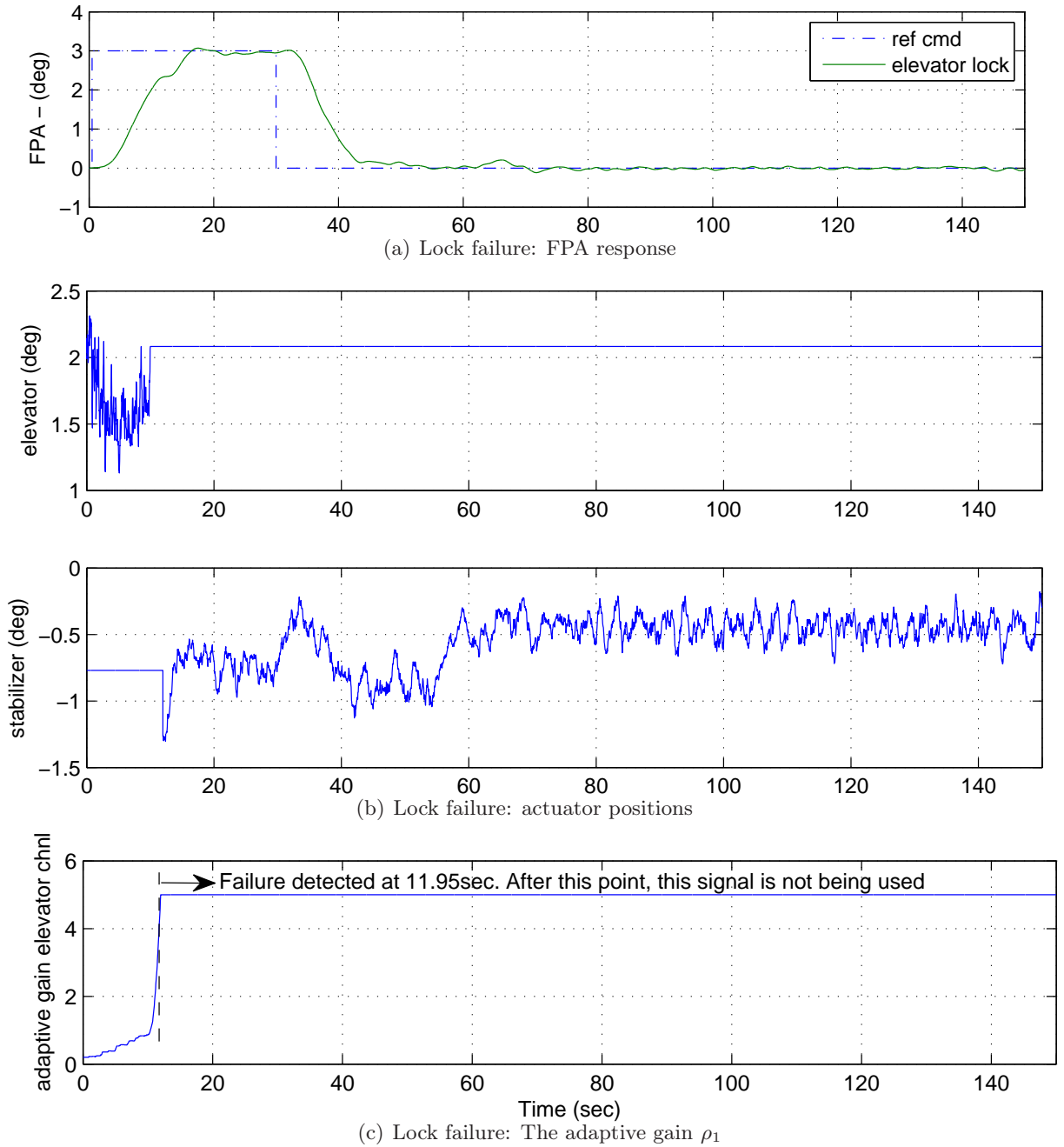


Figure 4.8: Responses of lock failure with wind & gust disturbances

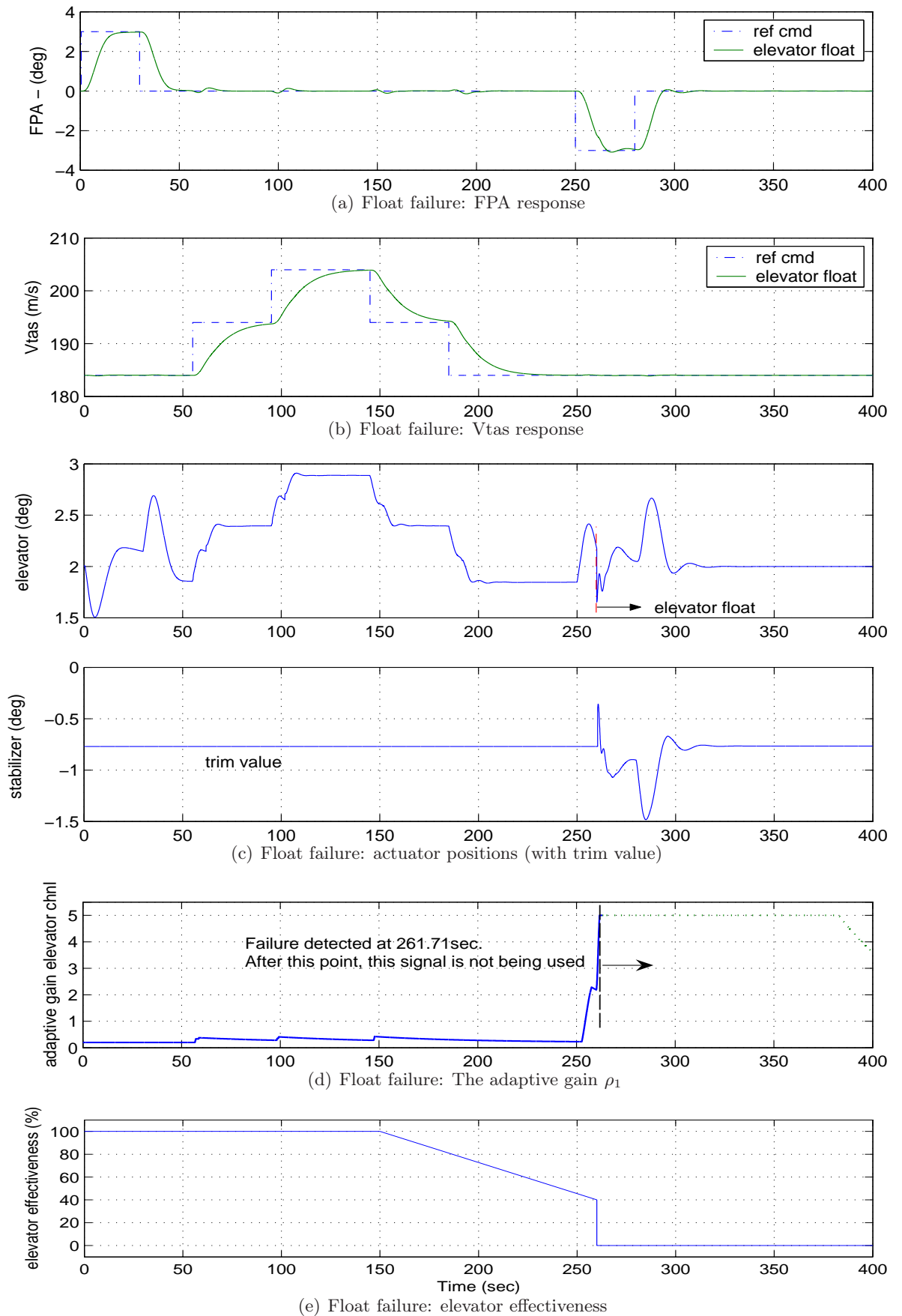


Figure 4.9: Responses of nominal, fault and failures (float failure)

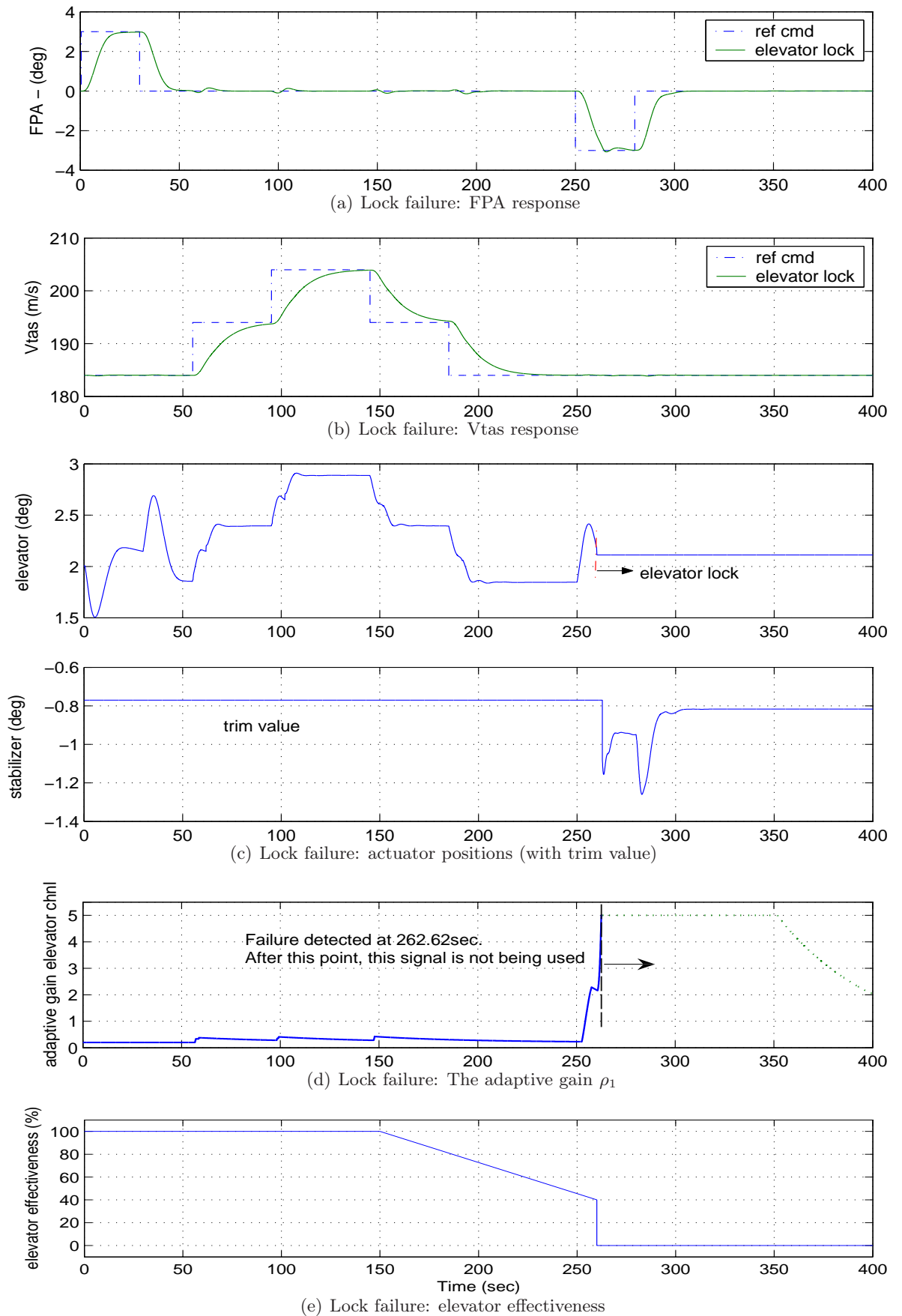


Figure 4.10: Responses of nominal, fault and failures (lock failure)

4.9(e) and 4.10(e), the elevator effectiveness degrades from (normal) 100% to 40% effectiveness. Subsequently the elevator develops floating and/or lock type actuator failures at 260sec. These simulate total failure of the elevator and therefore require stabilization of the aircraft using the ‘back-up’ controller (which uses the horizontal stabilizer). The failure is set to occur during the descent (pitch down) manoeuvre at 260sec for both failure scenarios. To simulate a floating actuator type of failure, the elevator signal is replaced with the angle of attack signal. Figure 4.9(a) shows that FPA tracking performance is slightly degraded and the response is slower. Figure 4.9(d) shows that the failure is detected at 261.71sec when the adaptive gain reaches its maximum set value. Some peaks can be seen in the horizontal stabilizer signal (Figure 4.9(c)) after activation due to the sudden change of control signal, but this stabilizes after a few seconds. Once the controller is switched to the horizontal stabilizer, that surface is used for the remainder of the simulation. Overall performance is satisfactorily maintained after detection of the failure and the change to the ‘back-up’ controller. To simulate lock failures, the elevator position is held at its value at 260sec. Fig 4.10(a) shows that the FPA tracking is slightly degraded. Failure is detected at 262.62sec (Figure 4.10(d)) and the stabilizer is activated (Figure 4.10(c)). Overall tracking performance is maintained.

4.4 Conclusions

This chapter has presented a novel SMC scheme for fault tolerant control of a civil aircraft. As in the work of [80], only longitudinal control with a fault and/or failure occurring in the elevator channel has been considered. The controller is based around a state-feedback sliding mode scheme and the gain associated with the nonlinear term is allowed to adaptively increase when the onset of a fault is detected. Compared to other FTC schemes which have been implemented on this model, the controller proposed here is simple and yet is shown to work across the entire ‘up and away’ flight envelope. It is not scheduled across any variables and its structure remains fixed (except for the adaptive gain associated with the nonlinear switching term). Unexpected deviation of the switching variable from its nominal condition initiates the adaptation mechanism. Total failure can also be detected from the switching function, and has in this example been used to trigger the use of a ‘back-up’ control surface. A range of realistic fault scenarios have been considered and the results of simulations using the full nonlinear aircraft model have been presented. The next chapter considers a similar flight regime but with sensor faults rather than actuator faults.

Chapter 5

Sliding Mode Fault Reconstruction and Sensor Fault Tolerant Control

In the previous chapter, the ability of a sliding mode controller to deal with actuator faults has been discussed. This chapter will explore and highlight the benefits of using sliding mode schemes for FDI: specifically for fault reconstruction. In general, the information obtained from a sliding mode fault reconstruction scheme can be used for detecting and isolating faults, controller reconfiguration (through estimation of the actuator effectiveness) or sensor fault tolerant control (by using the sensor fault estimation to correct a corrupted measurement). This chapter will demonstrate the capability of sliding mode observers for robust sensor fault estimation on the same high fidelity nonlinear model of the B747 aircraft which was used in the last chapter. In this chapter, the sensor fault estimation signals will be used to achieve sensor fault tolerant control as the corrupted sensor measurement signal can be corrected before being used by the controller. This removes the requirement for controller reconfiguration and removes the requirement for additional redundant sensors in the system.

5.1 Introduction

In the last chapter, a sliding mode controller has been shown to naturally handle actuator faults without requiring reconfiguration. The benefit of sliding modes does not stop there. Sliding mode observers have their own unique characteristics which are beneficial for FDI and for handling sensor faults.

In terms of sensor faults, SMC has the same drawback as most classical controllers: it cannot handle sensor faults directly. A very good controller design will become a very bad one when sensor faults occur, because the controller will ‘faithfully’ track the ‘wrong’ corrupted measurements from the faulty sensors.

Total sensor failures will not be considered in this thesis, as in aircraft systems as well as in many safety critical systems, key sensors possess double or even triple redundant units [36,37]. In the case of a total sensor failure, a voting system can be used to eliminate the failed sensor and therefore only the healthy sensors will be used for feedback control. The main concern in this thesis is therefore sensor faults with the assumption that other redundant sensors are not

used or are not available. Some types of sensor faults do not affect the stability of the aircraft, but some faults degrade the performance and affect stability.

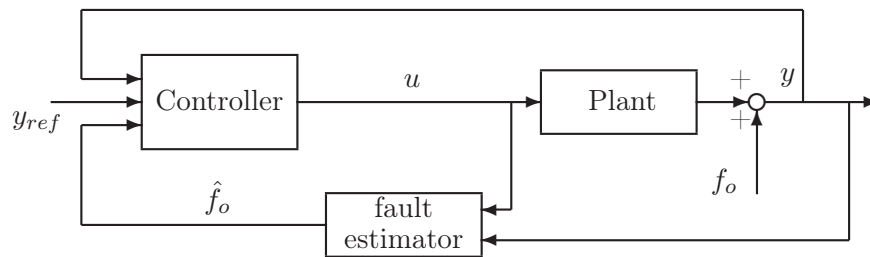


Figure 5.1: SMC sensor fault tolerant control schemes

5.2 Sliding Mode observers for FDI

Sliding mode observers are one of the nonlinear FDI approaches available in the literature. The idea is to design the observer gains so that the sliding surface is reached and maintained so that the error between the plant and the observer states is zero.

The first sliding mode observer designs used typical residual based FDI ideas [97, 229]. The idea was to ensure the sliding motion was broken when faults/failures occurred in the system and a residual was generated containing information about the fault. The more recent work by Edwards *et al* [68], Tan & Edwards [202], Jiang *et al* [111] and Kim *et al* [125] represent some of the approaches which have the capability to reconstruct/identify faults. Not only do these design approaches have the ability to detect and isolate the source of the fault/failure they also provide further information about the fault/failure which can be used especially for controller reconfiguration. In terms of FTC, the availability of a fault reconstruction signal means that sensor faults can be corrected before the measurement signals are used by the controller (see Figure 5.1), and the severity of an actuator fault (actuator effectiveness) can be estimated, which is beneficial for controller reconfiguration [227, 237, 242].

A generic FDI development in terms of the reconstruction of faults using sliding mode observers is given in Edwards *et al* [68]. The novelty of the work in Edwards *et al* [68], is the use of the concept of the ‘equivalent output error injection signal’ to reconstruct faults. Tan & Edwards [202] extended this work for robust reconstruction of sensor and actuator faults by minimizing the effect of modeling uncertainty on the reconstruction in an \mathcal{L}_2 sense [123].

One of the benefits of using the method proposed in [68, 201, 202] compared to other SMC observer based FDI methods is that the sliding motion is not broken even in the event of faults/failures. This allows the possibility of using the sliding mode observer not only for FDI but also as a state estimator. However, for FDI purposes, emphasis is placed on the fault estimation and not the state estimation.

In this chapter, actuator FDI is not of primary concern, as the sliding mode technique discussed in Chapter 4 has inherent robustness capabilities to actuator faults. Sensor FTC will take the form of using sensor fault estimates to correct the corrupt signals, therefore avoiding direct reconfiguration of the controller.

This chapter will include an introduction to a typical sliding mode observer and will show how sliding mode observers can be used for fault reconstruction as suggested in [68]. In order to show the true capabilities and the potential of sliding mode observers for FDI and fault reconstruction, this chapter will implement the work of Tan & Edwards [202] for robust sensor fault reconstruction with the emphasis on detecting, isolating and reconstructing sensor faults in a large civil aircraft using FTLAB747. The novelty lies in the application of the sensor fault reconstruction signal to correct the corrupted measured signals before they are used by the controller which therefore does not need to be reconfigured to adapt to sensor faults.

5.3 A typical sliding mode observer

The following section will briefly introduce one class of sliding mode observer. The one presented here evolved from the Utkin observer [210] and Walcott-Žak observer [216,217], and is known as the Edwards-Spurgeon observer [67].

Consider the following linear system with uncertainty

$$\dot{x}(t) = Ax(t) + Bu(t) + D\xi(t, x, u) \quad (5.1)$$

$$y(t) = Cx(t) \quad (5.2)$$

where $A \in \mathbb{R}^{n \times n}$, $B \in \mathbb{R}^{n \times m}$, $C \in \mathbb{R}^{p \times n}$, $D \in \mathbb{R}^{n \times q}$ and $p \geq q$. The function $\xi : \mathbb{R}_+ \times \mathbb{R}^n \times \mathbb{R}^m \rightarrow \mathbb{R}^q$ is unknown but bounded so that

$$\|\xi(t, x, u)\| \leq r_1 \|u\| + \alpha(t, y) \quad (5.3)$$

where r_1 is a known scalar and $\alpha : \mathbb{R}_+ \times \mathbb{R}^p \rightarrow \mathbb{R}_+$ is a known function.

Edwards & Spurgeon [67] proposed that for design purposes the system is transformed into an observer canonical form by using a transformation matrix T_o , so that $x \mapsto T_o x$ such that the system can be represented by

$$\begin{bmatrix} \dot{x}_1 \\ \dot{y} \end{bmatrix} = \begin{bmatrix} \mathcal{A}_{11} & \mathcal{A}_{12} \\ \mathcal{A}_{21} & \mathcal{A}_{22} \end{bmatrix} \begin{bmatrix} x_1 \\ y \end{bmatrix} + \begin{bmatrix} \mathcal{B}_1 \\ \mathcal{B}_2 \end{bmatrix} u + \begin{bmatrix} 0 \\ \mathcal{D}_2 \end{bmatrix} \xi \quad (5.4)$$

where $x_1 \in \mathbb{R}^{n-p}$, $y \in \mathbb{R}^p$, and \mathcal{A}_{11} has stable eigenvalues. In this new coordinate system, the new output distribution matrix is

$$CT_o^{-1} = \begin{bmatrix} 0 & I_p \end{bmatrix} \quad (5.5)$$

An observer associated with this system has the form

$$\dot{\hat{x}} = \mathcal{A}\hat{x} + \mathcal{B}u - \mathcal{G}_l e_y + \mathcal{G}_n \nu \quad (5.6)$$

where

$$\begin{bmatrix} \dot{\hat{x}}_1 \\ \dot{\hat{y}} \end{bmatrix} = \underbrace{\begin{bmatrix} \mathcal{A}_{11} & \mathcal{A}_{12} \\ \mathcal{A}_{21} & \mathcal{A}_{22} \end{bmatrix}}_{\mathcal{A}} \begin{bmatrix} \hat{x}_1 \\ \hat{y} \end{bmatrix} + \underbrace{\begin{bmatrix} \mathcal{B}_1 \\ \mathcal{B}_2 \end{bmatrix}}_{\mathcal{B}} u - \underbrace{\begin{bmatrix} \mathcal{A}_{12} \\ \mathcal{A}_{22} - \mathcal{A}_{22}^s \end{bmatrix}}_{\mathcal{G}_l} e_y + \underbrace{\begin{bmatrix} 0 \\ I_p \end{bmatrix}}_{\mathcal{G}_n} \nu \quad (5.7)$$

and \mathcal{A}_{22}^s is stable design matrix. The quantity $e_y = \hat{y} - y$ is the output estimation error and ν is defined as

$$\nu = \begin{cases} -\rho(t, y) \|\mathcal{D}_2\| \frac{P_2 e_y}{\|P_2 e_y\|} & \text{if } e_y \neq 0 \\ 0 & \text{otherwise} \end{cases} \quad (5.8)$$

The matrix P_2 is a s.p.d. matrix and satisfies the following Lyapunov equation

$$\mathcal{A}_{22}^{s\top} P_2 + P_2 \mathcal{A}_{22}^s = -I \quad (5.9)$$

The scalar ρ in (5.8) depends on the magnitude of the uncertainty and is any function which satisfies

$$\rho(t, y) \geq r_1 \|u\| + \alpha(t, y) + \gamma_o \quad (5.10)$$

where γ_o is a positive scalar. The sliding surface is the hyperplane represented by

$$\mathcal{S}_o = \{e \in \mathbb{R}^n : Ce = 0\} \quad (5.11)$$

where $e = \hat{x} - x$. The state estimation error system associated with e_y and $e_1 = \hat{x}_1 - x_1$ becomes

$$\begin{bmatrix} \dot{e}_1 \\ \dot{e}_y \end{bmatrix} = \begin{bmatrix} \mathcal{A}_{11} & 0 \\ \mathcal{A}_{21} & \mathcal{A}_{22}^s \end{bmatrix} \begin{bmatrix} e_1 \\ e_y \end{bmatrix} + \begin{bmatrix} 0 \\ I_p \end{bmatrix} \nu - \begin{bmatrix} 0 \\ \mathcal{D}_2 \end{bmatrix} \xi \quad (5.12)$$

Necessary and sufficient conditions for the existence of the canonical form (5.4) are given by Proposition 6.2 in [67] and are:

- $\text{rank}(CD) = q$
- any invariant zeros of (A, D, C) must lie in \mathbb{C}_-

In the original coordinates, the observer from Equation (5.6) and (5.7) can be written as

$$\dot{\hat{x}}(t) = A\hat{x}(t) + Bu(t) - G_l e_y(t) + G_n \nu \quad (5.13)$$

and the observer gains and parameters are given by

$$G_l = T_o^{-1} \begin{bmatrix} \mathcal{A}_{12} \\ \mathcal{A}_{22} - \mathcal{A}_{22}^s \end{bmatrix} \quad (5.14)$$

$$G_n = \|\mathcal{D}_2\| T_o^{-1} \begin{bmatrix} 0 \\ I_p \end{bmatrix} \quad (5.15)$$

$$\nu = \begin{cases} -\rho \frac{P_2 e_y}{\|P_2 e_y\|} & \text{if } e_y \neq 0 \\ 0 & \text{otherwise} \end{cases} \quad (5.16)$$

where T_o is the transformation matrix used to obtain the observer canonical form in (5.4). It can be shown that

$$\sigma((I - Gn(CGn)^{-1}C)A) = \sigma(\mathcal{A}_{11}) \cup \{0\}^p$$

and that the invariant zeros of (A, D, C) are a subset of $\sigma(\mathcal{A}_{11})$. For an appropriate choice of ρ , a sliding motion is obtained on \mathcal{S}_o in finite time [67].

5.4 The Edwards-Spurgeon observer for fault reconstruction

This section will describe one of the interesting properties of sliding mode observers which will be used for fault reconstruction/estimator based on the concept of the equivalent ‘output error injection signals’ which was proposed in [67, 68] and has become the basis for sensor FTC used in this chapter.

Consider a nominal linear system subject to faults described by

$$\dot{x}(t) = Ax(t) + Bu(t) + Df_i(t) \quad (5.17)$$

$$y(t) = Cx(t) + f_o(t) \quad (5.18)$$

It is assumed the matrices A, B, C, D are known. The signals f_i and f_o represent actuator and sensor faults respectively but it is assumed only $y(t)$ and $u(t)$ are measurable. Assume that an observer with the structure given in (5.13) has been designed. It is argued in [67, 68] that, *provided a sliding motion can be attained, estimates of f_i and f_o can be computed from approximating the equivalent control.*

5.4.1 Reconstruction of input faults

Consider the case when $f_o = 0$. During the sliding motion $\dot{e}_y = e_y = 0$. Therefore, the bottom partition of Equation (5.12) can be written as

$$0 = \mathcal{A}_{21}e_1 - \mathcal{D}_2f_i + \nu_{eq} \quad (5.19)$$

where ν_{eq} is the equivalent output error injection signal necessary to maintain sliding. Since \mathcal{A}_{11} is stable by construction and $\dot{e}_1 = \mathcal{A}_{11}e_1$, $e_1 \rightarrow 0$, therefore

$$\nu_{eq} \rightarrow \mathcal{D}_2f_i \quad (5.20)$$

As discussed in Chapter 3, the signal ν_{eq} is typically a discontinuous signal, and therefore an approximation must be used to recover the equivalent injection. In [67, 68], a continuous approximation

$$\nu_\delta = -\rho \|\mathcal{D}_2\| \frac{P_2 e_y}{\|P_2 e_y\| + \delta} \quad (5.21)$$

was proposed, where δ is a small positive scalar. Since $\text{rank}(\mathcal{D}_2) = q$ it follows from (5.20) that

$$f_i \approx -\rho \|\mathcal{D}_2\| (\mathcal{D}_2^T \mathcal{D}_2)^{-1} \mathcal{D}_2^T \frac{P_2 e_y}{\|P_2 e_y\| + \delta} \quad (5.22)$$

The right-hand side of the above ‘equation’ depends only on e_y and therefore can be computed online and so an approximation for f_i can be obtained in real time.

5.4.2 Reconstruction of output faults

Now consider the case when $f_i = 0$ but $f_o \neq 0$. Since the output of the plant is represented by Equation (5.18), it follows that

$$e_y = Ce - f_o \quad (5.23)$$

After some manipulation using (5.23), the new state estimation error system in the observer canonical form in (5.4) is given by

$$\begin{bmatrix} \dot{e}_1 \\ \dot{e}_y \end{bmatrix} = \begin{bmatrix} \mathcal{A}_{11} & 0 \\ \mathcal{A}_{21} & \mathcal{A}_{22}^s \end{bmatrix} \begin{bmatrix} e_1 \\ e_y \end{bmatrix} + \begin{bmatrix} 0 \\ I_p \end{bmatrix} \nu + \begin{bmatrix} \mathcal{A}_{12} \\ \mathcal{A}_{22} \end{bmatrix} f_o - \begin{bmatrix} 0 \\ I \end{bmatrix} \dot{f}_o \quad (5.24)$$

Note that f_o and \dot{f}_o appear as disturbances. Therefore, in order for sliding to be maintained, the nonlinear gain ρ in (5.16) must be sufficiently large in order to overcome the disturbance effect generated by f_o and \dot{f}_o . During sliding $\dot{e}_y = e_y = 0$, and therefore the bottom partition of Equation (5.24) becomes

$$0 = \mathcal{A}_{21}e_1 - \dot{f}_o + \mathcal{A}_{22}f_o + \nu_{eq} \quad (5.25)$$

when the dynamics of the sliding motion is fast, from the top partition of (5.24)

$$e_1 \approx -\mathcal{A}_{11}^{-1}\mathcal{A}_{12}f_o \quad (5.26)$$

When the output fault is slow varying, so that $\dot{f}_o \approx 0$, then substituting the above into (5.25) and rearranging, yields

$$\nu_{eq} \approx -(\mathcal{A}_{22} - \mathcal{A}_{21}\mathcal{A}_{11}^{-1}\mathcal{A}_{12})f_o \quad (5.27)$$

As in the actuator fault reconstruction case, the signal ν_{eq} can be calculated online using the approximation ν_{eq} given in (5.21). If $(\mathcal{A}_{22} - \mathcal{A}_{21}\mathcal{A}_{11}^{-1}\mathcal{A}_{12})$ is nonsingular, then

$$f_o \approx -(\mathcal{A}_{22} - \mathcal{A}_{21}\mathcal{A}_{11}^{-1}\mathcal{A}_{12})^{-1}\nu_{eq} \quad (5.28)$$

Note that even if $(\mathcal{A}_{22} - \mathcal{A}_{21}\mathcal{A}_{11}^{-1}\mathcal{A}_{12})$ is singular, Edwards *et al.* suggest in [67,68] that it may still be possible to reconstruct some of the sensor faults depending on the structure of the rank deficiency. Details and examples can be found in [67,68].

Remark: The above method as proposed in [67,68], has not included any modeling uncertainty in the analysis. Here, the idea has been to provide a simple analysis on how sliding mode observers can be used for fault reconstruction (see Figure 5.2). The above method was later improved for robust application in the presence by Tan & Edwards [201,202] using an LMI formulation. This approach will be used later in this chapter as a sensor fault estimator.

and the function $f_o : \mathbb{R}_+ \rightarrow \mathbb{R}^r$ is unknown but bounded so that

$$\|f_o(t)\| \leq \hat{a}(t) \quad (5.31)$$

where $\hat{a} : \mathbb{R}_+ \rightarrow \mathbb{R}_+$ is a known function. The signal $f_o(t)$ represents (additive) sensor faults and N_p represents a distribution matrix, which indicates which of the sensors providing measurements are prone to possible faults. Notice in this special case, all the states are assumed to be measured by sensors - which is normal for modern civil aircraft.

Remark: The assumption that only certain sensors are fault prone is a limitation. However in practical situations, some sensors may be more vulnerable to damage or may be more sensitive or delicate in construction than others, and so such a situation is not unrealistic. Also certain key sensors may have back-ups (hardware redundancy) and so essentially a fault-free signal can be assumed from a certain subset of the sensors.

The objective is to design a sliding mode observer in order to reconstruct the faults $f_o(t)$. As argued in [202] an effective way to do this is to first introduce a filter. Consider a new state $x_f \in \mathbb{R}^n$ that is a filtered version of y from (5.30), satisfying

$$\dot{x}_f(t) = -A_f x_f(t) + A_f(x_p(t) + N_p f_o(t)) \quad (5.32)$$

where $-A_f \in \mathbb{R}^{n \times n}$ is a stable matrix. Equations (5.29) and (5.32) can be combined to give a system of order $2n$ with states $x_a = \text{col}(x_p, x_f)$ in the form

$$\dot{x}_a(t) = A_a x_a(t) + B_a u(t) + F_a f_o(t) + M_a \xi(t, x_p) \quad (5.33)$$

$$x_f(t) = C_a x_a(t) \quad (5.34)$$

for appropriate $A_a \in \mathbb{R}^{(2n) \times (2n)}$, $B_a \in \mathbb{R}^{(2n) \times m}$, $C_a \in \mathbb{R}^{n \times (2n)}$, $F_a \in \mathbb{R}^{(2n) \times r}$ and $M_a \in \mathbb{R}^{(2n) \times q}$. For the uncertain system in (5.33) - (5.34) a sliding mode observer of the form

$$\dot{\hat{x}}_a(t) = A_a \hat{x}_a(t) + B_a u(t) - G_l e_y(t) + G_n \nu \quad (5.35)$$

will be considered. In (5.35) the discontinuous output error injection term

$$\nu = -\rho_o(t, y, u) \frac{P_o e_y}{\|P_o e_y\|} \quad \text{if } e_y \neq 0 \quad (5.36)$$

where $e_y(t) := C_a \hat{x}_a(t) - x_f(t)$ is the output estimation error and P_o is a symmetric positive definite matrix. The matrix G_l is a traditional observer gain used to make $(A_a - G_l C_a)$ stable and G_n must be chosen to ensure the nonzero eigenvalues of the matrix $(I - G_n (C_a G_n)^{-1} C_a) A_a$ (i.e. the poles of the associated reduced order sliding motion) are stable. The scalar function $\rho_o(\cdot)$ must be an upper bound on the uncertainty and the faults; for details see [202]. Tan & Edwards [202] have shown a sliding mode observer of the form (5.35)-(5.36), completely insensitive to the fault $f_o(t)$, exists if and only if

- A1) $\text{rank}(C_a F_a) = r$
- A2) no invariant zeros of (A_a, F_a, C_a) are in \mathbb{C}_+

It can be shown that provided the plant is open-loop stable these conditions can always be

met.¹ For an appropriate choice of $\rho_o(t, y, u)$ in (5.36), which must bound the uncertainty and the supremum of $\hat{a}(t)$ from (5.31), it can be shown that an ideal sliding motion takes place on $\mathcal{S}_o = \{e : C_a e = 0\}$ in finite time, where e is the state estimation error ($\hat{x}_a - x_a$). For details see [202]. During the ideal sliding motion, $e_y = \dot{e}_y = 0$ and the discontinuous signal ν must take on average a value to compensate for ξ and f_o to maintain sliding. The average quantity, denoted by ν_{eq} , is referred to as the *equivalent output error injection term*. The signal ν_{eq} can be approximated to any degree of accuracy, and is computable online as

$$\nu_\delta = -\rho_o(t, y, u) \frac{P_o e_y}{\|P_o e_y\| + \delta_o} \quad (5.37)$$

where δ_o is a small positive scalar. Consider as a fault reconstruction signal

$$\hat{f}_o := W \nu_\delta \quad (5.38)$$

where $W \in \mathbb{R}^{r \times n}$. In fact only $r \times (n - r)$ elements in W are freely assignable since W must be chosen to ensure that $W C_a F_a = I_r$. For details, see [202]. Then by straightforward manipulation it can be shown that the fault reconstruction signal from (5.38) satisfies

$$\hat{f}_o(t) = f_o(t) + \hat{G}(s) \xi(t, x_p) \quad (5.39)$$

where $\hat{G}(s)$ is a transfer function matrix which depends on the plant matrices A_a , M_a , the observer matrix G_n and the weighting matrix W . Tan & Edwards [202] propose minimizing the effect of ξ on the reconstruction \hat{f}_o by minimizing the \mathcal{L}_2 gain between ξ and \hat{f}_o . Because the relationship between the two signals is the transfer function matrix $\hat{G}(s)$, this is equivalent to minimizing the \mathcal{H}_∞ norm of $\hat{G}(s)$ [243]. With an appropriate change of variables, the problem of minimizing $\hat{\gamma} := \|\hat{G}(s)\|_\infty$ whilst satisfying the requirements of a feasible sliding mode observer design, can be cast as a well defined convex optimization problem and efficiently solved using Linear Matrix Inequality (LMI) methods [35]. In this chapter

$$G_l := \hat{\gamma}_0 P^{-1} C_a^T (D_1 D_1^T)^{-1} \quad (5.40)$$

where $\hat{\gamma}_0$ is a positive design scalar (an upper bound on $\hat{\gamma}$) and $D_1 \in \mathbb{R}^{n \times n}$ is a design parameter (which may be viewed as a covariance-like matrix associated with sensor noise). The s.p.d. matrix $P \in \mathbb{R}^{(2n) \times (2n)}$ is a Lyapunov matrix for the state estimation error system from which P_o in (5.36) and (5.37) is derived. Details of the formulae and the change of coordinates used to obtain a convex optimization problem are given in [202].

A general configuration representing the proposed sensor fault tolerant control scheme which will be used in this chapter is shown in Figure 5.3. In this particular figure, the specific output of the FDI component is the sensor fault estimate \hat{f}_o .

¹Open-loop stability is only a sufficient condition, more complicated necessary and sufficient conditions are discussed in [201] where unstable open-loop systems are considered.

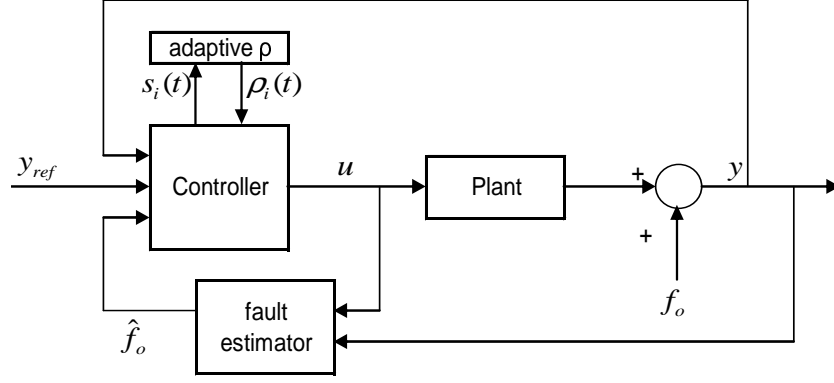


Figure 5.3: Schematic of the sensor fault implementation

5.5.2 closed-loop analysis

In this chapter, the estimated sensor fault \hat{f}_o will be used to correct the measured output signal so that $y - N_p \hat{f}_o$ will be the output of a ‘virtual sensor’ that will be used in the control law calculations to generate u . Suppose the corrected output measurement is given by \hat{x}_p then

$$\hat{x}_p := y - N_p \hat{f}_o = x_p + N_p (f_o - \hat{f}_o) \quad (5.41)$$

Also the integral action states from (4.6) in Chapter 4 are corrected so that

$$\dot{x}_d = y_c - C_c \hat{x}_p = y_c - C_c x_p - C_c N_p (f_o - \hat{f}_o) \quad (5.42)$$

After the coordinate change $x \mapsto T_r x = z$, and assuming for stability analysis purposes that $y_c \equiv 0$, then

$$\begin{bmatrix} \dot{z}_1 \\ \dot{z}_2 \end{bmatrix} = \begin{bmatrix} A_{11} & A_{12} \\ A_{21} & A_{22} \end{bmatrix} \underbrace{\begin{bmatrix} z_1 \\ z_2 \end{bmatrix}}_z + \underbrace{\begin{bmatrix} M_1 \\ M_2 \end{bmatrix}}_{T_r M} \xi - \underbrace{\begin{bmatrix} B_d^1 \\ B_d^2 \end{bmatrix}}_{T_r B_d C_c N_p} (f_o - \hat{f}_o) \quad (5.43)$$

where $z_2 \in \mathbb{R}^m$. By construction

$$f_o - \hat{f}_o = -\hat{G}(s)\xi(t, x_p)$$

and suppose $\hat{G}(s)$ has a state-space realization $(\hat{A}, \hat{B}, \hat{C}, \hat{D})$ with states $\hat{e} \in \mathbb{R}^{(n-p)}$ which implies $f_o - \hat{f}_o = -\hat{C}\hat{e} - \hat{D}\xi$. During a sliding motion, since \hat{x} is used in place of x in the control law (from Chapter 4), it follows $\hat{s}(t) = S\hat{x} = 0$ and so

$$S\hat{x} = 0 \Leftrightarrow ST_r^T T_r x + S\hat{N}_p (f_o - \hat{f}_o) = 0 \Leftrightarrow S_2 \begin{bmatrix} \mathcal{K} & I_m \end{bmatrix} z + S\hat{N}_p (f_o - \hat{f}_o) = 0 \quad (5.44)$$

where $\hat{N}_p^T = [0_{m \times m} \quad N_p^T]$ to account for the augmentation of the integral action states. From (5.44), during a sliding motion,

$$z_2(t) = -\mathcal{K}z_1(t) + S_2^{-1} S\hat{N}_p (\hat{C}\hat{e}(t) + \hat{D}\xi(t, x_p)) \quad (5.45)$$

Consequently, from (5.43), the reduced order sliding motion is governed by

$$\dot{z}_1(t) = (A_{11} - A_{12}\mathcal{K})z_1(t) + (A_{12}S_2^{-1}S\hat{N}_p + B_d^1)\left(\hat{C}\hat{e}(t) + \hat{D}\xi(t, x_p)\right) + M_1\xi(t, x_p) \quad (5.46)$$

$$\dot{\hat{e}}(t) = \hat{A}\hat{e}(t) + \hat{B}\xi(t, x_p) \quad (5.47)$$

By assumption $\|\xi(t, x_p)\| \leq \mathbf{C}_1\|z_p(t)\| + \mathbf{C}_2$. Consequently since

$$(\mathbf{C}_1\|z_p(t)\| + \mathbf{C}_2)^2 \leq 2\mathbf{C}_1^2\|z_p(t)\|^2 + 2\mathbf{C}_2^2$$

it follows from (5.45) that

$$\begin{aligned} \|\xi(t, x_p)\|^2 &\leq 2\mathbf{C}_1^2(\|z_1(t)\|^2 + \|z_2(t)\|^2) + 2\mathbf{C}_2^2 \\ &\leq 2\mathbf{C}_1^2\left((1+\|\mathcal{K}\|^2)\|z_1(t)\|^2 + \|S_2^{-1}S\hat{N}_p\hat{C}\|^2\|\hat{e}(t)\|^2 + \|S_2^{-1}S\hat{N}_p\|^2\|\hat{D}\|^2\|\xi(t, x_p)\|^2\right) + 2\mathbf{C}_2^2 \end{aligned}$$

Let $\alpha^2 := \max\{1 + \|\mathcal{K}\|^2, \|S_2^{-1}S\hat{N}_p\hat{C}\|^2\}$ and using the fact that

$$\|\hat{G}(s)\|_\infty < \hat{\gamma} \Rightarrow \|\hat{D}\| < \hat{\gamma}$$

means

$$\|\xi(t, x_p)\|^2 \leq 2\mathbf{C}_1^2\left(\alpha^2(\|z_1(t)\|^2 + \|\hat{e}(t)\|^2) + \|S_2^{-1}S\hat{N}_p\|^2\hat{\gamma}^2\|\xi(t, x_p)\|^2\right) + 2\mathbf{C}_2^2 \quad (5.48)$$

Suppose $2\mathbf{C}_1^2\hat{\gamma}^2\|S_2^{-1}S\hat{N}_p\|^2 < 1$, which will always be satisfied for a small enough $\hat{\gamma}$, then rearranging (5.48) yields

$$\begin{aligned} \|\xi(t, x_p)\|^2 &\leq \left(\underbrace{\frac{2\mathbf{C}_1^2\alpha^2}{(1 - 2\mathbf{C}_1^2\hat{\gamma}^2\|S_2^{-1}S\hat{N}_p\|^2)}}_{\hat{\mathbf{C}}_1^2} \left\| \begin{bmatrix} z_1(t) \\ \hat{e}(t) \end{bmatrix} \right\|^2 + \underbrace{\frac{2\mathbf{C}_2^2}{(1 - 2\mathbf{C}_1^2\hat{\gamma}^2\|S_2^{-1}S\hat{N}_p\|^2)}}_{\hat{\mathbf{C}}_2^2} \right) \\ &\leq \left(\hat{\mathbf{C}}_1 \left\| \begin{bmatrix} z_1(t) \\ \hat{e}(t) \end{bmatrix} \right\| + \hat{\mathbf{C}}_2 \right)^2 \end{aligned} \quad (5.49)$$

Notice that $\hat{\mathbf{C}}_1 \rightarrow 0$ as $\mathbf{C}_1 \rightarrow 0$, and so as the plant uncertainty decreases, the uncertainty in (5.46)-(5.47) diminishes. If $\xi(t, x_p) \equiv 0$ then (5.46)-(5.47) is stable since both $A_{11} - A_{12}\mathcal{K}$ and \hat{A} are stable by design. Consequently using Lyapunov arguments similar to those in §3.6 in [67], there exists a value of $\mathbf{C}_1 > 0$ for which the system (5.46)-(5.47) retains stability.

5.6 A Robust sensor fault reconstruction scheme for the B747

This section describes the development of the fault reconstruction scheme for the *full nonlinear high fidelity model* of the B747-100/200 aircraft. As in Section 4.2, a linearization of the B747 model about an operating condition of 300,000 Kg, 184 m/s true airspeed, and an altitude of

4000m at half maximum thrust has been obtained. The triple (A_p, B_p, C_p) is given by

$$A_p = \begin{bmatrix} -0.6803 & 0.0002 & -1.0490 & 0 \\ -0.1463 & -0.0062 & -4.6726 & -9.7942 \\ 1.0050 & -0.0006 & -0.5717 & 0 \\ 1 & 0 & 0 & 0 \end{bmatrix} \quad (5.50)$$

$$B_p = \begin{bmatrix} -1.5539 & 0.0154 \\ 0 & 1.3287 \\ -0.0398 & -0.0007 \\ 0 & 0 \end{bmatrix}, C_p = \begin{bmatrix} 1 & 0 & 0 & 0 \\ 0 & 1 & 0 & 0 \\ 0 & 0 & 1 & 0 \\ 0 & 0 & 0 & 1 \end{bmatrix} \quad (5.51)$$

A key aspect of the design is to establish the matrix M_p from (5.29) which captures the discrepancy between the nonlinear and linear models. A much more accurate model is required here for analytical redundancy purposes than for the controller design. Prior to obtaining the matrix M_p , the second state (V_{tas}) has been scaled by 0.1 and therefore the plant system triple (A_p, B_p, C_p) is transformed by the matrix given by $T_s = \text{diag}(1, 0.1, 1, 1)$. This has been done so that the magnitude of each of the states is comparable. Uniformly sampled data at 10Hz was collected from the nonlinear (open-loop) simulation which was excited using a PRBS signal (see Figure 5.4) with amplitude 1 deg in the elevator channel. An estimate of the derivatives of each of the state space vector components was obtained numerically (off-line) and an error vector $e_p := \dot{x} - Ax - Bu$ was then computed for each sample.

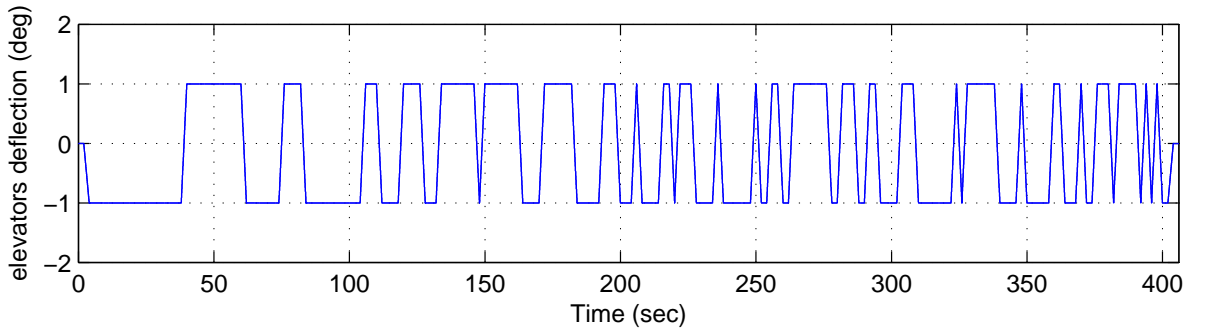
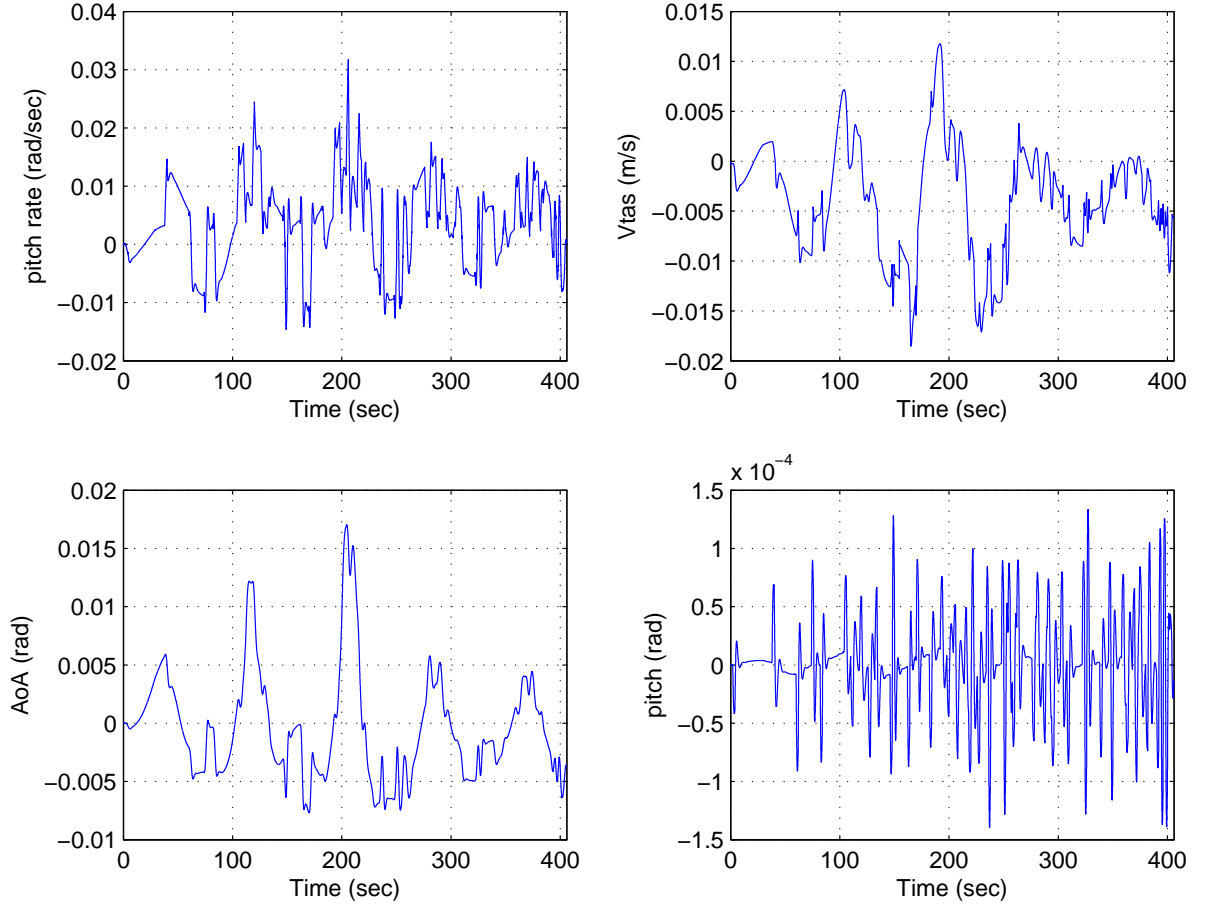


Figure 5.4: PRBS signal

In terms of the uncertainty model from (5.29) $\{e_p\} = M_p\{\xi\}$. Figure 5.5, shows the four components of the signals e_p . Principal component analysis on the signals e_p using singular value decomposition of the matrix $e_p^T e_p$ has been employed to compute M_p . This is based on the procedure proposed by Chen & Patton [50]. The singular values of the matrix $e_p^T e_p \in \mathbb{R}^{4 \times 4}$ are given by $\{3.2332, 1.9011, 0.3644, 0.0001\}$. The first two are significantly larger than the last two and so M_p has been chosen as the eigenvectors associated with the first two singular values giving

$$M_p = \begin{bmatrix} -0.8562 & 0.4262 \\ -0.3149 & -0.8786 \\ -0.4049 & -0.2155 \\ 0.0000 & -0.0000 \end{bmatrix} \quad (5.52)$$

Details of the justification of this appear in [50]. Note that the elements in the last row of

Figure 5.5: Plots of $e_p = \dot{x} - Ax - Bu$

M_p are small compared to the others. This is in accordance with the observation that pitch (the last state) is the integral of pitch rate, and therefore no modeling uncertainty is present. Once the matrix M_p from (5.33) has been obtained, the observer gains G_l and G_n and the reconstruction weighting matrix W can be synthesized using the LMI optimization proposed in [202]. The choice of the filter matrix A_f impacts on the performance of the system. If the absolute value of the eigenvalues of A_f are small then the bandwidth of the filtering properties is decreased. Consequently, during sliding, although the output of the observer may track the filtered outputs of the plant perfectly, the outputs of the observer no longer necessarily track the true output of the plant as accurately – consequently there is a reduction in performance in terms of the state estimation properties. Conversely, large negative eigenvalues for A_f improve the state estimation performance. However the state estimation performance is not the key criteria here. More importantly, the choice of A_f affects the optimal value of $\hat{\gamma} = \|\hat{G}(s)\|_\infty$. Often if the bandwidth of the filter associated with A_f is lower than the natural frequency of any oscillatory modes in the plant, then the optimal value of $\hat{\gamma}$ which is obtained from the LMIs may be reduced/improved, and consequently smaller eigenvalues for A_f maybe preferable. Therefore the selection of A_f is a crucial part of the initial design iteration. Here A_f from Equation (5.32) has been chosen as

$$A_f = 0.01 \times I_4$$

Assume that the pitch rate q , true air speed V_{tas} and angle of attack α measurements are

fault-free and therefore N_p from Equation (5.30) is defined as

$$N_p^T = [0 \ 0 \ 0 \ 1]$$

Using the fault reconstruction method based on the observer described in §5.5.1 applied to the augmented system, and choosing $D_1 = \text{diag}(0.1 \ 0.11 \ 0.1 \ 0.1)$ and $\hat{\gamma}_o = 0.003$, the following observer gains have been obtained from the LMI scheme proposed in [202]

$$G_l = \begin{bmatrix} 0.3325 & -4.5479 & -1.3616 & -0.6191 \\ -8.0016 & 74.7746 & -1.1413 & -12.9629 \\ 1.8657 & -0.0352 & 1.4094 & 1.7649 \\ 3.2872 & -11.6213 & 2.6326 & 4.8176 \\ 0.0324 & -0.1128 & 0.0248 & 0.0461 \\ -0.1365 & 1.6228 & -0.0029 & -0.2522 \\ 0.0248 & -0.0024 & 0.1640 & 0.1631 \\ 0.0461 & -0.2084 & 0.1631 & 0.3181 \end{bmatrix}$$

$$G_n = \begin{bmatrix} 8.0739 & -2.2555 & -9.5628 & -0.0000 \\ -81.3037 & 40.4364 & 6.0311 & 0.0000 \\ 85.9276 & 5.9437 & -4.2736 & 0.0000 \\ 99.8244 & -0.2224 & 0.9782 & 0.0000 \\ 1.0000 & 0 & -0.0000 & 0.0000 \\ 0.0000 & 1.0000 & 0.0000 & 0.0000 \\ 0 & 0 & 1.0000 & 0 \\ -0.0000 & 0.0000 & -0.0000 & 1.0000 \end{bmatrix}$$

where

$$P_o = \begin{bmatrix} 15.7240 & 1.0217 & -1.8273 & -0.5313 \\ 1.0217 & 0.2582 & -0.4207 & 0.2724 \\ -1.8273 & -0.4207 & 4.4240 & -2.3378 \\ -0.5313 & 0.2724 & -2.3379 & 2.4352 \end{bmatrix}$$

and the injection scaling matrix from (5.38) is

$$W = \begin{bmatrix} 0.8295 & 1.0211 & -2.5213 & 100.0000 \end{bmatrix}$$

It can be shown that with this choice of gains

$$\|\hat{G}(s)\|_\infty = 5.8668 \times 10^{-4}$$

The choice of the design matrix D_1 has been used to fine tune the observer gain G_l , while $\hat{\gamma}_o$ is chosen to be small to ensure that the \mathcal{H}_∞ norm of $\hat{G}(s)$ from Equation (5.39) is small (which means that the fault reconstruction will be less affected by the uncertainty). When trying to ensure that the \mathcal{H}_∞ norm of $\hat{G}(s)$ is small (using a small $\hat{\gamma}_o$), the observer gain G_l might become large and unrealistic for implementation. Therefore in terms of design there

is a tradeoff between obtaining a small $\hat{\gamma}$ and a realistic observer gain G_l . The simulation parameters from Equation (5.37) were chosen as $\rho_o = 50$ and $\delta_o = 0.005$. A large ρ_o is required to ensure that sliding still occurs in the presence of uncertainty and faults; and a small δ_o is necessary to closely approximate the discontinuous switching injection. The ν_{eq} signal used for the reconstruction is filtered using a first order low pass filter with time constant 0.1 before being scaled by the weighting matrix W . This filtering operation is quite in keeping with the notion of the equivalent injection being the low frequency component of ν [210]. In the same way, other observers can be designed to specifically reconstruct faults on the angle of attack and pitch rate measurement signals.

5.7 Sensor Fault Tolerant Control Simulation Results

The effect of feeding faulty sensor signals into the controller has been investigated. For comparison purposes, the performance of the scheme in Figure 5.3 has been measured using the root mean square (RMS) of the FPA tracking error. As in Section 4.3.5 in Chapter 4, the same flight conditions and controller have been used. The following subsections will discuss the different scenarios for testing the observer based schemes which have been designed. First a nominal no-fault condition is considered. Then the scenario in which a fault occurs and fault reconstruction is not used is discussed, to see the effect of the corrupted signals on the performance of the controller from Section 4.3. Finally the FTC scheme from Figure 5.3 is employed in the presence of faults, using a sliding mode fault reconstruction scheme. *Note that the simulations are done on the full 77 state nonlinear high fidelity model of the B747-100/200.*

5.7.1 Fault-free simulation

The fault-free performance of the controller is given in Figure 5.6. The reference command requests a change in flight path angle of 3 deg for 20 sec followed by a 20 m/s change in speed over a period of 45 sec (in 2 steps). The command sequence for the FPA demand is then reversed after 250 sec so that the aircraft is returned to (approximately) the initial flight conditions. (The results presented in the following figures do not include the trim values for ease of interpretation). Since the design of the FDI assume that the measurement for V_{tas} is free from faults, only the FPA tracking error is shown, and the RMS value is used as a measure of the controller performance. Figure 5.7(a) shows the FPA tracking error when no fault is present. The root mean square (RMS) of the error signal is 0.0150.

5.7.2 Fault simulations: FDI switched off

Figure 5.7(b) shows the FPA tracking error when the corrupted pitch signal (from a faulty sensor) is directly used by the controller. The fault signal was set as a sensor drift represented by a positive ramp signal starting from zero at the beginning of the simulation, with a peak of 5.73deg at 250 seconds and then a negative ramp back to zero at 500 seconds (as in Figure 5.9(a)). When the corrupted pitch signal is used directly by the controller, Figure 5.7(b) shows a significant degradation in the performance of the FPA tracking error. A RMS value of 0.1969

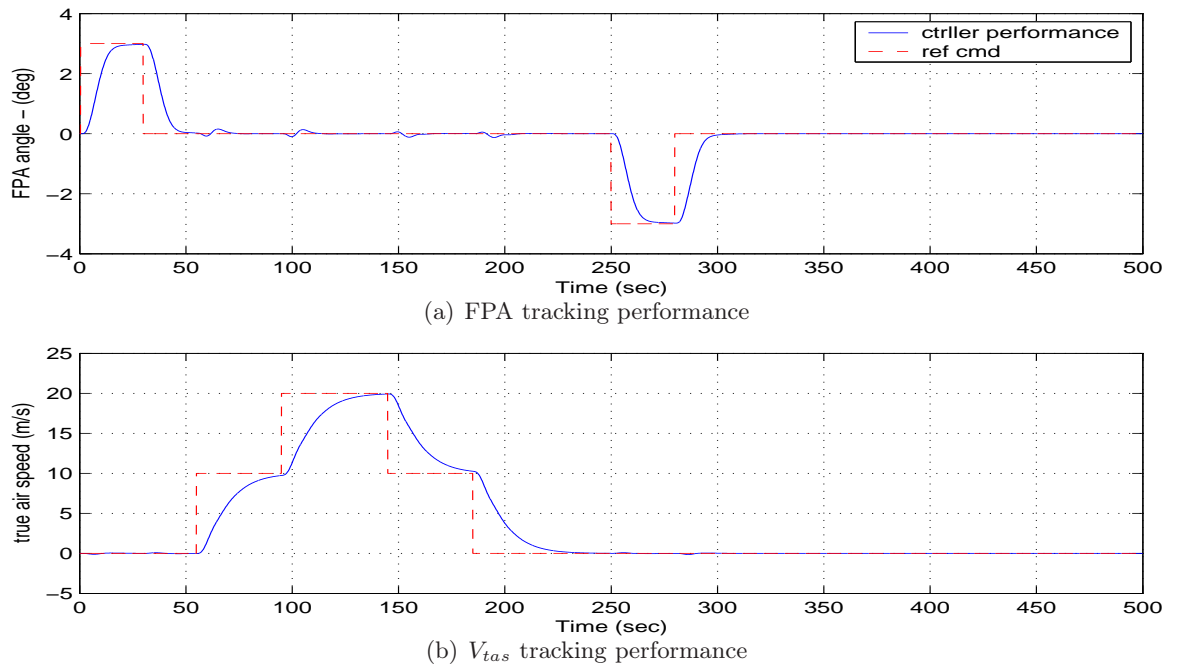


Figure 5.6: Fault-free controller responses

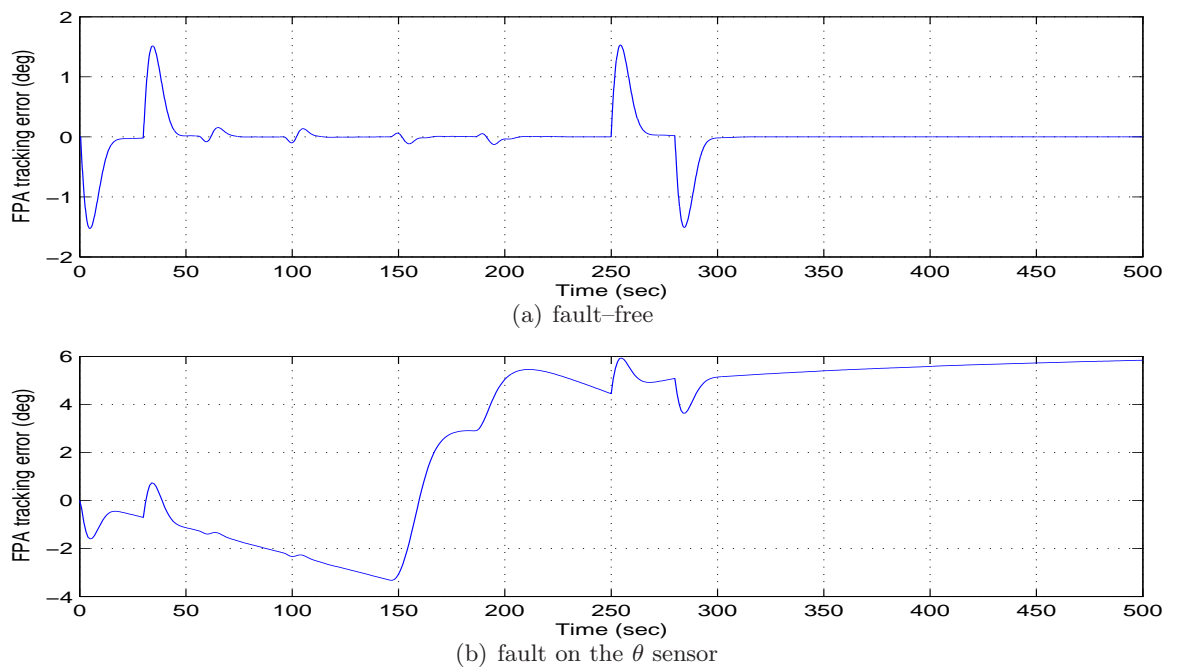


Figure 5.7: Fault simulation: FPA tracking error: fault-free & with fault (FDI switched off)

is observed compared to 0.0150 in the fault-free case (Figure 5.7(a)). In the subsequent tests, the FDI scheme will be switched on and the performance of the FTC from Figure 5.3 will be evaluated when the fault reconstruction signal is used to correct the corrupted sensor signal before being used by the controller. As before, the same set of flight conditions and tests, using the same controller and command references, will be performed under the scenario that there is a fault on the θ measurement.

5.7.3 Fault simulation: FDI switched on

Figure 5.8 shows the corrupted plant output with an error on the pitch (θ) measurement. Figure 5.8 also shows that the observer states track the filtered plant outputs closely (they overlap on top of each other). The filtering effect is clearly visible in Figure 5.8 where the filtered plant and observer output are different from the (actual) plant output. Here, the objective of the observer is to provide a good estimate of the faults; however, the plant state estimates are compromised by the low pass filter. Figure 5.9(a) shows the reconstructed θ sensor fault. The corrupted measured pitch signal (Figure 5.8) is corrected by the fault estimation signal in Figure 5.9(a) before being used by the controller. The closed-loop performance of the aircraft is given in Figure 5.9(b). The RMS of 0.0154 in Figure 5.9(b) is better than the one in Figure 5.7(b) (0.1969), which shows that the sensor fault reconstruction has enabled the controller to maintain the required performance in the presence of a sensor fault.

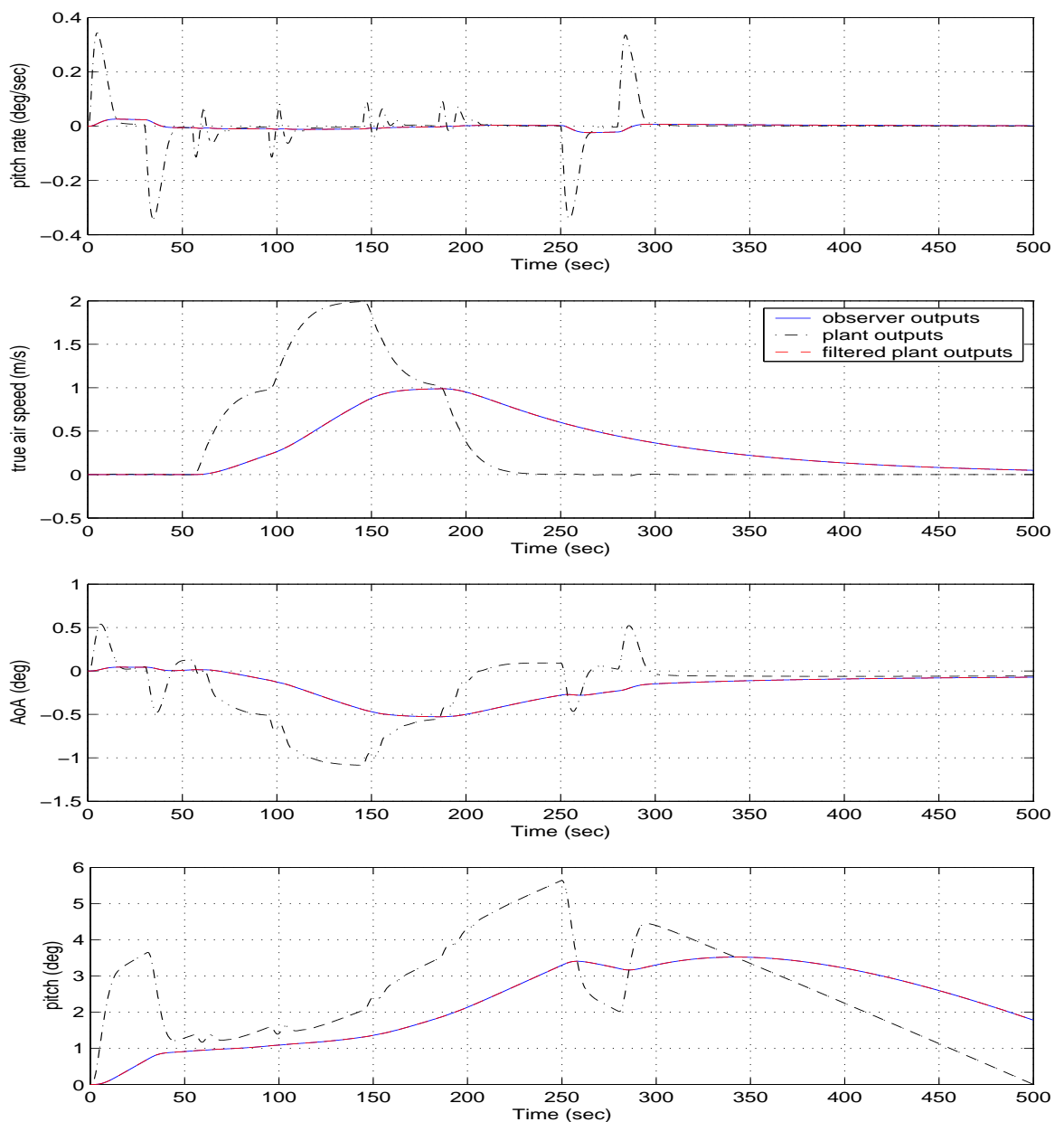


Figure 5.8: FDI on: fault simulation: corrupted plant outputs

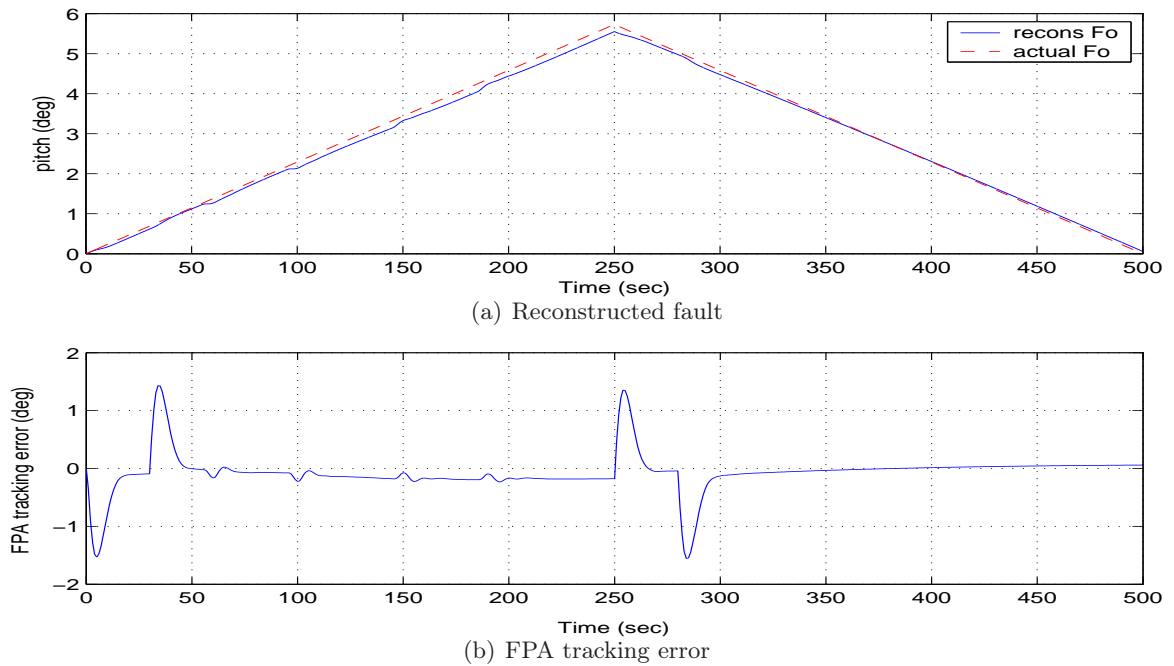


Figure 5.9: Fault simulation responses: FDI switched on (without trim values)

5.7.4 Fault simulations with sensor noise

Figure 5.10 shows the simulation results under similar conditions to the previous tests but with the addition of (bounded) sensor noise. The noise has been implemented using a scaling of the band limited white noise block in SIMULINK² with a noise power of 0.01 and sampling time of 0.1. Figure 5.10 shows satisfactory sensor fault reconstruction in the presence of noise.

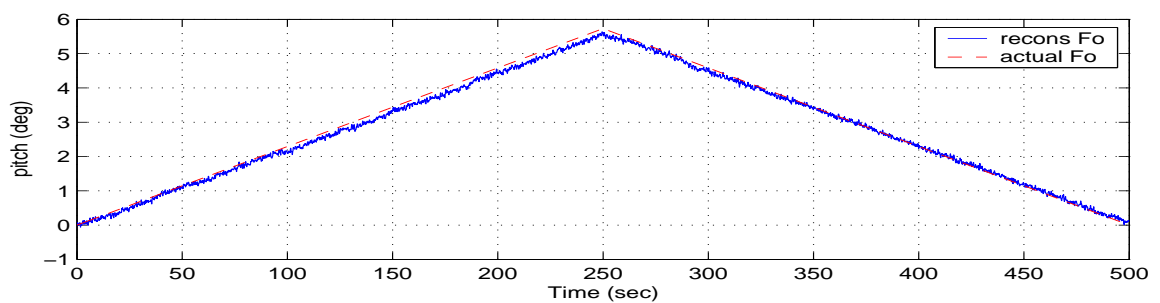


Figure 5.10: sensor fault reconstruction with noise

5.7.5 Threshold selection

The reconstruction schemes above have been implemented on the full nonlinear model of the B747-100/200 using FTLAB747 V6.5. The observers have been run under the assumption that the measurement of true air speed V_{tas} is fault-free. In the event of a pitch sensor fault, a reconstruction from the FDI provides the fault estimation. Note that in a nominal fault-free scenario, the FDI will not be switched on to correct the signals used in the controller because they would degrade the performance since the reconstructions are not perfect. The simplest approach would be to use the correction signals only if the fault estimate exceeds a predetermined

²®MATHWORKS trademark

threshold value indicating the presence of a fault. An initial estimate of the required thresholds can be obtained using the reconstruction scheme in a fault-free situation. Figure 5.11 shows the fault reconstruction signals when no fault is present. The selected threshold values need to be larger than the ‘normal’ variations in the fault estimation signals, to avoid false alarms, but not too large to miss faults. In the above simulations, the threshold values can be chosen as ± 0.3 deg for the pitch angle sensor.

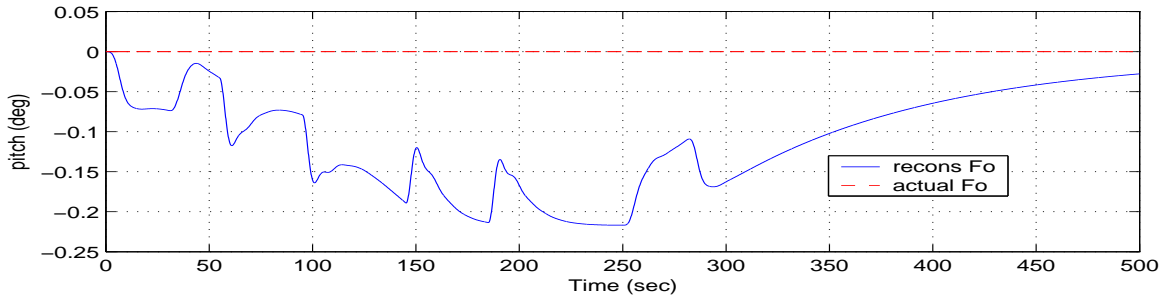


Figure 5.11: fault-free simulation: fault reconstruction signal - threshold selection

5.8 Conclusions

This chapter has introduced the concept of a sliding mode observer and highlighted the capabilities and benefits of sliding mode observers as a means of fault reconstruction and sensor fault tolerant control. Most of the existing results in the literature for the B747-100/200 civil aircraft benchmark (using FTLAB747) have focused on ‘actuator’ faults or parametric faults, this chapter has presented a sensor fault reconstruction and sensor fault tolerant control scheme. The scheme is based on the reconstruction of sensor faults using a sliding mode observer. The fault reconstructions are then used to correct the measured outputs before being used in the controller calculations and therefore the controller does not need to be reconfigured. Another contribution of this chapter is a theoretical analysis of the closed-loop system using a Lyapunov technique. The scheme is also shown to work in the presence of sensor noise.

Chapter 6

Fault Tolerant Control Using Sliding Modes with On–line Control Allocation

In Chapter 4, SMC has been shown to handle actuator faults without requiring any FDI. However, sliding mode methods are still hampered by one drawback; the inability to directly handle actuator failures¹. In Chapter 4, a simple example showed that when an elevator fails, the horizontal stabilizer can be used to generate the same pitch manoeuvre. In Chapter 4, the control signal to the elevator was simply rerouted to the stabilizer as the relationship between the stabilizer and the elevator is roughly known. The idea of using a single controller which can redistribute the control signals to ‘redundant’ actuators is appealing. It avoids the need of having many controllers or a bank of controllers for each type of fault or failure as required by other strategies in the FTC literature. It also removes the requirement of switching between controllers when faults/failures occur and the associated bumpless transfer issues.

This chapter will further explore the idea from Chapter 4 of rerouting control signals using a strategy called control allocation (CA). The combination of CA with SMC seems to have enormous benefit. The CA provides SMC with access to redundant actuators enabling SMC to handle actuator failures directly; thus opening new and exciting ways of achieving FTC. The combination of sliding modes and CA is not totally new – examples can be found in papers such as [185, 219] – however, none of these papers discussed in detail the analysis and conditions for stability of SMC when combined with CA. This will be explored further in this chapter. Furthermore, in this chapter, a novel control allocation strategy is applied where the control signal distribution is based on the actuator effectiveness.

6.1 Introduction

In most safety critical systems e.g. passenger aircraft [37] and modern fighter aircraft [75], there is actuator redundancy. This gives freedom to design FTC systems to maintain stability and acceptable performance during faults and failures. CA is one approach to manage the actuator redundancy for different control strategies handling actuator faults (see for example [40, 58]).

¹This drawback is also inherent in almost all traditional feedback control paradigms such as LQR , H_∞ and μ -synthesis

There is extensive literature on CA which discusses different algorithms, approaches and applications: [70] discusses two (broadly) linked approaches (linear and quadratic programming) based on finding the ‘best solution’ to a system of linear equations. The work in [95] compares control allocation with optimal control design for distributing the control effort among redundant actuators. In [41] the authors demonstrate that feedback control systems with redundant actuators can be reduced to a feedback control system without redundancy using a special case of CA known as ‘daisy chaining’. In this approach, a subset of the actuators, regarded as the primary actuators are used first, then secondary actuators are used if the primary actuators reach saturation. Other CA approaches which take into account actuator limits are discussed in [31, 34].

The work in [40, 58] uses CA as a means for FTC. The benefits of CA is that the controller structure does not have to be reconfigured in the case of faults and it can deal directly with total actuator failures without requiring reconfiguration/accommodation of the controller: the CA scheme automatically redistributes the control signal. This is the facet of CA that will be explored in this chapter. The work in [185, 219] provides practical examples of the combination of SMC and CA for FTC. The work by Shin *et al.* [181] uses control allocation ideas, but formulates the problem from an adaptive controller point of view. However neither of these papers provide a detailed stability analysis and discuss sliding mode controller design issues when using control allocation. Recent work by Corradini *et al.* [55] shows that total failures can be dealt with by SMC schemes provided that there is enough redundancy in the system. However [55] considers exact duplication of actuators to achieve redundancy, whereas in many over actuated systems, the redundant actuators do not have identical dynamics to the ‘primary’ actuators.

In this chapter, a combination of SMC and CA will be explored to achieve FTC. A rigorous design procedure is developed from a theoretical perspective. The proposed scheme has been tested in simulation on an aircraft model which has been used in the literature to demonstrate a CA scheme [95]. The control strategy uses the effectiveness level of the actuators and redistributes the control to the remaining actuators when faults/failures occur. This is the novelty of this chapter compared to the work in [55, 185, 219]. This chapter is structured as follows: Section 6.2 describes the problem formulation and develops the main results of the chapter including the stability analysis of the proposed sliding mode control allocation scheme and the design of the control laws; Section 6.5 gives a brief description of the ADMIRE aircraft model and the fault and failure scenarios used as examples to illustrate the proposed method; finally Section 6.6 draws some conclusions.

6.2 Controller Design

Consider the n th order linear time invariant system with m inputs given by

$$\dot{x}(t) = Ax(t) + Bu(t) \tag{6.1}$$

where $A \in \mathbb{R}^{n \times n}$ and $B \in \mathbb{R}^{n \times m}$ with $1 \leq m < n$. In most of the CA literature, it is assumed that B can be factorized as

$$B = B_\nu N \quad (6.2)$$

where $B_\nu \in \mathbb{R}^{n \times l}$, $N \in \mathbb{R}^{l \times m}$ and both have rank $l < m$ [95]. Then the ‘virtual control input’ [95] is defined as

$$\nu(t) := Nu(t) \quad (6.3)$$

where $\nu(t) \in \mathbb{R}^l$ can be interpreted as the total control effort produced by the actuators [95]. Typically the control law $\nu(t)$ is designed based on the pair (A, B_ν) which is assumed to be controllable. Direct manipulation of Equation (6.3) gives

$$u(t) = N^\dagger \nu(t) \quad (6.4)$$

where $N^\dagger \in \mathbb{R}^{m \times l}$ is a right pseudo-inverse of matrix N , so that $NN^\dagger = I_l$. Note that the choice of N^\dagger is not unique. One choice for N^\dagger is obtained from the following minimization problem:

$$\min_u u^T W^{-1} u \quad \text{subject to } Nu = \nu \quad (6.5)$$

where $W \in \mathbb{R}^{m \times m}$ is a symmetric positive definite (s.p.d) diagonal weighting matrix [95, 164]. This minimizes at each time instant the ‘weighted sum of squares’ cost, associated with the control vector u . The optimal solution to (6.5) is $u = N^\dagger \nu$ where

$$N^\dagger := WN^T(NWN^T)^{-1} \quad (6.6)$$

Often in the literature, W from (6.5) and (6.6) is set to the identity [181, 185, 219], which gives the classical Moore-Penrose pseudo-inverse [99]. Another approach is to choose the weighting W to be a diagonal matrix formed from the control surface limits squared [40, 58]. In this way, W scales each control surface based upon deflection limits to equally distribute the control effort [40] (assuming symmetric position limits and no rate limits).

6.2.1 Problem Formulation

This chapter considers a situation where a fault develops in system (6.1) associated with the actuators. It will be assumed that in the event of actuator faults or failures, Equation (6.1) can be rewritten as

$$\dot{x}(t) = Ax(t) + Bu(t) - BK(t)u(t) \quad (6.7)$$

with $K(t) = \text{diag}(k_1(t), \dots, k_m(t))$ where the $k_i(t)$ are scalars satisfying $0 \leq k_i(t) \leq 1$. These scalars, model a decrease in effectiveness of a particular actuator. If $k_i(t) = 0$, the i th actuator is working perfectly whereas if $k_i(t) > 0$, a fault is present, and if $k_i(t) = 1$ the actuator has failed completely.

In this chapter, a novel choice of weighting matrix W will be considered. If information about the actuator faults is available from a fault detection and isolation (FDI) scheme so that the actuator effectiveness values k_i are known, the control signal from the ‘virtual control’ $\nu(t)$ can be redistributed to the remaining working actuators using W in (6.6). Here, the weight W has

been chosen as

$$W = I - K \quad (6.8)$$

As a direct consequence, $W = \text{diag}\{w_1, \dots, w_m\}$ and the diagonal elements $w_i = 1 - k_i$. As $k_i \rightarrow 1$, $w_i \rightarrow 0$ and so the associated control component u_i in (6.5) is weighted heavily since $\frac{1}{w_i}$ becomes large. Note in a fault-free situation $W = I$ (a common choice in the CA literature [181, 185, 219]).

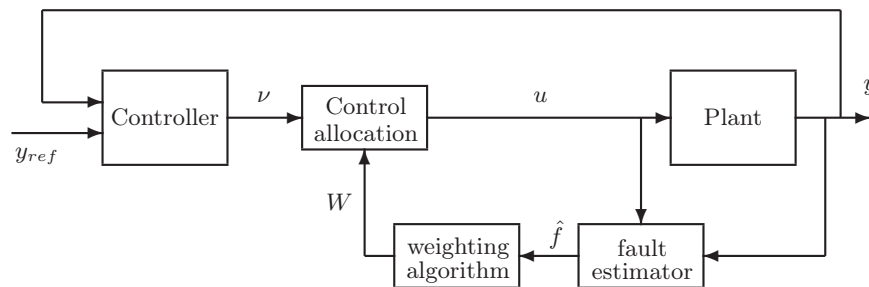


Figure 6.1: Control allocation strategy

Figure 6.1 illustrates the FTC control allocation strategy. The control allocation will depend on the effectiveness of the actuators. The information necessary to compute W on-line can be supplied by a fault reconstruction scheme as described in [202] for example, or by using a measurement of the actual actuator deflection compared to the demand which is available in many systems e.g. passenger aircraft [37]. Alternatively other fault reconstruction schemes based on Kalman filters [242] can be used. From (6.8) if an actuator fault occurs, the weighting W will be changed on-line and the control input $u(t)$ is reallocated to minimize the use of the faulty control surface. In the event of total failure of the i th control surface, $k_i \rightarrow 1$ and therefore the i th component of W^{-1} becomes large. Hence, $u_i(t)$ is totally re-routed to the other actuators (provided there is enough redundancy in the system).

In many systems with actuator redundancy, the assumption in Section 6.2 that $\text{rank}(B) = l$ is not valid and hence the perfect factorization in (6.2) cannot hold². However the system states can always be reordered, and the matrix B from (6.2) can be partitioned as:

$$B = \begin{bmatrix} B_1 \\ B_2 \end{bmatrix} \quad (6.9)$$

where $B_1 \in \mathbb{R}^{(n-l) \times m}$ and $B_2 \in \mathbb{R}^{l \times m}$ has rank l . The separating of the control law from the control allocation task comes naturally with design methods like feedback linearization and backstepping, which employ intermediate ‘virtual control’ signals [26, 94]. In most aircraft and submersible systems the control objectives can be achieved by commanding some desired moment to be generated by the control surfaces [26, 94]: in aircraft systems for example, the channels associated with B_2 are the equations of angular acceleration in roll, pitch and yaw [95]. Here it is assumed that the matrix B_2 will represent the dominant contribution of the control action on the system. This will be discussed formally later in the chapter. In [181], it is assumed that $B_1 = 0$. This represents the extreme situation where the total effect of the control is through B_2 only. Here $B_1 \neq 0$ will be considered explicitly in the controller design

²See for example (6.70), where $\text{rank}(B) = 4$ and l , which relates to the choice of B_2 in (6.9), is $l = \text{rank}(B_2) = 3$. Similarly in (7.2) and (7.4), $\text{rank}(B) = 3$ whilst $l = \text{rank}(B_2) = 2$.

and in the stability analysis. It will be assumed without loss of generality that the states of the system in (6.1) have been transformed so that $B_2 B_2^T = I_l$ and therefore $\|B_2\| = 1$. This is always possible since $\text{rank}(B_2) = l$. Let the ‘virtual control’

$$\nu(t) = B_2 u(t) \quad (6.10)$$

so that analogously to Section 6.2

$$u(t) = B_2^\dagger \nu(t) \quad (6.11)$$

where

$$B_2^\dagger := W B_2^T (B_2 W B_2^T)^{-1} \quad (6.12)$$

The fault term from (6.7), $BK u(t) = BK B_2^\dagger \nu(t)$; and therefore (6.7) becomes

$$\dot{x}(t) = Ax(t) + \underbrace{\begin{bmatrix} B_1 B_2^\dagger \\ I_l \end{bmatrix}}_{B_\nu} \nu(t) - \begin{bmatrix} B_1 K B_2^\dagger \\ B_2 K B_2^\dagger \end{bmatrix} \nu(t) \quad (6.13)$$

The objective is to use SMC techniques, to synthesize the ‘virtual control’ $\nu(t)$. Define a switching function $s(t) : \mathbb{R}^n \rightarrow \mathbb{R}^l$ to be

$$s(t) = Sx(t) \quad (6.14)$$

where $S \in \mathbb{R}^{l \times n}$ and $\det(SB_\nu) \neq 0$. Let \mathcal{S} be the hyperplane defined by $\mathcal{S} = \{x(t) \in \mathbb{R}^n : Sx(t) = 0\}$. If a control law can be developed which forces the closed-loop trajectories onto the surface \mathcal{S} in finite time and constrains the states to remain there, then an ideal sliding motion is said to have been attained. The selection of the sliding surface is the first part of any design and defines the system’s closed-loop performance. The sliding surface will be designed based on the nominal no fault condition ($K = 0$). The second aspect of the control design, is the synthesis of a control law to guarantee that the surface is reached in finite time and a sliding mode is subsequently maintained.

Using the fact that $K = I - W$ and $B_2 B_2^\dagger = I_l$, it follows that Equation (6.13) can be written as

$$\dot{x}(t) = Ax(t) + \begin{bmatrix} B_1 W^2 B_2^T (B_2 W B_2^T)^{-1} \\ B_2 W^2 B_2^T (B_2 W B_2^T)^{-1} \end{bmatrix} \nu(t) \quad (6.15)$$

If

$$\bar{\nu}(t) := (B_2 W B_2^T)^{-1} \nu(t) \quad (6.16)$$

then it is easy to see that (6.15) can be written as

$$\dot{x}(t) = Ax(t) + \begin{bmatrix} B_1 B_2^T \\ I \end{bmatrix} \bar{\nu}(t) - \begin{bmatrix} B_1 (I - W^2) B_2^T \\ B_2 (I - W^2) B_2^T \end{bmatrix} \bar{\nu}(t) \quad (6.17)$$

In the fault-free case $W = I$ and the nominal system is

$$\dot{x}(t) = Ax(t) + \begin{bmatrix} B_1 B_2^T \\ I \end{bmatrix} \bar{v}(t) \quad (6.18)$$

Notice that the virtual input distribution matrix in (6.17) and (6.18) is independent of W compared to the B_ν in (6.13). From the representation in (6.18), a coordinate transformation $x \mapsto T_r x(t) = \hat{x}(t)$ will be introduced to obtain ‘regular form’ which is a convenient representation from which to design the hyperplane. If

$$T_r := \begin{bmatrix} I & -B_1 B_2^T \\ 0 & I \end{bmatrix} \quad (6.19)$$

then it is easy to check that Equation (6.17) becomes:

$$\dot{\hat{x}}(t) = \hat{A}\hat{x}(t) + \underbrace{\begin{bmatrix} 0 \\ I \end{bmatrix}}_{\hat{B}_\nu} \bar{v}(t) - \begin{bmatrix} B_1 B_2^N (I - W^2) B_2^T \\ B_2 (I - W^2) B_2^T \end{bmatrix} \bar{v}(t) \quad (6.20)$$

where $\hat{A} := T_r A T_r^{-1}$ and

$$B_2^N := (I - B_2^T B_2) \quad (6.21)$$

Because by construction the matrix $B_2 B_2^T = I_l$, it follows that $B_2^N B_2^T = (I - B_2^T B_2) B_2^T = 0$, and therefore

$$B_1 B_2^N (I - W^2) B_2^T = -B_1 B_2^N W^2 B_2^T \quad (6.22)$$

Therefore Equation (6.20) becomes

$$\dot{\hat{x}}(t) = \hat{A}\hat{x}(t) + \begin{bmatrix} 0 \\ B_2 W^2 B_2^T \end{bmatrix} \bar{v}(t) + \begin{bmatrix} B_1 B_2^N W^2 B_2^T \\ 0 \end{bmatrix} \bar{v}(t) \quad (6.23)$$

The last term in (6.23) is zero in the fault-free case, but is treated as (unmatched) uncertainty when $W \neq I$. Define another nonsingular scaling of the virtual control signal as

$$\hat{v}(t) := (B_2 W^2 B_2^T) \bar{v}(t) \quad (6.24)$$

therefore, (6.23) becomes

$$\begin{bmatrix} \dot{\hat{x}}_1(t) \\ \dot{\hat{x}}_2(t) \end{bmatrix} = \begin{bmatrix} \hat{A}_{11} & \hat{A}_{12} \\ \hat{A}_{21} & \hat{A}_{22} \end{bmatrix} \begin{bmatrix} \hat{x}_1(t) \\ \hat{x}_2(t) \end{bmatrix} + \begin{bmatrix} 0 \\ I \end{bmatrix} \hat{v}(t) + \begin{bmatrix} B_1 B_2^N B_2^+ \\ 0 \end{bmatrix} \hat{v}(t) \quad (6.25)$$

where

$$B_2^+ := W^2 B_2^T (B_2 W^2 B_2^T)^{-1} \quad (6.26)$$

It is important to point out that there is an upper bound on the norm of the pseudo-inverse B_2^+ in (6.26) which is independent of W . Formally:

Proposition 2 *There exists a scalar γ_0 which is finite and independent of W such that*

$$\|B_2^+\| = \|W^2 B_2^T (B_2 W^2 B_2^T)^{-1}\| < \gamma_0 \quad (6.27)$$

for all $W = \text{diag}(w_1 \dots w_m)$ such that $0 < w_i \leq 1$.

Proof: This follows from a modification of the proof of Theorem 1 in [196]. The work in [196] considers left pseudo-inverses but since $(B_2^+)^T = (B_2^T)^+$, the result follows. ■

Remark 1: As shown in [196], if W is not diagonal, $\|B_2^+\|$ is no longer necessarily bounded.

The virtual control law will now be designed based on the nominal fault-free system in which the top partition of the last term in (6.25) is zero since $B_1 B_2^N B_2^+|_{W=I} = 0$. In the $\hat{x}(t)$ coordinates in (6.25), a suitable choice for the sliding surface is

$$\hat{S} = S T_r^{-1} = \begin{bmatrix} M & I_l \end{bmatrix} \quad (6.28)$$

where $M \in \mathbb{R}^{l \times (n-l)}$ represents design freedom. Introduce another transformation so that $(\hat{x}_1, \hat{x}_2) \mapsto (\hat{x}_1, s(t))$, associated with the nonsingular matrix

$$T_s = \begin{bmatrix} I & 0 \\ M & I \end{bmatrix} \quad (6.29)$$

Equation (6.25) then becomes

$$\begin{bmatrix} \dot{\hat{x}}_1(t) \\ \dot{s}(t) \end{bmatrix} = \begin{bmatrix} \tilde{A}_{11} & \tilde{A}_{12} \\ \tilde{A}_{21} & \tilde{A}_{22} \end{bmatrix} \begin{bmatrix} \hat{x}_1(t) \\ s(t) \end{bmatrix} + \begin{bmatrix} B_1 B_2^N B_2^+ \\ I + M B_1 B_2^N B_2^+ \end{bmatrix} \hat{v}(t) \quad (6.30)$$

where B_2^+ is defined in (6.26) and $\tilde{A}_{11} := \hat{A}_{11} - \hat{A}_{12} M$, $\tilde{A}_{21} := M \tilde{A}_{11} + \hat{A}_{21} - \hat{A}_{22} M$. If a control law can be designed to induce sliding, then during sliding $\dot{s}(t) = s(t) = 0$ and so the equivalent control necessary to maintain sliding is obtained from solving for $\hat{v}_{eq}(t)$ from the lower equations of (6.30) to give

$$\hat{v}_{eq}(t) = -(I + M B_1 B_2^N B_2^+)^{-1} \tilde{A}_{21} \hat{x}_1(t) \quad (6.31)$$

where B_2^N is defined in (6.21).

Define

$$\gamma_1 := \|M B_1 B_2^N\| \quad (6.32)$$

It follows that $\|M B_1 B_2^N B_2^+\| < \|M B_1 B_2^N\| \|B_2^+\| < \gamma_0 \gamma_1$. Since B_2^+ is independent of M , the term γ_0 can be calculated a-priori using the boundedness result from Proposition 2. If (A, B_ν) is controllable, then $(\hat{A}_{11}, \hat{A}_{12})$ is controllable and so M can always be chosen to make $\hat{A}_{11} - \hat{A}_{12} M$ stable. If the design matrix M can also be chosen so that γ_1 from (6.32) satisfies $\gamma_0 \gamma_1 < 1$, this guarantees the inverse in (6.31) exists for all W .

Substituting (6.31) into the top partition of (6.30), yields the following reduced order system

which governs the sliding motion:

$$\dot{\hat{x}}_1(t) = \tilde{A}_{11}\hat{x}_1(t) - B_1B_2^NB_2^+(I + MB_1B_2^NB_2^+)^{-1}\tilde{A}_{21}\hat{x}_1(t) \quad (6.33)$$

Remark 2: In a fault-free condition, $W = I$ and therefore $B_2^+|_{W=I} = B_2^T$ since $B_2B_2^T = I$. Also

$$B_2^NB_2^+ = (I - B_2^TB_2)B_2^+ = (I - B_2^TB_2)B_2^T = 0$$

and the system in (6.33) ‘collapses’ to $\dot{\hat{x}}_1(t) = \tilde{A}_{11}\hat{x}_1(t)$ which is the nominal sliding mode reduced order system for which M has been designed to guarantee stability. The system in (6.33) depends on W and so stability needs to be established. The stability analysis which follows examines what will happen to the reduced order sliding motion when the system is subjected to faults and failures. The idea is to use available design tools from the literature e.g. [67, 210], to design the sliding surface for the fault-free condition, and then extend the stability analysis to the faulty situation.

6.2.2 Stability analysis

The stability of the sliding mode is dependent on the reduced order system (6.33). Typically in SMC the stability of the system only depends on \tilde{A}_{11} which is guaranteed to be stable by choice of M . Note that M can be designed using standard sliding hyperplane design methods (such as Section 3.4) assuming a nominal no fault condition – i.e. $W = I$ in (6.25). To facilitate the subsequent analysis, define

$$\tilde{G}(\mathbf{s}) := \tilde{A}_{21}(sI - \tilde{A}_{11})^{-1}B_1B_2^N \quad (6.34)$$

where \mathbf{s} represents the Laplace variable. By construction the transfer function matrix $\tilde{G}(\mathbf{s})$ is stable. Suppose

$$\gamma_2 = \|\tilde{G}(\mathbf{s})\|_\infty \quad (6.35)$$

Proposition 3 *During a fault or failure condition, for any combination of $0 < w_i \leq 1$, the closed-loop system will be stable if*

$$0 \leq \frac{\gamma_2\gamma_0}{1 - \gamma_1\gamma_0} < 1 \quad (6.36)$$

where the positive scalar γ_0 is defined in Proposition 2, the positive scalar γ_1 is defined in (6.32) and $\gamma_2 = \|\tilde{G}(\mathbf{s})\|_\infty$.

Proof: Consider the reduced order system from Equation (6.33) rewritten as follows:

$$\dot{\hat{x}}_1(t) = \tilde{A}_{11}\hat{x}_1(t) - B_1B_2^N\tilde{u}(t) \quad (6.37)$$

$$\tilde{y}(t) = \tilde{A}_{21}\hat{x}_1(t) \quad (6.38)$$

where

$$\tilde{u}(t) := B_2^+(I + MB_1B_2^NB_2^+)^{-1}\tilde{y}(t) \quad (6.39)$$

Let $\tilde{G}(\mathbf{s})$ be defined as (6.34). Consequently (6.33) may be viewed as the closed-loop dynamics of the negative feedback interconnection of $\tilde{G}(\mathbf{s})$ and the varying (with respect to W) ‘feedback

gain' associated with (6.39). Since (6.36) is assumed to hold, $\gamma_0\gamma_1 < 1$ and it follows that $\|MB_1B_2^NB_2^+\| < \|MB_1B_2^N\|\|B_2^+\| < \gamma_0\gamma_1 < 1$. Consequently, $\det(I + MB_1B_2^NB_2^+) \neq 0$. Furthermore, using the fact that in general $\|(I + X)^{-1}\| \leq (I - \|X\|)^{-1}$ if $\|X\| < 1$ (page 301 [99]), then

$$\|B_2^+(I + MB_1B_2^NB_2^+)^{-1}\| < \|B_2^+\|(I + MB_1B_2^NB_2^+)^{-1}\| < \frac{\gamma_0}{1 - \gamma_1\gamma_0} \quad (6.40)$$

From the Small Gain Theorem [123], if

$$\|\tilde{G}(s)\|_\infty \|B_2^+(I + MB_1B_2^NB_2^+)^{-1}\| < 1 \quad (6.41)$$

then (6.33) is stable. Using (6.40) and the fact that $\|\tilde{G}(s)\|_\infty < \gamma_2$, inequality (6.36) implies (6.41) holds and so (6.33) is stable. ■

Remark 3: Both γ_1 and γ_2 depend on the design of the sliding surface since they depend on M , however they are independent of W . The scalar γ_0 depends on W but is independent of M .

Remark 4: If $B_1 = 0$ (which is an assumption in many schemes: for example [181]), then $\gamma_1 = 0$ and $\gamma_2 = 0$ and Proposition 3 is trivially satisfied. Furthermore, as $\|B_1\| \rightarrow 0$, the scalar $\frac{\gamma_2\gamma_0}{1 - \gamma_1\gamma_0} \rightarrow 0$ and so the requirements of Proposition 3 are satisfied. This means loosely speaking, for weakly coupled systems in which $\|B_1\|$ is small, the approach will be feasible. The situation where $B_1 = 0$ can be regarded as the special extreme case as $\|B_1\| \rightarrow 0$.

Equation (6.36) represents a test to guarantee the stability of the closed-loop system when faults occur (i.e. when the w_i vary). One important feature is that in order for (6.33) to hold, the norm of the pseudo-inverse B_2^+ which depends on W must be bounded for all $0 < w_i \leq 1$ (which was proved in Proposition 2).

6.2.3 Sliding Mode Control laws

Next, a sliding mode controller is designed based on the system in (6.30) with respect to $\hat{\nu}$. The proposed control law has a structure given by $\hat{\nu}(t) = \hat{\nu}_l(t) + \hat{\nu}_n(t)$ where

$$\hat{\nu}_l(t) := -\tilde{A}_{21}\hat{x}_1(t) - \tilde{A}_{22}s(t) \quad (6.42)$$

and the nonlinear component is defined to be

$$\hat{\nu}_n(t) := -\rho(t, x) \frac{s(t)}{\|s(t)\|} \quad \text{for } s(t) \neq 0 \quad (6.43)$$

where $s(t) = \hat{S}\hat{x}(t)$.

Proposition 4 Suppose the hyperplane matrix M has been chosen so that $\tilde{A}_{11} = \hat{A}_{11} - \hat{A}_{12}M$ is stable and condition (6.36) from Proposition 3 holds, then choosing

$$\rho(t, x) := \frac{\gamma_1\gamma_0\|\hat{\nu}_l(t)\| + \eta}{1 - \gamma_1\gamma_0} \quad (6.44)$$

ensures a sliding motion takes place on \mathcal{S} in finite time.

Proof: Notice if (6.36) holds, then $\gamma_0\gamma_1 < 1$ and so the gain defined in (6.44) is well defined. From (6.30),

$$\begin{aligned}\dot{s}(t) &= \tilde{A}_{21}\hat{x}_1(t) + \tilde{A}_{22}s(t) + (I + MB_1B_2^NB_2^+)\hat{\nu}(t) \\ &= (I + MB_1B_2^NB_2^+)\hat{\nu}_n(t) + (MB_1B_2^NB_2^+)\hat{\nu}_l(t)\end{aligned}$$

and so

$$\begin{aligned}s^T\dot{s} &= -\rho\|s\| + s^TMB_1B_2^NB_2^+\hat{\nu}_n(t) + s^T(MB_1B_2^NB_2^+)\hat{\nu}_l(t) \\ &\leq \|s\|(\rho\|MB_1B_2^NB_2^+\| + \|MB_1B_2^NB_2^+\|\|\hat{\nu}_l(t)\| - \rho) \\ &\leq \|s\|(\rho\gamma_1\gamma_0 + \gamma_1\gamma_0\|\hat{\nu}_l(t)\| - \rho)\end{aligned}\tag{6.45}$$

So choosing $\rho(\cdot)$ as described in (6.44) and substituting into (6.45) implies

$$s(t)^T\dot{s}(t) \leq -\eta\|s(t)\|\tag{6.46}$$

The differential inequality (6.46) is a standard ‘reachability condition’ and implies $s(t) = 0$ in finite time and a sliding motion is maintained for all subsequent time. ■

Remark 5: It can be shown that $\hat{\nu}_l(t)$ as defined in (6.42) can be written as $\hat{\nu}_l(t) = -(\hat{S}\hat{B})^{-1}\hat{S}\hat{A}\hat{x}(t)$ which is more in keeping with the notation in [67]. Note here $\hat{S}\hat{B} = I_l$ and so this simplifies to $\hat{\nu}_l(t) = -\hat{S}\hat{A}\hat{x}(t)$.

It follows that the actual control which is sent to the actuators is resolved from the ‘virtual control law’ $\nu(t)$ (from (6.42)-(6.43)), using (6.11), (6.12), (6.16) and (6.24). Therefore $u(t)$ is defined as

$$u(t) = WB_2^T(B_2W^2B_2^T)^{-1}\hat{\nu}(t)\tag{6.47}$$

i.e. the control which is sent to the actuators depends on the effectiveness gains k_i (through the matrix W).

Note that in most of the literature, whilst SMC has been successfully tested on systems with faulty actuators, it was claimed that SMC cannot deal directly with total failures [114]. However, in this chapter, provided that the matrix M satisfies the stability condition (6.36), the sliding mode controller for the ‘virtual’ system proposed above, can handle total actuator failures in the original system provided that $\det(B_2WB_2^T) \neq 0$.

Remark 6: In this chapter, formally, the effect of position and rate limits on the actuators is not considered. However, if a rate limit or position limit is exceeded, it would be interpreted by the estimation mechanism as a fault, because the actual actuator position would be different from the expected one based on the commanded control signal. This would result in a $k_i > 0$ in the channel in which the saturation or rate limit is reached. The proposed scheme would then inherently attempt to reduce the burden in this channel and redistribute the control effort to other actuators, which would mitigate the effect of the saturation.

So far, it has been assumed that the effectiveness gains $k_i(t)$ that make up K and hence W are known perfectly. In real engineering systems, there will always be some error in the computation measurements of the $k_i(t)$. The next section considers the impact of this on the

proposed scheme.

6.3 The effect of non-perfect fault reconstruction

Consider a faulty system represented by Equation (6.7). Let \bar{K} correspond to the estimated reduction of the actuator efficiency based on the information provided by the FDI scheme. Define

$$\bar{W} = I - \bar{K} \quad (6.48)$$

and suppose $\bar{K} \neq K$, where, as described earlier, K represents the actual reduction in actuator efficiency. Suppose

$$W = (I - \Delta)\bar{W} \quad (6.49)$$

where $\Delta = \text{diag}(\delta_1, \dots, \delta_m)$ and (the unknown) δ_i are elements which represent the level of imperfection in the fault reconstruction. Since $(I - K) = W$, from (6.7)

$$\dot{x}(t) = Ax(t) + B(I - K)u(t) = Ax(t) + B(I - \Delta)\bar{W}u(t) \quad (6.50)$$

Now suppose $u(t) = \bar{B}_2^\dagger \nu(t)$ where

$$\bar{B}_2^\dagger := \bar{W}B_2^T(B_2\bar{W}B_2^T)^{-1} \quad (6.51)$$

This represents the fact that \bar{W} (i.e. the estimate rather than the true value of W) will be used to compute the controller. Then (6.50) becomes

$$\dot{x}(t) = Ax(t) + B(I - \Delta)\bar{W}\bar{B}_2^\dagger \nu(t) \quad (6.52)$$

Also define $\bar{\nu}(t) = (B_2\bar{W}B_2^T)^{-1}\nu(t)$, then it follows from (6.52) that

$$\begin{aligned} \dot{x}(t) &= Ax(t) + \begin{bmatrix} B_1\bar{W}^2B_2^T \\ B_2\bar{W}^2B_2^T \end{bmatrix} \bar{\nu}(t) - \begin{bmatrix} B_1\Delta\bar{W}^2B_2^T \\ B_2\Delta\bar{W}^2B_2^T \end{bmatrix} \bar{\nu}(t) \\ &= Ax(t) + \begin{bmatrix} B_1B_2^T \\ I \end{bmatrix} \bar{\nu}(t) - \begin{bmatrix} B_1(I - \bar{W}^2)B_2^T \\ B_2(I - \bar{W}^2)B_2^T \end{bmatrix} \bar{\nu}(t) - \begin{bmatrix} B_1\Delta\bar{W}^2B_2^T \\ B_2\Delta\bar{W}^2B_2^T \end{bmatrix} \bar{\nu}(t) \end{aligned} \quad (6.53)$$

Notice that compared with (6.17), Equation (6.53) has an additional term dependent on both the faults and the error in fault reconstruction. Again consider a transformation to regular form using the transformation matrix T_r defined in (6.19). Equation (6.53) becomes

$$\begin{aligned} \dot{\hat{x}} &= \hat{A}\hat{x}(t) + \begin{bmatrix} 0 \\ I \end{bmatrix} \bar{\nu}(t) - \begin{bmatrix} -B_1B_2^N\bar{W}^2B_2^T \\ I - B_2\bar{W}^2B_2^T \end{bmatrix} \bar{\nu}(t) - \begin{bmatrix} B_1B_2^N\Delta\bar{W}^2B_2^T \\ B_2\Delta\bar{W}^2B_2^T \end{bmatrix} \bar{\nu}(t) \\ &= \hat{A}\hat{x}(t) + \begin{bmatrix} 0 \\ B_2\bar{W}^2B_2^T \end{bmatrix} \bar{\nu}(t) + \begin{bmatrix} B_1B_2^N\bar{W}^2B_2^T \\ 0 \end{bmatrix} \bar{\nu}(t) - \begin{bmatrix} B_1B_2^N\Delta\bar{W}^2B_2^T \\ B_2\Delta\bar{W}^2B_2^T \end{bmatrix} \bar{\nu}(t) \end{aligned} \quad (6.54)$$

where B_2^N is defined in (6.21). Define $\hat{v}(t) := B_2 \bar{W}^2 B_2^T \bar{v}(t)$ and $\bar{B}_2^+ := \bar{W}^2 B_2^T (B_2 \bar{W}^2 B_2^T)^{-1}$ then (6.54) becomes

$$\dot{\hat{x}} = \hat{A}\hat{x}(t) + \begin{bmatrix} 0 \\ I \end{bmatrix} \hat{v}(t) + \begin{bmatrix} B_1 B_2^N (I - \Delta) \bar{B}_2^+ \\ -B_2 \Delta \bar{B}_2^+ \end{bmatrix} \hat{v}(t) \quad (6.55)$$

Consider another coordinate transformation T_s defined in (6.29), then the above becomes

$$\begin{bmatrix} \dot{\hat{x}}_1(t) \\ \dot{s}(t) \end{bmatrix} = \begin{bmatrix} \tilde{A}_{11} & \tilde{A}_{12} \\ \tilde{A}_{21} & \tilde{A}_{22} \end{bmatrix} \begin{bmatrix} \hat{x}_1(t) \\ s(t) \end{bmatrix} + \begin{bmatrix} 0 \\ I \end{bmatrix} \hat{v}(t) + \begin{bmatrix} B_1 B_2^N (I - \Delta) \bar{B}_2^+ \\ M B_1 B_2^N (I - \Delta) \bar{B}_2^+ - B_2 \Delta \bar{B}_2^+ \end{bmatrix} \hat{v}(t) \quad (6.56)$$

where $\tilde{A}_{11} := \hat{A}_{11} - \hat{A}_{12}M$, $\tilde{A}_{21} := M\hat{A}_{11} + \hat{A}_{21} - \hat{A}_{22}$.

If a control law can be designed to induce sliding, then during sliding $\dot{s}(t) = s(t) = 0$ and so the equivalent control necessary to maintain sliding is obtained from solving for $\hat{v}_{eq}(t)$ from the lower equations of (6.56) to give

$$\hat{v}_{eq}(t) = -(I + M B_1 B_2^N (I - \Delta) \bar{B}_2^+ - B_2 \Delta \bar{B}_2^+)^{-1} \tilde{A}_{21} \hat{x}_1(t) \quad (6.57)$$

Substituting into the first equation of (6.56) gives the following reduced order system:

$$\dot{\hat{x}}_1(t) = \tilde{A}_{11} \hat{x}_1(t) - B_1 B_2^N (I - \Delta) \bar{B}_2^+ (I + M B_1 B_2^N (I - \Delta) \bar{B}_2^+ - B_2 \Delta \bar{B}_2^+)^{-1} \tilde{A}_{21} \hat{x}_1(t) \quad (6.58)$$

Remark 7: If the information on the actual degradation of the control surface efficiency is ‘perfect’, then $\Delta = 0$, and (6.58) reduces to (6.33) in the stability analysis that follows. However in the event of non-perfect fault reconstruction, there is a bound on Δ for which stability is still guaranteed.

Proposition 5 *Assume (as in Proposition 3), that Equation (6.36) holds. During a fault or failure condition, for any combinations of $0 < w_i \leq 1$, the closed-loop system will be stable if the mismatch between the actual and reconstructed fault Δ satisfies:*

$$\|\Delta\| < \frac{1 - \gamma_1 \gamma_0 - \gamma_2 \gamma_0}{\gamma_0 (\gamma_1 + \gamma_2 + 1)} \quad (6.59)$$

where γ_0 and γ_1 are defined in Proposition 2 and 3 respectively and γ_2 is defined in (6.35).

Proof: Consider the reduced order system from Equation (6.58) which can be rewritten as (6.37)-(6.39), where now

$$\tilde{u}(t) := (I - \Delta) \bar{B}_2^+ (I + M B_1 B_2^N (I - \Delta) \bar{B}_2^+ - B_2 \Delta \bar{B}_2^+)^{-1} \tilde{y}(t) \quad (6.60)$$

Assume that (6.36) and (6.59) hold. Inequality (6.59) implies

$$\|\Delta\| < \frac{1 - \gamma_1 \gamma_0}{\gamma_0 (\gamma_1 + 1)} \quad (6.61)$$

because

$$\frac{1 - \gamma_1 \gamma_0}{\gamma_0 (\gamma_1 + 1)} > \frac{1 - \gamma_1 \gamma_0 - \gamma_2 \gamma_0}{\gamma_0 (\gamma_1 + \gamma_2 + 1)} > 0$$

Since

$$\|MB_1B_2^N(I - \Delta)\bar{B}_2^+ - B_2\Delta\bar{B}_2^+\| \leq \|MB_1B_2^N\|(1 + \|\Delta\|)\|\bar{B}_2^+\| + \|B_2\|\|\Delta\|\|\bar{B}_2^+\|$$

and in addition $\|B_2\| = 1$ and $\|\bar{B}_2^+\| \leq \gamma_0$ (since $\|B_2^+\| \leq \gamma_0 \Rightarrow \|\bar{B}_2^+\| \leq \gamma_0$), inequality (6.61) implies

$$\|MB_1B_2^N(I - \Delta)\bar{B}_2^+ - B_2\Delta\bar{B}_2^+\| \leq \gamma_1\gamma_0 + \|\Delta\|\gamma_0(\gamma_1 + 1) < 1 \quad (6.62)$$

Therefore $(I + MB_1B_2^N(I - \Delta)\bar{B}_2^+ - B_2\Delta\bar{B}_2^+)^{-1}$ exists for all $0 < w_i \leq 1$. Furthermore, using arguments similar to those in the proof of Proposition 3

$$\|(I - \Delta)\bar{B}_2^+(I + MB_1B_2^N(I - \Delta)\bar{B}_2^+ - B_2\Delta\bar{B}_2^+)^{-1}\| < \frac{(1 + \|\Delta\|)\gamma_0}{(1 - \gamma_1(1 + \|\Delta\|)\gamma_0 - \|\Delta\|\gamma_0)} \quad (6.63)$$

From Small Gain Theorem, since (6.58) is the closed-loop system obtained from $\tilde{G}(s)$ interconnected with (6.60) if

$$\frac{(1 + \|\Delta\|)\gamma_0}{(1 - \gamma_1(1 + \|\Delta\|)\gamma_0 - \|\Delta\|\gamma_0)} < \frac{1}{\gamma_2} \quad (6.64)$$

holds, then (6.58) is stable. By direct manipulation, (6.64) holds if (6.59) holds, and the proof is complete. \blacksquare

As in Section 6.2.3, a sliding mode controller will now be designed based on the ‘virtual’ system in (6.56) with respect to $\hat{\nu}$, as defined in (6.42) and (6.43).

Proposition 6 *Suppose that the hyperplane matrix M has been chosen so that $\tilde{A}_{11} = \hat{A}_{11} - \hat{A}_{12}M$ is stable and*

$$\|\Delta\| \leq \Delta_{max} < \frac{1 - \gamma_1\gamma_0}{\gamma_0(1 + \gamma_1)} \quad (6.65)$$

where γ_0 , γ_1 and γ_2 are defined in (6.27), (6.32) and (6.35) respectively and Δ_{max} is a fixed positive scalar. Then choosing

$$\rho(t, x) = \frac{(\gamma_1(1 + \Delta_{max})\gamma_0 + \Delta_{max}\gamma_0)\|\hat{\nu}_l(t)\| + \eta}{1 - \gamma_1(1 + \Delta_{max})\gamma_0 - \Delta_{max}\gamma_0} \quad (6.66)$$

ensures a sliding motion takes place on \mathcal{S} in finite time.

Proof: The assumption on Δ in (6.65) implies $\gamma_0\gamma_1 + (1 + \gamma_1)\Delta_{max}\gamma_0 < 1$ and so the gain $\rho(t, x)$ in (6.66) is well defined. From (6.56),

$$\begin{aligned} \dot{s}(t) &= \tilde{A}_{21}\hat{x}_1(t) + \tilde{A}_{22}s(t) + \left(I + MB_1B_2^N(I - \Delta)\bar{B}_2^+ - B_2\Delta\bar{B}_2^+\right)\hat{\nu}(t) \\ &= \left(I + MB_1B_2^N(I - \Delta)\bar{B}_2^+ - B_2\Delta\bar{B}_2^+\right)\hat{\nu}_n(t) + \left(MB_1B_2^N(I - \Delta)\bar{B}_2^+ - B_2\Delta\bar{B}_2^+\right)\hat{\nu}_l(t) \end{aligned}$$

after substituting for $\nu_l(t)$ from (6.42). Consequently substituting $\nu_n(t)$ from (6.43) into the

above yield

$$\begin{aligned}
s^T \dot{s} &= -\rho \|s\| + s^T \left(MB_1 B_2^N (I - \Delta) \bar{B}_2^+ - B_2 \Delta \bar{B}_2^+ \right) \hat{\nu}_n(t) + s^T \left(MB_1 B_2^N (I - \Delta) \bar{B}_2^+ - B_2 \Delta \bar{B}_2^+ \right) \hat{\nu}_l(t) \\
&\leq \|s\| \left(\rho \left\| MB_1 B_2^N (I - \Delta) \bar{B}_2^+ - B_2 \Delta \bar{B}_2^+ \right\| + \left\| MB_1 B_2^N (I - \Delta) \bar{B}_2^+ - B_2 \Delta \bar{B}_2^+ \right\| \|\hat{\nu}_l(t)\| - \rho \right) \\
&\leq \|s\| \left(-\rho \left(1 - \gamma_1 (1 + \Delta_{max}) \gamma_0 - \Delta_{max} \gamma_0 \right) + \left(\gamma_1 (1 + \Delta_{max}) \gamma_0 + \Delta_{max} \gamma_0 \right) \|\hat{\nu}_l(t)\| \right) \quad (6.67)
\end{aligned}$$

So choosing $\rho(\cdot)$ as described in (6.66) and substituting into (6.67) implies

$$s(t)^T \dot{s}(t) \leq -\eta \|s(t)\| \quad (6.68)$$

Again, as in Section 6.2.3, the differential inequality (6.68) implies that the ‘reachability condition’ is achieved. Therefore $s(t) = 0$ in finite time and a sliding motion is maintained for all subsequent time. ■

6.4 Sliding mode design issues

Based on the stability analysis above, the sliding mode design problem can be summarized as follows:

1. Pre-design calculations:

- (a) Make an appropriate re-ordering of the states in (6.7) so that the input distribution matrix B is partitioned to identify B_1 and B_2 .
- (b) Scale the states so that $B_2 B_2^T = I$.
- (c) Change coordinates using the linear transformation $x(t) \mapsto \hat{x}(t) = T_r x(t)$, where T_r is given in (6.19), to achieve the canonical form in (6.25) and isolate the matrices \hat{A}_{11} , \hat{A}_{12} , \hat{A}_{21} and \hat{A}_{22} .
- (d) Compute the smallest possible scalar γ_0 so that $\|W^2 B_2^T (B_2 W^2 B_2^T)^{-1}\| < \gamma_0$, $\forall 0 < W \leq I$. This value is an a-priori calculation and is independent of the choice of sliding surface and control law.

2. Design of matrix M :

- (a) The design objective is to compute M from (6.28) so that $\tilde{A}_{11} := \hat{A}_{11} - \hat{A}_{12} M$ is stable. This is always possible if (A, B_ν) is controllable.

3. Stability analysis:

- (a) Compute and check if $\gamma_1 := \|MB_1 B_2^N\| < \frac{1}{\gamma_0}$ is satisfied. Otherwise re-design M .
- (b) Calculate $\tilde{G}(\mathbf{s}) := \tilde{A}_{21}(\mathbf{s}I - \tilde{A}_{11})^{-1} B_1 B_2^N$. If $\|\tilde{G}(\mathbf{s})\|_\infty := \gamma_2 < \frac{1}{\gamma_0} - \gamma_1$, the closed-loop is guaranteed to be stable $\forall 0 < W \leq I$. Since $\gamma_2 < \frac{1}{\gamma_0} - \gamma_1$ ensures inequality (6.36) in Proposition 3 holds. Otherwise consider re-designing the matrix M .
- (c) Calculate $\|\Delta\|$ from Proposition 6. This is the maximum tolerable mismatch between the actual and the estimated fault that guarantees the closed-loop system to be stable $\forall 0 < W \leq I$. This might dictate the choice of the fault estimation scheme.

4. Obtain the virtual control law using (6.42), (6.43) and the actual control law using (6.47).

6.5 ADMIRE simulations

6.5.1 Controller design

The ADMIRE model has been used by several researchers (e.g. [95]) and within the Group for Aeronautical Research and Technology in Europe (GARTEUR) AG11 and AG12. The ADMIRE model represents a rigid small fighter aircraft with a delta-canard configuration based on a real fighter aircraft called GRIPEN. Details of the model can be found in [75]. The linear model used here has been obtained at a low speed flight condition of Mach 0.22 at an altitude of 3000m and is similar to the one in [95]. The states are $x = [\alpha \ \beta \ p \ q \ r]^T$ with controlled outputs α, β, p ; where α is angle of attack (AoA) (rad), β is sideslip angle (rad), p is roll rate (rad/sec), q is pitch rate (rad/sec) and r is yaw rate (rad/sec). The control surfaces are $\delta = [\delta_c \ \delta_{re} \ \delta_{le} \ \delta_r]^T$, which represent the deflections (rad) of the canard, right elevon, left elevon and rudder respectively. A linearized model [95] is:

$$A = \begin{bmatrix} -0.5432 & 0.0137 & 0 & 0.9778 & 0 \\ 0 & -0.1179 & 0.2215 & 0 & -0.9661 \\ 0 & -10.5128 & -0.9967 & 0 & 0.6176 \\ 2.6221 & -0.0030 & 0 & -0.5057 & 0 \\ 0 & 0.7075 & -0.0939 & 0 & -0.2127 \end{bmatrix} \quad (6.69)$$

$$B = \left[\begin{array}{cccc|cccc} 0.0069 & -0.0866 & -0.0866 & 0.0004 & & & & \\ 0 & 0.0119 & -0.0119 & 0.0287 & & & & \\ \hline 0 & -4.2423 & 4.2423 & 1.4871 & & & & \\ 1.6532 & -1.2735 & -1.2735 & 0.0024 & & & & \\ 0 & -0.2805 & 0.2805 & -0.8823 & & & & \end{array} \right] \begin{array}{l} \left. \vphantom{\begin{matrix} 0.0069 \\ 0 \end{matrix}} \right\} B_1 \\ \left. \vphantom{\begin{matrix} 0 \\ 1.6532 \\ 0 \end{matrix}} \right\} B_2 \end{array} \quad (6.70)$$

The partition of B in (6.70) shows the terms B_1 and B_2 (although a further change of coordinate is necessary to scale B_2 to ensure $B_2 B_2^T = I$). It can be shown that in the coordinates in which $\|B_2\| = 1$, $\|B_1\| = 0.1227$ and so the dominant effect of the control signal is through the B_2 channels. To include a tracking facility, integral action (as discussed in Section 3.5.1) has been included. Let $x_r(t)$ represent integral action states. Define

$$\dot{x}_r(t) = r(t) - C_c x(t) \quad (6.71)$$

where

$$C_c = \begin{bmatrix} I_3 & 0_{3 \times 2} \end{bmatrix} \quad (6.72)$$

is the distribution matrix associated with the controlled outputs, and the differentiable (filtered reference) signal $r(t)$ satisfies

$$\dot{r}(t) = \Gamma (r(t) - r_c) \quad (6.73)$$

with $\Gamma \in \mathbb{R}^{3 \times 3}$ is a stable design matrix and r_c is a constant demand vector. Augmenting

the states from (6.70) with the integral action states and defining $x_a(t) = \text{col}(x_r(t), x(t))$ (as discussed in Section 3.5.1) it follows that

$$\dot{x}_a(t) = A_a x_a(t) + B_a u(t) + B_r r(t) \quad (6.74)$$

where

$$A_a = \begin{bmatrix} 0 & -C_c \\ 0 & A \end{bmatrix} \quad B_a = \begin{bmatrix} 0 \\ B \end{bmatrix} \quad B_r = \begin{bmatrix} I_3 \\ 0 \end{bmatrix} \quad (6.75)$$

If (A, B) is controllable and (A, B, C_c) does not have any zeros at the origin then (A_a, B_a) is controllable. Define a switching function $s_a(t) : \mathbb{R}^{(n+l)} \rightarrow \mathbb{R}^l$ to be

$$s_a(t) = S_a x_a(t) \quad (6.76)$$

where $S_a \in \mathbb{R}^{l \times (n+l)}$. As in Equation (6.42)-(6.43), the proposed ‘virtual control’ law comprises two components $\hat{v}(t) = \hat{v}_l(t) + \hat{v}_n(t)$. Now because of the reference signal $r(t)$, the linear component has a feed-forward reference term and so $\hat{v}_l(t) = Lx_a(t) + L_r r(t)$ where $L = -\hat{S}_a \hat{A}_a$ and $L_r = -\hat{S}_a \hat{B}_r$. Here \hat{A} , \hat{B}_r and \hat{S} are the matrices from (6.75) and (6.76) after a transformation to achieve regular form (analogous to (6.19)) has been performed. Note that an extract term L_r has appeared in this tracking formulation compared to the one in Section 6.2.3. The nonlinear component is defined as

$$\hat{v}_n(t) = -\rho(t, x_a) \frac{s_a(t)}{\|s_a(t)\|} \quad \text{for } s_a(t) \neq 0 \quad (6.77)$$

The actual control sent to the actuator is given in (6.47). A quadratic optimal design has been used to obtain the sliding surface matrix S_a (see for example Section 3.4.1). The symmetric positive definite weighting matrix has been chosen as $Q = \text{diag}(20, 20, 20, 7, 10, 10, 1, 1)$. The pre-filter from (6.73) has been chosen as $\Gamma = -20I_3$. In the simulations the discontinuity in the nonlinear control term in (6.77) has been smoothed (as in Section 3.2.2) by using a sigmoidal approximation $\frac{s_a}{\|s_a\| + \delta_a}$, where the scalar δ_a has been chosen as $\delta_a = 0.001$. This removes the discontinuity and introduces a further degree of tuning to accommodate the actuator limits, especially during actuator fault or failure conditions.

In normal flight, either the canard or elevons (left & right) are sufficient to provide the pitch moment and therefore redundancy is available. In the event of faults or failures, elevons can replace the canard to obtain a pitch moment. However for roll, the elevons will become the only active control surface (the rudder is used for yaw). During the design stage, and based on analysis from (6.44), it was found that, $\text{rank}(B_2 W B_2^T) < 3$ when the rudder completely fails or any two surfaces from the set consisting of the canard and the left and right elevons completely fail. This is an expected result since there is no redundancy for the rudder to provide yaw; and when two actuators fail from either the canard or elevons, it means that there is no redundancy left in the system and all possible actuators to provide pitch or roll have failed. Based on this assumption, it can be verified from a numerical search that $\gamma_0 = 2.0913$. Simple calculations show that $\gamma_1 = 0.0980$, therefore $\gamma_1 \gamma_0 = 0.2050 < 1$ and so, the requirement of Proposition 3 is satisfied. Also for this particular choice of sliding surface $\|\tilde{G}(\mathbf{s})\|_\infty < \gamma_2 = 0.0819$. Therefore

from Proposition 3,

$$\frac{\gamma_2\gamma_0}{1 - \gamma_1\gamma_0} = 0.2154 < 1$$

which shows that the closed-loop system is stable for all choices of $0 < w_i \leq 1$. From Proposition 5, the limits of the tolerable mismatch between the actual and estimated fault signal (for guaranteed stability) is $\Delta_{max} = 0.3519$.

6.5.2 Actuator fault estimation using a sliding mode observer

In many systems e.g. passenger aircraft [37], the information necessary to compute W on-line can be obtained by using a measurement of the actual actuator deflection compared to the demand signals. If measurements of the actual actuator deflections are not available, a sliding mode fault reconstruction scheme, as described in [68] or [202] for example, can be employed. Alternatively other fault reconstruction schemes based on Kalman filters [242] can also be used. Here it is assumed that direct measurements of the actuator deflections are not available and a sliding mode reconstruction approach similar to the one in [68] will be used. This is based on the novel concept of using the ‘equivalent output error injection signal’ to reconstruct faults. Consider the system affected by actuator faults described by Equation (6.7). The objective is to design a sliding mode observer in order to reconstruct $Ku(t)$.

Suppose all the states are available as measured output information, therefore the proposed sliding mode observer has the form:

$$\dot{z}(t) = Az(t) + Bu(t) + \vartheta(t) \quad (6.78)$$

where $u(t)$ is the actual control signal sent to each actuator. The discontinuous injection term is defined as

$$\vartheta(t) := -\rho_o(t, y, u) \frac{e(t)}{\|e(t)\|} \quad \text{if } e(t) \neq 0 \quad (6.79)$$

where $e(t) := z(t) - x(t)$ is the (state) estimation error. It can be shown [68] that, a sliding mode observer of the form (6.78)-(6.79) is completely insensitive to faults. For an appropriate choice of $\rho_o(t, y, u)$ in (6.79), which must bound the fault signal $\|Ku(t)\|$, it can be shown that an ideal sliding motion takes place on $\mathcal{S}_o = \{e(t) : e(t) = 0\}$ in finite time [68]. During the ideal sliding motion, $e(t) = \dot{e}(t) = 0$ and the discontinuous signal $\vartheta(t)$ must take an average value to compensate for $Ku(t)$ to maintain sliding. The average quantity, denoted by $\vartheta_{eq}(t)$, is referred to as the equivalent error injection term, which can be approximated to any degree of accuracy, and is computable on-line as

$$\vartheta_\delta(t) = -\rho_o(t, y, u) \frac{e(t)}{\|e(t)\| + \delta_o} \quad (6.80)$$

where $\delta_o > 0$ is a (small) design parameter. The observer state estimation error system is given by:

$$\dot{e}(t) = Ae(t) + \vartheta(t) + BKu(t) \quad (6.81)$$

During ideal sliding, $\dot{e}(t) = e(t) = 0$, and therefore (6.81) reduces to $-BKu(t) = \vartheta_{eq}(t)$. Using the on-line computed approximation $\vartheta_\delta(t)$ from (6.80), the fault reconstruction can be obtained as:

$$-Ku(t) \approx (B^T B)^{-1} B^T \vartheta_\delta(t) \quad (6.82)$$

Then, provided that $u_i(t) \neq 0$, the effectiveness gains k_i can be computed from (6.82).

For this example, the observer gains $\rho_o = 30$ and $\delta_o = 0.0001$ from (6.78) have been chosen. A saturation $(0, 1]$ block has been included to ‘clip’ the w_i before they are used for the on-line control allocation. This ensures that the weight W stays within the theoretical limits. During implementation, as $u_i(t) \rightarrow 0$, the estimation of the actuator effectiveness K from (6.7), becomes unreliable. A small threshold has been introduced so that if t_ϵ is the time when $|u_i(t)| \leq \epsilon$, then

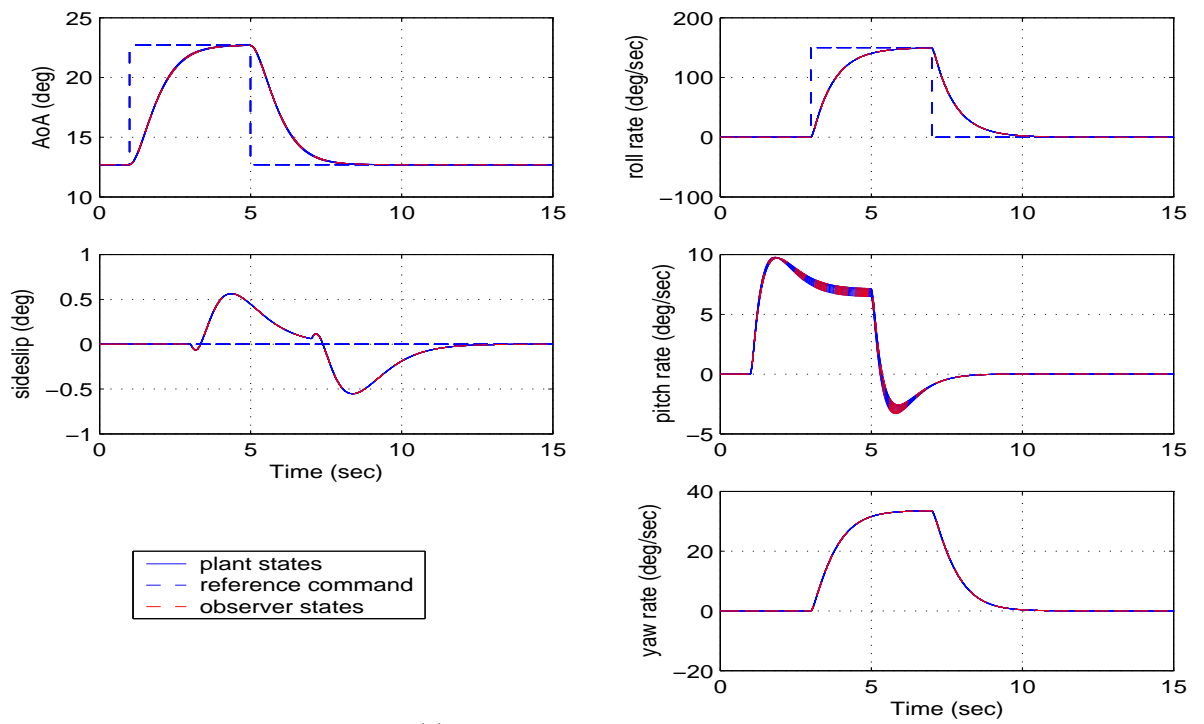
$$k_i(t) = \begin{cases} ((B^T B)^{-1} B^T \nu_\delta)_i / u_i(t) & \text{if } |u_i(t)| > \epsilon \\ k_i(t_\epsilon) & \text{otherwise} \end{cases} \quad (6.83)$$

The idea is to hold the component of the weighting matrix $w_i := 1 - k_i$ constant if $|u_i(t)| \leq \epsilon$, otherwise $k_i(t)$ is provided by the fault estimator. Here, the threshold defined in (6.83) is set as $\epsilon = 1 \times 10^{-3}$ (rad).

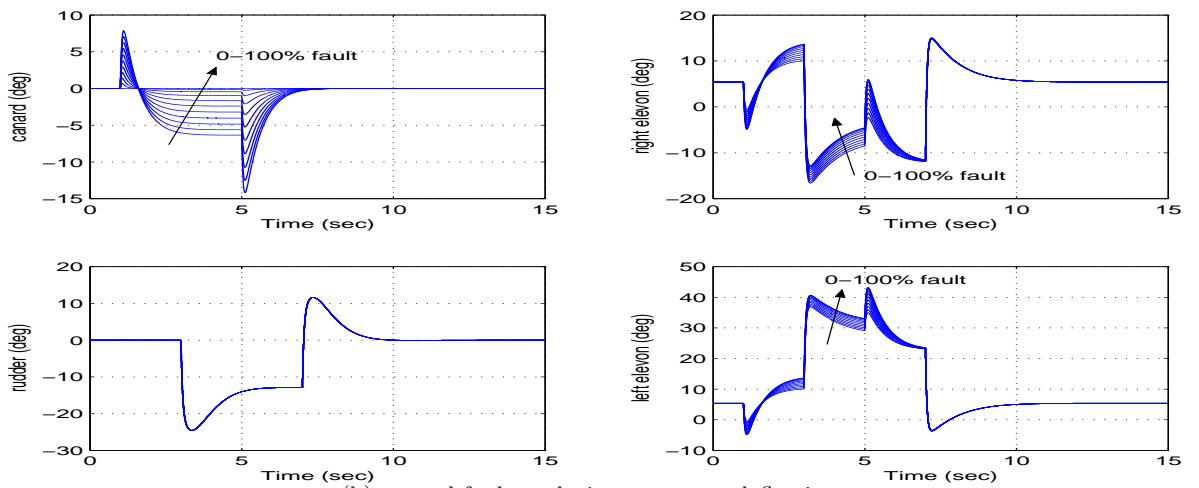
6.5.3 ADMIRE: simulation results

In the following simulations (which assume that there is no saturation or rate limits on the actuators), the linear aircraft model from [95] undertakes a manoeuvre called ‘ α roll’ [95], where a step demand of magnitude 10 deg is applied to α during 1-5 sec and a step of 150 deg for p is applied during 3-7 sec. (There is no reference command for β – see Figure 6.2(a)). Figures 6.2(a), 6.2(b), 6.2(c) and 6.2(d) show the responses of the closed-loop system under 11 different canard fault conditions ranging from 0% \rightarrow 100% (including total failure). It can be seen that the control signal is systematically re-routed to the right and left elevon (Figure 6.2(b)). The tracking responses (Figure 6.2(a)) show no degradation in performance. The control allocation redistributes the control signal to obtain the required performance. Figure 6.2(a) shows that the observer designed for fault reconstruction, tracks the plant output ‘perfectly’. Figure 6.2(c) shows the evolution of the fault reconstruction signal from the observer. These signals are used for the on-line control allocation through the term W as shown in Figure 6.2(d).

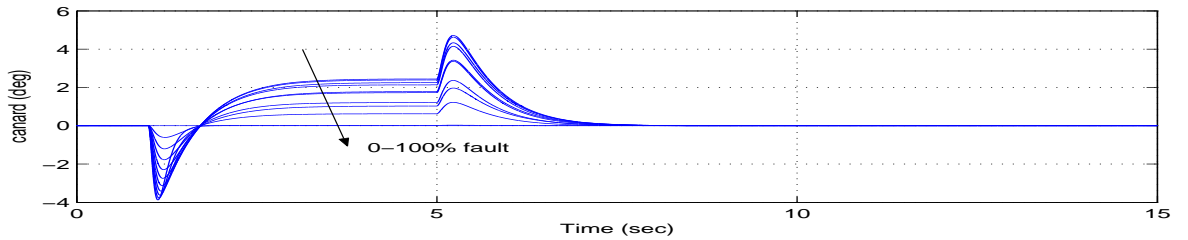
Figures 6.3(a), 6.3(b), 6.3(c) and 6.3(d) show that in the event the left elevon fails, the control signal is redistributed to the remaining actuators without reconfiguring the structure of the controller. The control signals are re-routed to other control surfaces when the fault is detected and estimated (Figure 6.3(c)). Initially in Figure 6.3(b), a control signal is sent to the failed actuator. After the failure has been detected by the observer (Figure 6.3(c)), the weight w_i in the control allocation is changed (Figure 6.3(d)) and the control signal sent to the left elevon is ‘switched off’ and redistributed to the canard and right elevon.



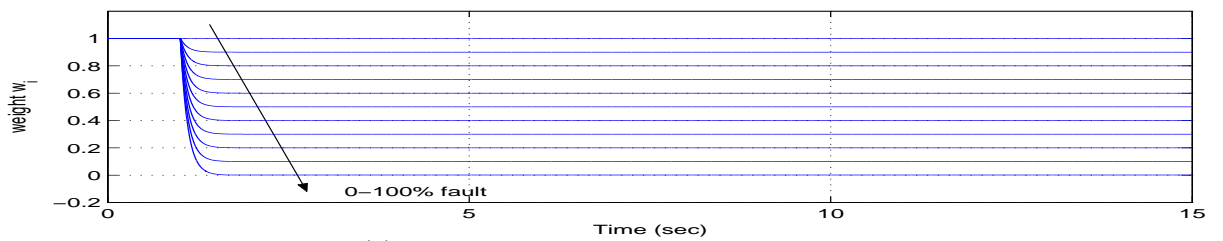
(a) canard fault evolution: states



(b) canard fault evolution: actuator deflection

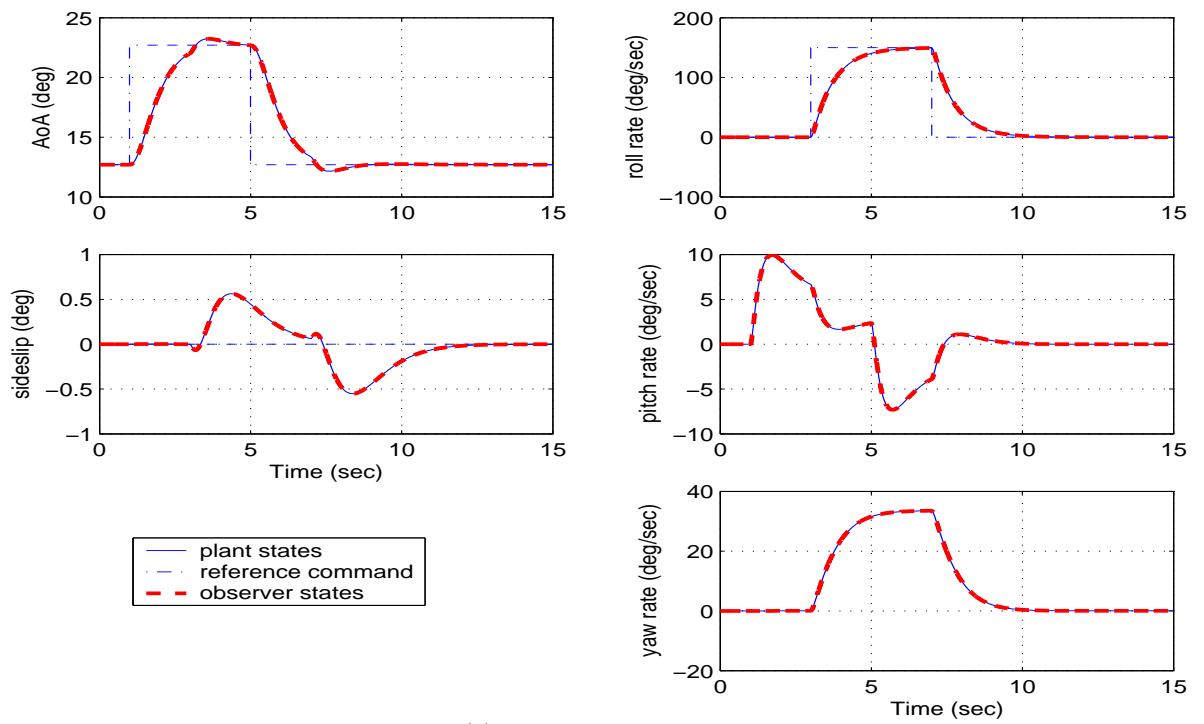


(c) canard fault evolution: fault reconstruction ($k_i u_i(t)$) signals

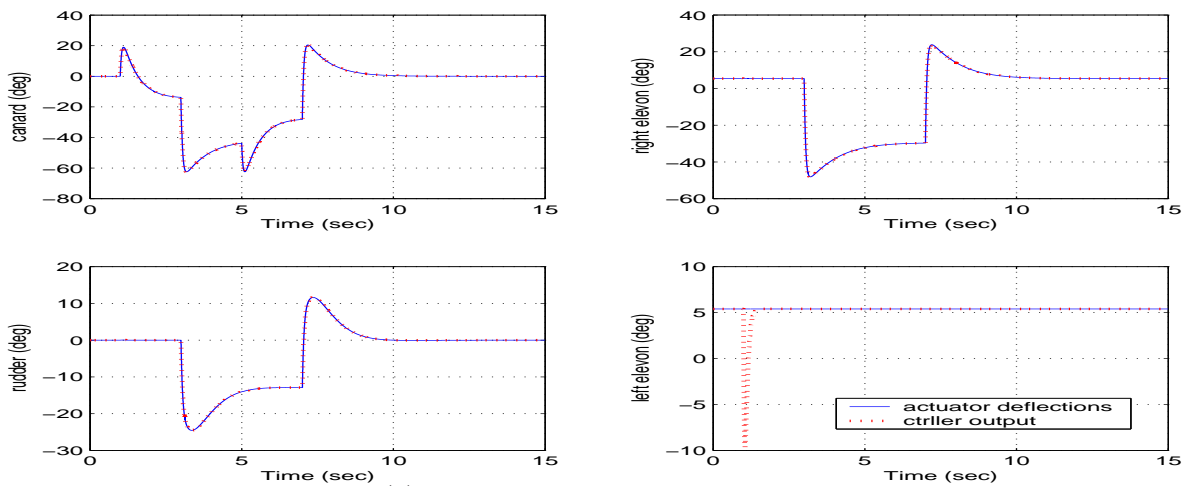


(d) canard fault evolution: weight w_i signals

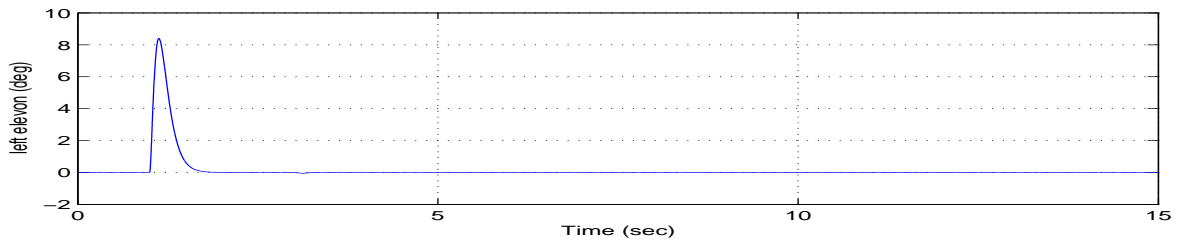
Figure 6.2: Responses of fault & failure on canard



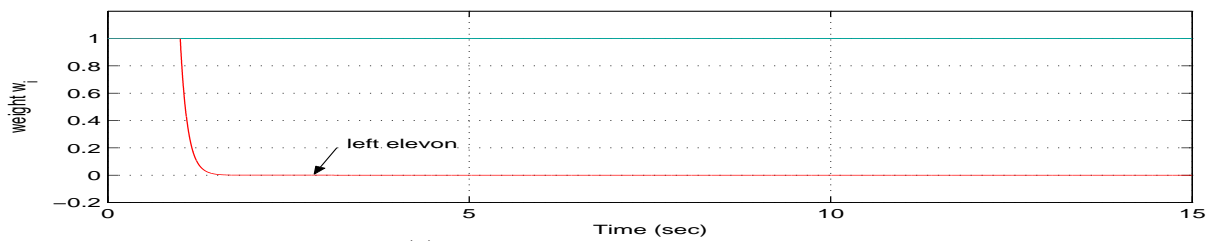
(a) left elevon fail: states



(b) left elevon fail: actuator deflection



(c) left elevon fail: fault reconstruction ($k_i u_i(t)$) signals



(d) left elevon fail: weight w_i signals

Figure 6.3: Responses of failure on left elevon

6.6 Conclusions

This chapter has presented an on-line sliding mode control allocation scheme for fault tolerant control. The effectiveness level of the actuators is used by the CA scheme to redistribute the control signals to the remaining ‘healthy’ actuators when a fault or failure occurs. This chapter has provided an analysis of the proposed sliding mode control allocation scheme and has determined the nonlinear gain required to maintain sliding. The on-line sliding mode control allocation scheme implemented on the ADMIRE model has shown that faults and total actuator failures can be handled directly without reconfiguring the controller.

Chapter 7

SIMONA Implementation Results

The previous chapter proposed and analyzed new fault tolerant schemes using a combination of CA and SMC. Practical issues arising from implementing the proposed controller will be presented in this chapter for controlling both the longitudinal and lateral axes of a nonlinear B747 aircraft on a 6-DOF flight motion simulator called SIMONA (SIMulation, MOtion and NAVigation). Here, a ‘proof of concept’ controller will be presented to highlight the practicality of the sliding mode controllers for real time application. The implementation of the SMC controller on the SIMONA flight simulator was made possible through the co-operation of the faculty of Aerospace Engineering, Delft University of Technology, the Netherlands, under the Group for Aeronautical Research and Technology in Europe, Flight Mechanics, Action Group 16 (GARTEUR AG16) program.

7.1 Introduction

The combination of sliding modes and control allocation developed in the last chapter provides a powerful tool for the development of simple, robust fault tolerant flight controllers that work for a wide range of faults and failures without requiring any reconfiguration (provided there is still enough redundancy in the system). The work in Shtessel *et al.* [185] and Wells & Hess [219] provides practical examples of the combination of SMC and CA for FTC. The work by Shin *et al.* [181] uses CA ideas, but formulates the problem from an adaptive controller point of view. However none of these papers provide a detailed stability analysis and discuss sliding mode controller design issues when using control allocation. The scheme in Chapter 6 uses a control law which depends on (an estimate of) the ‘efficiency/effectiveness’ of the actuators. In this chapter, these ideas are extended and the potential of SMC and CA is demonstrated through an implementation of these ideas on an aircraft research motion simulator. The sliding mode control allocation schemes have been designed and tested on a 6 degree of freedom (6-DOF) research flight simulator called SIMONA running a high fidelity nonlinear aircraft model based on FTLAB747 V6.5/7.1/2006b [190].

7.2 Test facilities (SIMONA)

Testing a fault tolerant controller is an important process in assessing its effectiveness during faults or failures. Typically a newly developed controller is first designed and tested on a benchmark model, and then tested on a flight simulator before being certified by actual flight testing. Flight testing is very expensive. For the study of faults and failures, a high fidelity nonlinear aircraft model can simulate closely real life conditions and the performance of an aircraft with high accuracy, and apart from the cost saving, is much safer. Flight simulators are also used before an actual flight for training and to get precious feedback from pilots on the effectiveness of the controller systems. The work in this chapter is based on a high fidelity nonlinear B747 model for design and desktop simulations, and has subsequently been implemented on a flight simulator. The details of the high fidelity nonlinear B747 model and the flight simulator are described in the subsections below.

7.2.1 The SIMONA research simulator

The SIMONA Research Simulator (SRS) in Figure 7.1 is a research project of the Delft University of Technology. During its design and fabrication the university employed new techniques and insights from various fields to optimize performance and operational flexibility. The resulting flight simulator provides researchers with a powerful tool that can be adapted to various uses [197]. In the years since it has been operational, the SRS has been used for research into human (motion) perception [96, 165, 236], aircraft handling qualities [72, 86], fly-by-wire control algorithms and flight deck displays [132, 158], flight procedures [76, 172] and air traffic control [215]. The flexible software architecture and high-fidelity cueing environment allows the integration of the B747 model from Smali *et al.* [190], complete with failures and the assessment of the controller in a realistic aircraft environment.

The flight deck of the SRS provides the two pilots with simulated instruments that match the aircraft under investigation (Figure 7.1(b) and 7.1(c)). The pilots can interface with the aircraft through a conventional control column or a sidestick controller, a centre pedestal with engine controls and a Mode Control Panel (MCP) for the autopilot. The windows give a wide view on a virtual environment and a motion system moves the entire cabin to simulate aircraft accelerations.

A modular network of personal computers (PCs) provides the processing power to run the simulator. Each PC has a specific task, e.g. driving the pilot controls, generating the instrument graphics, running the aircraft model or logging data. A high-speed fibre-optic network provides synchronization and communication services for all the computers. The modular approach makes it easy to exchange for example the aircraft model for another, without affecting the rest of the simulation software. In particular, the software is able to interface with MATLAB SIMULINK¹ models.

¹MATWORKS trademark

7.2.2 Benchmark V2.2 - FTLAB747 V6.5/7.1/2006b

The FTLAB747 software running under MATLAB² has been developed for the study of FTC and FDI schemes [147]. It represents a ‘real world’ model of a B747-100/200 aircraft, where the technical data and the underlying differential equations have been obtained from NASA [91,92]. The software was originally developed at Delft University of Technology by van der Linden (Delft University Aircraft Simulation and Analysis Tool, DASMAT) [212] and Smaili (Flight Lab 747, FTLAB747) [189], and later developed and enhanced for use in terms of fault detection and fault tolerant control by Marcos & Balas [147] (FTLAB747 V6.1/V6.5). More recently this software has been upgraded to V6.5/7.1/2006b by Smaili *et al.* [190] to allow all the control surfaces to be controlled independently offering more degrees of control flexibility especially during faults or failures. This model is the basis for the results in this chapter. This ‘modified’ aircraft is essentially a fly by wire aircraft [37] where all the control surfaces are controlled electronically compared to the ‘classical’ B747 aircraft which uses mechanical linkages which therefore limit the usability of some of the control surfaces in fault or failure conditions. The high fidelity nonlinear model has 77 states incorporating rigid body variables, sensors, actuators and aeroengine dynamics. All the control surfaces and engine dynamics are modeled with realistic position limits and rate limits. The specific aerodynamic coefficients are taken from Hanke [91] and Hanke & Nordwall [92], which have been obtained from extensive wind tunnel experiments, simulations and test flights. The amount of redundancy available on this aircraft model [147] makes it suitable to test the proposed fault tolerant scheme. The capabilities of this software as a realistic platform to test FTC and FDI schemes is demonstrated by its use by many researchers (see for example Marcos *et al.* [149], Ganguli *et al.* [80], Szaszi *et al.* [199], Maciejowski & Jones [141] and Aravena *et al.* [19]). *However most of the published results are based only on the longitudinal axis.* Here, two sliding mode controllers for lateral and longitudinal control have been designed and tested under multiple fault and failure conditions before being implemented on the 6-DOF SIMONA flight simulator to show the capabilities of the proposed method.

To be able to fly with a pilot in the loop, the benchmark B747 model [190] (from FTLAB747) was slightly adapted from the offline model. The aircraft model was isolated from peripheral utility functions such as the autopilot, to follow the reference scenario and MATLAB logging functions. Its inputs and outputs were standardized to fit in the SRS software environment and the SIMULINK model was converted to C code using the Real-Time Workshop³. Finally the model was integrated with the pilot controls, aircraft instruments and cueing devices of the SRS. Section 7.4 describes in more detail similar steps that were taken for the controller described in the next section, which was subsequently integrated in the SRS and coupled with the B747 model.

7.3 Controller Design

The 12 rigid body states of the B747 aircraft can be divided into 6 longitudinal axis states and 6 lateral and directional axes states which are all determined from the 6-degree of freedom

²MATWORKS trademark

³MATWORKS trademark



(a) Outside view



(b) Flight deck - centre view



(c) Flight deck - right view

Figure 7.1: SIMONA research simulator

equations of motion. The states are given by $x = [p \ q \ r \ V_{tas} \ \alpha \ \beta \ \phi \ \theta \ \psi \ h_e \ x_e \ y_e]^T$. For the longitudinal axis, the states are pitch rate q , true airspeed V_{tas} , angle of attack α , pitch angle θ and altitude h_e . Meanwhile for the lateral and directional axes, the states are roll rate p , yaw rate r , sideslip angle β , roll angle ϕ and yaw angle ψ . The control surfaces comprise 4 ailerons (inner and outer on each wing), 12 spoilers (2 inner spoilers and 4 outer spoilers on each wing), 2 rudders (upper and lower), 4 elevators (an inner and outer on each left and right elevator), a horizontal stabilizer and 4 engine thrusts (which are controlled through engine pressure ratios (EPR)).

In this chapter both lateral and longitudinal control is considered. One of the controller design objectives considered here is to bring a faulty aircraft to a near landing condition. This can be achieved by a change of direction through a ‘banking turn’ manoeuvre [38], followed by a decrease in altitude and speed. This can be achieved by tracking appropriate roll angle (ϕ) and sideslip angle (β) commands using the lateral controller, and tracking flight path angle (FPA) and airspeed (V_{tas}) commands using the longitudinal controller. For lateral control, the settling time when there is no fault/failure should be approximately 20sec for ϕ and 20sec for β . If a fault/failure occurs, the tracking requirement is 25sec for ϕ and β . These specifications are chosen to ensure that there is almost zero side force and therefore passenger comfort is maintained (page 233 of Bryson [38]). For longitudinal control, the settling time when there is no failure should be 20sec for FPA and 45sec for V_{tas} . If a failure occurs, the tracking requirement is 30sec for FPA with no difference in the V_{tas} tracking. These specifications are taken from Ganguli *et al.* [80].

A linearization has been obtained around an operating condition of 263,000 Kg, 92.6 m/s true airspeed, and an altitude of 600m at 25.6% of maximum thrust and at a 20deg flap position. The result is a 12th order linear model (separated into two 6th order models) associated with the lateral and longitudinal states. For design purposes, only the first four longitudinal ($x_{long} = [q \ V_{tas} \ \alpha \ \theta]^T$) and lateral states ($x_{lat} = [p \ r \ \beta \ \phi]^T$) have been retained. For lateral control, the 4 individual engine pressure ratios (EPR) and the 4 individual ailerons have been used. The 10 spoilers⁴ have been aggregated to produce two control inputs on each wing (spoilers 1-4, 5, 8 and 9-12 have been grouped respectively). The other input represents rudder deflection (the upper and lower rudder has been aggregated to produce a single control signal). For longitudinal control, the 4 elevators have been aggregated to produce one control input while the 4 longitudinal EPRs can be controlled independently. The other input represents horizontal stabilizer deflection. The following state-space system pairs represent the lateral and longitudinal systems about the trim condition:

⁴Spoilers 6 & 7 are ground spoilers and are not used during flight [92].

$$A_{lat} = \begin{bmatrix} -1.0579 & 0.1718 & -1.6478 & 0.0004 \\ -0.1186 & -0.2066 & 0.2767 & -0.0019 \\ 0.1014 & -0.9887 & -0.0999 & 0.1055 \\ 1.0000 & 0.0893 & 0 & 0 \end{bmatrix} \quad (7.1)$$

$$B_{lat} = \begin{bmatrix} -0.0832 & 0.0832 & -0.2285 & 0.2285 & -0.2625 & -0.0678 & 0.0678 \\ -0.0154 & 0.0154 & -0.0123 & 0.0123 & -0.0180 & -0.0052 & 0.0052 \\ \hline 0 & 0 & 0 & 0 & 0.0017 & 0.0006 & -0.0006 \\ 0 & 0 & 0 & 0 & 0 & 0 & 0 \\ \hline 0.2625 & 0.1187 & 0.0246 & 0.0140 & -0.0140 & -0.0246 \\ 0.0180 & -0.2478 & 0.1269 & 0.0724 & -0.0724 & -0.1269 \\ \hline -0.0017 & 0.0174 & 0.0005 & 0.0005 & -0.0005 & -0.0005 \\ 0 & 0 & 0 & 0 & 0 & 0 \end{bmatrix} \left. \begin{array}{l} \\ \\ \\ \\ \\ \\ \end{array} \right\} \begin{array}{l} B_{lat,2} \\ \\ \\ B_{lat,1} \end{array} \quad (7.2)$$

and

$$A_{long} = \begin{bmatrix} -0.5137 & 0.0004 & -0.5831 & 0 \\ 0 & -0.0166 & 1.7171 & -9.8046 \\ 1.0064 & -0.0021 & -0.6284 & 0 \\ 1.0000 & 0 & 0 & 0 \end{bmatrix} \quad (7.3)$$

$$B_{long} = \begin{bmatrix} -0.6228 & -1.3578 & 0.0082 & 0.0218 & 0.0218 & 0.0082 \\ 0 & -0.1756 & 1.4268 & 1.4268 & 1.4268 & 1.4268 \\ \hline -0.0352 & -0.0819 & -0.0021 & -0.0021 & -0.0021 & -0.0021 \\ 0 & 0 & 0 & 0 & 0 & 0 \end{bmatrix} \left. \begin{array}{l} \\ \\ \\ \end{array} \right\} \begin{array}{l} B_{long,2} \\ \\ B_{long,1} \end{array} \quad (7.4)$$

where the states represent $x_{lat} = [p \ r \ \beta \ \phi]^T$ and $x_{long} = [q \ V_{tas} \ \alpha \ \theta]^T$. The lateral control surfaces are $\delta_{lat} = [\delta_{air} \ \delta_{ail} \ \delta_{aor} \ \delta_{aol} \ \delta_{sp1-4} \ \delta_{sp5} \ \delta_{sp8} \ \delta_{sp9-12} \ \delta_r \ e_{1lat} \ e_{2lat} \ e_{3lat} \ e_{4lat}]^T$ which represent aileron deflection (right & left - inner & outer)(rad), spoiler deflections (left: 1-4 & 5 & right: 8 & 9-12) (rad), rudder deflection (rad) and lateral engine pressure ratios (EPR). The longitudinal control surfaces are $\delta_{long} = [\delta_e \ \delta_s \ e_{1long} \ e_{2long} \ e_{3long} \ e_{4long}]^T$ which represent elevator deflection (rad), horizontal stabilizer deflection (rad), and longitudinal EPR. The partition of B in (7.2) and (7.4) shows the terms B_1 and B_2 (although a further change of coordinates is necessary to obtain the form in (6.9) to scale B_2 to ensure $B_2 B_2^T = I$). The controlled output distribution matrices are

$$C_{c_{lat}} = \begin{bmatrix} 0 & 0 & 1 & 0 \\ 0 & 0 & 0 & 1 \end{bmatrix}, \quad C_{c_{long}} = \begin{bmatrix} 0 & 0 & -1 & 1 \\ 0 & 1 & 0 & 0 \end{bmatrix}$$

which represent the states ϕ and β for lateral control and flight path angle (FPA) and V_{tas} for longitudinal control. These linear models will be used to design the control schemes which will be described in the next sections.

To include a tracking facility, integral action (as discussed in Section 3.5.1) has been included for both longitudinal and lateral control. For the generic system in (6.7), let $x_r(t)$ represent

integral action states:

$$\dot{x}_r(t) = r(t) - C_c x(t) \quad (7.5)$$

where $C_c \in \mathbb{R}^{l \times n}$ is the distribution matrix associated with the controlled outputs and the differentiable (filtered reference) signal $r(t)$ satisfies

$$\dot{r}(t) = \Gamma (r(t) - r_c) \quad (7.6)$$

with $\Gamma \in \mathbb{R}^{l \times l}$ a stable design matrix and r_c a constant demand vector. Augmenting the states from (7.1)-(7.4) with the integral action states and defining $x_a(t) = \text{col}(x_r(t), x(t))$ it follows that

$$\dot{x}_a(t) = A_a x_a(t) + B_a u(t) + B_r r(t) \quad (7.7)$$

where

$$A_a = \begin{bmatrix} 0 & -C_c \\ 0 & A \end{bmatrix} \quad B_a = \begin{bmatrix} 0 \\ B \end{bmatrix} \quad B_r = \begin{bmatrix} I_p \\ 0 \end{bmatrix} \quad (7.8)$$

If (A, B) is controllable and (A, B, C_c) does not have any zeros at the origin then (A_a, B_a) is controllable. Define a switching function $s_a(t) : \mathbb{R}^{(n+l)} \rightarrow \mathbb{R}^l$ to be

$$s_a(t) = S_a x_a(t) \quad (7.9)$$

where $S_a \in \mathbb{R}^{l \times (n+l)}$ and $S_a B_a = I_l$. As in Equation (6.42)-(6.43), the proposed ‘virtual control’ law comprises two components $\hat{v}(t) = \hat{v}_l(t) + \hat{v}_n(t)$. Now because of the reference signal $r(t)$, the linear component has a feed-forward reference term and so $\hat{v}_l(t) = L x_a(t) + L_r r(t)$ where $L = -\hat{S}_a \hat{A}_a$ and $L_r = -\hat{S}_a \hat{B}_r$. Here \hat{A}_a , \hat{B}_r and \hat{S}_a are the matrices from (7.8) and (7.9) after a transformation to achieve the regular form in Equation (6.19) has been performed. The nonlinear component is defined as

$$\hat{v}_n(t) = -\rho(t, x_a) \frac{s_a(t)}{\|s_a(t)\|} \quad \text{for } s_a(t) \neq 0 \quad (7.10)$$

From (6.47)

$$u(t) = W B_2^T (B_2 W^2 B_2^T)^{-1} \hat{v}(t) \quad (7.11)$$

i.e. the control sent to the actuators is dependent on the effectiveness gains k_i (through the diagonal weighting matrix W).

7.3.1 Lateral Controller Design

In normal operation, the ailerons will be the primary control surface for ϕ tracking, whilst the spoilers introduce redundancy. Meanwhile for β tracking, the rudder will be the primary control surface and differential engine thrust is the associated redundancy. It will be assumed that at least one of the control surfaces for both ϕ and β tracking will be available when a fault or failure occurs (i.e. one of either the four ailerons or the four spoilers will be available and one of either the rudder or the four engine thrusts are available). Based on these assumptions, it can be verified from a numerical search that $\gamma_{0_{lat}}$ from (6.27) is $\gamma_{0_{lat}} = 8.1314$.

The matrix which defines the hyperplane must now be synthesized so that the conditions of

(6.36) are satisfied. As in the previous chapters, a quadratic optimal design (as in Section 3.4.1) has been used to obtain the sliding surface $S_{a_{lat}}$ which depends on the matrix M_{lat} in Equation (6.28). Here the symmetric positive definite state weighting matrix has been chosen as $Q_{lat} = \text{diag}(0.005, 0.1, 6, 6, 1, 1)$. The first two terms of Q_{lat} are associated with the integral action and are less heavily weighted. The third and fourth term of Q_{lat} are associated with the equations of the angular acceleration in roll and yaw (i.e. $B_{lat,2}$ term partition in (6.9)) and thus weight the virtual control term. Thus by analogy to a more typical LQR framework, they effect the speed of response of the closed-loop system. Here, the third and fourth terms of Q_{lat} have been heavily weighted compared to the last two terms to reflect a reasonably fast closed-loop system response. The poles associated with the reduced order sliding motion are $\{-0.0707, -0.3867, -0.3405 \pm 0.1484i\}$. Based on this value of M_{lat} , simple calculations from (6.32) show that $\gamma_{1_{lat}} = 0.0145$, therefore $\gamma_{0_{lat}}\gamma_{1_{lat}} = 0.1180 < 1$ and so the requirements of (6.36) are satisfied. Also for this particular choice of sliding surface, $\|\tilde{G}_{lat}(\mathbf{s})\|_{\infty} = \gamma_{2_{lat}} = 0.0764$ from (6.35). Therefore from (6.36),

$$\frac{\gamma_{2_{lat}}\gamma_{0_{lat}}}{1 - \gamma_{1_{lat}}\gamma_{0_{lat}}} = 0.7043 < 1$$

which shows that the system is stable for $0 < w_i \leq 1$. The pre-filter matrix from (7.6) has been designed to be $\Gamma_{lat} = \text{diag}(-0.5, -0.5)$. This may be viewed as representing the ideal response in the ϕ and the β channels. For implementation, the discontinuity in the nonlinear control term in (7.10) has been smoothed by using a sigmoidal approximation described in Section 3.2.2 where the scalar $\delta_{lat} = 0.05$. This removes the discontinuity and introduces a further degree of tuning to accommodate the actuator rate limits – especially during actuator fault or failure conditions.

To emulate a real aircraft flight control capability, an outer loop heading control was designed based on a proportional plus derivative controller, to provide a roll command to the inner loop sliding mode controller. In the SIMONA implementation, this outer loop heading control can be activated by a switch in the cockpit. The proportional gain was set as $K_{p_{lat}} = 0.5$ and the derivative gain was set as $K_{d_{lat}} = 0.1$

7.3.2 Longitudinal Controller Design

In normal operation, the elevators will be the primary control surface for FPA tracking, whilst the horizontal stabilizer introduces redundancy. For V_{tas} tracking, the collective thrust (from the four engines) will be the actuator. It will be assumed that at least one of the control surfaces for FPA tracking will still be available when a fault or failure occurs. It is also assumed that at least one of the four engines is available for V_{tas} tracking. Based on these assumptions, it can be verified from a numerical search that $\gamma_{0_{long}} = 8.2913$ from (6.27).

As in the lateral controller, a quadratic optimal design has been used to obtain the sliding surface matrix (and therefore the matrix M_{long}). The weighting matrix has been chosen as $Q_{long} = \text{diag}(0.1, 0.1, 10, 50, 1, 1)$. Again, similar to the lateral controller design, the first two terms of Q_{long} are associated with the integral action and are less heavily weighted. The third and fourth terms of Q_{long} are associated with the $B_{long,2}$ term partition in (6.9) (i.e. states q and V_{tas}) which weight the virtual control term, and have been heavily weighted

compared to the last two terms. The poles associated with the reduced order sliding motion are $\{-0.7066, -0.2393 \pm 0.1706i, -0.0447\}$. Based on this value of M_{long} , simple calculations from (6.32) show that $\gamma_{1_{long}} = 1.9513 \times 10^{-4}$: therefore $\gamma_{0_{long}}\gamma_{1_{long}} = 0.0016 < 1$ and so the requirements of Equation (6.36) are satisfied. For this choice of sliding surface, $\|\tilde{G}_{long}(\mathbf{s})\|_{\infty} = \gamma_{2_{long}} = 0.0112$ from (6.35). Therefore from (6.36),

$$\frac{\gamma_{2_{long}}\gamma_{0_{long}}}{1 - \gamma_{1_{long}}\gamma_{0_{long}}} = 0.0931 < 1$$

which shows that the system is stable for $0 < w_i \leq 1$. The pre-filter matrix from (7.6) has been designed to be $\Gamma_{long} = \text{diag}(-0.5, -0.125)$. The discontinuity in the nonlinear control term in (7.10) has been smoothed by using a sigmoidal approximation where the scalar $\delta_{long} = 0.05$.

An outer loop altitude control scheme was designed based on a proportional plus derivative controller to provide a FPA command to the inner loop sliding mode controller. In the SIMONA implementation, this outer loop altitude control can be activated by a switch in the cockpit. The proportional and the derivative gains were set as $K_{p_{long}} = 0.001$ and $K_{d_{long}} = 0.05$ respectively.

Note that both the lateral and longitudinal controller manipulate the engine EPRs. For lateral control, differential engine EPR is required as a secondary ‘actuator’ for β tracking; whilst for longitudinal control, collective EPR is used for V_{tas} tracking. In the trials, ‘control mixing’ was employed, where the signals from both the lateral controller ($e_{1_{lat}}, e_{2_{lat}}, e_{3_{lat}}$ and $e_{4_{lat}}$) and longitudinal controller ($e_{1_{long}}, e_{2_{long}}, e_{3_{long}}$ and $e_{4_{long}}$) were added together before being applied into each of the engines (page 14 of Burcham *et al.* [43]). This is similar to the control strategy used for the NASA propulsion control aircraft described in Burcham *et al.* [43].

7.4 SIMONA Implementations

The controller was implemented as a MATLAB SIMULINK (version 2006b) model with appropriate inputs and outputs to connect it with the aircraft model and the SIMONA hardware, as described in Table 7.1 and Figure 7.2.

Input	Source	Output	Destination
Reference signals e.g. ψ_{cmd}	MCP	Actuator commands	Aircraft model
Aircraft states e.g. ψ	Aircraft model	Controller data	Data logger
Configuration switches e.g. ψ or ϕ	Pilot switches	Configuration choice	Controller

Table 7.1: SIMONA hardware interconnections

The controller/aircraft model combination contains an algebraic loop, with the controller requiring input from the model whilst producing the required input for the aircraft model. In the SRS this was solved by the controller module using the aircraft state data from the previous time step. All data is time stamped, ensuring consistency across different modules within the simulation, even when they are on physically different processors.

The controller was set up to work with an Ode4 solver with a fixed time step of 0.01 sec. Using the Real-Time Workshop, the SIMULINK controller block diagram was converted to C-code and integrated into the SRS, where it runs on a dual Pentium III 1 GHz processor, together with

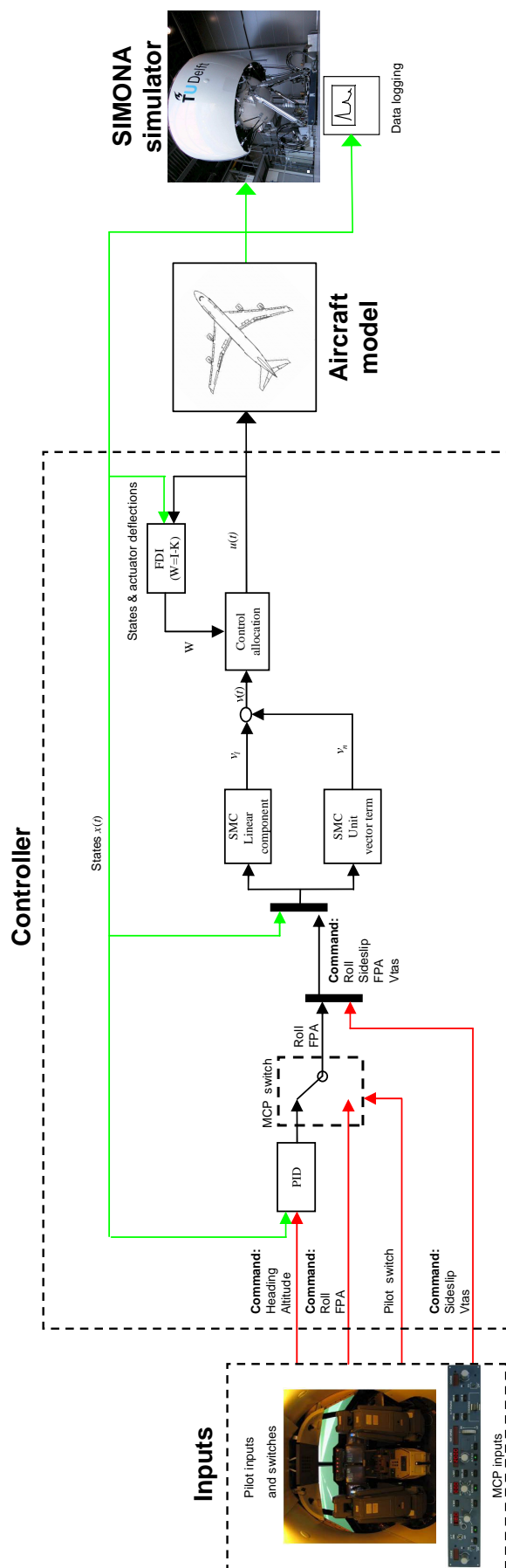


Figure 7.2: SIMONA interconnections



Figure 7.3: Mode control panel (MCP)

the aircraft model and motion control software. The available processing power is sufficient to run the controller in real time, i.e. within 10 ms per time step.

A connection with the Mode Control Panel (MCP) on the flight deck (Figure 7.3) enables the selection of ‘control modes’ e.g. altitude hold, heading select and reference values. The simulator trials were performed with the speed, altitude and heading select modes active. The pilot commands new headings, speeds or altitudes by adjusting the controls on the MCP.

7.5 Results

The results presented in this chapter are all from the 6–DOF SIMONA research simulator based on the full 77 state nonlinear B747 model. For passenger comfort during turning manoeuvres, the reference command for ϕ was limited to 25deg and a 0deg reference applied to β to force the nose of the aircraft to point towards the heading angle. It was assumed that the aircraft has recently taken off and reached an altitude of 600m. After a few seconds of straight and level flight, failures occur on the actuators. The immediate action requested by the pilot is to change the heading to 180deg and to head back to the runway. The altitude is then changed from 600m (1967.2ft) to 30.5m (100ft) before the V_{tas} is reduced from 92.8m/s(180kn) to 82.3m/s(160kn), to approximate a landing manoeuvre.

Five different control surface failures have been tested on the simulator: all elevators jam with a 3deg offset, all ailerons jam with a 3deg offset, a stabilizer runaway, all rudders runaway and finally both rudders detach from the vertical fin [190]. All the trials have been done with and without wind and turbulence. However due to space limitations, only the most significant results are shown in this chapter.

7.5.1 No fault

Figures 7.4–7.6 show the fault–free responses of the controller. Figure 7.4 shows that there is a small amount of coupling between roll and sideslip during a heading change. There is also a small change in altitude during heading change. The heading is changed by means of two 90deg step inputs followed by a change in altitude from 600m to 30m in 3 steps: 600m to 366m to 183m and finally to 30m above the runway. Figure 7.4 shows good tracking by the states of the command signals. Figure 7.5 shows the nominal variation in the norm of the switching function signals. Finally Figure 7.6 shows the overall trajectory of the aircraft in 3D. Here, the change in heading and altitude can be seen more clearly.

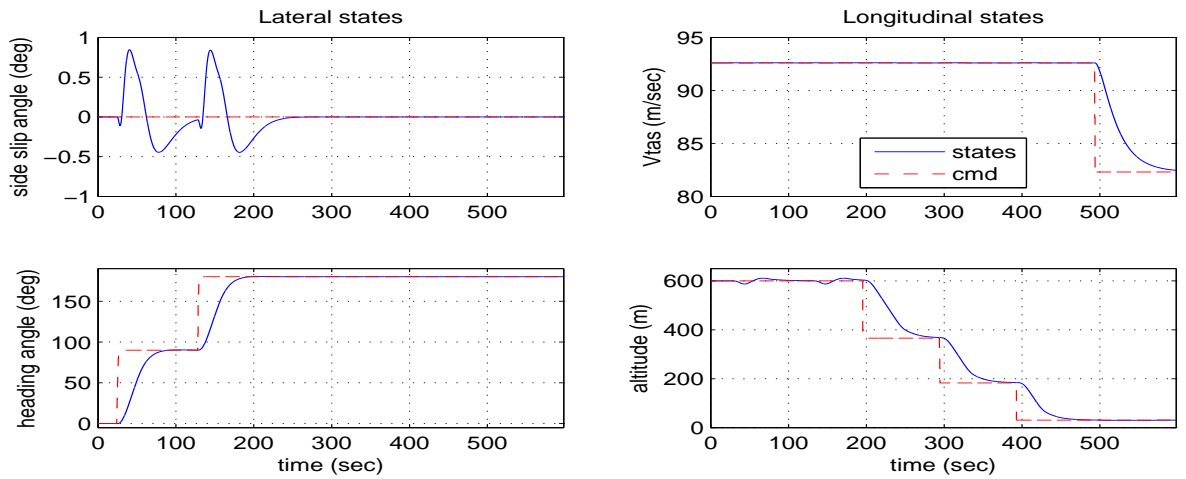


Figure 7.4: no fault condition: controlled states

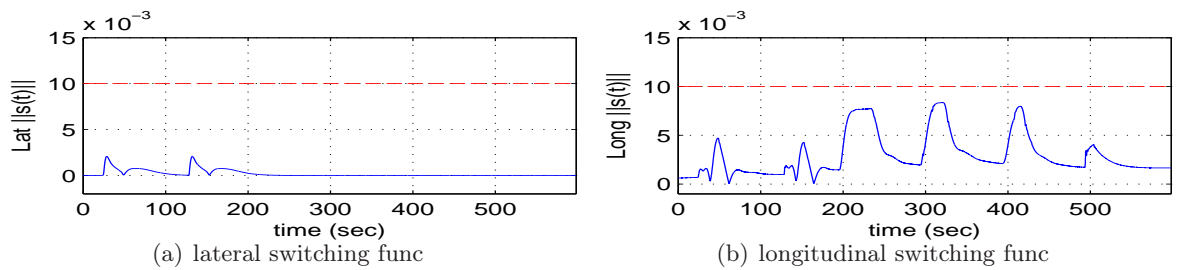


Figure 7.5: No fault conditions

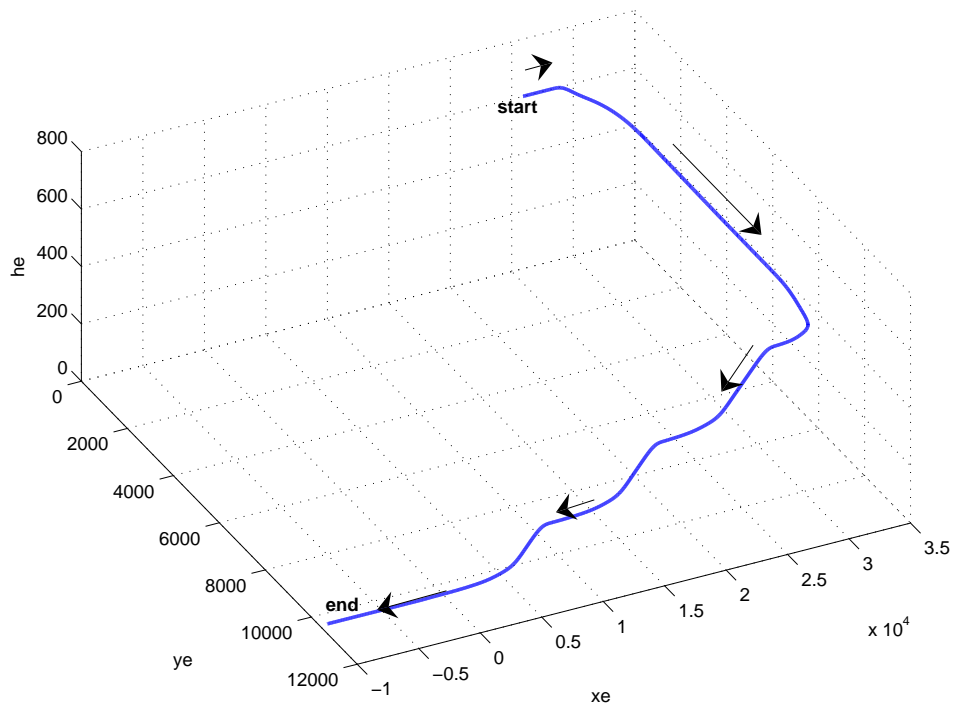


Figure 7.6: no fault condition: flight trajectory

7.5.2 Actuator effectiveness

In (7.11), the weighting matrix W depends on information about the actuator fault. In this chapter, it will be assumed that a measurement of the actual actuator deflection is available. This is not an unrealistic assumption in aircraft systems [37]. Information provided by the actual actuator deflection can be compared with the signals from the controller to indicate the effectiveness of the actuator. The idea is to use a ‘least squares’ method to estimate the coefficients w_i and c_i in a relationship of the form

$$u_{(i,a)} = w_i u_i + c_i$$

where $u_{(i,a)}$ represents the actual deflection and u_i represents the demanded deflection i.e. the controller output. The scalars w_i and c_i can be obtained from a least squares optimization and $W := \text{diag}(w_1, \dots, w_m)$. If the i th actuator is working perfectly, $w_i = 1$ and $c_i = 0$. If $w_i < 1$ then a fault is present. In the SIMONA implementation, 10 data samples from a ‘moving window’, collected at 100Hz are used to compute the w_i and c_i . In the SIMONA implementation, both the lateral and longitudinal controller has its own fault estimation block.

7.5.3 Stabilizer runaway

Figures 7.7-7.9, showing a stabilizer runaway failure, are comparable to those in Figures 7.4-7.6. As before, Figure 7.7 shows no visible degradation in performance. The only difference that can be seen is in the switching function shown in Figure 7.9. Here the switching function exceeds the nominal condition briefly after failure occurs but immediately returns and remains close to zero. Figure 7.8 shows the stabilizer runaway to a maximum positive deflection of 3deg at its maximum deflection rate of 0.5deg/sec [92]. During the stabilizer runaway, Figure 7.8 shows the elevator moves to the negative deflection to counteract the effect of stabilizer runaway. Figure 7.8 also shows that to counteract the stabilizer deflection change of about 6deg (from a trim deflection of -3deg to maximum deflection of 3deg), the elevator deflection has offset approximately 12deg from its trim deflection of approximately 2deg. Finally, Figure 7.9(a) shows that the effectiveness of the stabilizer has been successfully estimated.

7.5.4 Elevator jam with offset

Figures 7.10 -7.12 show the system responses when the elevator jams with an offset in the presence of wind and gusts. Figure 7.10 shows that the states maintain the required performance (as in the no fault condition in Figure 7.4) throughout the manoeuvre. A small change in altitude during the elevator jams is visible at approximately 50sec, since the effect of the elevator offset to 5deg from the trim deflection (see Figure 7.11) creates an unwanted pitch moment. Figure 7.11 also shows that when the elevator jams occur, the stabilizer becomes more active and offset from approximately -3deg to -5deg deflection to counteract the effect of elevator offset jam. Figure 7.12(a) shows that the elevator effectiveness has been successfully estimated. Figure 7.12(b) shows that during the elevator jam, the switching function momentarily deviates from the nominal conditions; but once the control signal redistribution takes place, the switching function returns to near zero.

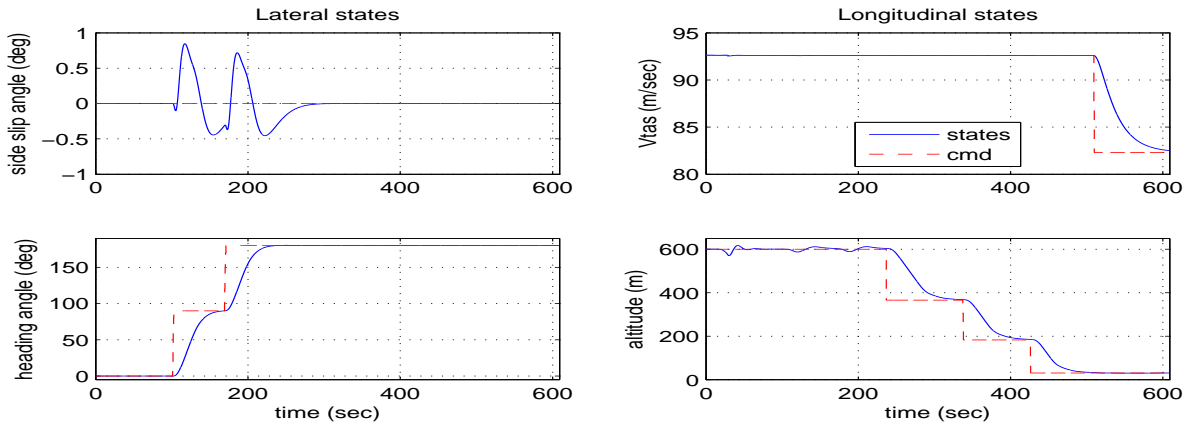


Figure 7.7: stabilizer runaway: controlled states

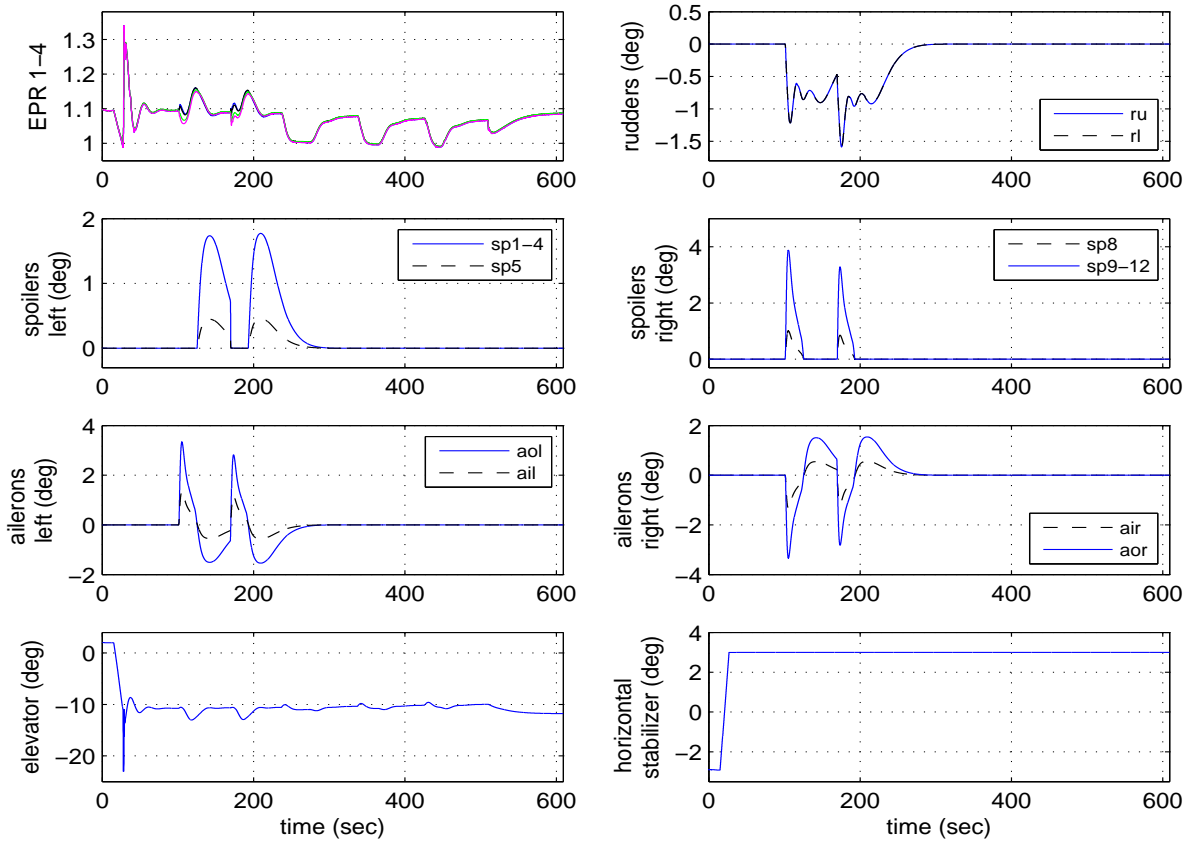


Figure 7.8: stabilizer runaway: actuator positions

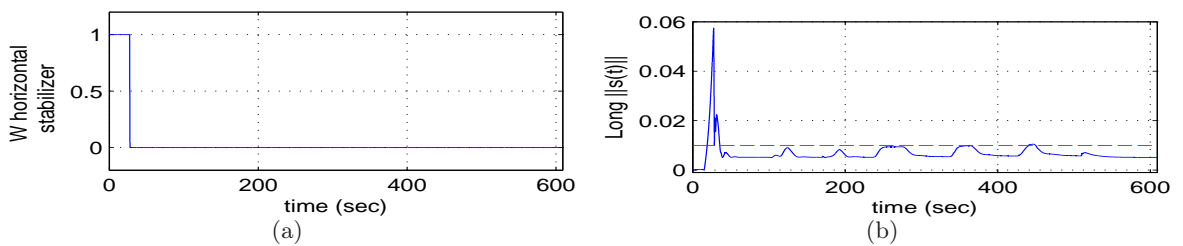


Figure 7.9: stabilizer runaway: actuator effectiveness and switching function

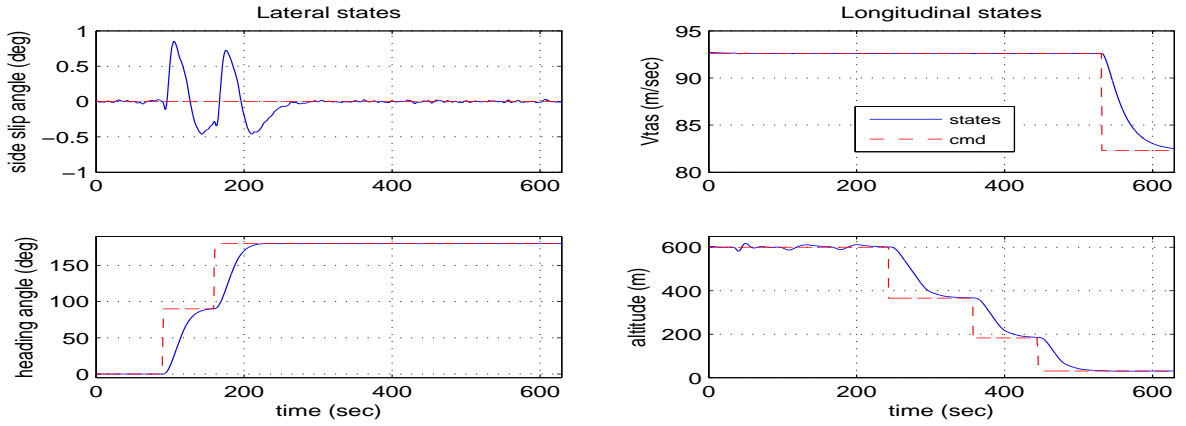


Figure 7.10: elevator jam with offset: controlled states

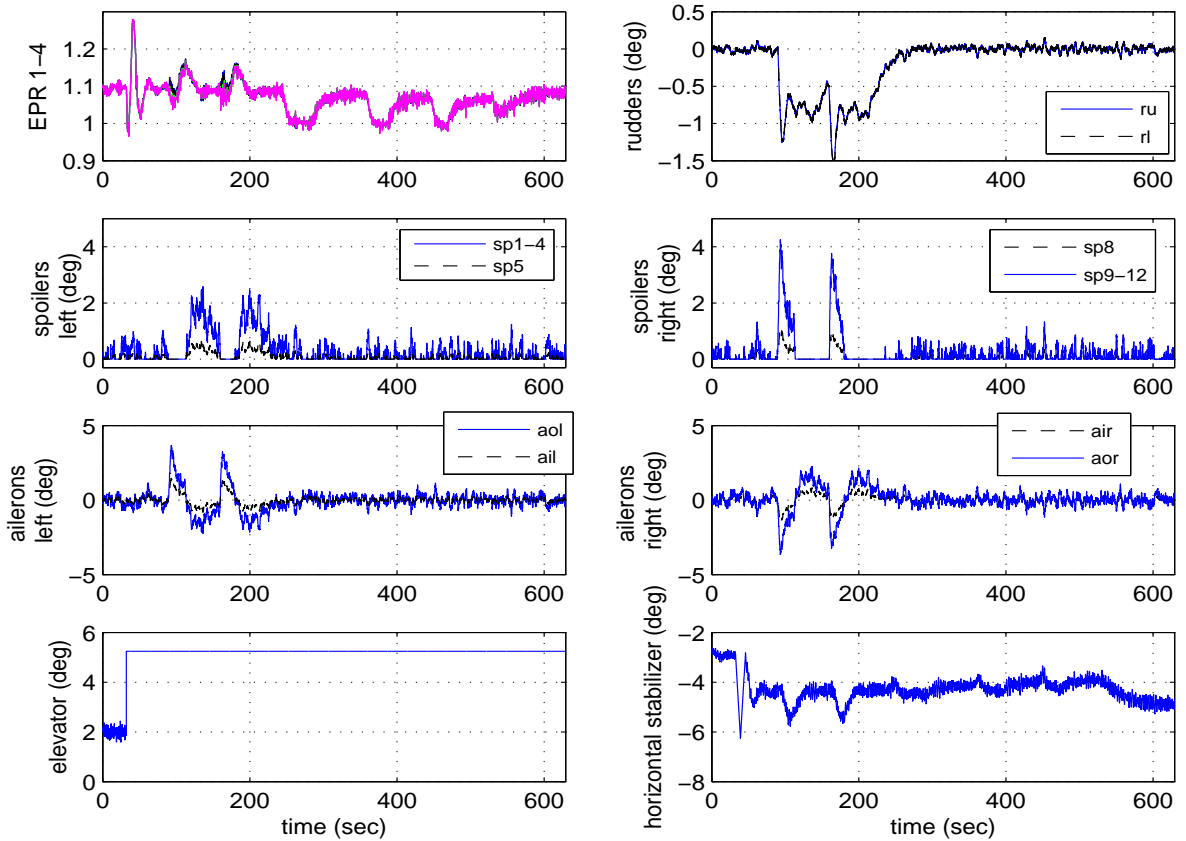


Figure 7.11: elevator jam with offset: actuator positions

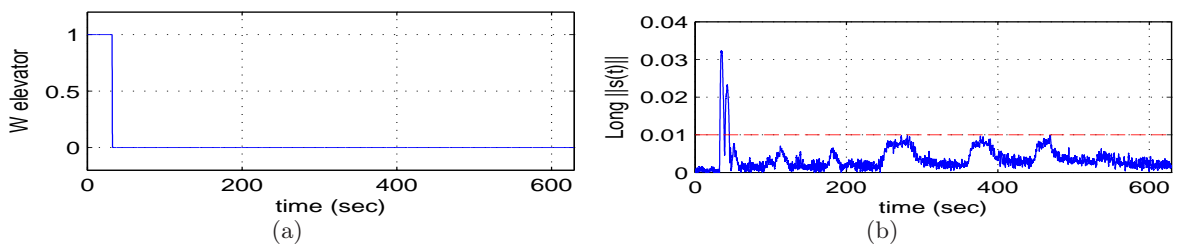


Figure 7.12: elevator jam with offset: actuator effectiveness and switching function

7.5.5 Aileron jam with offset

Figures 7.13 -7.15 show the system responses when the aileron jams with an offset. Figure 7.13 shows no visible difference in terms of tracking performance compared to the no fault condition. Figure 7.14 shows the offset deflection of the aileron from 0deg to an offset deflection of 3deg. After the aileron jams, the aileron effectiveness estimation (Figure 7.15(a)) drops to zero, and therefore the control signals sent to the ailerons are shut off and redistributed to the spoilers. Figure 7.15(a) shows that after the aileron jams, the spoilers become more active to provide roll. Finally Figure 7.15(b) shows that the switching function is maintained close to zero, indicating that a nominal performance is maintained despite the failure.

7.5.6 Rudder missing

Figures 7.16 -7.18 show the system responses when the upper and lower rudder detaches from the vertical fin in the presence of wind and gusts. This is shown clearly in Figure 7.17 where at the start of the simulation, the rudder moves due to wind and gusts, and when the rudders are detached, there is no longer any deflection detected by the sensor. Figure 7.16 shows that without the rudders, the aircraft manages to maintain the required level of performance even in challenging wind and gust conditions. There is visually no difference in the sideslip performance compared to the nominal situation in Figure 7.4. Finally Figure 7.18 shows accurate rudder effectiveness estimation and that the switching function is maintained close to zero despite the failure and the presence of wind and gusts.

7.5.7 Rudder runaway

Figure 7.20 shows that the upper and lower rudders runaway to the 5deg position. Not only does the rudder runaway cause a tendency to turn to one side (and therefore affecting the lateral performance), it also creates difficulties in the longitudinal axis and results in a tendency to pitch up. Figure 7.19 shows that the controller is tested on a slightly different manoeuvre. The sideslip command is kept at 0deg and has only a small degradation in its performance. The heading is changed by 180deg by banking to the right and at the same time the speed is increased to 113.18m/s (220kn) adding further difficulties to the banking manoeuvre. Then a bank left is tested by changing the demanded heading back to 135deg, followed by a reduction in speed to 92.6m/s. The altitude is also decreased to 30m, before a small increase in altitude to 182m above the runway. In these tests, only a small degradation in performance is visible. Figure 7.21 shows that the switching function just exceeds the nominal condition at high speed indicating that, the effect of the rudder runaway is harder to control. However, using the rudder effectiveness information in Figure 7.21, the control signal sent to the rudder is shut-off and the control signals are sent to the remaining functioning actuators causing a visible split in the control surface deflections as seen in Figure 7.20. Figure 7.20 shows the 4 EPR have split to counteract the effect of the banking turn. Engine 3 (red line) and 4 (green line) on the right wing show less EPR compared to Engine 1 (red line) and 2 (green line) on the left wing, to counteract the tendency to turn to the left. The spoilers and ailerons also show a visible split in terms of the deflections to counteract the effect of the rudder runaway.

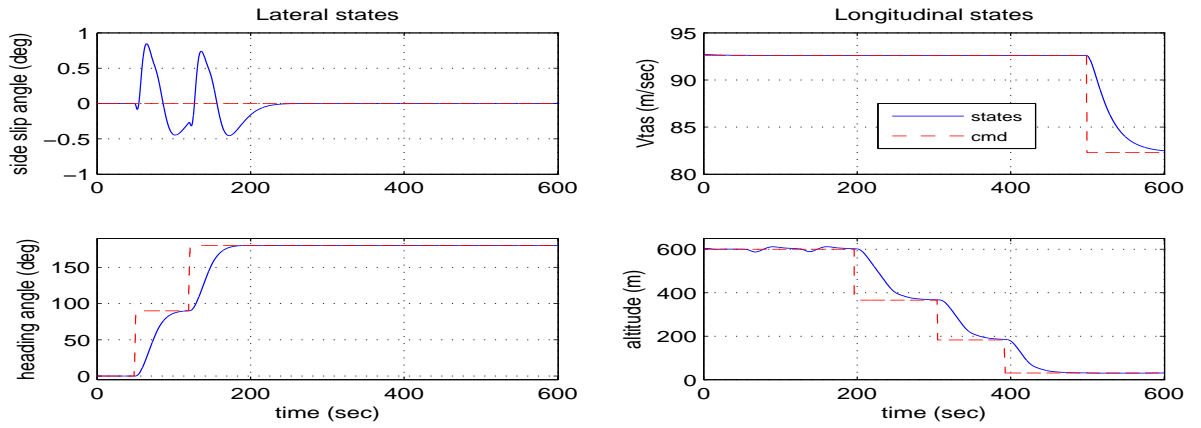


Figure 7.13: aileron jam with offset: controlled states

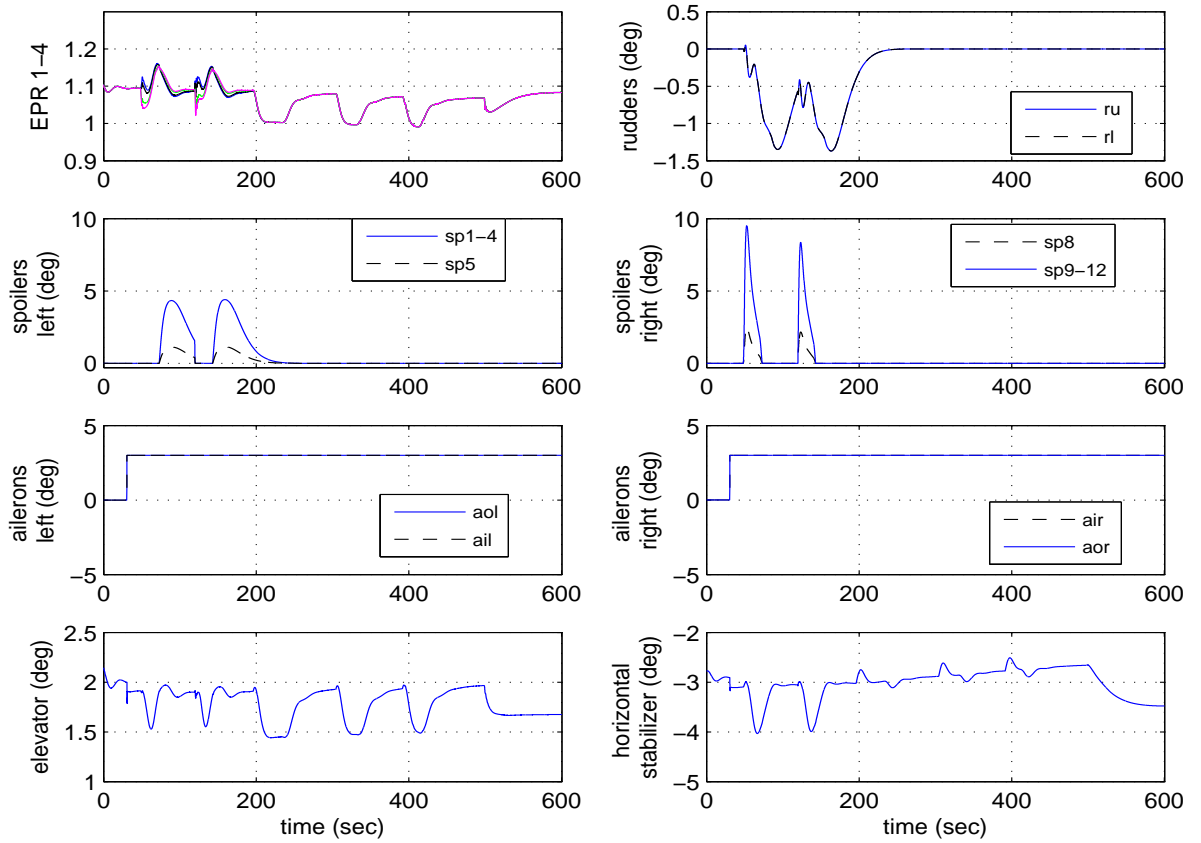


Figure 7.14: aileron jam with offset: actuator positions

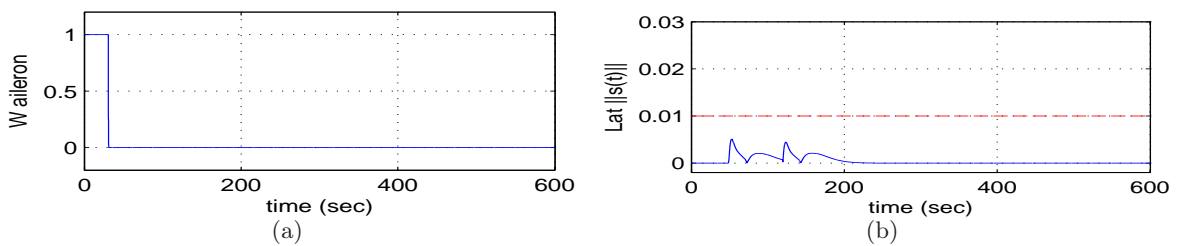


Figure 7.15: aileron jam with offset: actuator effectiveness and switching function

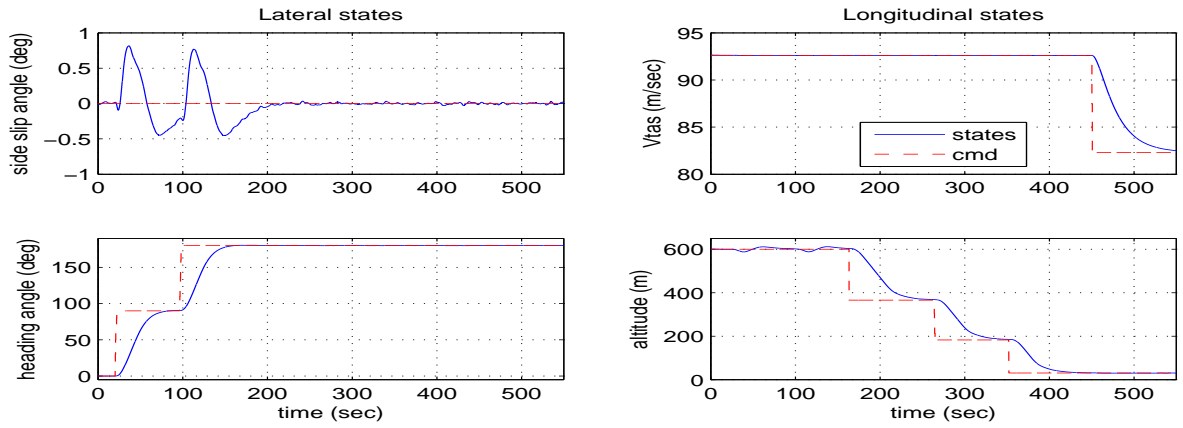


Figure 7.16: rudder missing with wind & gust: controlled states

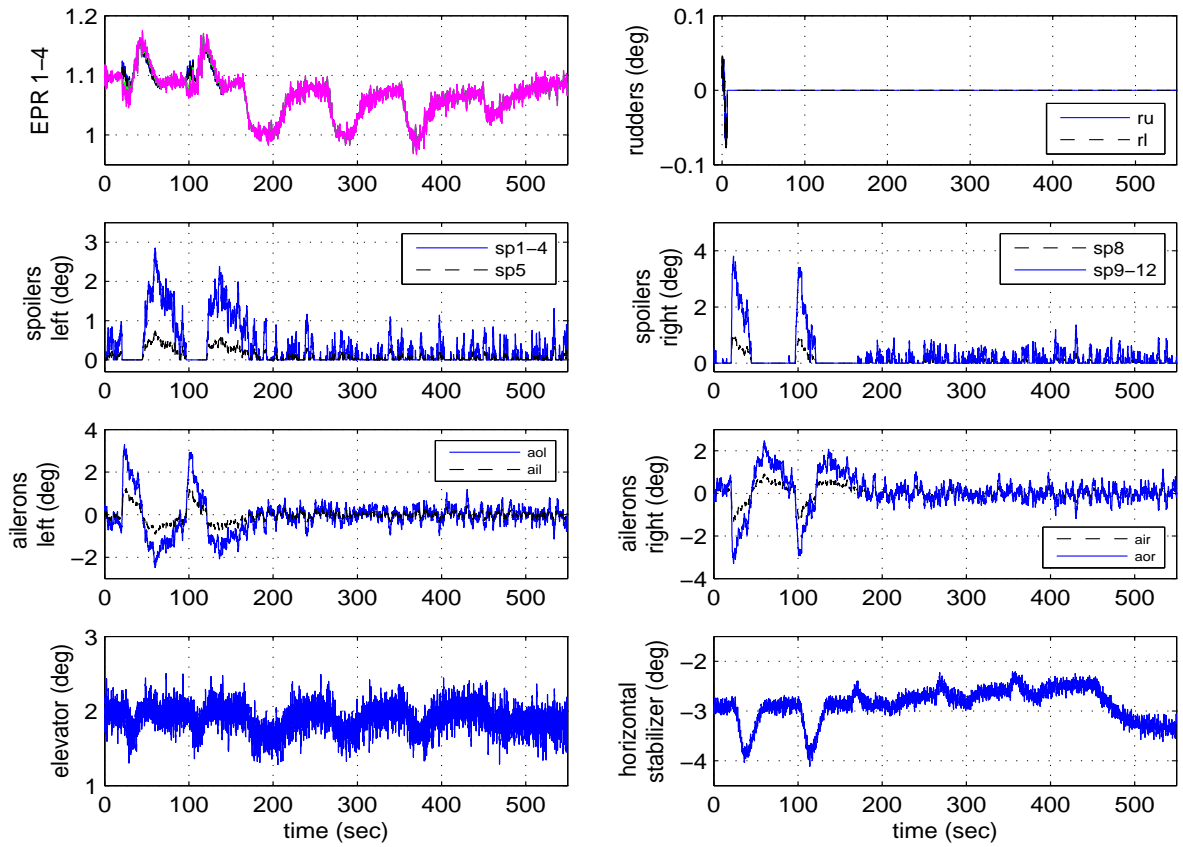


Figure 7.17: rudder missing with wind & gust: actuator positions

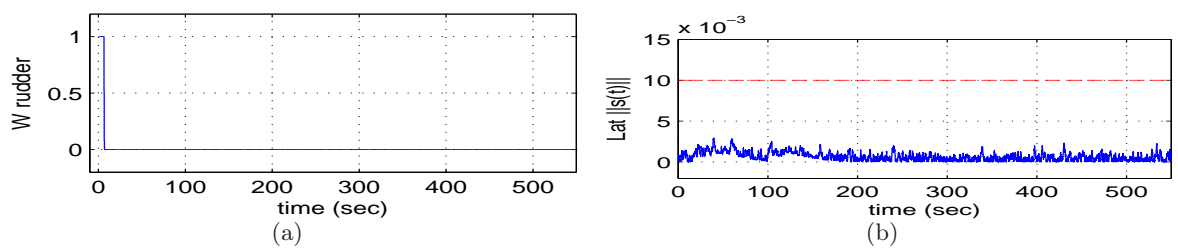


Figure 7.18: rudder missing with wind & gust: actuator effectiveness and switching function

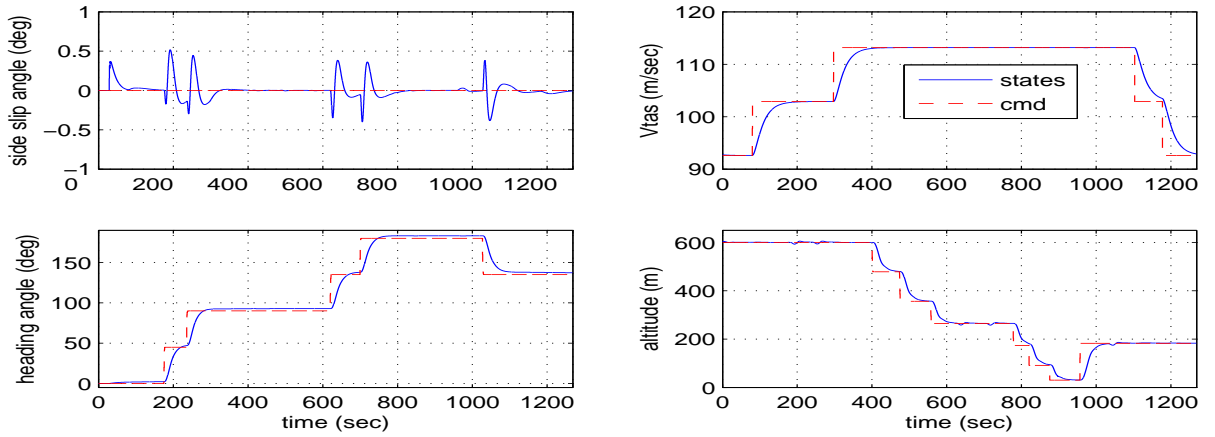


Figure 7.19: rudder runaway: controlled states

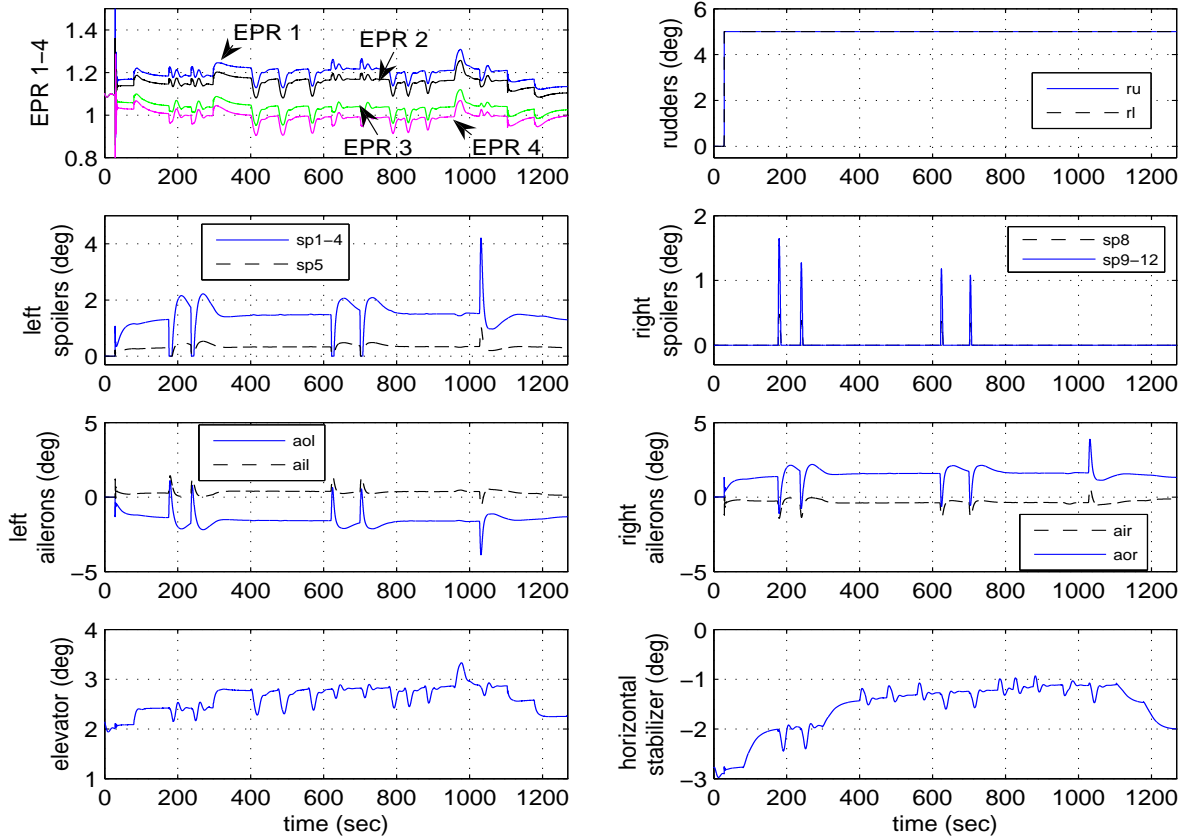


Figure 7.20: rudder runaway: actuator positions

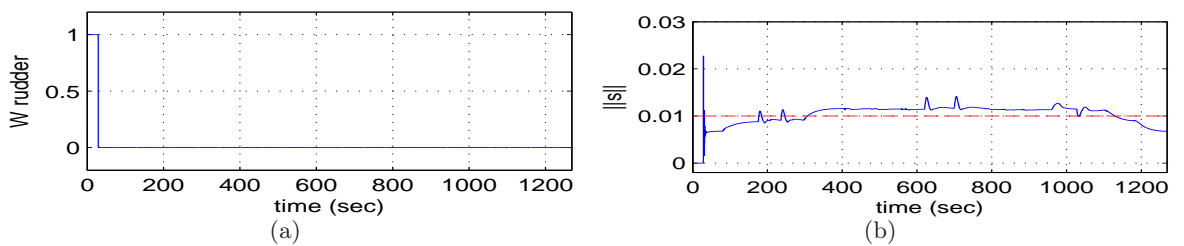


Figure 7.21: rudder runaway: actuator effectiveness and switching function

7.6 Conclusions

This chapter has presented sliding mode control allocation schemes for fault tolerant control. The control allocation aspect is used to allow the sliding mode controller to redistribute the control signals to the remaining functioning actuators when a fault or failure occurs, without reconfiguring or switching to another controller. This chapter has provided a proof of concept to highlight the practicality of the real time application of the proposed scheme. The scheme, implemented on the SIMONA research flight simulator has shown good performance not only in nominal conditions, but also in the case of total actuator failures, even in wind and gust conditions.

Chapter 8

Model Reference Sliding Mode FTC

In the last two chapters, a combination of CA and SMC has been introduced. A rigorous stability analysis and a practical implementation have been presented in the framework of integral action for tracking purposes. In this chapter, two different CA strategies will be considered. The first CA strategy is based on the effectiveness of the actuators. In the second CA strategy, the control signal will be distributed equally among all actuators. The main difference of this chapter compared to the previous chapter, will be the use of a model reference framework (similar to the one in Section 3.5.2) for tracking purposes. The use of a model reference tracking strategy is well known in the literature to have the benefit of avoiding the problem of ‘windup’ which may be suffered by integral action tracking methods – especially when significant faults/failures occur. This chapter will highlight the benefit of combining SMC, CA and a model reference framework for achieving FTC. An adaptive gain and an adaptive reference model are used to increase the flexibility of the design and to provide further tuning for the controller.

8.1 Introduction

The so-called model reference framework is one of the many ways of achieving control reconfiguration or adaptation [133]. Therefore it is not surprising that model reference control is quite synonymous with FTC. The work described in [112] and [56] describes some recent research that uses model reference schemes for active FTC. The popularity of the model reference framework for adaptation and FTC is due to several advantageous features. Many performance specifications are given in the time domain e.g. rise time, damping ratio, decoupling effects etc. These can be represented in terms of an ideal transfer function response, which become the reference signals the closed-loop system must follow for tracking purposes. Another advantage of using a model reference framework for FTC is that it allows the reference model to be changed online to cope with changes in the operational conditions especially during faults or failure.

In the SMC literature, model reference schemes have been used for tracking (as seen in Section 3.5.2 and [24, 57, 59, 194, 246]). In terms of FTC, work such as [56] has investigated combining model reference and SMC. This chapter explores the use of a model reference framework combined with SMC (as in Section 3.5.2) and CA. Two novel adaptive gain approaches are also proposed to achieve and maintain sliding. One advantage of the approach in this chapter

is the absence of integrators; this eliminates the dangers of windup in the face of saturation and rate limits being exceeded (because of the increased burden imposed on the remaining working actuators as a result of the faults). The introduction of the adaptive gain in the SMC controller obviates the need for unnecessarily large gains in the non-linear control terms in the fault-free case. An adaptive reference model is also discussed to provide a safe level of degraded performance.

8.2 Controller Design

As in Chapter 6, this chapter considers a situation where a fault associated with the actuators develops in a system. It will be assumed that the system subject to actuator faults or failures, can be written as

$$\dot{x}(t) = Ax(t) + Bu(t) - BK(t)u(t) \quad (8.1)$$

where $A \in \mathbb{R}^{n \times n}$ and $B \in \mathbb{R}^{n \times m}$. The effectiveness gain $K(t) := \text{diag}(k_1(t), \dots, k_m(t))$, where the $k_i(t)$ are scalars satisfying $0 \leq k_i(t) \leq 1$. These scalars model a decrease in effectiveness of a particular actuator. In most CA strategies, the control signal is distributed equally among all the actuators [181, 185, 219] or distributed based on the limits (position and rate) of the actuators [95]. In this chapter, two different CA strategy will be considered. First, (as in Chapter 6) information about $K(t)$ will be incorporated into the allocation algorithm through a weighting matrix W , so that the control is redistributed to the remaining actuators when faults/failures occur. The idea is that if an actuator fault occurs, the control input $u(t)$ is reallocated to minimize the use of the faulty control surface. The second strategy is based on a widely used CA approaches from the literature; i.e. fixed and equal distribution of the control signals. This is motivated by the fact that the information about K in (8.1) is not always available. Here, the CA is set to be fixed and the control signals are distributed equally to all actuators and is therefore independent of the fault information.

Again as in Chapter 6, assume that the system states can be reordered, and the input distribution matrix B from (8.1) can be partitioned as:

$$B = \begin{bmatrix} B_1 \\ B_2 \end{bmatrix} \quad (8.2)$$

where $B_1 \in \mathbb{R}^{(n-l) \times m}$ and $B_2 \in \mathbb{R}^{l \times m}$ has rank l . It will be assumed without loss of generality that the states of the system in (8.1) have been transformed so that $B_2 B_2^T = I_l$ and therefore $\|B_2\| = 1$. As in Chapter 6, let the ‘virtual control’

$$\nu(t) := B_2 u(t) \quad (8.3)$$

so that

$$u(t) = B_2^\dagger \nu(t) \quad (8.4)$$

where the right pseudo inverse is chosen as

$$B_2^\dagger := \Omega B_2^T (B_2 \Omega B_2^T)^{-1} \quad (8.5)$$

and $\Omega \in \mathbb{R}^{m \times m}$ is a symmetric positive definite diagonal weighting matrix.

8.3 On-line Control Allocation

In this section, the idea is to use the information about $K(t)$ and incorporate this into the allocation algorithm through a weighting matrix W . Therefore the control is redistributed to the remaining actuators when faults/failures occur to minimize the use of the faulty control surface.

Equation (8.1) can be written as

$$\dot{x}(t) = Ax(t) + B(I - K)u(t) \quad (8.6)$$

Define

$$W := I - K \quad (8.7)$$

Using (8.7), (8.2) and (8.4), Equation (8.6) can be written as

$$\dot{x}(t) = Ax(t) + \begin{bmatrix} B_1 W B_2^\dagger \\ B_2 W B_2^\dagger \end{bmatrix} \nu(t) \quad (8.8)$$

where B_2^\dagger is defined in (8.5). In this section, the weight Ω in (8.5) will be chosen as

$$\Omega = W \quad (8.9)$$

Using (8.9) and (8.5), Equation (8.8) can be written as

$$\dot{x}(t) = Ax(t) + \begin{bmatrix} B_1 W^2 B_2^\top (B_2 W B_2^\top)^{-1} \\ B_2 W^2 B_2^\top (B_2 W B_2^\top)^{-1} \end{bmatrix} \nu(t) \quad (8.10)$$

If a new virtual control is selected as

$$\bar{\nu}(t) := (B_2 W B_2^\top)^{-1} \nu(t) \quad (8.11)$$

then as shown in Chapter 6 (see Equation (6.17)), Equation (8.10) can be written as

$$\dot{x}(t) = Ax(t) + \underbrace{\begin{bmatrix} B_1 B_2^\top \\ I \end{bmatrix}}_{B_\nu} \bar{\nu}(t) - \underbrace{\begin{bmatrix} B_1 (I - W^2) B_2^\top \\ B_2 (I - W^2) B_2^\top \end{bmatrix}}_{\bar{B}_\nu} \bar{\nu}(t) \quad (8.12)$$

In the fault-free case $W = I$ and \bar{B}_ν in (8.12) is zero. As in Section 3.5.2, consider a reference model defined as

$$\dot{x}_m(t) = A_m x_m(t) + B_m y_d(t) \quad (8.13)$$

where $y_d(t)$ is the reference signal and $A_m \in \mathbb{R}^{n \times n}$, $B_m \in \mathbb{R}^{n \times l}$ with A_m is stable. Define

$$e(t) = x(t) - x_m(t) \quad (8.14)$$

and therefore from (8.12) and (8.13) the error system

$$\dot{e}(t) = Ae(t) + (A - A_m)x_m(t) + B_\nu\bar{\nu}(t) - \bar{B}_\nu\bar{\nu}(t) - B_my_d(t) \quad (8.15)$$

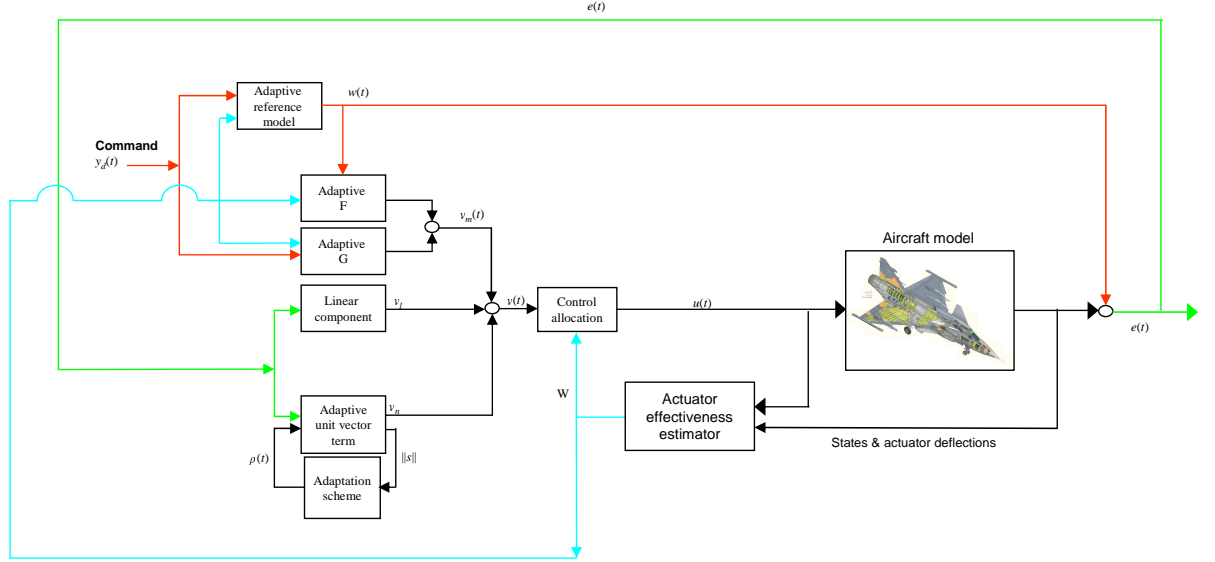


Figure 8.1: overall structure of proposed FTC

Suppose the reference model matrices A_m and B_m are given by

$$A_m = A + B_\nu F, \quad B_m = B_\nu G \quad (8.16)$$

and

$$\nu_m(t) = Fx_m(t) + Gy_d(t) \quad (8.17)$$

SMC techniques, will now be used to synthesize $\bar{\nu}(t)$. Define a switching function $s : \mathbb{R}^n \rightarrow \mathbb{R}^l$ to be

$$s(t) = Se(t) \quad (8.18)$$

where $S \in \mathbb{R}^{l \times n}$ and $\det(SB_\nu) \neq 0$. Let \mathcal{S} be the hyperplane defined by

$$\mathcal{S} = \{e(t) \in \mathbb{R}^n : Se(t) = 0\}$$

If a control law can be developed which forces the closed-loop trajectories onto the surface \mathcal{S} in finite time and constrains the states to remain there, then an ideal sliding motion is said to have been attained. The sliding surface is typically designed based on the nominal no fault condition ($K = 0$). Using (8.16), Equation (8.15) can be rewritten as

$$\dot{e}(t) = Ae(t) - \bar{B}_\nu\bar{\nu}(t) + B_\nu(\bar{\nu}(t) - \underbrace{Fx_m(t) - Gy_d(t)}_{-\nu_m(t)}) \quad (8.19)$$

where B_ν and \bar{B}_ν are defined in (8.12). As in Chapter 6, a coordinate transformation $e \mapsto$

$T_r e(t) = \hat{e}(t)$ is introduced to obtain ‘regular form’. If

$$T_r := \begin{bmatrix} I & -B_1 B_2^T \\ 0 & I \end{bmatrix} \quad (8.20)$$

then it is easy to check that Equation (8.19) becomes:

$$\dot{\hat{e}}(t) = \hat{A} \hat{e}(t) + \underbrace{\begin{bmatrix} 0 \\ I \end{bmatrix}}_{\hat{B}_\nu} (\bar{\nu}(t) - \nu_m(t)) - \begin{bmatrix} B_1 B_2^N (I - W^2) B_2^T \\ B_2 (I - W^2) B_2^T \end{bmatrix} \bar{\nu}(t) \quad (8.21)$$

where $\hat{A} := T_r A T_r^{-1}$ and

$$B_2^N := (I - B_2^T B_2) \quad (8.22)$$

Because by construction the matrix $B_2 B_2^T = I_l$, it follows that $B_2^N B_2^T = (I - B_2^T B_2) B_2^T = 0$, and

$$B_1 B_2^N (I - W^2) B_2^T = -B_1 B_2^N W^2 B_2^T \quad (8.23)$$

Define another scaling of the virtual control signal as

$$\hat{\nu}(t) := (B_2 W^2 B_2^T) \bar{\nu}(t) \quad (8.24)$$

Then using similar arguments to those in Chapter 6, (8.21) becomes

$$\begin{bmatrix} \dot{\hat{e}}_1(t) \\ \dot{\hat{e}}_2(t) \end{bmatrix} = \begin{bmatrix} \hat{A}_{11} & \hat{A}_{12} \\ \hat{A}_{21} & \hat{A}_{22} \end{bmatrix} \begin{bmatrix} \hat{e}_1(t) \\ \hat{e}_2(t) \end{bmatrix} + \begin{bmatrix} 0 \\ I \end{bmatrix} (\hat{\nu}(t) - \nu_m(t)) + \begin{bmatrix} B_1 B_2^N B_2^+ \\ 0 \end{bmatrix} \hat{\nu}(t) \quad (8.25)$$

where

$$B_2^+ := W^2 B_2^T (B_2 W^2 B_2^T)^{-1} \quad (8.26)$$

As shown in Proposition 2 in Chapter 6, there exists a scalar γ_0 which is finite and independent of W such that

$$\|B_2^+\| = \|W^2 B_2^T (B_2 W^2 B_2^T)^{-1}\| < \gamma_0 \quad (8.27)$$

for all $W = \text{diag}(w_1 \dots w_m)$ such that $0 < w_i \leq 1$.

The virtual control law will now be designed based on the nominal fault-free system in which the last term in (8.25) is zero since $B_1 B_2^N B_2^+|_{W=I} = 0$. In the $\hat{e}(t)$ coordinates, a suitable choice for the sliding surface matrix is

$$\hat{S} = S T_r^{-1} = \begin{bmatrix} M & I \end{bmatrix} \quad (8.28)$$

where $M \in \mathbb{R}^{l \times (n-l)}$ represents design freedom. Introduce another transformation $(\hat{e}_1, \hat{e}_2) \mapsto (\hat{e}_1, s)$, associated with

$$T_s = \begin{bmatrix} I & 0 \\ M & I \end{bmatrix} \quad (8.29)$$

Equation (8.25) then becomes

$$\begin{bmatrix} \dot{\hat{e}}_1(t) \\ \dot{s}(t) \end{bmatrix} = \begin{bmatrix} \tilde{A}_{11} & \tilde{A}_{12} \\ \tilde{A}_{21} & \tilde{A}_{22} \end{bmatrix} \begin{bmatrix} \hat{e}_1(t) \\ s(t) \end{bmatrix} + \begin{bmatrix} 0 \\ I \end{bmatrix} (\hat{\nu}(t) - \nu_m(t)) + \begin{bmatrix} B_1 B_2^N B_2^+ \\ M B_1 B_2^N B_2^+ \end{bmatrix} \hat{\nu}(t) \quad (8.30)$$

where

$$\tilde{A}_{11} := \hat{A}_{11} - \hat{A}_{12} M \quad (8.31)$$

and

$$\tilde{A}_{21} := M \tilde{A}_{11} + \hat{A}_{21} - \hat{A}_{22} M \quad (8.32)$$

If a control law can be designed to induce a sliding motion, then during sliding $\dot{s}(t) = s(t) = 0$ and the equivalent control necessary to maintain sliding is obtained from solving for $\hat{\nu}_{eq}(t)$ from the lower equations of (8.30) to give

$$\hat{\nu}_{eq}(t) = -(I + M B_1 B_2^N B_2^+)^{-1} (\tilde{A}_{21} \hat{e}_1(t) - \nu_m(t)) \quad (8.33)$$

where B_2^N is defined in (8.22).

By design, assume the sliding surface matrix M has been designed, so that $\tilde{A}_{11} := \hat{A}_{11} - \hat{A}_{12} M$ is stable and $\|M B_1 B_2^N B_2^+\| < 1$ for all $0 < W \leq I$.

Note: $\|M B_1 B_2^N B_2^+\| < 1$ guarantees the inverse in (8.33) exists and uses the boundedness result from Proposition 2 in Chapter 6. If (A, B_ν) is controllable, then $(\hat{A}_{11}, \hat{A}_{12})$ is controllable and so M can be chosen to make $\hat{A}_{11} - \hat{A}_{12} M$ stable. Substituting (8.33) into the top partition of (8.30), yields the following reduced order system which governs the sliding motion:

$$\dot{\hat{e}}_1(t) = (\tilde{A}_{11} - B_1 B_2^N B_2^+ (I + M B_1 B_2^N B_2^+)^{-1} \tilde{A}_{21}) \hat{e}_1(t) + B_1 B_2^N B_2^+ (I + M B_1 B_2^N B_2^+)^{-1} \nu_m(t) \quad (8.34)$$

As shown in (6.33), when $W = I$ (fault-free situation), $B_2^+|_{W=I} = B_2^T$ and the system in (8.34) ‘collapses’ to $\dot{\hat{e}}_1(t) = \tilde{A}_{11} \hat{e}_1(t)$ which is the nominal sliding mode reduced order system for which M has been designed to guarantee stability. However, during fault/failure conditions, stability of the system in (8.34) (which depends on W through B_2^+) needs to be established.

8.3.1 Stability analysis

The stability of the sliding mode is dependent on the reduced order system (8.34). Since by construction, the reference model is stable, for a bounded signal $y_d(t)$, the signal $x_m(t)$ is bounded and hence ν_m is bounded. Therefore the stability of the reduced order system which governs the sliding motion depends on:

$$\dot{\hat{e}}_1(t) = (\tilde{A}_{11} - B_1 B_2^N B_2^+ (I + M B_1 B_2^N B_2^+)^{-1} \tilde{A}_{21}) \hat{e}_1(t) \quad (8.35)$$

To facilitate the subsequent analysis, define

$$\tilde{G}(s) := -\tilde{A}_{21} (sI - \tilde{A}_{11})^{-1} B_1 B_2^N \quad (8.36)$$

where \mathbf{s} represents the Laplace variable. By construction $\tilde{G}(\mathbf{s})$ is stable. Define scalars γ_1 and γ_2 so that

$$\gamma_2 = \|\tilde{G}(\mathbf{s})\|_\infty \quad (8.37)$$

and

$$\gamma_1 := \|MB_1B_2^N\| \quad (8.38)$$

As proven in Proposition 3 in Chapter 6, during a fault or failure condition, for any combination of $0 < w_i \leq 1$, the closed-loop system will be stable if

$$0 \leq \frac{\gamma_2\gamma_0}{1 - \gamma_1\gamma_0} < 1 \quad (8.39)$$

where the positive scalar γ_0 is defined in (8.27).

8.3.2 A Sliding Mode Control Law

Next, a sliding mode controller will be designed based on the system in (8.30) with respect to the virtual control $\hat{\nu}$. The proposed control law is given by $\hat{\nu}(t) = \hat{\nu}_l(t) + \hat{\nu}_n(t)$ where

$$\hat{\nu}_l(t) := -\tilde{A}_{21}\hat{e}_1(t) - \tilde{A}_{22}s(t) + \nu_m(t) \quad (8.40)$$

and $\nu_m(t)$ is defined in (8.17). The nonlinear component is defined to be

$$\hat{\nu}_n(t) := -(\rho(t) + \eta) \frac{s(t)}{\|s(t)\|} \quad \text{for } s(t) \neq 0 \quad (8.41)$$

where $s(t) = \hat{S}\hat{x}(t)$ and η is a positive scalar.

It follows that the actual control which is sent to the actuators is resolved from the ‘virtual control law’ $\nu(t)$ (from (8.40)-(8.41)), using (8.4), (8.5), (8.11) and (8.24). Therefore $u(t)$ is defined as

$$u(t) = WB_2^T(B_2W^2B_2^T)^{-1}\hat{\nu}(t) \quad (8.42)$$

i.e. the control which is sent to the actuators depends on the effectiveness gains k_i (through the weighting matrix W). Note that in most of the literature, whilst SMC has been successfully tested on systems with faulty actuators, it was claimed that SMC cannot deal directly with total failures. However, in this chapter, provided the stability condition (8.39) is satisfied, the sliding mode controller for the ‘virtual’ system proposed above, can handle total actuator failures in the original system provided that $\det(B_2WB_2^T) \neq 0$.

In a fault-free situation it is not necessary and indeed is not advisable to have a large gain on the switched term – therefore ideally the term $\rho(t)$ should only adapt to the onset of a fault and react accordingly. It is easy to see from (8.40) that, if $y_d(t)$ is bounded, $\hat{\nu}_l(t)$ is bounded by

$$\|\hat{\nu}_l(t)\| < l_1\|e(t)\| + l_2 \quad (8.43)$$

where l_1 and l_2 are known positive constants. The gain from (8.41) is defined to be

$$\rho(t) = r(t)(l_1\|e(t)\| + l_2) \quad (8.44)$$

The scalar variable $r(t)$ is an adaptive gain which varies according to

$$\dot{r}(t) = a(l_1\|e(t)\| + l_2)D_\epsilon(\|s(t)\|) - br(t) \quad (8.45)$$

where $r(0) = 0$ and the a and b are positive design constants. The function $D_\epsilon : \mathbb{R} \mapsto \mathbb{R}$ is the nonlinear function

$$D_\epsilon(\|s\|) = \begin{cases} 0 & \text{if } \|s\| < \epsilon \\ \|s\| & \text{otherwise} \end{cases} \quad (8.46)$$

where ϵ is a positive scalar. Here, ϵ is set to be small and helps define a boundary layer about the surface \mathcal{S} , inside which an acceptably close approximation to ideal sliding takes place. Provided the states evolve with time inside the boundary layer, no adaptation of the switching gains takes place. If a fault occurs, which starts to make the sliding motion degrade so that the states evolve outside the boundary layer i.e. $\|s(t)\| > \epsilon$, then the dynamic coefficients $r(t)$ increase in magnitude, (according to (8.45)), to force the states back into the boundary layer around the sliding surface.

As in Section 4.2.1, the choice of the design parameters η , a , b and ϵ depends on the closed-loop performance specifications and requires some design iteration. The choice of these design parameters will be discussed further in Section 8.6. Similar to Proposition 1 in Chapter 4, the following lemma will show that $r(t)$ is bounded and motion inside a boundary layer around \mathcal{S} is obtained.

Proposition 7 *Consider the potentially faulty error system represented by (8.15) with the control law in (8.40)-(8.41); then the adaptive gain $r(t)$ remains bounded and the switching states $s(t)$ enter a boundary layer around \mathcal{S} in finite time.*

Proof: Define a scalar

$$\zeta := 1/(1 - \gamma_1\gamma_0) > 0 \quad (8.47)$$

This is guaranteed to exist, since in the requirements of Equation (8.27), the inequality $\gamma_1\gamma_0 < 1$ must hold. Consider as a candidate Lyapunov function

$$V = \frac{1}{2} \left(\|s\|^2 + \frac{1}{a}(1 - \gamma_1\gamma_0)(r(t) - \zeta)^2 \right) \quad (8.48)$$

where a is the positive scalar from (8.45). Clearly $V(\cdot)$ is positive definite with respect to $\|s\|$, the adaptive gain error $r(t) - \zeta$, and is radially unbounded. Taking derivatives along trajectories

$$\dot{V} = s^T \dot{s} + \frac{1}{a}(1 - \gamma_1\gamma_0)(r(t) - \zeta)\dot{r}(t) \quad (8.49)$$

From (8.30) and using (8.40)

$$\begin{aligned} \dot{s}(t) &= \tilde{A}_{21}\hat{e}_1(t) + \tilde{A}_{22}s(t) + (\hat{v}(t) - Fx_m(t) - Gr(t)) + (MB_1B_2^N B_2^+) \hat{v}(t) \\ &= (I + MB_1B_2^N B_2^+) \hat{v}_n(t) + (MB_1B_2^N B_2^+) \hat{v}_l(t) \end{aligned} \quad (8.50)$$

and so

$$\begin{aligned}
s^T \dot{s} &= s^T (MB_1 B_2^N B_2^+) \hat{\nu}_n(t) + s^T (MB_1 B_2^N B_2^+) \hat{\nu}_l(t) - (\rho(t) + \eta) \|s\| \\
&\leq \|s\| (\rho(t) + \eta) \|MB_1 B_2^N B_2^+\| + \|s\| \|MB_1 B_2^N B_2^+\| \|\hat{\nu}_l(t)\| - \|s\| (\rho(t) + \eta) \\
&\leq \|s\| ((\rho(t) + \eta) \gamma_1 \gamma_0 + \gamma_1 \gamma_0 \|\hat{\nu}_l(t)\| - (\rho(t) + \eta))
\end{aligned} \tag{8.51}$$

Using the fact that $\gamma_1 \gamma_0 = 1 - (1 - \gamma_1 \gamma_0)$, the inequality above can be written as

$$s^T \dot{s} \leq -\|s\| (1 - \gamma_1 \gamma_0) (\rho(t) + \eta) - \|s\| (1 - \gamma_1 \gamma_0) \|\hat{\nu}_l(t)\| + \|s\| \|\hat{\nu}_l(t)\| \tag{8.52}$$

Using (8.47), the inequality above can be written as

$$s^T \dot{s} \leq -\|s\| (1 - \gamma_1 \gamma_0) (\eta + \|\hat{\nu}_l(t)\|) - \|s\| (1 - \gamma_1 \gamma_0) (\rho - \|\hat{\nu}_l(t)\| \zeta) \tag{8.53}$$

since $(1 - \gamma_1 \gamma_0) \zeta = 1$. Therefore, using (8.43)

$$s^T \dot{s} \leq -\|s\| (1 - \gamma_1 \gamma_0) (\eta + \|\hat{\nu}_l(t)\|) - \|s\| (1 - \gamma_1 \gamma_0) (\rho - (l_1 \|e(t)\| + l_2) \zeta) \tag{8.54}$$

Substituting from (8.44) into the above yields

$$s^T \dot{s} \leq -\|s\| (1 - \gamma_1 \gamma_0) (\eta + \|\hat{\nu}_l(t)\|) - \|s\| (1 - \gamma_1 \gamma_0) (l_1 \|e(t)\| + l_2) (r(t) - \zeta) \tag{8.55}$$

Finally, substituting (8.45) and (8.55) into (8.49) yields

$$\begin{aligned}
\dot{V} &\leq -\|s\| (1 - \gamma_1 \gamma_0) (\eta + \|\nu_l(t)\|) - \|s\| (1 - \gamma_1 \gamma_0) (l_1 \|e(t)\| + l_2) (r(t) - \zeta) \\
&\quad + \frac{1}{a} (1 - \gamma_1 \gamma_0) (r(t) - \zeta) a (l_1 \|e(t)\| + l_2) D_\epsilon (\|s(t)\|) - \frac{1}{a} (1 - \gamma_1 \gamma_0) (r(t) - \zeta) b r(t)
\end{aligned} \tag{8.56}$$

If $\|s\| > \epsilon$ then $D_\epsilon (\|s\|) = \|s\|$ and so substituting in (8.56) and simplifying terms yields

$$\dot{V} \leq -\|s\| (1 - \gamma_1 \gamma_0) (\eta + \|\nu_l(t)\|) - \frac{b}{a} (1 - \gamma_1 \gamma_0) (r(t) - \zeta) r(t) \tag{8.57}$$

Notice by construction $0 \leq \gamma_1 \gamma_0 < 1$ and $r(t) \geq 0$. Further manipulation of (8.57) and using (8.47) yields

$$\dot{V} \leq -\|s\| (1 - \gamma_1 \gamma_0) (\eta + \|\nu_l(t)\|) - \frac{b}{a} (1 - \gamma_1 \gamma_0) \left(\frac{1}{2} \zeta - r(t) \right)^2 + \frac{b}{4a(1 - \gamma_1 \gamma_0)} \tag{8.58}$$

since expanding the quadratic term on the right-hand side of (8.58) gives the right-hand side of (8.57). If $\|s\| > \epsilon$, then $\|s\| (1 - \gamma_1 \gamma_0) \eta \geq (1 - \gamma_1 \gamma_0) \epsilon \eta$. The quantities ϵ, η, a and b are design parameters and so if they are chosen to satisfy

$$\epsilon \eta \geq \frac{b}{4a(1 - \gamma_1 \gamma_0)^2} \tag{8.59}$$

then

$$\dot{V} \leq -\|s\| (1 - \gamma_1 \gamma_0) \|\nu_l(t)\| - \frac{b}{a} (1 - \gamma_1 \gamma_0) \left(\frac{1}{2} \zeta - r(t) \right)^2 \leq 0$$

If $\|s\| < \epsilon$ then $D_\epsilon(\|s\|) = 0$ and so substituting in (8.56) and simplifying terms yields

$$\begin{aligned} \dot{V} \leq & -\|s\|(1 - \gamma_1\gamma_0)(\eta + \|\nu_l(t)\|) - \|s\|(1 - \gamma_1\gamma_0)(l_1\|e(t)\| + l_2)(r(t) - \zeta) \\ & - \frac{b}{a}(1 - \gamma_1\gamma_0)(r(t) - \zeta)r(t) \end{aligned} \quad (8.60)$$

Notice again by construction $\gamma_1\gamma_0 < 1$ and $r(t) \geq 0$ and therefore for $\|s\| < \epsilon$ and $r(t) > \zeta$, it follows $\dot{V} < 0$. Define a rectangle in \mathbb{R}^2 as

$$\mathcal{R} = \{(\|s\|, r) \mid \|s\| \leq \epsilon, 0 \leq r \leq \zeta\} \quad (8.61)$$

Also define $\mathcal{R}_+ \in \mathbb{R}^2$ as $\mathcal{R}_+ = \{(\|s\|, r) \mid r \geq 0\}$. By construction of the adaptive gains, $r(t) \geq 0$ for all time and so the trajectory of $(\|s(t)\|, r(t)) \in \mathcal{R}_+$ for all time, and so outside the set $\mathcal{R} \cap \mathcal{R}_+ = \mathcal{R}$, from (8.58) and (8.60), the derivative of the Lyapunov function $\dot{V} < 0$. Let \mathcal{V}_d denote the truncated ellipsoid

$$\mathcal{V}_d = \{(\|s\|, r) \mid V(\|s\|, r) \leq d\} \cap \mathcal{R}_+$$

where $V(\cdot)$ is defined in (8.48). Because \mathcal{R} in (8.61) is a compact set, there exists a unique $d_0 > 0$ such that $d_0 = \min\{d \in \mathbb{R}_+ \mid \mathcal{R} \subset \mathcal{V}_d\}$ and in fact $d_0 = \frac{1}{2}(\epsilon^2 + \frac{\zeta}{a})$. As shown in Figure 8.2, since $\mathcal{R} \subset \mathcal{V}_{d_0}$, it follows outside \mathcal{V}_{d_0} the derivative of the Lyapunov function $\dot{V} < 0$ and so \mathcal{V}_{d_0} is an invariant set which is entered in finite time t_0 . Since \mathcal{V}_{d_0} is entered in finite time, $V(\|s\|, r) \leq d_0$ for all $t > t_0$ which implies $\|s\| \leq \sqrt{2d_0}$ for all time $t > t_0$, and hence s enters and remains in a boundary layer of size $\sqrt{2d_0}$ around the ideal sliding surface \mathcal{S} . ■

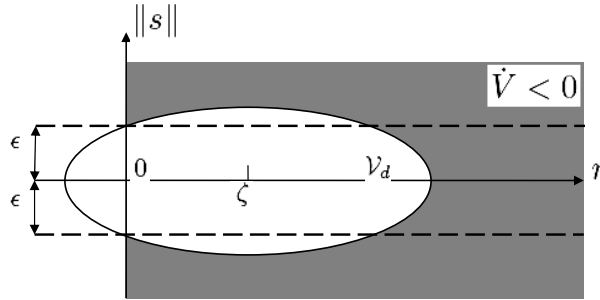


Figure 8.2: Level set of the Lyapunov functions V

From the arguments above, for an appropriate choice of a , b and ϵ , close approximation to ideal sliding can be maintained even in the presence of faults.

Remark 5: As discuss in Section 4.2.1, if $\epsilon=0$ and $b=0$, then ideal sliding can be guaranteed since it follows from (8.57) that $\dot{V}(s) \leq -\|s\|(1 - \gamma_1\gamma_0)(\eta + \|\nu_l(t)\|)$ and therefore ideal sliding can be attained and maintained in finite time. However this scheme is not practical since $r(t)$ may become unbounded in the presence of noise.

8.4 Fixed Control Allocation

The analysis in this section is similar to that in Section 8.3 above. The difference here is the assumption that there is no FDI or actuator effectiveness estimation available. Here the CA

will be fixed, i.e. $\Omega = I$ will be used in Equation (8.5) instead of $\Omega = W = I - K$ as proposed in Section 8.3.

The effect of choosing the weighting matrix to be $\Omega(t) = W(t)$ as in Section 8.3 above is that, $u(t)$ in (8.4) depends explicitly on $K(t)$. Here instead, and perhaps more conventionally,

$$\Omega := I \quad (8.62)$$

will be considered. With this choice of weighting matrix, Equation (8.4) becomes

$$u(t) = B_2^\dagger \nu(t) = B_2^\top \underbrace{(B_2 B_2^\top)^{-1}}_I \nu(t) = B_2^\top \nu(t) \quad (8.63)$$

then it can be shown that (8.1) can be written as

$$\dot{x}(t) = Ax(t) + \underbrace{\begin{bmatrix} B_1 B_2^\top \\ I \end{bmatrix}}_{B_\nu} \nu(t) - \underbrace{\begin{bmatrix} B_1 K B_2^\top \\ B_2 K B_2^\top \end{bmatrix}}_{\bar{B}_k} \nu(t) \quad (8.64)$$

Note that the last term in Equation (8.64) above is different from the last term in Equation (8.12). Consider a reference model as defined in (8.13), then using the definition of the error signal from (8.14), from (8.64) and (8.13) the error system

$$\dot{e}(t) = Ae(t) + (A - A_m)x_m(t) + B_\nu \nu(t) - \bar{B}_k \nu(t) - B_m y_d(t) \quad (8.65)$$

where $e(t)$ is defined in (8.14), B_ν and \bar{B}_k are defined in Equation (8.64) above, and the reference model matrices A_m and B_m are defined in (8.16).

Define

$$\nu(t) = \nu_l(t) + \nu_n(t) \quad (8.66)$$

and ν_m as in (8.17). Using (8.16) and (8.17), Equation (8.65) can be rewritten as

$$\dot{e}(t) = Ae(t) - \bar{B}_k \nu(t) + B_\nu \underbrace{(\nu(t) - Fx_m(t) - Gy_d(t))}_{-\nu_m(t)} \quad (8.67)$$

As in Section 8.3, a coordinate transformation $e \mapsto T_r e(t) = \hat{e}(t)$ is introduced to obtain ‘regular form’, where T_r is defined in (8.20). By construction the matrix $B_2 B_2^\top = I_l$, then it is easy to check that Equation (8.67) becomes:

$$\dot{\hat{e}}(t) = \hat{A} \hat{e}(t) + \underbrace{\begin{bmatrix} 0 \\ I \end{bmatrix}}_{\hat{B}_\nu} (\nu(t) - \nu_m(t)) - \begin{bmatrix} -B_1 B_2^N (I - K) B_2^\top \\ I - B_2 (I - K) B_2^\top \end{bmatrix} \nu(t) \quad (8.68)$$

where $\hat{A} := T_r A T_r^{-1}$ and B_2^N is defined in (8.22). The fact that $B_2^N B_2^\top = (I - B_2^\top B_2) B_2^\top = 0$ has also been used to obtain the top partition of the last term in (8.68). The last term in (8.68) is zero in the fault-free case ($K = 0$), but is treated as (unmatched) uncertainty when

$K \neq 0$. Define

$$B_2^\dagger := WB_2^T(B_2WB_2^T)^{-1} \quad (8.69)$$

where W is defined in (8.7). It is shown in Section 8.3 there is an upper bound on the norm of the pseudo-inverse B_2^\dagger in (8.69) which is independent of W (as proven in Proposition 2 in Chapter 6); also

$$\|B_2^\dagger\| = \|WB_2^T(B_2WB_2^T)^{-1}\| = \|W^2B_2^T(B_2W^2B_2^T)^{-1}\| < \gamma_0 \quad (8.70)$$

for all $W = \text{diag}(w_1 \dots w_m)$ such that $0 < w_i \leq 1$.

In the $\hat{e}(t)$ coordinates, a suitable choice for the sliding surface matrix is given by (8.28). Introduce another transformation $(\hat{e}_1, \hat{e}_2) \mapsto (\hat{e}_1, s)$, where T_s is defined in (8.29). Therefore Equation (8.68) becomes

$$\begin{aligned} \begin{bmatrix} \dot{\hat{e}}_1(t) \\ \dot{s}(t) \end{bmatrix} &= \begin{bmatrix} \tilde{A}_{11} & \tilde{A}_{12} \\ \tilde{A}_{21} & \tilde{A}_{22} \end{bmatrix} \begin{bmatrix} \hat{e}_1(t) \\ s(t) \end{bmatrix} + \begin{bmatrix} 0 \\ I \end{bmatrix} (\nu(t) - \nu_m(t)) \\ &\quad - \begin{bmatrix} -B_1B_2^NWB_2^T \\ I - MB_1B_2^NWB_2^T - B_2WB_2^T \end{bmatrix} \nu(t) \end{aligned} \quad (8.71)$$

where \tilde{A}_{11} and \tilde{A}_{21} are defined in (8.31) and (8.32) respectively. Note that Equation (8.71) has a similar structure to the one in (8.30) which uses the on-line CA in Section 8.3. One clear difference is the last term of both equation.

As in Section 8.3, if (A, B_ν) is controllable, from (8.28), M can always be chosen to make \tilde{A}_{11} stable. If a control law can be designed to induce a sliding motion, then during sliding $\dot{s}(t) = s(t) = 0$ and the equivalent control necessary to maintain sliding is obtained from solving for $\nu_{eq}(t)$ from the lower equations of (8.71) to give

$$\nu_{eq}(t) = (B_2WB_2^T)^{-1}(I + MB_1B_2^NB_2^\dagger)^{-1}(-\tilde{A}_{21}\hat{e}_1(t) + \nu_m(t)) \quad (8.72)$$

where B_2^N is defined in (8.22) and B_2^\dagger is defined in (8.69). Substituting (8.72) into the top partition of (8.71), yields the reduced order system (which governs the sliding motion) given as

$$\dot{\hat{e}}_1(t) = (\tilde{A}_{11} - B_1B_2^NB_2^\dagger(I + MB_1B_2^NB_2^\dagger)^{-1}\tilde{A}_{21})\hat{e}_1(t) + B_1B_2^NB_2^\dagger(I + MB_1B_2^NB_2^\dagger)^{-1}\nu_m(t) \quad (8.73)$$

Note that Equation (8.73) has the same structure as the one in (8.34). The difference is the term B_2^\dagger is replaced by B_2^+ in (8.34). Since γ_1 from (8.38) and γ_2 from (8.37) correspond to the same elements in both the reduced order systems (8.34) and (8.73); and the fact that $\|B_2^\dagger\| = \|B_2^+\| < \gamma_0$, therefore the closed-loop system described in (8.73) will be stable if Equation (8.39) is satisfied. Although the CA strategy proposed in this section is different from the one in Section 8.3, the stability analysis of the reduced order sliding motion is the same.

8.4.1 A Sliding Mode Control Law

In this section, a sliding mode controller will be designed based on the nominal no fault ‘virtual’ system in (8.71) with respect to ν . Here, the proposed control law is given by Equation (8.66),

where

$$\nu_l(t) := -\tilde{A}_{21}\hat{e}_1(t) - \tilde{A}_{22}s(t) + \nu_m(t) \quad (8.74)$$

and $\nu_m(t)$ is defined in (8.17). The nonlinear component is defined to be

$$\nu_n(t) := -(\rho(t) + \eta) \frac{s(t)}{\|s(t)\|} \quad \text{for } s(t) \neq 0 \quad (8.75)$$

where $s(t) = \hat{S}\hat{e}(t)$ and η is a positive scalar. The choice of the varying gain $\rho(t)$ will be discussed next.

It follows that the actual control which is sent to the actuators is resolved from the ‘virtual control law’ $\nu(t)$ defined in (8.3). Therefore $u(t)$, as defined in (8.63), is

$$u(t) = B_2^T \nu(t)$$

and the control signal distribution is independent of the actuator effectiveness K .

As argued in Section 8.3.2, $\nu_l(t)$ in (8.74) is bounded by

$$\|\nu_l(t)\| < l_1 \|e(t)\| + l_2 \quad (8.76)$$

where l_1 and l_2 are known positive constants as in (8.43). The gain $\rho(t)$ from (8.75) is defined as in (8.44), where the scalar variable $r(t)$ also varies according to (8.45) and (8.46).

Let \mathcal{W} be the set of faults such that

$$\mathcal{W} = \left\{ (w_1 \dots w_m) \in \underbrace{[0, 1] \times [0, 1] \dots \times [0, 1]}_{m \text{ times}} \mid \underline{\lambda}(B_2 W B_2^T) := w > 0 \right\} \quad (8.77)$$

where w is a strictly positive scalar and $\underline{\lambda}(B_2 W B_2^T)$ is the smallest eigenvalues of $(B_2 W B_2^T)$. Notice that $(w_1, \dots, w_m) \in \mathcal{W} \Rightarrow \det(B_2 W B_2^T) \neq 0$.

Using similar analysis as Proposition 1, in Chapter 4, and in Section 8.3.2 the following lemma will show that $r(t)$ is bounded.

Proposition 8 *Consider the potentially faulty system represented by (8.1) with the control law in (8.74)-(8.75); then the adaptive gain $r(t)$ from (8.44)-(8.46) remains bounded, and the switching states $s(t)$ enter a boundary layer around \mathcal{S} in finite time for any fault condition $(w_1 \dots w_m) \in \mathcal{W}$.*

Proof: Define a scalar

$$\varsigma := \frac{(2 + \gamma_1)}{w^2(1 - \gamma_1\gamma_0)} \quad (8.78)$$

The expression for ς in (8.78) is guaranteed to be positive, since in the requirements of Equation (8.39), the inequality $\gamma_1\gamma_0 < 1$ must hold. Assume that $\dot{K}(t) = 0$ almost always, this implies $\dot{W}(t) = 0$ almost always and so only isolated abrupt step changes in the effectiveness are considered here. Using the fact that $(B_2 W B_2^T) > 0$, the following candidate Lyapunov function

$$V = \frac{1}{2} \left(s^T (B_2 W B_2^T) s + \frac{1}{a} \underline{\lambda}(B_2 W B_2^T)^2 (1 - \gamma_1\gamma_0) (r(t) - \varsigma)^2 \right) \quad (8.79)$$

where a is the positive scalar from (8.45), is positive definite with respect to s , the adaptive gain error $r(t) - \varsigma$, and is radially unbounded and $\underline{\lambda}(B_2WB_2^T)^2$ is the smallest eigenvalues of $(B_2WB_2^T)^2$. Taking derivatives along trajectories

$$\dot{V} = s^T(B_2WB_2^T)\dot{s} + \frac{1}{a}\underline{\lambda}(B_2WB_2^T)^2(1 - \gamma_1\gamma_0)(r(t) - \varsigma)\dot{r}(t) \quad (8.80)$$

where from (8.71) (and using (8.66) and (8.74)),

$$\dot{s}(t) = \tilde{A}_{21}\hat{x}_1(t) + \tilde{A}_{22}s(t) + (\nu(t) - \nu_m(t)) - (I - MB_1B_2^NWB_2^T - B_2WB_2^T)\nu(t) \quad (8.81)$$

$$= (I + MB_1B_2^NB_2^\dagger)(B_2WB_2^T)\nu_n(t) - (I - MB_1B_2^NWB_2^T - B_2WB_2^T)\nu_l(t) \quad (8.82)$$

Using the fact that

$$s(t)^T(B_2WB_2^T)(B_2WB_2^T)s(t) = \|B_2WB_2^Ts\|^2$$

where $\|(B_2WB_2^T)\| \leq \|B_2B_2^T\| = 1$, and $\|WB_2^T\| \leq \|W\|\|B_2^T\| \leq 1$ for all $(w_1, \dots, w_m) \in \mathcal{W}$, it follows that when $s \neq 0$

$$\begin{aligned} s^T(B_2WB_2^T)\dot{s} &= -\frac{(\rho + \eta)}{\|s\|}\|B_2WB_2^Ts\|^2 - (\rho + \eta)s^T(B_2WB_2^T)(MB_1B_2^NB_2^\dagger)(B_2WB_2^T)\frac{s}{\|s\|} \\ &\quad - s^T(B_2WB_2^T)(I - MB_1B_2^NWB_2^T - B_2WB_2^T)\nu_l(t) \\ &\leq -\frac{(\rho + \eta)}{\|s\|}\|B_2WB_2^Ts\|^2 + \frac{(\rho + \eta)}{\|s\|}\|B_2WB_2^Ts\|^2\|(MB_1B_2^NB_2^\dagger)\| \\ &\quad + \|B_2WB_2^Ts\|\|(I - MB_1B_2^NWB_2^T - B_2WB_2^T)\|\|\nu_l(t)\| \\ &\leq \|B_2WB_2^Ts\|\left(-\frac{(\rho + \eta)}{\|s\|}\|B_2WB_2^Ts\|(1 - \gamma_1\gamma_0) + (2 + \gamma_1)\|\nu_l(t)\|\right) \end{aligned} \quad (8.83)$$

since $\|MB_1B_2^NB_2^\dagger\| \leq \|MB_1B_2^N\|\|B_2^\dagger\| \leq \gamma_0\gamma_1$, and

$$\|I - MB_1B_2^NWB_2^T - B_2WB_2^T\| \leq 1 + \|MB_1B_2^NWB_2^T\| + \|B_2WB_2^T\| \leq 2 + \gamma_1$$

Using the Rayleigh principle, $-\|B_2WB_2^Ts\|^2 \leq -\underline{\lambda}(B_2WB_2^T)^2\|s\|^2 = -w^2\|s\|^2$, and using the fact that $\bar{\lambda}(B_2WB_2^T) = 1$, inequality (8.83) implies

$$\begin{aligned} s^T(B_2WB_2^T)\dot{s} &\leq -w^2\|s\|(\rho + \eta)(1 - \gamma_1\gamma_0) + \|s\|(2 + \gamma_1)\|\nu_l(t)\| \\ &= w^2\|s\|(1 - \gamma_1\gamma_0)\left(-(\rho + \eta) + \varsigma\|\nu_l(t)\|\right) \end{aligned} \quad (8.84)$$

where ς is defined in (8.78). Using (8.76) and (8.44), the inequality above can be written as

$$s^T(B_2WB_2^T)\dot{s} \leq -w^2\|s\|(1 - \gamma_1\gamma_0)\eta - w^2\|s\|(1 - \gamma_1\gamma_0)(l_1\|x(t)\| + l_2)(r(t) - \varsigma) \quad (8.85)$$

Finally, substituting (8.45) and (8.85) into (8.80) yields

$$\begin{aligned} \dot{V} &\leq -w^2\|s\|(1 - \gamma_1\gamma_0)\eta - w^2\|s\|(1 - \gamma_1\gamma_0)(l_1\|x(t)\| + l_2)(r(t) - \varsigma) \\ &\quad + w^2(1 - \gamma_1\gamma_0)(r(t) - \varsigma)\left(l_1\|x(t)\| + l_2\right)D_\epsilon(\|s(t)\|) \\ &\quad - \frac{b}{a}w^2(1 - \gamma_1\gamma_0)(r(t) - \varsigma)r(t) \end{aligned} \quad (8.86)$$

If $\|s\| > \epsilon$ then $D_\epsilon(\|s\|) = \|s\|$ and so substituting in (8.86) and simplifying terms yields

$$\dot{V} \leq -w^2\|s\|(1 - \gamma_1\gamma_0)\eta - \frac{b}{a}w^2(1 - \gamma_1\gamma_0)(r(t) - \varsigma)r(t) \quad (8.87)$$

By construction $0 \leq \gamma_1\gamma_0 < 1$ and $r(t) \geq 0$. Further manipulation of (8.87), and using (8.78) yields

$$\dot{V} \leq -w^2\|s\|(1 - \gamma_1\gamma_0)\eta - \frac{b}{a}w^2(1 - \gamma_1\gamma_0)\left(\frac{1}{2}\varsigma - r\right)^2 + \frac{b}{4a} \frac{(2 + \gamma_1)^2}{w^2(1 - \gamma_1\gamma_0)} \quad (8.88)$$

since expanding the quadratic term on the right-hand side of (8.88) gives the right-hand side of (8.87). If $\|s\| > \epsilon$, then $w^2\|s\|(1 - \gamma_1\gamma_0)\eta \geq w^2(1 - \gamma_1\gamma_0)\eta\epsilon$. The quantities ϵ, η, a and b are design parameters and so if they are chosen to satisfy

$$\epsilon\eta \geq \frac{b}{4a} \frac{(2 + \gamma_1)^2}{w^4(1 - \gamma_1\gamma_0)^2} = \frac{b}{4a}\varsigma^2 \quad (8.89)$$

then from (8.88)

$$\dot{V} \leq -\frac{b}{a}w^2(1 - \gamma_1\gamma_0)\left(\frac{1}{2}\varsigma - r\right)^2 \leq 0$$

If $\|s\| < \epsilon$ then $D_\epsilon(\|s\|) = 0$ and so substituting in (8.86) and simplifying terms yields

$$\begin{aligned} \dot{V} \leq & -w^2\|s\|(1 - \gamma_1\gamma_0)\eta - w^2\|s\|(1 - \gamma_1\gamma_0)(l_1\|x(t)\| + l_2)(r(t) - \varsigma) \\ & - \frac{b}{a}w^2(1 - \gamma_1\gamma_0)(r(t) - \varsigma)r(t) \end{aligned} \quad (8.90)$$

Notice by construction $\gamma_1\gamma_0 < 1$ and $r(t) \geq 0$ and therefore for $\|s\| < \epsilon$ and $r(t) > \varsigma$, it follows $\dot{V} < 0$. Define a rectangle in \mathbb{R}^2 as

$$\mathcal{R} = \{(\|s\|, r) \mid \|s\| \leq \epsilon, 0 \leq r \leq \varsigma\} \quad (8.91)$$

Also define $\mathcal{R}_+ \in \mathbb{R}^2$ as $\mathcal{R}_+ = \{(\|s\|, r) \mid r \geq 0\}$. By construction of the adaptive gains, $r(t) \geq 0$ for all time and so the trajectory of $(\|s(t)\|, r(t)) \in \mathcal{R}_+$ for all time, and so outside the set $\mathcal{R} \cap \mathcal{R}_+ = \mathcal{R}$, from (8.88) and (8.90), the derivative of the Lyapunov function $\dot{V} < 0$. Let \mathcal{V}_d denote the truncated ellipsoid

$$\mathcal{V}_d = \{(\|s\|, r) \mid V(\|s\|, r) \leq d\} \cap \mathcal{R}_+$$

where $V(\cdot)$ is defined in (8.79). Because \mathcal{R} in (8.91) is a compact set, for a given $w > 0$, there exists a unique $d_0 > 0$ such that $d_0 = \min\{d \in \mathbb{R}_+ \mid \mathcal{R} \subset \mathcal{V}_d\}$. As shown in Figure 8.2, since $\mathcal{R} \subset \mathcal{V}_{d_0}$, it follows outside \mathcal{V}_{d_0} the derivative of the Lyapunov function $\dot{V} < 0$ and so \mathcal{V}_{d_0} is an invariant set which is entered in finite time t_0 . Since \mathcal{V}_{d_0} is entered in finite time, $V(\|s\|, r) \leq d_0$ for all $t > t_0$ which implies $\|s\| \leq \sqrt{2d_0/w}$ for $t > t_0$, and hence s enters and remains in a boundary layer of size $\sqrt{2d_0/w}$ around the ideal sliding surface \mathcal{S} . ■

Remark 5: Close approximation to ideal sliding can be maintained even in the presence of faults for an appropriate choice of a, b and ϵ . If $\epsilon = 0$ and $b = 0$, it follows from (8.87) that $\dot{V} \leq -w^2\|s\|(1 - \gamma_1\gamma_0)\eta$, which means that ideal sliding can be attained and maintained in finite time. However, in the presence of noise $r(t)$ may become unbounded.

8.5 Adaptive Reference Model

One benefit of using a model reference framework is it allows the possibility of changing the reference model when a fault or failure occurs. This can be done using multiple pre-designed reference models or alternatively by adapting the reference model online. In some fault conditions, to reduce the demands on the damaged actuators, a ‘slower’ reference model is desirable. In this chapter, the reference model will be allowed to adapt to faults. Assume that two reference models have been designed, one will be the nominal reference model designed for a fault-free situation represented by (8.13), and the other will be the conservative reference model for the faulty situation. The idea is to blend the two models so that

$$A_m = \lambda(A + B_\nu F_1) + (1 - \lambda)(A + B_\nu F_2) \quad (8.92)$$

$$B_m = \lambda B_\nu G_1 + (1 - \lambda) B_\nu G_2 \quad (8.93)$$

where $\lambda \in [0 \ 1]$ and is a function of the w_i from W in (8.7). The matrices F_1 and G_1 are associated with the nominal ideal model, while F_2 and G_2 are associated with the conservative one. In the fault-free case, the nominal reference model will be used; when significant failures occur, the ‘slow’ reference model will be used and when partial faults occur, a mix of both reference models will be used.

8.6 ADMIRE simulations: on-line control allocation

8.6.1 Controller design

The linear model from Chapter 6 has been used here and is associated with a low speed flight condition of Mach 0.22 at an altitude of 3000m. The states are angle of attack (AoA) (rad), sideslip angle (rad), roll rate (rad/sec), pitch rate (rad/sec) and yaw rate (rad/sec). The controlled outputs are AoA, sideslip and roll rate. The control surfaces are $\delta = [\delta_c \ \delta_{re} \ \delta_{le} \ \delta_r]^T$, which represent the deflections (rad) of the canard, right elevon, left elevon and rudder respectively. Recalling (6.69) and (6.70), the system and input distribution matrices are:

$$A = \begin{bmatrix} -0.5432 & 0.0137 & 0 & 0.9778 & 0 \\ 0 & -0.1179 & 0.2215 & 0 & -0.9661 \\ 0 & -10.5128 & -0.9967 & 0 & 0.6176 \\ 2.6221 & -0.0030 & 0 & -0.5057 & 0 \\ 0 & 0.7075 & -0.0939 & 0 & -0.2127 \end{bmatrix}$$

$$B = \begin{bmatrix} 0.0069 & -0.0866 & -0.0866 & 0.0004 \\ 0 & 0.0119 & -0.0119 & 0.0287 \\ \hline 0 & -4.2423 & 4.2423 & 1.4871 \\ 1.6532 & -1.2735 & -1.2735 & 0.0024 \\ 0 & -0.2805 & 0.2805 & -0.8823 \end{bmatrix} \left. \begin{array}{l} \vphantom{B} \\ \vphantom{B} \end{array} \right\} B_1$$

$$\left. \begin{array}{l} \vphantom{B} \\ \vphantom{B} \end{array} \right\} B_2$$

The partition of B above shows the terms B_1 and B_2 (although a further change of coordinates is necessary to scale B_2 to ensure $B_2 B_2^T = I$). The feedback matrices for the ideal model from (8.16) have been designed using an LQR approach for the triple (A, B_ν, C_c) where

$$C_c = \begin{bmatrix} I_3 & 0_{3 \times 2} \end{bmatrix} \quad (8.94)$$

is the distribution matrix associated with the controlled outputs. The state weighting matrix has been chosen as $Q_m = C_c Q_c C_c$. Here, $Q_c = \text{diag}(1, 5000, 0.1)$ in the fault-free case, and the control penalty weight is $2I_3$. In the faulty case, $Q_c = \text{diag}(0.01, 50, 0.001)$ and I_3 has been chosen as the control penalty. Alternatively, other methods such as eigenstructure assignment [71, 137] could also be used to design the ideal models. The feed-forward matrix G has been designed using the inverse steady-state gain for the virtual triple system (A, B_ν, C_c) , specifically

$$G = -(C_c(A + B_\nu F)^{-1} B_\nu)^{-1}$$

Based on the above, the feed-back matrices from (8.92) and (8.93) are given by

$$F_1 = \begin{bmatrix} 0.0006 & -30.4857 & -1.1726 & 0.0003 & 4.8569 \\ -1.5365 & -0.0276 & -0.0006 & -0.8933 & 0.0022 \\ -0.0003 & 36.3096 & 1.0527 & -0.0002 & -4.9790 \end{bmatrix}$$

$$F_2 = \begin{bmatrix} -0.0003 & -3.8030 & -0.3749 & -0.0002 & 1.7039 \\ -1.3459 & -0.0072 & -0.0002 & -0.8304 & 0.0010 \\ 0.0006 & 3.4436 & 0.3142 & 0.0004 & -1.4496 \end{bmatrix}$$

and the feed-forward matrices are given by

$$G_1 = \begin{bmatrix} -0.0007 & 32.7235 & 0.2213 \\ 1.1753 & 0.0128 & 0.0001 \\ -0.0003 & -37.8584 & 0.1885 \end{bmatrix}$$

$$G_2 = \begin{bmatrix} 0.0005 & 5.7154 & 0.1294 \\ 0.9441 & -0.0069 & 0.0001 \\ -0.0015 & -4.6283 & 0.1371 \end{bmatrix}$$

where the matrices F_1 and G_1 are associated with the nominal ideal model, while F_2 and G_2 are associated with the conservative one.

A quadratic optimal design (similar to the one in Section 3.4.1) has been used to obtain the sliding surface matrix S . The symmetric positive definite weighting matrix has been chosen as $Q = \text{diag}([30, 30, 1, 1, 1])$. This results in

$$M = \begin{bmatrix} 0.0002 & 0.2906 \\ 1.9922 & -0.0019 \\ -0.0088 & -5.5060 \end{bmatrix}$$

In the simulations the discontinuity in the nonlinear control term in (8.41) has been smoothed by using a sigmoidal approximation from (3.60), where the scalar δ has been chosen as $\delta = 0.001$.

This removes the discontinuity and introduces a further degree of tuning to accommodate the actuator limits.

During the design stage, and based on analysis from §8.3.2, it was found $\text{rank}(B_2WB_2^T) < 3$ when the rudder completely fails or any two surfaces from the set consisting of the canard and the left and right elevons completely fail. This is an expected result since there is no redundancy for the rudder to provide yaw; and when two actuators fail from either the canard or elevons, it means that there is no redundancy left in the system, and all possible actuators to provide pitch or roll have failed. From (8.27), it can be verified that $\gamma_0 = 2.0913$. Simple calculations show that $\gamma_1 = 0.1549$, therefore $\gamma_1\gamma_0 = 0.3239 < 1$ and so one of the stability requirements in (8.39) is satisfied. Also for this particular choice of sliding surface $\|\tilde{G}(s)\|_\infty = 0.1277 = \gamma_2$. Therefore, from (8.39)

$$\frac{\gamma_2\gamma_0}{1 - \gamma_1\gamma_0} = 0.3951 < 1$$

which shows that the closed-loop system is stable for all $0 < w_i \leq 1$. The variables related to the adaptive non-linear gain (§8.3.2) have been chosen as follows: it was found that choosing $l_1 = 0$ and $l_2 = 1$ gave sufficiently good performance. This removes the dependance of $r(t)$ on $e(t)$ and simplifies the implementation. The parameter η from (8.41) was chosen as $\eta = 1$. The adaptation parameters from (8.45) have been chosen as $a = 1000$, $b = 0.1$ and $\epsilon = 2 \times 10^{-5}$. The parameter ϵ was chosen to be able to tolerate the variation in $\|s(t)\|$ due to normal changes in flight condition but small enough to enable the adaptive gain to be sensitive enough to deviation from zero due to faults or failures. Here a has been chosen to be large to enable small changes in $\|s(t)\|$ to cause significant changes in the gain, so that the control system reacts quickly to a fault. The parameter b on the other hand dictates the rate at which $\rho(t)$ will decrease, after $\|s(t)\|$ has returned below the threshold ϵ . For practical reason, the adaptive gain is limited at a maximum of $\rho_{max} = 5$. From (8.59), $(1 - \gamma_1\gamma_0)\epsilon\eta = 3 \times 10^{-5}$ and $b/4a(1 - \gamma_1\gamma_0) = 2.5 \times 10^{-5}$ and therefore the condition in Proposition 7 is satisfied.

8.6.2 Actuator fault estimation using least square method

In (8.7), the weighting matrix W which is used for the control signal redistribution, depends on information about the actuator fault. In this chapter, it will be assumed that a measurement of the actual actuator deflection is available. This is not an unrealistic assumption in aircraft systems [37]. Information provided by the actual actuator deflection can be compared with the signals from the controller to indicate the effectiveness of the actuator. The idea is to use a ‘least squares’ method to estimate the coefficients w_i and c_i in a relationship of the form

$$u_{(i,a)} = w_i u_i + c_i$$

where $u_{(i,a)}$ represents the actual deflection and u_i represents the demanded deflection i.e. the controller output. The scalars w_i and c_i are obtained from a least squares optimization and $W = \text{diag}(w_1, \dots, w_m)$. If the i th actuator is working perfectly, $w_i = 1$ and $c_i = 0$. If $w_i < 1$ then a fault is present. In the Admire simulation, 10 data samples from a ‘moving window’, collected at 100Hz are used to compute the w_i and c_i .

8.6.3 Simulation results

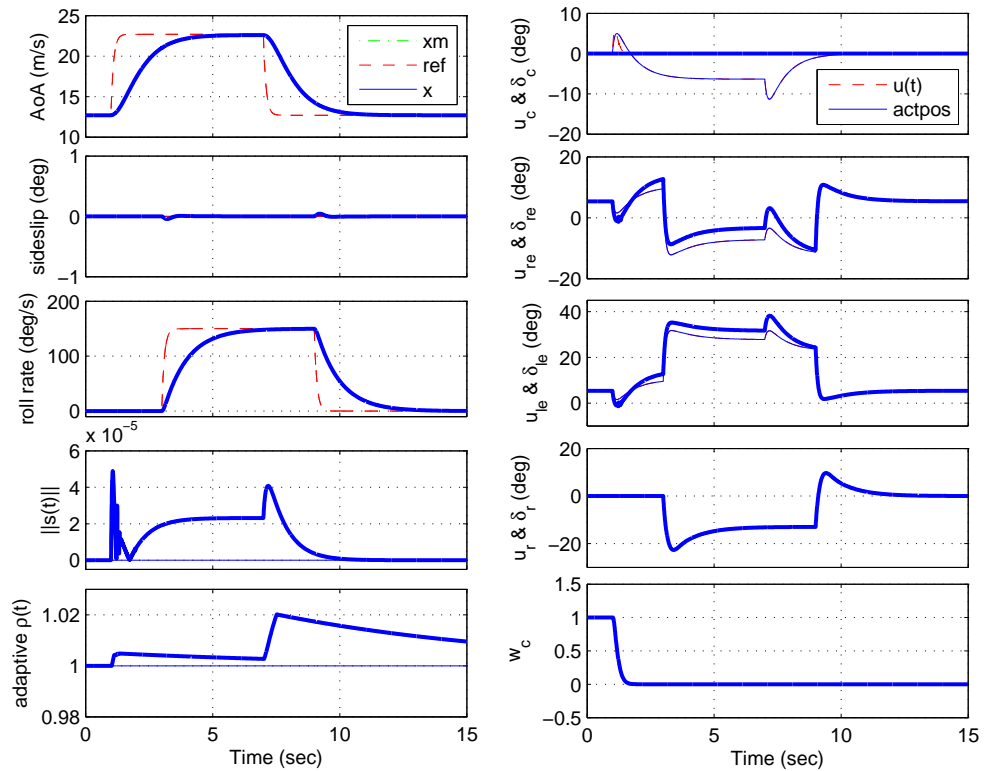


Figure 8.3: on-line CA: nominal no fault condition (solid thin line) vs. canard lock failure (solid thick line): system responses

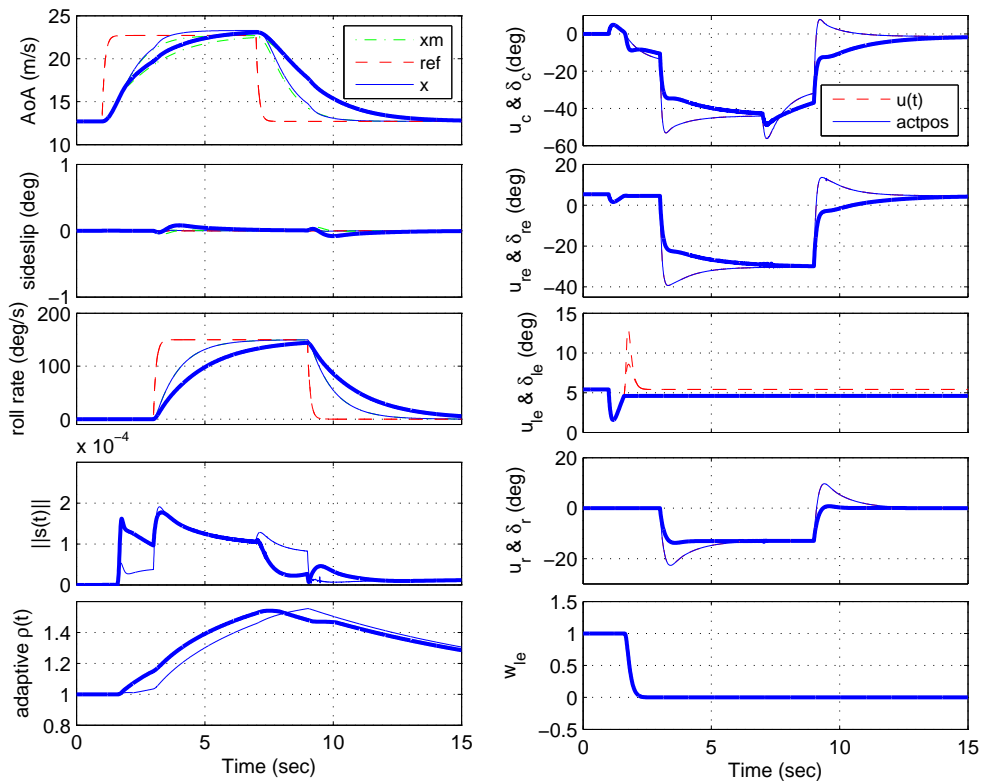


Figure 8.4: on-line CA: left elevon lock with offset: without (solid thin line) & with adaptive reference model (solid thick line).

In the following simulations, the aircraft model undertakes a manoeuvre called ‘ α roll’. In this chapter, step demand of magnitude 10 deg is applied to AoA during 1-7 sec and a step of 150 deg/sec for roll rate is applied during 3-9 sec. (There is no reference command for sideslip angle – see Figure 8.3). Figure 8.3 shows the response of the closed-loop system and compares the nominal no-fault condition (solid thin line) and a situation when the canard jams at 2sec (solid thick line). Note that some of the thick solid line overlaps the thin solid line. It can be seen that the control signal is systematically re-routed to the right and left elevon to maintain the required performance. The tracking responses show no degradation in performance and the commanded state responses show that the controller tracks the reference model ‘perfectly’. Figure 8.3 also shows accurate canard effectiveness estimation (w_c) from the least squares method.

Figure 8.4 shows a non-symmetric type of actuator failure where the left elevon locks with an offset at 1.6sec (i.e. a lock at a non-trim position). This scenario is much more difficult compared to the one considered in [95]. Initially in Figure 8.4, a control signal is sent to the left elevon. After the failure has been detected, the weight w_i for the left elevon (w_{le}) in the control allocation is changed and the control signal sent to the left elevon is ‘switched off’ and redistributed to the canard and right elevon. Figure 8.4 shows much more significant non-linear gain adaptation (for both with and without reference model adaptation) when the fault occurs. Figure 8.4 also shows comparisons between the controller with (solid thick line) and without (solid thin line) reference model adaptation. It can be seen that in the event of a severe failure, by ‘slowing down’ the reference model the control surface deflections become less aggressive compared with the non-adapted reference model. Therefore (as observed in the literature e.g. [112]), a much slower response is desirable to provide a safe level of degraded performance and to prevent further damage to the aircraft.

8.7 ADMIRE simulations: fixed control allocation

8.7.1 Controller design

Note that in both the actuator effectiveness based CA scheme and the fixed and equally distributed CA scheme, the controller is designed based on the system in (8.21) and (8.68) when $K = 0$: i.e. based on the pair (\hat{A}, \hat{B}_ν) . The same sliding surface design as in Section 8.6.1 is used here. The only difference is the actual control signal being sent to the actuators. In Section 8.6.1, the control signals sent to the actuators are based on (8.42) while in this section, the control signals sent to the actuators are based on (8.63). Note also, as mentioned in Section 8.4, although the CA strategy proposed in this section is different from the one in Section 8.3, the stability analysis of the reduced order sliding motion must satisfy the same condition i.e. Equation (8.39). This is due to the fact that γ_1 from (8.38) and γ_2 from (8.37) correspond to the same elements in the reduced order systems (8.34) and (8.73), and the fact that $\|B_2^\ddagger\| = \|B_2^+\|$. Therefore, the analysis in Section 8.6.1 is also valid for the case of the fixed CA scheme.

The variables related to the adaptive non-linear gain in Section 8.4.1 have been chosen as follows: it was found that choosing $l_1 = 0$ and $l_2 = 1$ gave sufficiently good performance. The parameter η from (8.75) was chosen as $\eta = 1$. The adaptation parameters from Section 8.4.1 have been chosen as $a = 3200$, $b = 0.0001$ and $\epsilon = 3 \times 10^{-5}$. As in Section 8.6, the parameter

ϵ was chosen to be able to tolerate the variation in $\|s(t)\|$ due to normal changes in flight condition but small enough to enable the adaptive gain to be sensitive enough to deviations from zero due to faults or failures. Here a has been chosen to be large to enable small changes in $\|s(t)\|$ to cause significant changes in the gain, so that the control system reacts quickly to a fault. The parameter b on the other hand dictates the rate at which $\rho(t)$ will decrease, after $\|s(t)\|$ has returned below the threshold ϵ . As in Section 8.6.1, $\text{rank}(B_2WB_2^T) < 3$ when the rudder completely fails or any two surfaces from the set consisting of the canard and the left and right elevons completely fail. Using the fact that, as in Section 8.6.3, only a single actuator failure is considered, w from (8.77) has been found to be $w = 0.2286$. Therefore from (8.78), $\varsigma = 60.9629$ (where γ_1 and γ_0 are defined in Section 8.6.1). From (8.89), $\epsilon\eta = 3 \times 10^{-5}$ and $b\varsigma^2/4a = 2.903 \times 10^{-5}$ and therefore the condition in Proposition 8 is satisfied.

8.7.2 Simulation results

The same manoeuvre and failure test conditions as in Section 8.6.3 is considered here. Figure 8.5 shows the aircraft responses when the canard fails at 2 sec, while Figure 8.6 shows when the left elevon fails at 1.6 sec. Figure 8.5 shows the response of the closed-loop system and compares the controller with (solid thick line) and without (solid thin line) reference model adaptation. It can be seen that the tracking responses show no degradation in performance and the commanded state responses show that the controller tracks the reference model ‘perfectly’. Similar responses to those in Section 8.6.3 have been obtained. The controller with the adaptive reference model (solid thick line) shows much less aggressive control surface deflection compared to the one with a fixed reference model (thin line). There are a few differences in Figure 8.5 compared to Figure 8.3 associated with the signal $\|s(t)\|$, the adaptive gain $\rho(t)$, and the control signal to the canard $u_c(t)$. Figure 8.5 shows that in the absence of the actuator effectiveness estimation, the fixed CA scheme continues to send signals to the canard even after it has failed. The absence of the actuator effectiveness estimate gives much larger deviations from the sliding surface ($\|s(t)\|$) compared to the one in Figure 8.3. As a consequence of the larger $\|s(t)\|$, the adaptive gain $\rho(t)$ is much higher than the one in Figure 8.3. The higher gain $\rho(t)$ gives larger control signals than in the nominal condition, which are sent to all actuators to compensate for the jammed canard. This replicates the condition of passive FTC using sliding modes without any FDI as shown in Chapter 4. The difference in this section is that total actuator failures can be handled. The slow rate at which $\rho(t)$ is decreasing in Figure 8.5 is due to the choice of b for the adaptive gain.

Figure 8.6 shows a non-symmetric type of actuator failure where the left elevon locks with an offset. This figure also shows a similar trend as in Figure 8.5. The control signal sent to the jammed left elevon is not shut off (because of the absence of any FDI schemes). The deviation from the sliding surface ($\|s(t)\|$ signal) is much higher compared to the one in Figure 8.4; and this causes the adaptive gain $\rho(t)$ to reach the maximum set gain. The large adaptive gain increases the magnitude of the control signals sent to all the actuators and thus enables the desired AoA, sideslip and roll rate performance to be maintained. Again, the slow rate at which $\rho(t)$ is decreasing in Figure 8.6 is due to the choice of b for the adaptive gain. Figure 8.6 also shows comparisons between the controller with (solid thick line) and without (solid thin line) reference model adaptation. By ‘slowing down’ the reference model, especially in the event

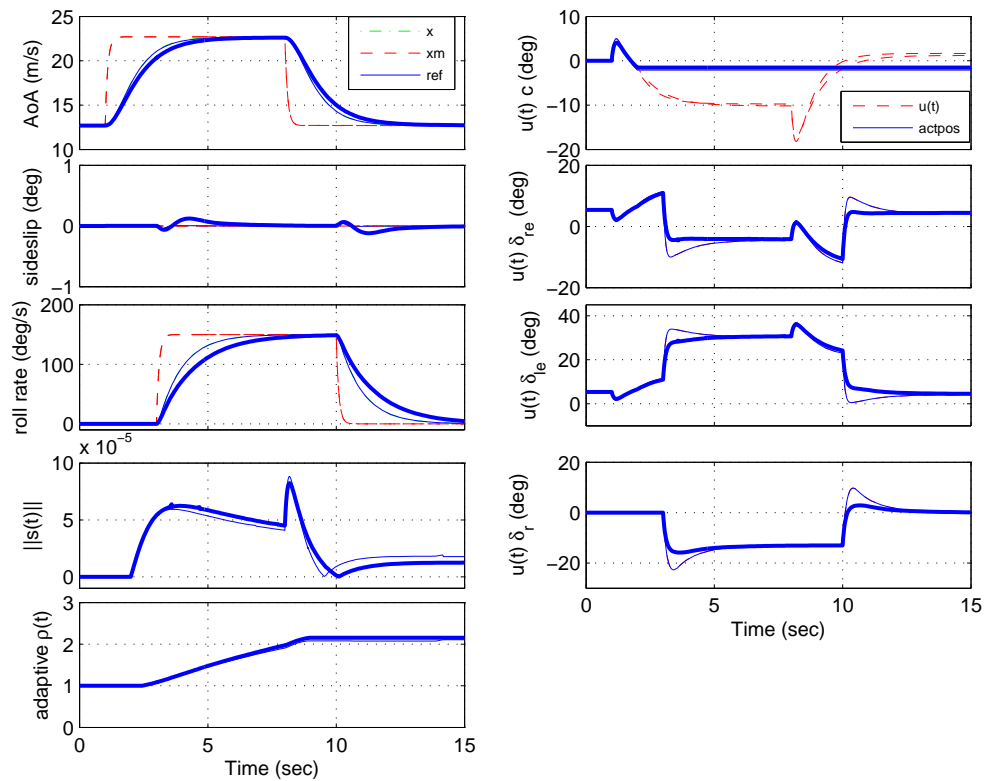


Figure 8.5: fixed CA: canard lock with offset: without (solid thin line) & with adaptive reference model (solid thick line).

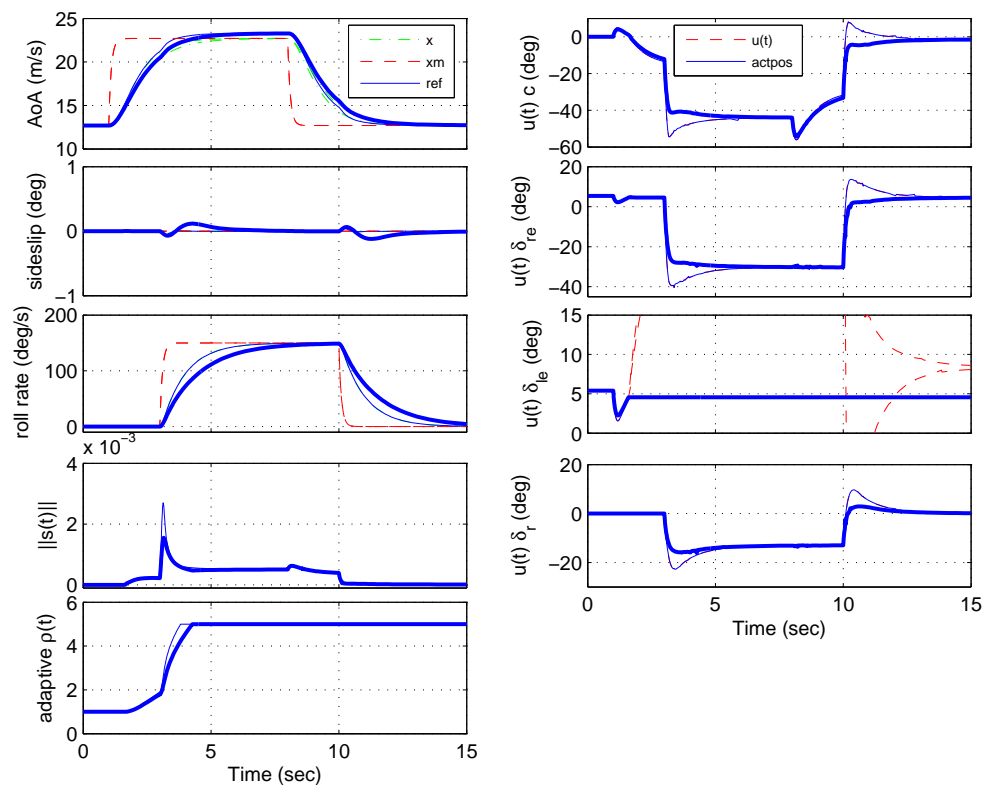


Figure 8.6: fixed CA: left elevon lock with offset: without (solid thin line) & with adaptive reference model (solid thick line).

of a severe failure, the control surface deflections become less aggressive compared with the non-adapted reference model.

8.8 Conclusions

This chapter has proposed two new CA strategies using a model reference framework. One is based on an on-line control redistribution and the other uses an equally distributed CA scheme. An adaptive non-linear gain and an adaptive reference model, for FTC, have also been proposed. In the first CA strategy, the effectiveness level of the actuators is used by the CA scheme to redistribute the control signals to the remaining actuators when a fault or failure occurs. The second CA scheme is based on fixed equally distributed control to all actuators even in the case of faults or failures. The adaptive non-linear gain and reference model provide on-line tuning for the controller. This chapter has presented a rigorous stability analysis for the two proposed schemes and has proposed two adaptive non-linear gain strategies to maintain sliding. The schemes have been implemented on the ADMIRE aircraft model and have shown that faults and total actuator failures can be handled. The simulation results have shown good performance even in worse failure scenarios than those considered in the existing literature.

Chapter 9

GARTEUR AG16 Case Study: ELAL Flight 1862 Bijlmermeer Incident

The flight simulator results shown in Chapter 7 concentrated on individual control surface failures (jams with offsets or runaways). In this chapter, the model reference controller from Chapter 8 will be applied to the more challenging task of landing the aircraft under the ELAL flight 1862 Bijlmermeer scenario under the assumption that no actuator effectiveness estimation is available. This represents the actual situation in the Bijlmermeer incident, where there was not enough information and no FDI available to inform the pilots of the actual damage to the aircraft. This is one of the challenges and the ultimate goal set at the beginning of this thesis.

9.1 Introduction

Learning from previous incidents, where pilots successfully landed crippled aircraft – such as Flight 232 in Sioux City, Iowa 1989¹, the Kalita Air freighter in Detroit, Michigan, October 2004² and the DHL freighter incident in Baghdad, November 2003³ – suggests that in many cases, the damaged/faulty aircraft is still ‘flyable’, controllable and some level of performance can still be achieved, to allow the pilot to safely land the aircraft. A successful program by NASA on propulsion controlled aircraft [43–46, 208] which considered the scenario of total hydraulic loss, showed the proposed controller helped the pilots land the aircraft safely [208].

An independent investigation by Delft University of Technology [188] on the ELAL flight 1862 which crashed into an apartment building in Bijlmermeer, Amsterdam, suggested that there was still some control and flying capability associated with the crippled aircraft. This is backed up by an early publication of FTC on the ELAL 1862 scenario in [141] which showed that it was possible to control the crippled aircraft (although in [141], an exact damage model is assumed to be available).

This chapter presents the flight simulator results obtained by experienced pilots on the ELAL flight 1862 (Bijlmermeer incident) scenario – which is one of the case studies associated with

¹Flight 232 suffered tail engine failure that caused the total loss of hydraulics [42, 84].

²The freighter shed engine no. 1, but the crew managed to land safely without any casualties.

³The DHL A300B4 was hit by a missile on its left wing and lost all hydraulics, but still landed safely [42].

the GARTEUR AG16. The results in this chapter are the outcome of the controller evaluation ‘flight testing’ campaign and the GARTEUR AG16 final workshop at Delft University of Technology, the Netherlands in November 2007. The results represent the successful real-time implementation of the SMC controller proposed in Section 8.4 on the SIMONA 6-DOF flight simulator with actual pilots flying and evaluating the controller. The simulator tests by the pilots were done with the ELAL flight 1862 scenario which was previously used in the independent investigation of the Bijlmermeer incident by Delft University of Technology [188].

The ELAL flight 1862 incident represents a challenging scenario for any FTC strategy. In this chapter, it will be assumed that the controller has no knowledge of the failure and damage to the airframe, and that there is no FDI or fault estimation available.

The controller that has been used is the model reference sliding mode controller proposed in Chapter 8. Here, since there is no FDI and no actuator effectiveness estimation available, fixed control allocation (specifically $\Omega = I$ from (8.62)) will be used. In this situation, there is no control signal redistribution to the healthy control surfaces. Instead, the fixed and equally distributed control allocation scheme is sufficient to access the remaining available control surfaces and ‘passively’ control the aircraft while ensuring stability and some nominal performance.

An outer loop inertial landing system (ILS) PID is used in order to provide an outer loop command (roll and flight path demand) to guide the aircraft to capture the localizer (LOC) and glide slope (GS), and therefore landing the aircraft using a typical landing procedure. This is a typical controller configuration used by the pilot to reduce the work-load, although this setup can be changed from the Mode Control Panel (MCP – see Figure 7.3) to allow the pilot to manually land the aircraft.

9.2 ELAL flight 1862: the incident

A brief discussion of the actual incident will be discussed in this section. This summary is based on the actual incident report by The Netherlands Aviation Safety Board [2].

On the 4th October 1992, the ELAL flight 1862 freighter aircraft – a Boeing 747-200 (Figure 9.1) – departed from Schiphol Airport, Amsterdam after refueling. This was a scheduled flight from New York JFK airport to Tel Aviv Israel, stopping in Amsterdam for refueling and a crew change [2]. Two runways were in use that day, 01L for takeoff and 06 for landing.

The aircraft takeoff started from runway 01L at 17:21 with a gross weight of 338.3 metric tons. The centre of gravity (CG) for takeoff was 23.1 percent of the mean aerodynamic chord (MAC). The aircraft initial climb was normal. At about 17:27.30, as the aircraft reached an altitude of about 6500ft, the pilots transmit an emergency call as the aircraft was turning to the right. The pilots were operating under extreme workload conditions trying to control the aircraft. Straight and level flight required full positive rudder pedal deflection and 60% to 70% maximum lateral control (the wheel almost full to the left) [2]. At around 17:28.06, the air traffic controller (ATC) instructed the pilot to turn to a heading of 260deg. At 17:28.17 the crew reported a fire in engine no. 3 and reported the loss of thrust in engine no. 3 and 4. At 17:28.57, the crew was initially informed that runway 06 was in use for landing but the crew requested runway 27 which was much closer to their current location in order to land quickly. However the aircraft



Figure 9.1: ELAL flight 1862: the aircraft



Figure 9.2: ELAL flight 1862: the impact area at the Bijlmermeer apartment building

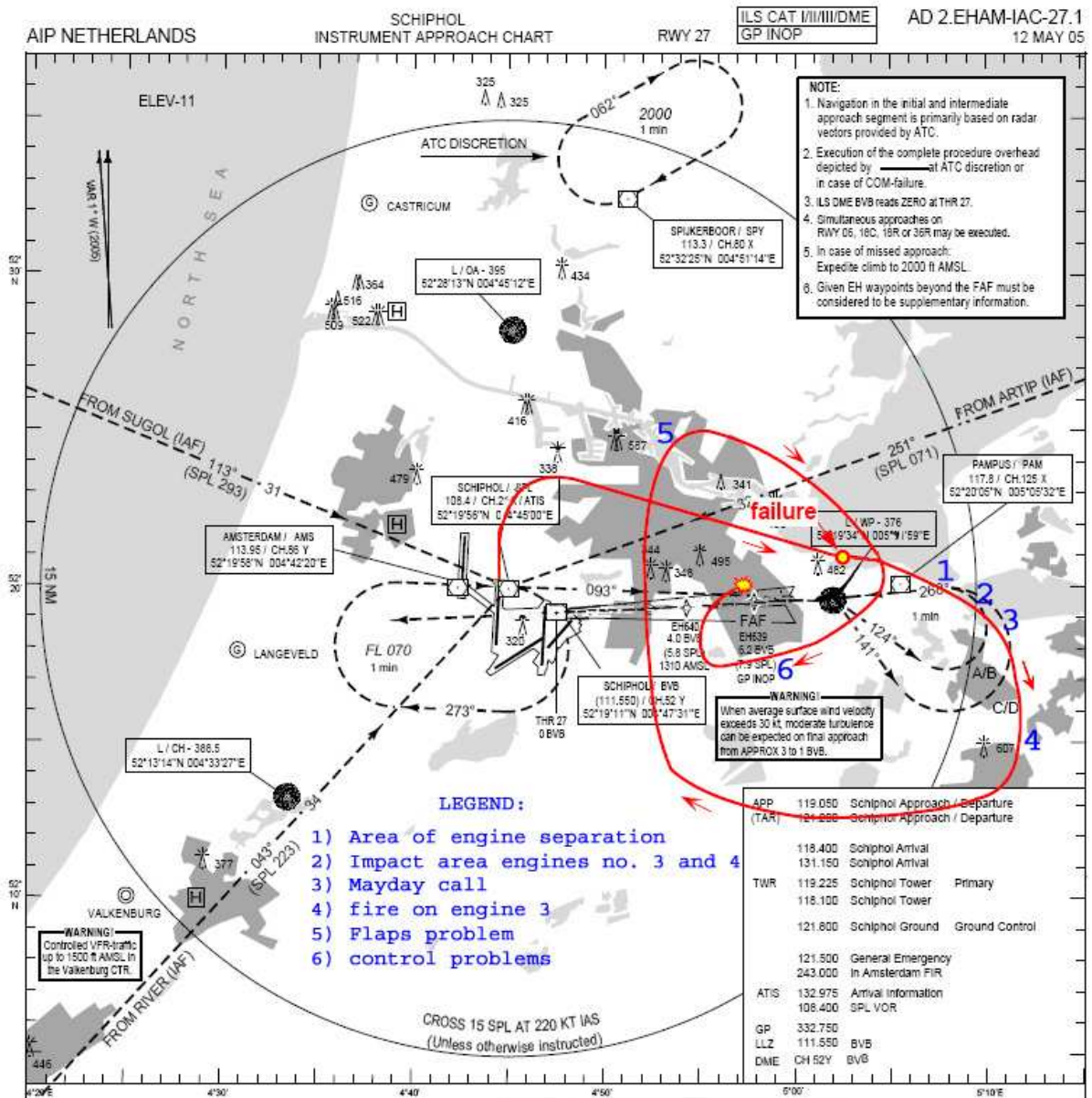


Figure 9.3: ELAL flight 1862: flight trajectory

was only 7 miles away from runway 27 at an altitude of 5000ft i.e. too high for a landing approach. The crew was instructed by the ATC to turn right to a heading of 360deg and descend to 2000ft. At 17:31.17 ‘flap 1’ setting could be heard in the cockpit. The ATC then instructed a heading change to 100deg and asked for the current status of the aircraft. The crew reported that engines no. 3 and 4 were inoperative and reported a problem on the wing flaps. The aircraft passed through the required heading of 100deg and maintained a heading of 120deg with airspeed 260 knots in a gradual descent to 2000ft. As the aircraft was still heading to the required localizer (associated with runway 27), no correction in heading was instructed by the ATC. The ATC then instructed another right turn to a heading of 270deg to intercept the localizer and align for the final approach course. At this point the aircraft was at 4000ft, 260 knots ground speed and at a heading of 120deg, 3 nautical miles north of runway 27 centre-line and 11 miles away from the runway. The heading change took about 30 seconds

and it was realized that the aircraft was going to overshoot the localizer. The ATC instructed another right turn and a change of heading to 290deg in an attempt to capture the localizer from the south. After 20 seconds the ATC instructed a heading and altitude change to 310deg and 1500ft respectively. At 17:35.03 the flight crew acknowledged the instruction and immediately reported control difficulties. At approximately 17:35.28, the co-pilot reported that the aircraft was 'going down' while the pilot was raising all flaps and lowering the landing gear. At 17:35.42 the aircraft crashed 13km east of Schiphol airport into an eleven floor apartment building in Bijlmermeer, a suburb of Amsterdam (Figure 9.2). The aircraft was destroyed during impact and due to the subsequent fire. Investigation of the crash site indicated that the impact was at a very steep flight path angle with bank angle slightly over 90deg to the right and with the nose down approximately 70deg [2]. All the 4 flight crew and approximately 43 other people on the ground were fatally injured. The trajectory of the ELAL flight 1862 can be seen in Figure 9.3. Further details on the incident can be found in [2].

9.3 ELAL flight 1862: aircraft damage analysis

This section provides a summarized version of the incident report [2] describing the actual damage on the aircraft:

Unknown to the flight crew, the inboard fuse-pin⁴ that held engine no. 3 to the pylon⁵ broke due to fatigue. This caused no. 3 engine and its pylon to also separate from the right wing shortly after takeoff causing damage to the leading edge of the right wing. The shedding of engine no. 3 from the right wing in an outboard and rearward direction resulted in a collision with no. 4 engine (see Figure 9.4), causing it and its pylon to separate from the wing. The damage was extensive to the right wing structure (see Figure 9.4). Several parts of the leading edge flaps and leading edge structures such as the leading edge flap no. 18 drive unit, the top skin panel above pylon no. 3, the adjacent inboard top skin panel (located above the most outboard Krügerflap⁶) and the pneumatic duct of the bleed air system (which is normally located in the wing leading edge, between engines no. 3 and 4) detached from the wing when engines no. 3 and 4 were lost. It is assumed that due to the speed of the aircraft, the aerodynamic distortion, and turbulence, some other parts were also blown off the leading edge of the right hand wing up to the front spar. Right wing leading edge damage is assumed to have occurred up to the front spar of the right hand wing over an area approximately 1 metre left of pylon no. 3, to approximately 1 metre to the right of pylon no. 4. Figure 9.4 illustrates the estimated damage to the right wing. (The amount of damage on the wing leading edge after the separation of pylon no. 2 from a B747 accident at Anchorage on March 31, 1993 (Figure 9.5), is indicative of the amount of damage probably inflicted on the El Al 1862 right wing leading edge [2]).

In summary, the damage and the effect to the ELAL flight 1862 aircraft after the engine no. 3 and 4 separation are:

⁴The role of the fuse pin is to allow the engine to separate from the wing under a strong impact load that occurs in the event of a crash or hard landing in order to protect the fuselage from engine fire.

⁵The pylon is the structural component connecting the jet engine to the main wing.

⁶The Krügerflap is the hinged flap on the leading edge.

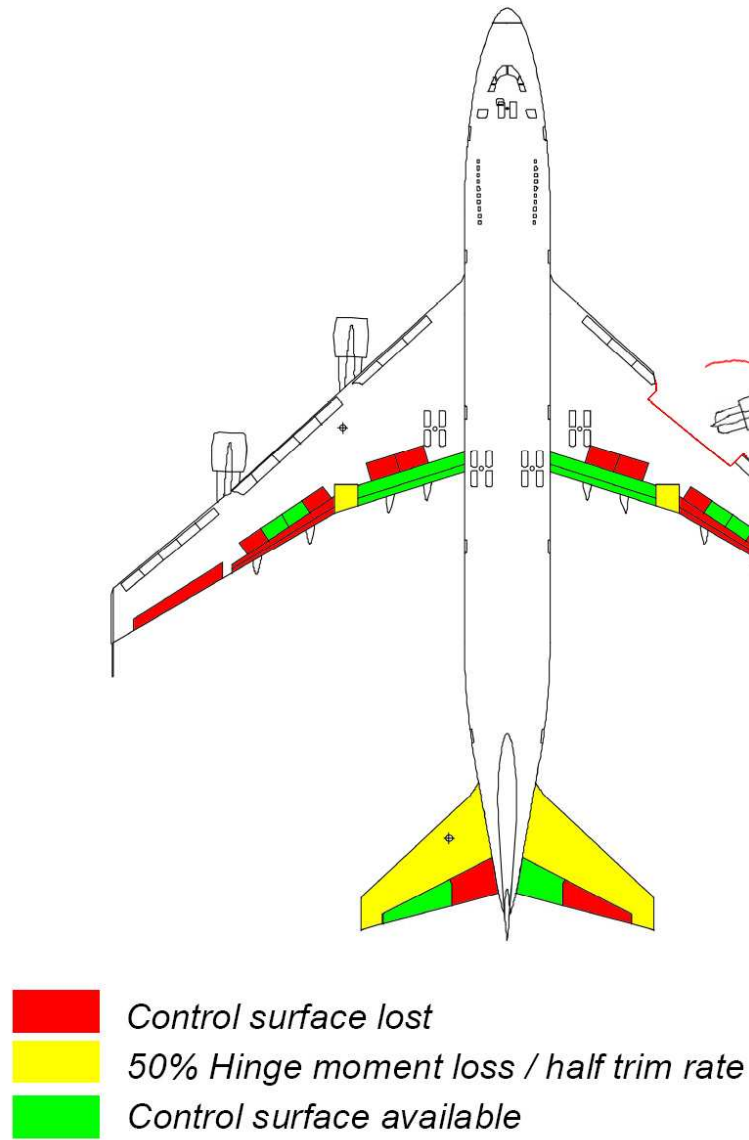


Figure 9.4: ELAL flight 1862: actuator fault/failure and structural damage (adapted from [2, 188])

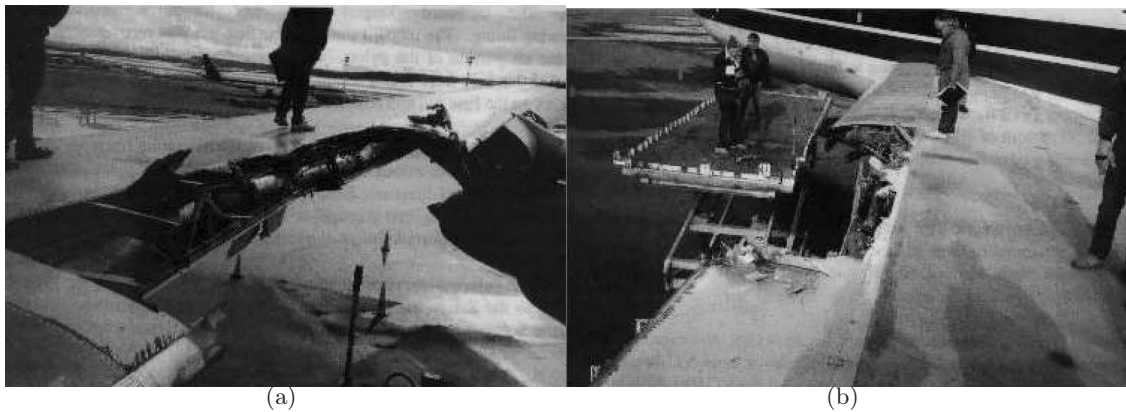


Figure 9.5: Wing damage due to separation of engine no. 2, Anchorage, 1993 (Figure adapted from [190]).

1. loss of thrust from engine no. 3 and 4;
2. right wing leading edge damage causing changes to the wing aerodynamic (higher drag and less lift due to the disrupted airflow over the damaged wing);
3. right inboard aileron and remaining spoilers 10 and 11 are less effective due to the airflow disruption resulting from the damage to the leading edge of the right wing;
4. limited roll control due to the loss of the outboard aileron (which is required during slow speed) and only partially available spoilers due to hydraulic no. 3 and 4 system loss;
5. weight loss of about 10 tonnes due to the separation of two engines;
6. hydraulic and pneumatic system no. 3 and 4 pressure loss;
7. loss and partial loss (half trim rate) of several control surfaces due to the loss of hydraulics system no. 3 and 4 (see Figure 9.4);
8. lateral CG displacement due to the loss of the engines;
9. degraded lateral control due to lower rudder lag as a result of hydraulic pressure loss;
10. positive yawing moment to the right due to asymmetric thrust from engine no. 1 and 2;
11. partial loss of the right wing leading edge flaps and the loss of outboard trailing edge flaps means that a high speed landing is necessary.

9.3.1 ELAL flight 1862: controllability and performance of the damage aircraft

When the flight crew transmitted the emergency call at 17:27.30, the aircraft was turning to the right. In order to stabilize the aircraft at 260 knots and maintain straight and level flight, an almost full positive rudder deflection and almost maximum wheel (60%-70%) deflection was applied by the pilot [2]. The amount of corrections in order to obtain straight and level flight was something unexpected for the pilot, indicating something unusual had occurred.

A few paragraphs from [190] best describe the expected effect when engine failure occurs (but the engine still intact) compared to the ELAL 1862 scenario; “. . . *The aircraft design and certification requirements state that there should be enough controllability to handle a multiple engine failure on one side in order to continue flight. The air minimum control speed (V_{mca}) is defined as the minimum speed during a failure of the most critical engine, at which aircraft control and a fixed heading can be maintained with full rudder and with sufficient lateral control authority to bank 5 degrees into the operating engine. The first sign of an engine failure will be a sudden roll of the aircraft. If directional control is not applied, or with a fixed rudder deflection, thrust asymmetry will cause the aircraft to yaw. Assuming a right multiple engine failure for a nominal case with no structural wing damage, the resulting yaw will create a negative side slip angle that creates a positive roll moment to the right. Instant control compensation in an engine failure flight condition consists of applying a rudder pedal input to counteract the yawing moment, a control wheel deflection to counteract the rolling moment or applying a thrust reduction on the*

remaining engines to decrease the yawing moment.

For the case of ELAL Flight 1862, the wing damage caused an additional lift loss and drag increase on the right wing. Because these effects are a function of angle of attack, increase of angle of attack will create an additional rolling moment and yawing moment into the direction of the dead engines. This in turn will require more opposite control wheel deflection, especially to counteract bank steepening during manoeuvring. Banking into the dead engines will increase the minimum control speed and therefore reduce the available controllability.

The Flight 1862 accident aircraft was designed to have enough rudder authority to keep the control wheel almost neutral with two engines inoperative on one side. However, in the case of Flight 1862, the DFDR (digital flight data recorder) indicates that control wheel deflections between 20 to 60 degrees to the left were needed for lateral control and straight flight. The aerodynamic effects due to the wing damage and degraded effectiveness of the right wing inboard aileron, required larger left wing down control wheel deflections than in the nominal case. ...”

The extensive damage to the right wing caused severe disruption of the airflow at the leading edge of the right wing, causing major aerodynamic changes thus reducing its lift generating capability and increasing drag. “... At small angles of attack the lift on both wings was essentially equal, at higher angles of attack the increase in lift on the damaged wing was less than the increase of lift on the undamaged wing. An increase in angle of attack therefore generates a roll moment. In the case of El Al 1862 this increase caused bank steepening during the right turns in the direction of the damaged wing. This effect was confirmed by the DFDR data ...” [2].

Later studies [188] managed to estimate the total drag using the reconstruction of the ELAL 1862 aircraft in simulation. When compared with the DFDR a reasonable match was obtained. It is further stated in [188] that a 10% drag increase at low angle of attack was estimated compared to the undamaged wing. At higher angle of attack, a 20% to 30% increase in drag was estimated, due to flow separation behind the damaged leading edge. The extensive damage to the leading edge of the right wing (which caused flow separation and turbulence) meant that the right inboard elevator and the remaining spoilers 10 and 11 became less effective. This required more aileron deflection on the left inboard wing just to maintain straight and level flight. This is reflected in the almost maximum wheel deflection to the left applied by the pilot.

It is further reported in [2] that “... An energy analysis was performed based upon altitude and airspeed data from the DFDR. It should be realized that this method does not allow extrapolation of performance capabilities in other conditions than those encountered during this flight. Based on this analysis the following conclusions were made:

- Marginal level flight capability was available at 270 knots and go-around power with a limited manoeuvring capability
- Performance degraded below about 260 knots at increased angles of attack. Deceleration to 256 knots resulted in a considerable sink rate.

... Until the last phase of the flight, aircraft control was possible but extremely difficult. The aircraft was in a right turn to intercept the localizer and the crew was preparing for the final approach and may have selected the leading edge flaps electrically. During the last minute, the following occurred, as derived from DFDR data: the aircraft decelerated when the pitch attitude

was increased probably to reduce the rate of descent. The associated increase in angle of attack caused increased drag. The additional drag from a side slip and possibly extended leading edge flaps resulted in a further speed decay. This speed decay was probably the reason for increasing thrust on the two remaining engines. All this generated an increased roll moment to the right by:

1. asymmetric lift generation at an increased angle of attack;
2. high thrust asymmetry;
3. loss of aerodynamic efficiency of the right hand inboard aileron at increased angle of attack;
4. possible asymmetric lift due to leading edge flaps operation.

The resulting roll moment exceeded the available roll control ...” This contributed to the excessive roll, loss of altitude and loss of control during the last phase of the flight. A similar effect was also seen during the GATREUR AG16 flight evaluation test by three experienced pilots in the SIMONA motion flight simulator when using the classical/existing B747 controller (see the discussions in Section 9.6).

In one of the conclusions of the incident report [2], it was mentioned that in the case of ELAL 1862 “... Performance and controllability were so severely limited that the airplane was marginally flyable ... Because of the marginal controllability a safe landing became highly improbable, if not virtually impossible ...”. The independent investigation done later in Delft University of Technology [152, 188], which also looked into the performance capabilities using simulations, suggests that there was still some control and flying capability and that the aircraft was still “... recoverable ...”. It is further elaborated in [190] that “... from a technical point of view, the accident aircraft was recoverable if unconventional control strategies were used ...”. Further studies using [141] showed that it is possible to control the crippled aircraft (although in this FTC paper, an exact model of the damaged aircraft was assumed to be available).

One of the main findings in [152] is that “... a significant improvement in available performance and controllability was available at lower weight if more fuel had been jettisoned ...” [188].

It is also interesting to highlight that, for the duration of the incident, the flight crew was unaware engines no. 3 and 4 had separated from the wing despite reporting loss of thrust from both engines. In [2] “... Information regarding the separation of both engines did not reach the ATC controllers concerned with the emergency, and was therefore not relayed to the crew. Although it remains questionable if, when relayed, this knowledge would have changed the course of events, it could have given the crew at least a better understanding of the unusual situation ...”. This is the motivation for the tests in this chapter to be carried out under the assumption that the type of failure is unknown and in the absence of any FDI or fault reconstruction strategy.

9.4 Controller design

In this chapter both lateral and longitudinal control is considered. The main objective of the controller design is to bring the damaged ELAL 1862 aircraft to a near landing condition on

Runway 27 at Schiphol airport (through a proper landing approach using localizer (LOC) and glide slope (GS) capture procedures if possible). It is assumed that no FDI or fault reconstruction is available to replicate the actual ELAL 1862 scenario – indeed the flight crew were even unaware that engine no. 3 and 4 had detached from the right wing.

As in Chapter 7, a linearization of the nominal aircraft has been obtained around an operating condition of 263,000 Kg, 92.6 m/s true airspeed, and an altitude of 600m at 25.6% of maximum thrust and at a 20deg flap position. The result is a 12th order linear model (separated into two 6th order models) associated with the lateral and longitudinal states. For design purposes, only the first four longitudinal and lateral states have been retained. The state-space system pairs, representing the lateral and longitudinal systems about the trim condition, can be found in (7.1), (7.2), (7.3) and (7.4) in Chapter 7. The states represent $x_{lat} = [p \ r \ \beta \ \phi]^T$ and $x_{long} = [q \ V_{tas} \ \alpha \ \theta]^T$. The lateral control surfaces are $\delta_{lat} = [\delta_{air} \ \delta_{ail} \ \delta_{aor} \ \delta_{aol} \ \delta_{sp1-4} \ \delta_{sp5} \ \delta_{sp8} \ \delta_{sp9-12} \ \delta_r \ e_{1_{lat}} \ e_{2_{lat}} \ e_{3_{lat}} \ e_{4_{lat}}]^T$ which represent aileron deflection (right & left - inner & outer)(rad), spoiler deflections (left: 1-4 & 5 & right: 8 & 9-12) (rad), rudder deflection (rad) and lateral engine pressure ratios (EPR). The longitudinal control surfaces are $\delta_{long} = [\delta_e \ \delta_s \ e_{1_{long}} \ e_{2_{long}} \ e_{3_{long}} \ e_{4_{long}}]^T$ which represent elevator deflection (rad), horizontal stabilizer deflection (rad), and longitudinal EPR.

As in Chapter 7, the controlled output distribution matrices are

$$C_{c_{lat}} = \begin{bmatrix} 0 & 0 & 1 & 0 \\ 0 & 0 & 0 & 1 \end{bmatrix}, \quad C_{c_{long}} = \begin{bmatrix} 0 & 0 & -1 & 1 \\ 0 & 1 & 0 & 0 \end{bmatrix}$$

which represent the states ϕ and β for lateral control, and flight path angle (*FPA*) and V_{tas} for longitudinal control. These linear models of the *nominal damage free aircraft* will be used to design the control schemes which will be described in the next sections. This is a major difference compared to [141] where the MPC controller is designed based on the exact knowledge of the damaged aircraft.

In the original coordinates, the control law can be summarized as:

$$\nu_l(t) = Le(t) + Fx_m(t) + Gy_d(t)$$

where $L = -SA$ and SB_ν has been scaled so that $SB_\nu = I$. The nonlinear term $\nu_n(t)$ is given in (8.75), where the nonlinear gain $\rho(t)$ is based on the adaptive law (8.44)-(8.46). The final control law is given in (8.63) i.e. a fixed CA scheme which does not depend on estimates of $K(t)$.

9.4.1 Lateral Controller Design

The feedback matrices for the ideal lateral model from (8.17) have been designed using eigenstructure assignment [137]. The eigenvalues were chosen as $\{-0.3500 \pm 0.1500i, -0.5000, -0.4000\}$ and the desired and obtained eigenstructure are respectively:

$$\underbrace{\begin{bmatrix} * + *i & * - *i & * & 0 \\ 0 & 0 & 0 & 0 \\ * + *i & * - *i & 0 & 0 \\ 1 + *i & 1 - *i & 1 & 1 \end{bmatrix}}_{desired} \Rightarrow \underbrace{\begin{bmatrix} 0.3195 - 0.1369i & 0.3195 + 0.1369i & 0.4498 & 0.3748 \\ -0.0000 - 0.0000i & -0.0000 + 0.0000i & -0.0430 & -0.0526 \\ 0.1619 + 0.1412i & 0.1619 - 0.1412i & 0.0182 & 0.0275 \\ -0.9127 & -0.9127 & -0.8919 & -0.9252 \end{bmatrix}}_{obtained}$$

which yields

$$F_{lat} = \begin{bmatrix} 0.5592 & -0.8808 & -0.6384 & 0.1010 \\ 0.0823 & 1.3729 & 2.5265 & -0.5851 \end{bmatrix}$$

As in Section 8.6.1, the feed-forward matrix G_{lat} has been designed using the inverse steady-state gain for the virtual triple $(A_{lat}, B_{\nu_{lat}}, C_{c_{lat}})$: specifically

$$G_{lat} = -(C_{c_{lat}}(A_{lat} + B_{\nu_{lat}}F_{lat})^{-1}B_{\nu_{lat}})^{-1}$$

Here

$$G_{lat} = \begin{bmatrix} -0.3078 & 0.0651 \\ 0.7310 & 0.3891 \end{bmatrix}$$

As in Chapter 7, it will be assumed that at least one of the control surfaces for both ϕ and β tracking will be available when a fault or failure occurs (i.e. one of either the four ailerons or the four spoilers will be available, and one of either the rudder or the four engine thrusts are available). Based on these assumptions, it can be verified from a numerical search that $\gamma_{0_{lat}}$ from (8.70) is $\gamma_{0_{lat}} = 8.1314$, which is the same as in Chapter 7, as $\gamma_{0_{lat}}$ only depends on the linear plant model.

The matrix which defines the hyperplane must now be synthesized so that the conditions of (8.39) are satisfied. A quadratic optimal design (as discussed in Section 3.4.1) has been used to obtain the sliding surface S_{lat} which depends on the matrix M_{lat} in Equation (8.28). The symmetric positive definite state weighting matrix has been chosen as $Q_{lat} = \text{diag}(2, 2, 1, 1)$. The first and second terms of Q_{lat} are associated with the equations of angular acceleration in roll and yaw (i.e. $B_{lat,2}$ term partition in (7.2)) and thus weight the virtual control term. Thus by analogy to a more typical LQR framework, they affect the speed of response of the closed-loop system. Here, the first and second terms of Q_{lat} have been more heavily weighted compared to the last two terms, to give a reasonably fast closed-loop system response. The poles associated with the reduced order sliding motion are $\{-0.7136 \pm 0.0522i\}$, where

$$M_{lat} = \begin{bmatrix} 0.0813 & -1.9138 \\ 1.3455 & 0.1854 \end{bmatrix}$$

Based on this value of M_{lat} , simple calculations from (8.38) show that $\gamma_{1_{lat}} = 0.0230$, therefore $\gamma_{0_{lat}}\gamma_{1_{lat}} = 0.1870 < 1$ and so the requirements of (8.39) are satisfied. Also for this particular choice of sliding surface, $\|\tilde{G}_{lat}(\mathbf{s})\|_{\infty} = \gamma_{2_{lat}} = 0.0563$ from (8.37). Therefore from (8.39),

$$\frac{\gamma_{2_{lat}}\gamma_{0_{lat}}}{1 - \gamma_{1_{lat}}\gamma_{0_{lat}}} = 0.5627 < 1$$

which shows that the system is stable for all $0 < w_i \leq 1$. For implementation, the discontinuity in the nonlinear control term in (8.41) has been smoothed by using a sigmoidal approximation as in Section 3.2.2 where the scalar $\delta_{lat} = 0.05$. This removes the discontinuity and introduces a further degree of tuning to accommodate the actuator rate limits – especially during actuator fault or failure conditions.

For simplicity, the variables related to the adaptive nonlinear gain have been chosen as $l_{1lat} = 0$ and $l_{2lat} = 1$, as in the last chapter. The parameter η_{lat} from (8.41) was chosen as $\eta_{lat} = 1$. In practice, a maximum limit ρ_{max} for the adaptive nonlinear gain in (8.44) has been imposed to avoid the actuators becoming too aggressive. Here, the maximum gain was set at $\rho_{max_{lat}} = 5$. The adaptation parameters from (8.45) have been chosen as $a_{lat} = 100$, $b_{lat} = 0.01$ and $\epsilon_{lat} = 5 \times 10^{-2}$. As in the last chapter, the parameter ϵ_{lat} was chosen to be able to tolerate the variation in $\|s_{lat}(t)\|$ due to normal changes in flight condition, but small enough to enable the adaptive gain to be sensitive enough to deviation from zero due to faults or failures. Here a_{lat} has been chosen to be large to enable small changes in $\|s_{lat}(t)\|$ to cause significant changes in the gain, so that the control system reacts quickly to a fault. The parameter b_{lat} on the other hand dictates the rate at which $\rho_{lat}(t)$ will decrease after $\|s_{lat}(t)\|$ has returned below the threshold ϵ_{lat} .

To emulate real aircraft flight control capability, an outer loop heading control law was designed based on a PID, to provide a roll command to the inner-loop sliding mode controller. In the SIMONA implementation, this outer loop heading control can be activated by a switch in the cockpit. The proportional gain as $K_{p_{lat}} = 3$, the integrator gain was set as $K_{i_{lat}} = 0.1$ and the derivative gain was set as $K_{d_{lat}} = 3$. Note that the integrator component is only activated when the heading angle error is less than 5deg to remove unwanted oscillation during manoeuvres but to still eliminate steady state error.

9.4.2 Longitudinal Controller Design

As in the lateral controller, the feedback matrices for the ideal longitudinal model from (8.17) have been designed using eigenstructure assignment [137]. The eigenvalues were chosen as $\{-0.2400 \pm 0.1700 - 0.7000 - 0.1250\}$ and the desired and obtained eigenstructure are

$$\underbrace{\begin{bmatrix} 0.5 + *i & 0.5 - *i & 0 & 0 \\ 0 & 0 & 0 & 1 \\ 0.5 + *i & 0.5 - *i & 0 & 0 \\ 0 & 0 & 1 & 0 \end{bmatrix}}_{desired} \Rightarrow \underbrace{\begin{bmatrix} 0.1812 - 0.1283i & 0.1812 + 0.1283i & -0.1057 & 0.0001 \\ -0.0020 + 0.0015i & -0.0020 - 0.0015i & -0.0060 & 1.0000 \\ 0.3220 - 0.5264i & 0.3220 + 0.5264i & 0.9829 & -0.0037 \\ -0.7549 & -0.7549 & 0.1510 & -0.0012 \end{bmatrix}}_{obtained}$$

respectively which yields

$$F_{long} = \begin{bmatrix} -0.0012 & -0.0380 & -0.6113 & 3.4367 \\ -0.0523 & 0.0017 & 0.4395 & -0.2396 \end{bmatrix}$$

As in the lateral control design, the feed-forward matrix G_{long} has been designed using the

inverse steady-state gain for the virtual triple so that

$$G_{long} = -(C_{c_{long}}(A_{long} + B_{v_{long}}F_{long})^{-1}B_{v_{long}})^{-1}$$

Here, the lateral feed-forward matrix G_{lat} is given by

$$G_{long} = \begin{bmatrix} -0.0015 & 0.0438 \\ 0.0665 & -0.0024 \end{bmatrix}$$

As in Chapter 7, it will be assumed that at least one of the control surfaces for *FPA* tracking will still be available when a fault or failure occurs. It is also assumed that at least one of the four engines is available for V_{tas} tracking. Based on these assumptions, it can be verified from a numerical search that $\gamma_{0_{long}} = 8.2913$ from (8.70).

As in the lateral controller, a quadratic optimal design has been used to obtain the sliding surface matrix. The weighting matrix has been chosen as $Q_{long} = \text{diag}(2, 2, 1, 1)$. Again, the first two terms of Q_{long} are associated with the $B_{long,2}$ term partition in (8.2) (i.e. the q and V_{tas} states) which weight the virtual control term. These have been more heavily weighted compared to the last two terms. The poles associated with the reduced order sliding motion are $\{-1.1157, -0.3737\}$ where

$$M_{long} = \begin{bmatrix} -0.0124 & -0.0037 \\ 0.4786 & 0.1247 \end{bmatrix}$$

Based on this value of M_{long} , simple calculations from (8.38) show that $\gamma_{1_{long}} = 3.0160 \times 10^{-4}$. Therefore $\gamma_{0_{long}}\gamma_{1_{long}} = 0.0025 < 1$ and so the requirements of Equation (8.39) are satisfied. For this choice of sliding surface, $\|\tilde{G}_{long}(\mathbf{s})\|_{\infty} = \gamma_{2_{long}} = 0.0066$ from (8.37). Therefore from (8.39),

$$\frac{\gamma_{2_{long}}\gamma_{0_{long}}}{1 - \gamma_{1_{long}}\gamma_{0_{long}}} = 0.0551 < 1$$

which shows that the system is stable for all $0 < w_i \leq 1$. The discontinuity in the nonlinear control term in (8.41) has been smoothed by using a sigmoidal approximation where the scalar $\delta_{long} = 0.05$.

As in the lateral design, the variables related to the adaptive nonlinear gain have been chosen as $l_{1_{long}} = 0$ and $l_{2_{long}} = 1$. This was also found to give sufficiently good performance and removes the dependence of $r(t)$ on $x(t)$ and simplifies the implementation. The parameter η_{long} from (8.41) was chosen as $\eta_{long} = 1$. In practice, a maximum limit ρ_{max} for the adaptive nonlinear gain in (8.44) is imposed to avoid the actuators from becoming too aggressive. Here, the maximum gain was set as $\rho_{max_{long}} = 2$. The adaptation parameters from (8.45) have been chosen similar to those in the lateral design; i.e. $a_{long} = 100$, $b_{long} = 0.01$ and $\epsilon_{long} = 5 \times 10^{-2}$.

Again, to emulate real aircraft flight control capability, an outer loop altitude control law was designed based on a PID, to provide a *FPA* command to the inner loop sliding mode controller. In the SIMONA implementation, this outer loop altitude control can be activated by a switch in the cockpit. The proportional gain was set as $K_{p_{long}} = 0.001$, the integrator gain was set as $K_{i_{long}} = 0.00004$ and the derivative gain was set as $K_{d_{long}} = 0.02$. Note that the integrator

component is only activated when the altitude error is less than 15m to remove unwanted oscillation during manoeuvres but to eliminate steady state error.

Note that both the lateral and longitudinal controllers manipulate the engine EPRs. For lateral control, differential engine EPR is required as a secondary ‘actuator’ for β tracking; whilst for longitudinal control, collective EPR is used for V_{tas} tracking. In the trials, ‘control mixing’ was employed, where the signals from both the lateral controller ($e_{1_{lat}}$, $e_{2_{lat}}$, $e_{3_{lat}}$ and $e_{4_{lat}}$) and longitudinal controller ($e_{1_{long}}$, $e_{2_{long}}$, $e_{3_{long}}$ and $e_{4_{long}}$) were added together before being applied into each of the engines.

9.5 SIMONA implementation

The designed controller was implemented on the SIMONA flight simulator. The command input from the pilot is through the MCP. The new additional item in this control scheme is the implementation of the APP (approach) button which is engaged in order to intercept the LOC⁷ (localizer) and GS⁸ (glide slope) for the desired runway.

The controller was implemented as a SIMULINK (version 2006b) model with appropriate inputs and outputs to connect it with the SIMONA hardware, as described in Figure 9.6. In Figure 9.6, one major difference compared to the implementation in Chapter 7 is the addition of the ILS landing capability which has been added to the control loop to allow the aircraft to land on Runway 27 at Schiphol.

The controller was set up to work with an Ode4 solver with a fixed time step of 0.01sec. The available processing power is sufficient to run the controller in real time, i.e. within 10 ms per time step.

A connection with the MCP on the flight deck (Figure 9.7) enables the selection of ‘control modes’ e.g. altitude hold, heading select and reference values. The simulator trials were performed with the speed, altitude and heading select modes active. The pilot commands new headings, speeds or altitudes by adjusting the controls on the MCP.

9.5.1 ILS landing

A sensor which measures the deviation from the LOC angle/beam error (which is available in typical transport aircraft) combined with the current aircraft heading and VOR (VHF Omni-directional Radio Range⁹) course radial is used for aligning the aircraft towards the runway. The output of this outer loop is a roll demand for the LOC controller and an FPA demand for the

⁷A localizer is one component of an Instrument Landing System (ILS). The localizer provides runway centre-line guidance to an aircraft. The Localizer is placed at the far end of the approached runway. Its covers a distance of up to 46.3km in a cone of up to 10deg either side of the course.

⁸The Glideslope provides vertical guidance to the aircraft during descent. The standard glide-slope path is 3deg. The glideslope signal is emitted by an antenna, located near the end of the runway. The glideslope provides the precise required altitude leading to the touchdown zone of the runway.

⁹VOR is a type of radio navigation system for aircraft. VORs broadcast a VHF composite radio signal and data that allows the airborne receiving equipment to derive a magnetic bearing from the station to the aircraft (the direction from the VOR station in relation to the earth’s magnetic North at the time of installation). This line of position is called the "radial" in VOR parlance. The intersection of two radials from different VOR stations on a chart allow a "fix" of the specific position of the aircraft.

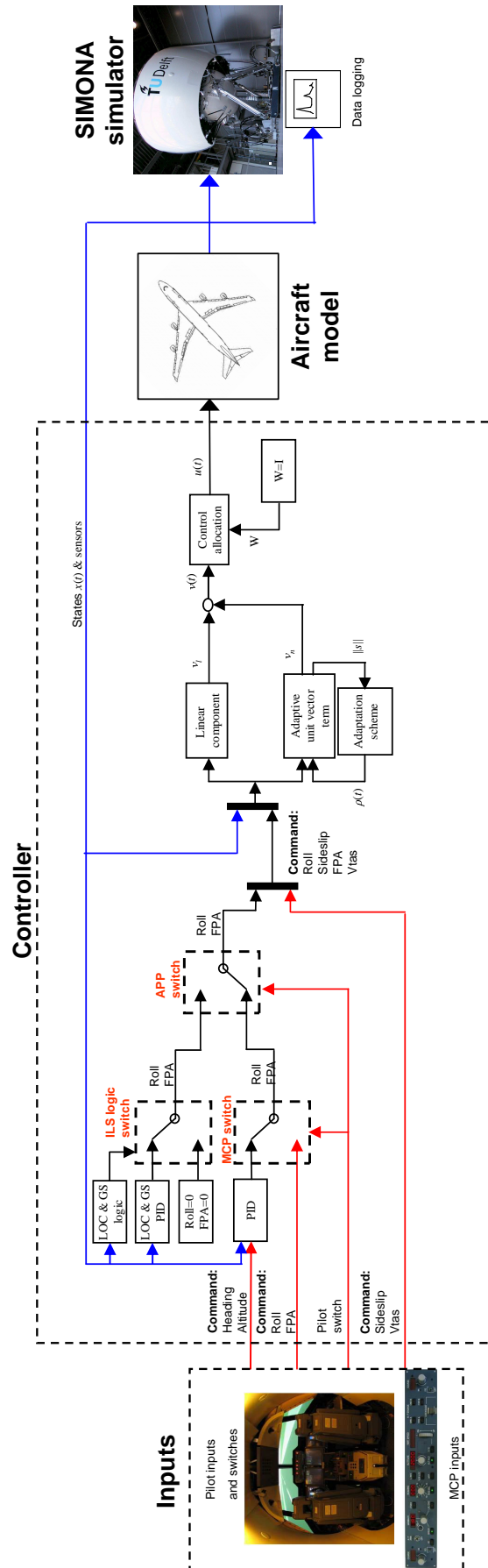


Figure 9.6: SIMONA interconnections



Figure 9.7: Mode control panel (MCP)

GS controller. These demand signals replace the pilot commands to the main SMC controller to allow for an almost automatic landing procedure. The outer loop controller (LOC and GS) is armed by the pilot by engaging the APP (approach) button on the MCP (see Figure 9.7) when the aircraft is near the LOC signal coverage. In normal operation, the LOC will be the first to be engaged (LOC valid) when the aircraft is inside the LOC coverage (the DME¹⁰ is less than 46.3km when the aircraft is inside the coverage angle of ± 10 deg from the LOC beacon and $(-7, -0.75)$ deg inside the glideslope (GS) beacon). During the armed phase, the LOC controller is in standby mode and the aircraft is controlled either by heading or roll commands from the pilot. When the LOC is engaged (LOC valid), the LOC controller will provide the inner roll command to the core lateral sliding mode controller and the whole process becomes an automatic landing mode: i.e. no input from the pilot is needed. The GS is then engaged (GS valid) when the aircraft is inside the GS coverage (i.e. the DME is less than 18.5km, LOC is within ± 8 deg and the GS is within $(-1.35, -5.25)$ deg inside coverage). The GS is in an armed phase (after the APP button is engaged), and the GS controller is in a standby mode with the aircraft controlled using altitude or via FPA commands from the pilot. When the GS controller is engaged (GS valid), the GS controller will provide the FPA command to the core longitudinal SMC controller: again no input from the pilot is needed. If for some reason, during the LOC and GS manoeuvre to the runway, the LOC or GS becomes invalid (i.e. if the aircraft goes outside the LOC and GS coverage ‘cones’), then the LOC and GS controller provide zero roll and FPA commands respectively. Then, the pilot can disengage the APP button to retake full control of the aircraft.

9.6 SIMONA flight simulator results with experienced pilots

The controller has been flown by three different pilots with experience on B747, B767, A330 and Citation II aircraft. Prof. J.A. Mulder, an experienced B767 and Citation II pilot, has rigorously tested the controller during the flight evaluation campaign before the GARTEUR AG16 final workshop in November 2007. During the AG16 final workshop, Hessel Benedictus, an experienced B747 pilot, flew the damaged ‘aircraft’ on the SIMONA simulator, during a presentation to the general public, including the local Dutch press (TV news, radio and newspapers). The results presented here are from tests flown by Arun Karwal, an experienced A330 KLM (Royal Dutch Airlines) pilot and test pilot for NLR (National Aerospace Laboratory, the Netherlands) during the pilot evaluation campaign in November 2007.

Note that even though the controller has been designed based on the linearization using a weight

¹⁰DME (Distance Measuring Equipment) is a transponder-based radio navigation technology that measures the distance between the LOC beacon and the aircraft by timing the propagation delay of VHF or UHF radio signals.

of approximately 263 000kg, the controller was tested with a heavy trim weight of 317 000Kg as per the actual ELAL 1862 aircraft. This removes the advantage of low weight and low speed manoeuvrability and higher performance and controllability compared to the heavy trim weight as discussed in Section 9.3, which was one of the main findings in [152]. The heavy trim weight for the flight test also replicates the actual ELAL 1862 scenario and fits with the assumption that the exact damage and condition of the aircraft, post faults, is unknown, thus making the challenge even harder.

The flight test was made as realistic as possible. As in the actual ELAL 1862 scenario, the aircraft flew in a northerly direction from runway 01L before starting to make a right turn. Immediately after the right turn, the ELAL failure scenario occurred (see Figure 9.8) whereby engines no. 3 and 4 detached from the right wing and caused significant damage to the right wing. The chosen runway, Runway 27, faced west at an angle of approximately 269deg from the north. Therefore in order for the aircraft to land, two 90deg turns must be performed before aligning the aircraft on Runway 27. During the third right turn, the aircraft was required to capture a localizer signal which guides the heading of the aircraft to line it up with the runway. During this normal procedure for landing, the aircraft will also be required to intercept a glide slope signal to enable the aircraft to descend at about a 3deg flight path angle, which will bring the aircraft to the landing target zone. The flare¹¹ and the actual landing of the aircraft were not carried out and the simulation was stopped at a point 50ft above the ground level.

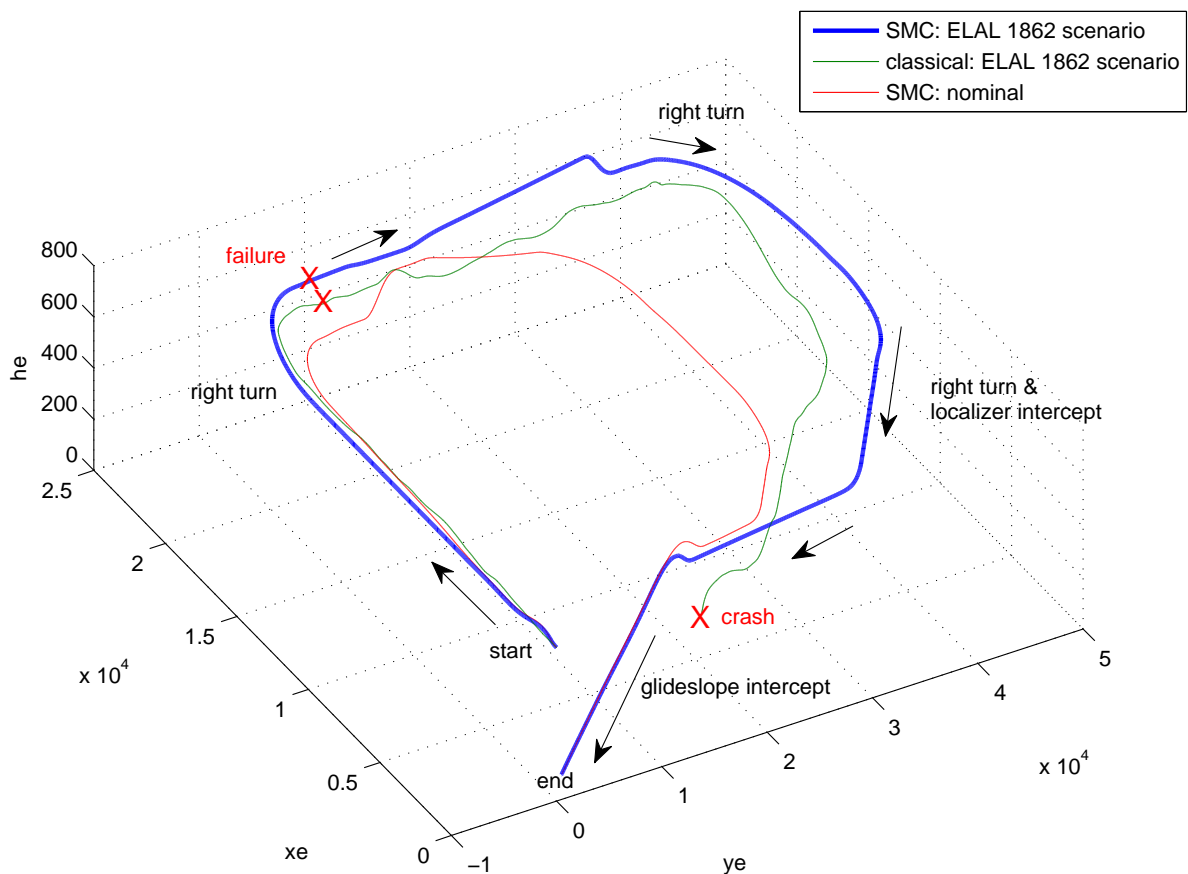


Figure 9.8: Classical & SMC controller: 3-D flight trajectory

¹¹Flare is the nose up manoeuvre of the aircraft, used at the final part of landing i.e. just before touch down to arrest the descent rate.

9.6.1 Classical Controller

Figures 9.9-9.11 show the results of the piloted evaluation using the classical controller tested under the ELAL flight 1862 scenario. The classical controller was tested by the experienced pilots to give them some ‘feel’ and an idea of the severity of the actual ELAL scenario. The classical controller makes the pilot appreciate the controllability challenges and difficulties experienced during the failure, especially when compared to the FTC schemes.

Figure 9.8 shows an example of the flight trajectory of the piloted classical controller in the ELAL 1862 scenario. After the failure, the aircraft is still able to do right turns. Only during the final stage of the test flight does the aircraft lose control and crash before being able to line up with the runway.

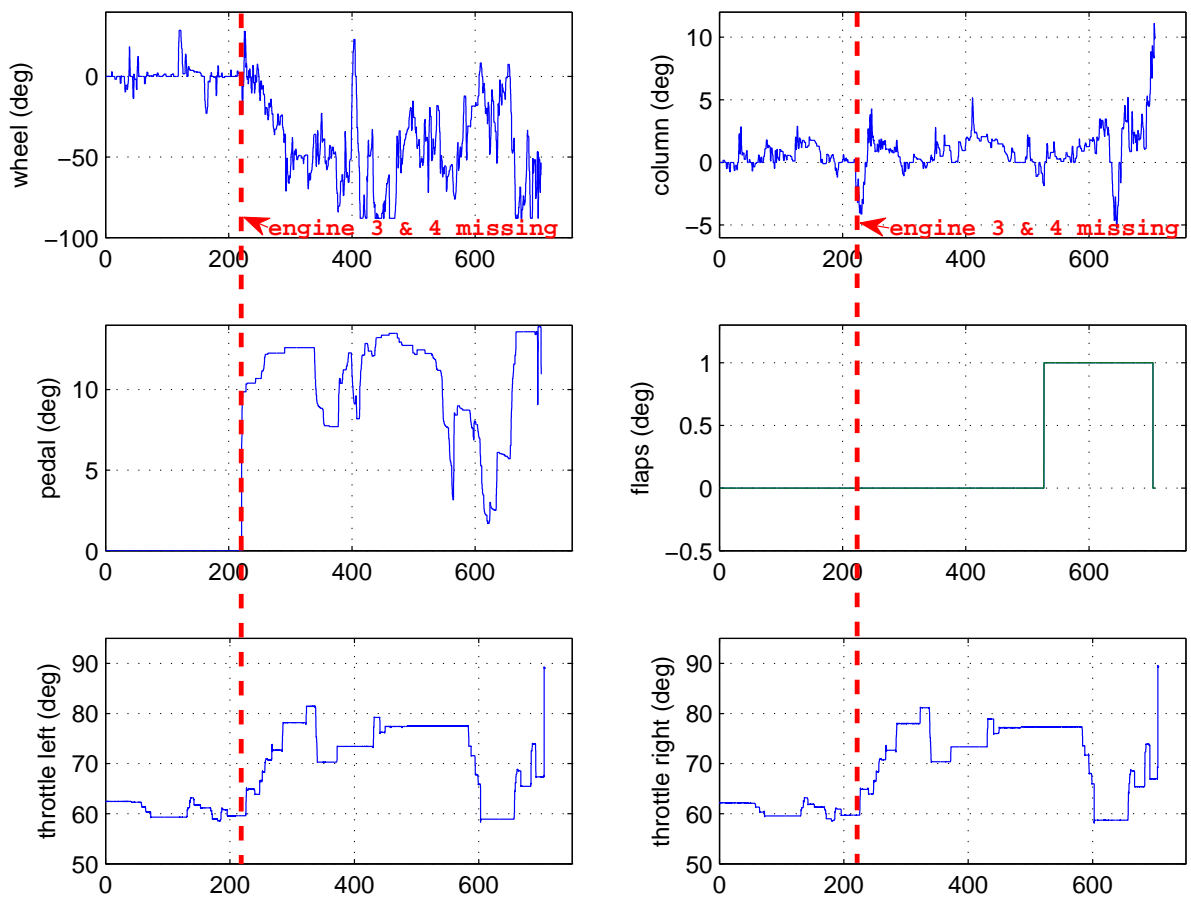


Figure 9.9: ELAL 1862 scenario: classical controller: pilot deflection

The results shown in Figures 9.9-9.11 have been carried out with the heavy trim weight. Figure 9.9 shows the pilot control deflections. As described in Section 9.3 above, and in the incident studies in [2,152], similar patterns appear. Immediately after the failure, the deflection of wheel, column and pedal increase in magnitude. As in the ELAL 1862 flight, almost maximum wheel deflection to the left to counter the right turn is visible. Also visible is the pedal deflection to counteract the yawing moment of the asymmetric thrust. Figure 9.9 also shows that near to the final stages of the test, a flap setting of 1deg is selected to prepare for landing. At about 600 sec, the power lever angle (throttle) is also reduced for landing. However, when the speed reaches 110 m/s (approx 220 Kn) near 700sec (Figure 9.10), the aircraft becomes hard to control and banks to the right. Figure 9.9 shows that maximum left pilot wheel deflection is applied. Still

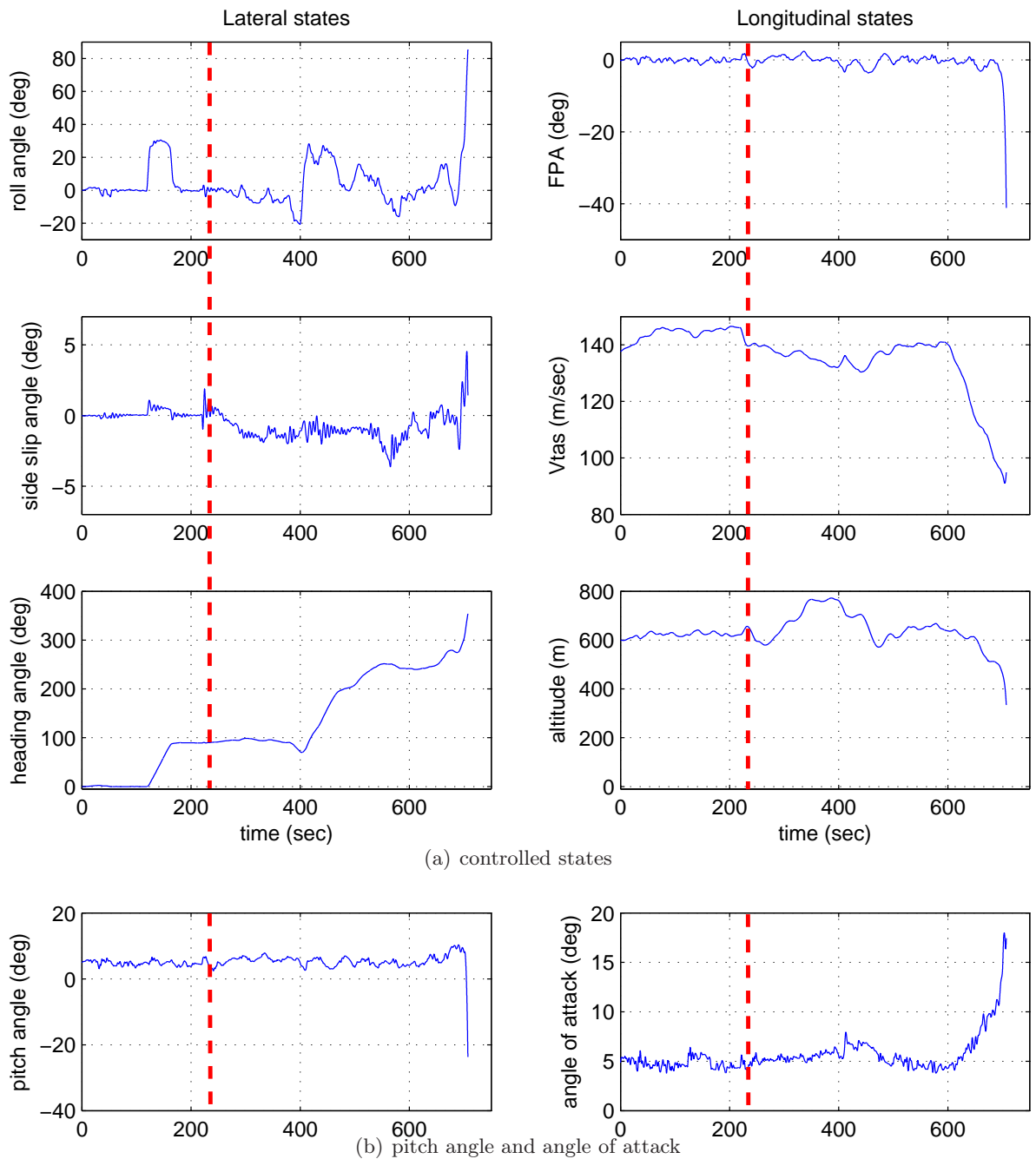


Figure 9.10: ELAL 1862 scenario: classical controller: states

unable to recover from the right bank, the flap is returned to a zero degree setting, and the throttle input is increased in order to regain control. However the aircraft still rolls to the right and loses altitude and speed. The loss of altitude and FPA tries to be compensated for by the high positive (pull towards the pilot) column deflection. At this stage, all control is lost and the aircraft rolls at almost 80deg right with the FPA nearing -40deg and the pitch angle passing -20deg. This is similar to what is described in the incident report in [2] when the ELAL 1862 aircraft hit the apartment building in Bijlmermeer, Amsterdam.

Analyzing the plots further, it can be seen that when the throttle is reduced in preparation for landing, the speed becomes low, and during descent, the angle of attack becomes high. As discussed in Section 9.3.1 and in [2, 152, 188, 190], the increase in the angle of attack causes high

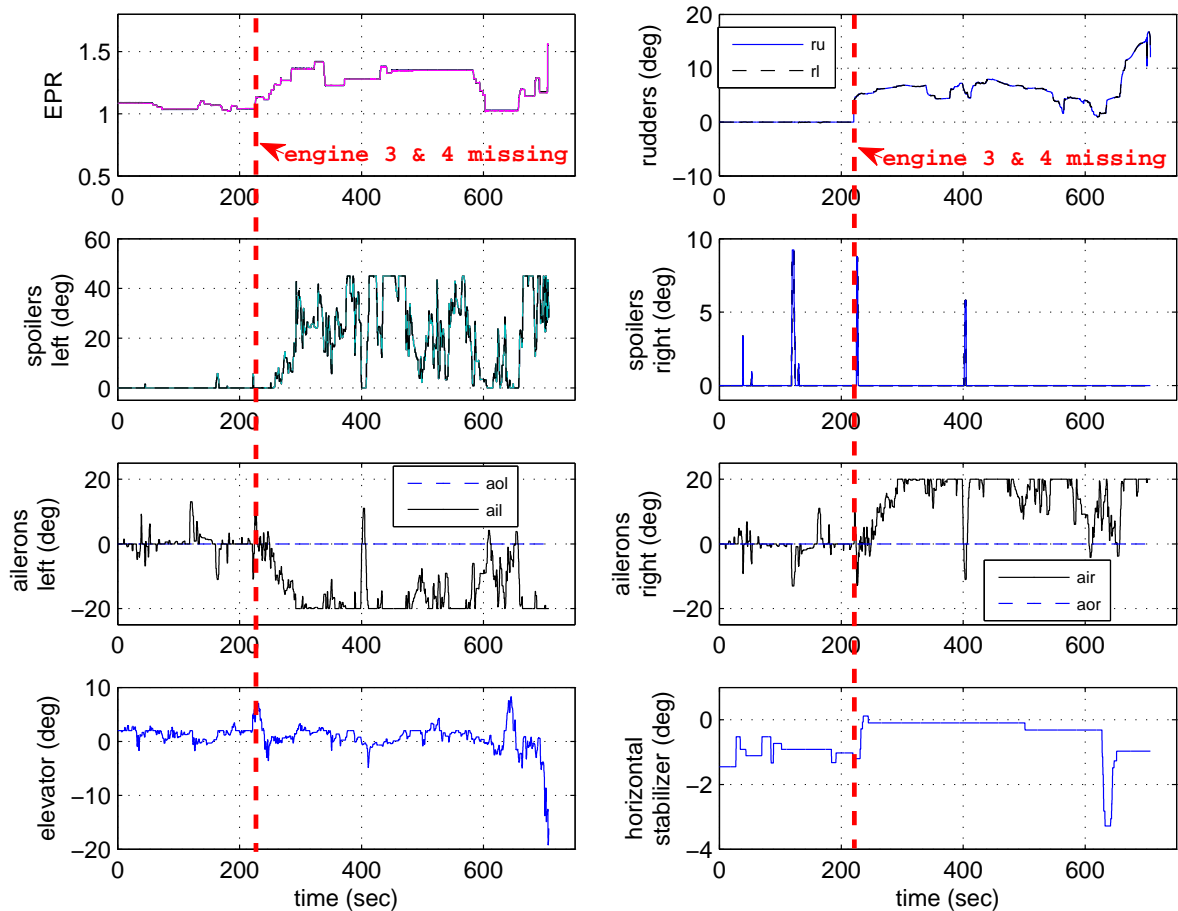


Figure 9.11: ELAL 1862 scenario: classical controller: control surfaces deflection

flow separation and turbulence behind the damaged right wing leading edge, resulting in the loss of lift and high drag (compared to the left wing). This increases the rolling and yawing moment to the right which results in a further drop in altitude and speed.

Figure 9.11 shows the control surface deflections of the classical controller. One major feature of the classical controller is that most of the control surfaces are mechanically linked. For example, the outer ailerons on the left and right wing is only fully active when a flap setting of more than 5deg is used [91,92]. This can be seen in Figure 9.11, where the outboard aileron is inactive throughout the flight test. The high deflection of the left aileron and spoilers up to the saturation limits (-20deg for the aileron and 40deg for the spoiler) after the engine failure shows that there is limited control even at a speed of 130-140kn. Note that a positive deflection for ailerons is a deflection down, and for the spoilers, positive is deflected up [91,92]. The high deflections of the control surfaces on the left wing compensate for the loss of efficiency of the right inboard aileron and the remaining spoilers (10 and 11), and for the higher drag and loss of lift due to flow separation/turbulence caused by the damage to the leading edge of the right wing. This is also due to the fact that there is no direct authority to the outer ailerons due to mechanical linkages preventing the outboard aileron being functional in the classical controller setup [91,92]. (This is one of the motivations for fly by wire (FBW) aircraft control). Figure 9.11 shows that the aileron deflections are most of the time at the saturation limits after the loss of engine 3 and 4 in order to obtain straight and level flight, and therefore most of the roll manoeuvre capability is assisted by the spoiler deflections. Shortly after the reduction in speed

i.e. approximately after 600sec, the left aileron and spoilers saturate again, but due to the lower speed and higher angle of attack, the control surface deflections are insufficient to regain control as the aircraft has gone beyond the capability of the control surfaces to provide enough controllability and performance. Note that the general control surface deflections and behaviour in Figures 9.9-9.11 closely follow the findings of the actual ELAL 1862 incident reported in [2].

Figure 9.8 shows the flight trajectory of the test. Three different trajectories are shown; the ELAL 1862 scenario with classical and SMC controllers and one with the SMC without any failure. With the classical controller, the pilot manages to maintain some performance and managed two banking turn manoeuvres. During the preparation for landing and capture of the localizer, the aircraft loses control and the simulation was stopped. The other two trajectories associated with safe landings by the SMC controller will be discussed in the next section.

9.6.2 SMC controller

As described in the last section, Figure 9.8 shows two trajectories of flight tests using the SMC. The fault-free test of the SMC is to give the pilot the feel of the capability of the controller in the nominal condition. Initially the aircraft was flown straight and level, before a heading change of 90deg to the east was performed. The pilot tested the aircraft's capability to climb to a pre-specified altitude from 600m altitude to approximately 800m. Then the pilot commands a return to an altitude of 600m and performs another right turn to capture the LOC. At this stage, the pilot 'arms' the APP in order to prepare for an automated landing approach. Once the aircraft captures the LOC signal, a final turn towards the centre-line of Runway 27 is started, and after a while, the GS signal is captured and the aircraft descends towards the runway at around a 3deg glide slope. Note that starting from the moment the pilot activates the APP button in the MCP and the LOC signal has been captured, the aircraft is in a fully automated landing mode and no other pilot input is required.

Note that as discussed in Section 9.4, the controller has been designed based on a linearization obtained around an operating condition of 263,000 Kg, 92.6 m/s true airspeed, and an altitude of 600m at 25.6% of maximum thrust and at a 20deg flap position. The actual pilot test was performed at 317,000Kg, a speed of 133.8m/s and a flap setting of 1deg. The test was done at a different trim condition to allow the pilot to rigorously test the controller and access the controller performance under different operating conditions. Also note that the B747 aircraft setup in the GARTEUR AG16 program using the FTLAB747 software, has been modified to include a state of the art fly by wire capability, 'removing' mechanical links and locks from the classical B747 configuration. This allows more flexibility in the control strategy exploiting independent control of all available surfaces thus increasing the ways redundant control surfaces can be used to achieve fault tolerant control.

Figure 9.8 also shows the trajectory of the SMC controller tested with the ELAL 1862 failure scenario. The same controller as that used in the nominal fault-free case is applied. In general, the controller performs the same right turn manoeuvres, LOC and GS intercept and lands on Runway 27. The SMC with the ELAL 1862 failure manages to bring the aircraft near to landing on the desired runway. Figure 9.12 shows the controlled states of the damaged aircraft with the SMC controller. Note at the beginning of the simulation, before the failure occurs at around

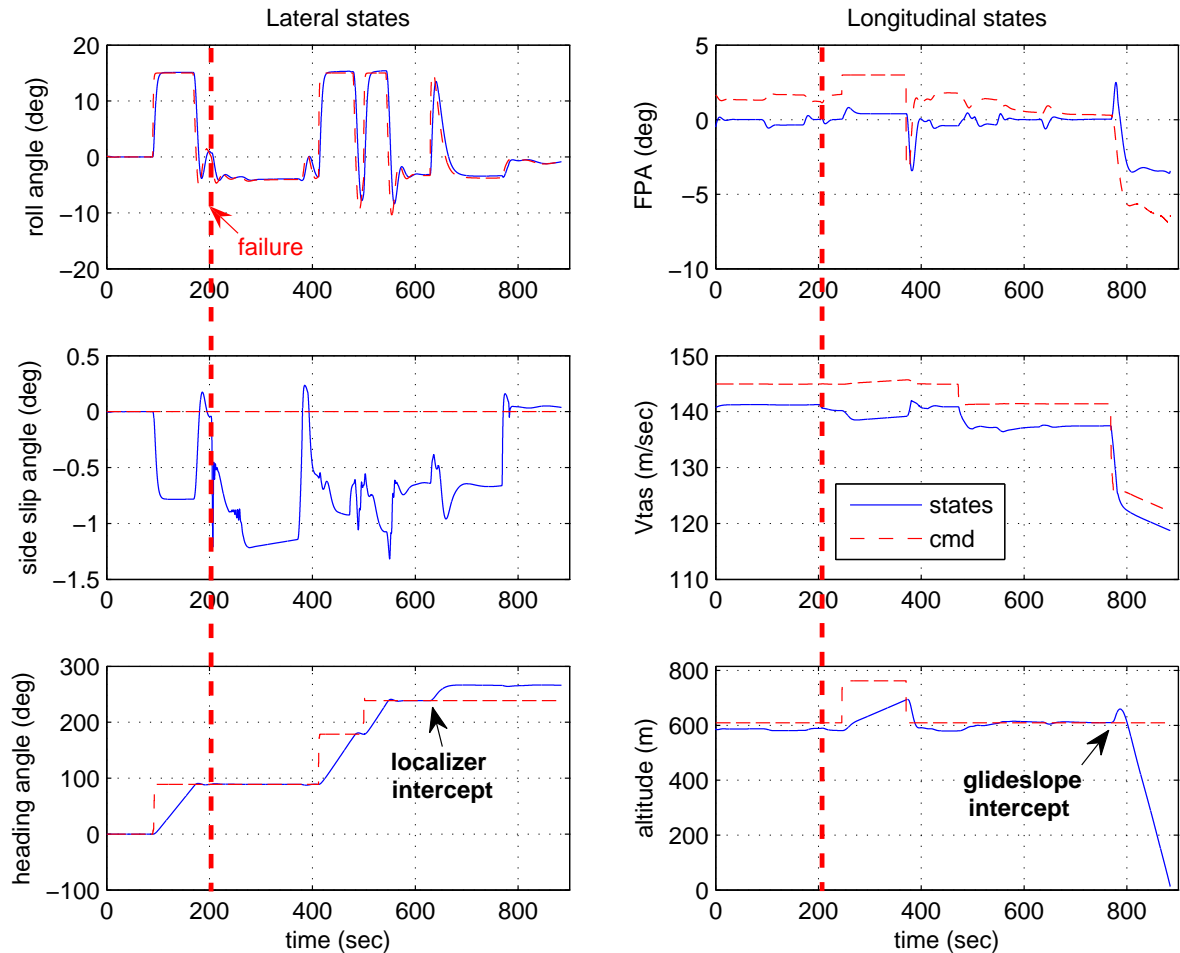


Figure 9.12: ELAL 1862 scenario: SMC controller: controlled states

200sec, the FPA, Vtas and altitude show small steady state errors due to the mismatch between the designed trim conditions and the test conditions as described earlier. This is due to the absence of integrators in the main SMC controller. The mismatch between the designed and test trim conditions demonstrate the controller coping with uncertainty and allows the pilot to rigorously test the controller outside its ‘comfort zone’.

Figure 9.12 shows that after the failure occurs, at approximately 200sec, the climb capability of the aircraft is slightly degraded when the pilot requests an increase in altitude to 800m (from 600m). On the other hand, the more important descent capability of the SMC controller is not degraded as it is able to follow the glide slope of 3deg towards the runway. This is shown in Figure 9.13. The glide slope error is maintained below 0.5deg. Figure 9.12 also shows that the side slip angle of the damaged aircraft has been maintained in the interval (0.5,-1.5) deg which is an improvement on the classical controller in Figure 9.12. Heading changes of the damaged aircraft with the SMC controller in Figure 9.12 also show a more systematic and higher level of performance of the controller – even when subjected to the ELAL 1862 failures. This shows that the lateral controller is able to deal with the asymmetric change in CG, weight and the asymmetric thrust conditions, and maintains the desired change in heading. Decreasing the speed to approximately 120m/s does not have the devastating and unstable effect seen in the classical controller. In fact, as suggested in [2, 152], reducing the speed helps in terms of lateral control. This is seen in terms of the deviation of the side slip angle in Figure 9.12. The side

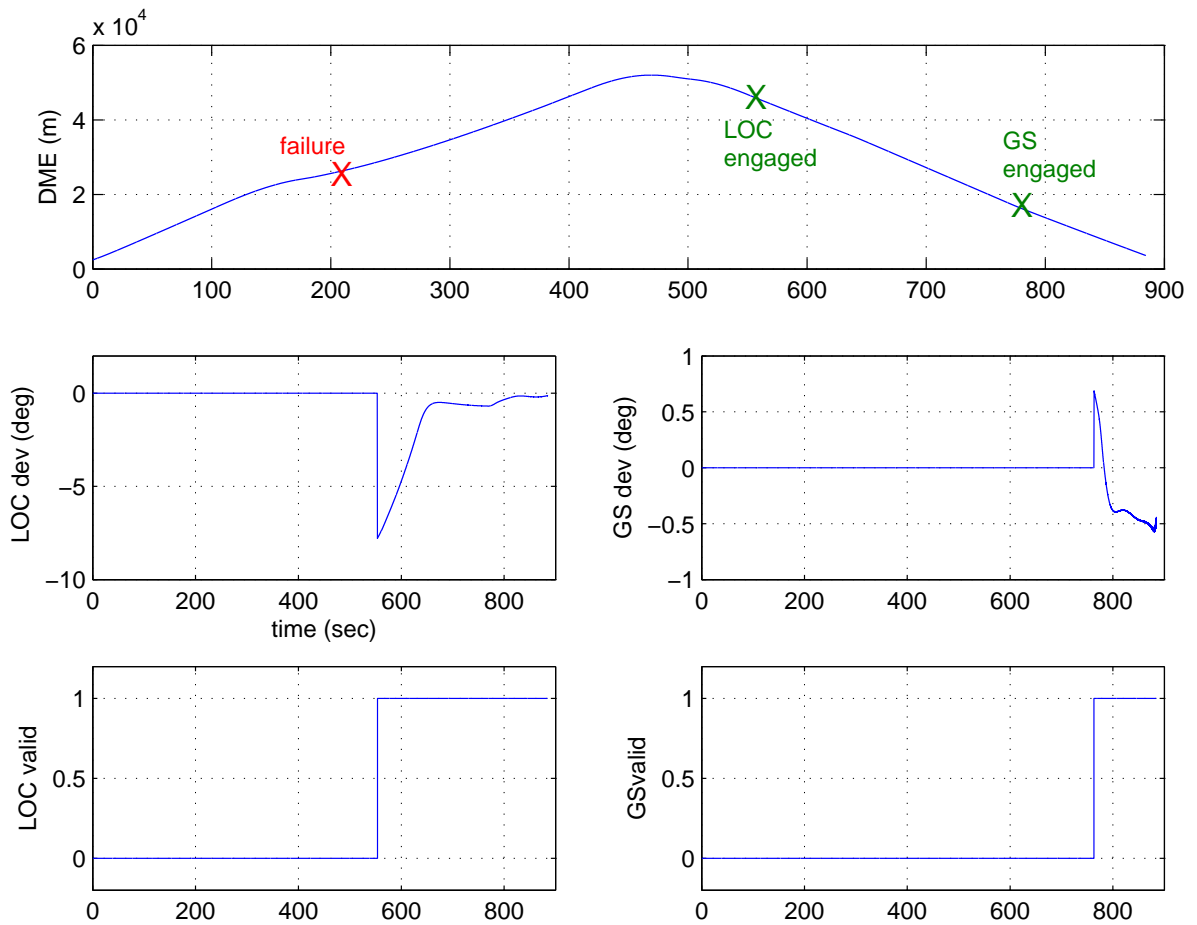


Figure 9.13: ELAL 1862 scenario: SMC controller: LOC and GS deviation angle

slip angle is much smaller than at higher speed after the failure has occurred. The roll angle tracking again shows good performance even after the loss of the engines and the hydraulics associated with the ELAL 1862 scenario.

Figure 9.13 shows the signals from the ILS sensors. It represents the DME , LOC & GS deviation and the moment when the LOC and the GS is engaged (valid/engaged) after being ‘armed’ using the APP button in the MCP. As usual, the LOC is engaged before the GS. The LOC coverage is much further than the GS and this allows the aircraft to be aligned to the extended centre–line of the runway before following the specified 3deg glide slope descent.

Figure 9.14 shows the control surface deflections under the ELAL 1862 scenario. This figure highlights the major difference between the classical controller (which is mechanically linked) and the FBW aircraft that has been provided by the GARTEUR AG16 modification [190]. In this figure, the outer ailerons can be seen to be independently mobile before the occurrence of the failure. After the failure, the outer ailerons (left and right) ‘float’ due to the loss of hydraulic systems 3 and 4. Independent control can also be seen in the spoilers, elevators, rudders and EPR. The effect of losing the hydraulic system can also be seen in the floating of the inner left and outer right elevators (see Figure 9.14) where a clear distinction between the control surface deflection can also be seen. The spoilers also show similar patterns. Before the loss of engines 3 and 4, all the spoilers seem to be moving independently; and when the failure occurs, only spoilers 2,3,10 and 11 are active, the rest remain at zero deflection. In

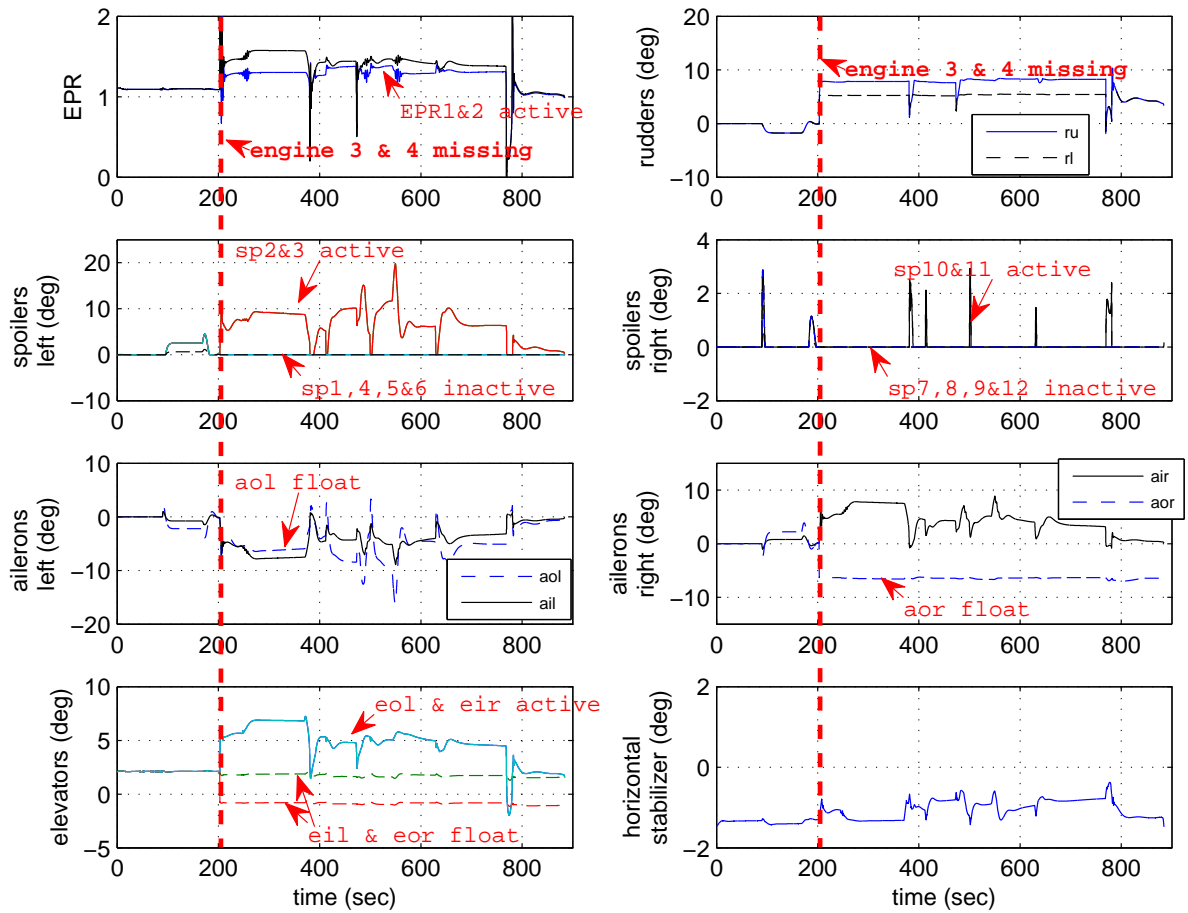


Figure 9.14: ELAL 1862 scenario: SMC controller: control surfaces deflection

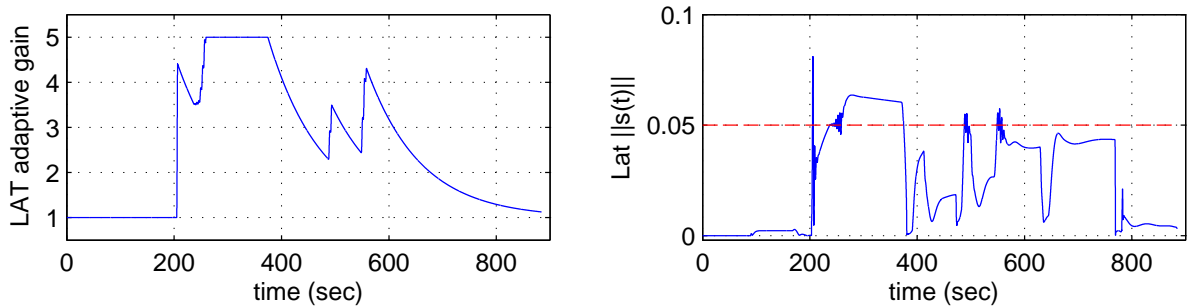


Figure 9.15: ELAL 1862 scenario: SMC controller: lateral adaptive gain

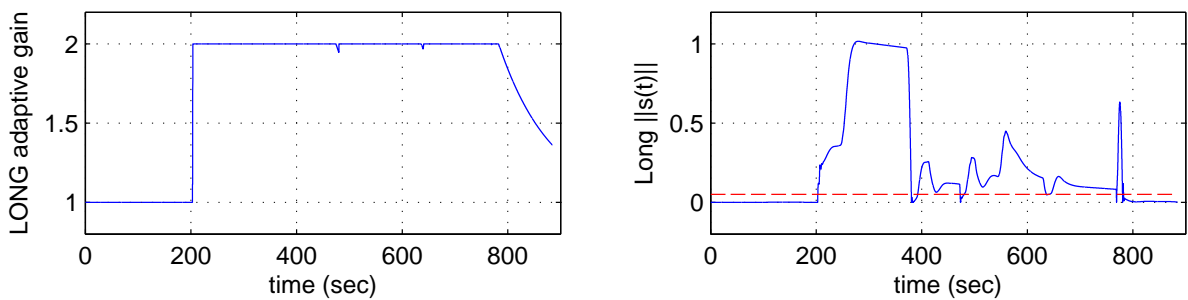


Figure 9.16: ELAL 1862 scenario: SMC controller: longitudinal adaptive gain

general, the control surface deflections of the elevators, ailerons and spoilers are almost half of the ones using the classical controller (see Figure 9.14). The control surface deflections from the SMC controller do not reach the saturation limits of the surfaces and the spoilers and the ailerons, are generally less aggressive. Engine EPR shows that differential thrust has been used to achieve the desired performance, obtain a small side slip angle and roll angle. Note that all the surfaces are controlled independently by the CA SMC scheme. The pilot input only comes from supplying the higher level commands such as heading and altitude change (or roll or FPA commands through the MCP panel). This reduces the pilot's workload compared to the classical controller where the demand is high.

Figure 9.15 and 9.16 show the adaptive gain and the associated $\|s(t)\|$ signals that initiate the gain adaptation. Before the occurrences of the failure, the sliding signal $s(t)$ is below the selected threshold. Once the threshold is exceeded, the gain is adapted from a minimum of 1 up to the maximum of 5, and 2 for the lateral and longitudinal axes respectively. High deviation from the sliding surface $s(t) = 0$ shows the severity of the faults (as discussed in Chapter 4). After the failure has occurred and during manoeuvres, the switching function plot $s(t)$ deviates away from the ideal sliding surface. However, during or near landing conditions, the switching function returns below the adaptation threshold, near to zero. During this time, the adaptive gain reduces to the minimum value of 1.

Although the SMC controller can be implemented in such a way that pilot inputs (such as column, wheel and pedal) can also be used, the purpose here is to show that, as a proof of concept, the SMC controller is more than able to handle all the rigorous tests and failures it is subjected to using the minimal amount of input from the pilot, thus lowering the workload during such an emergency condition. This will allow pilots to concentrate on higher level decisions.

Figure 9.17(a) is one of the SIMONA output alternative views and provides the aircraft position on the Netherlands map near Sciphol airport (and Amsterdam itself). This figure shows the actual SMC controller trajectory under the ELAL 1862 failure. The overall trajectory shows that the aircraft manages to reach Runway 27. A zoom of the overall trajectory near the runway (Figure 9.17(b)) shows that the SMC controller manages to reach the desired landing position – although slightly out to the right of the runway. Finally Figure 9.18 shows the actual pilot's view inside the SIMONA cockpit near to landing.

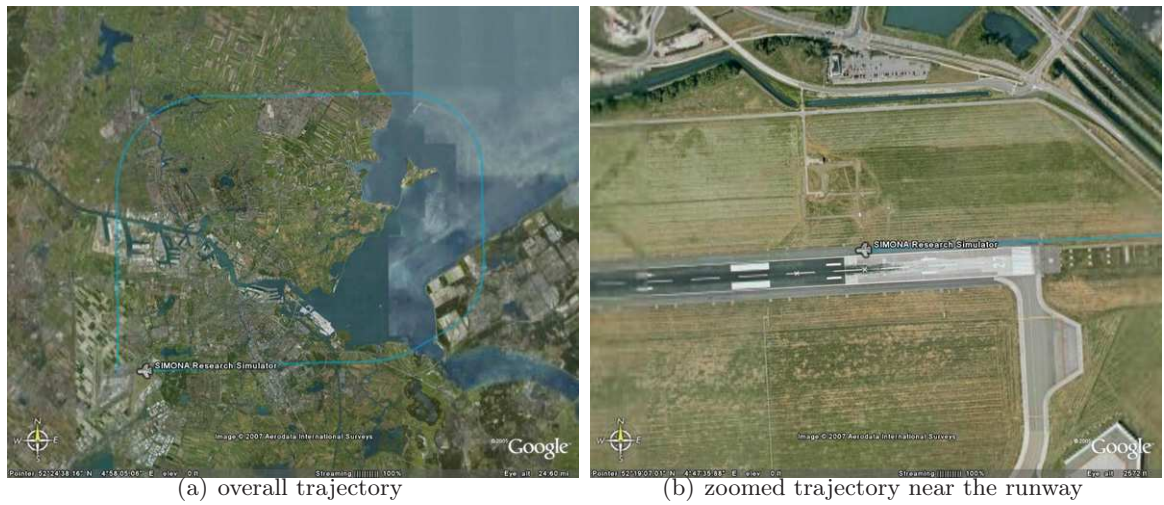


Figure 9.17: SIMONA flight trajectory of ELAL 1862 scenario with model reference SMC controller with control allocation with pilot Arun Karwal.

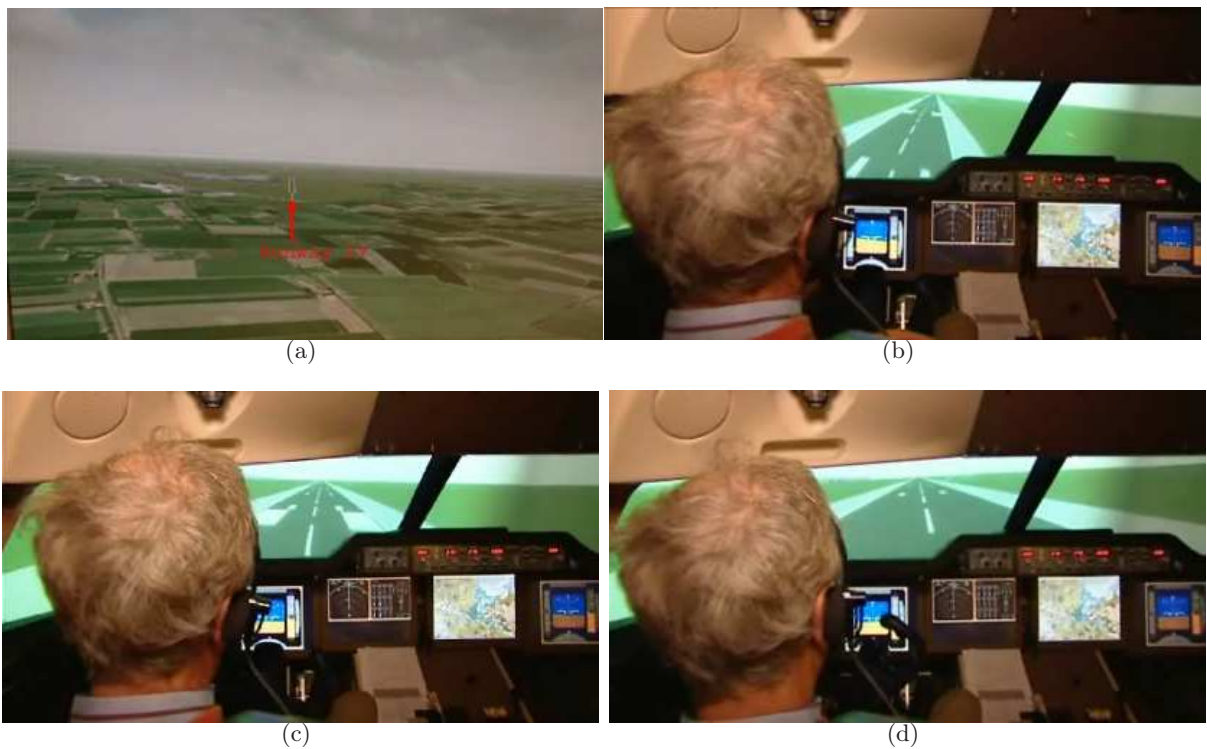


Figure 9.18: Pilot view inside SIMONA during landing manoeuvre (snapshot taken from video courtesy of RTL news, the Netherlands and International Research Institute SIMONA, Delft University of Technology, the Netherlands.)

9.7 Conclusions

This chapter has presented piloted flight simulator results associated with the ELAL flight 1862 (Bijlmermeer incident) scenario which is one of the case studies of the GARTEUR action group AG16. The results represent the successful implementation of a FTC SMC controller on the SIMONA 6-DOF flight simulator configured to represent a B747 with pilots flying and testing the controller. Results from the classical controller show the same behavior as witnessed in the investigation reports, indicating the high fidelity and capability of the nonlinear model to reproduce the performance of the damaged aircraft before the crash. The results from the proposed SMC controller show that the control surface deflections are also much lower than that of the classical controller. A significant reduction in the pilot's workload, especially with the implementation of the ILS landing approach, is also shown from the SMC controller tests. The comments and feedback from the experienced pilots after the rigorous simulator flight test show that the proposed SMC scheme has the ability to help pilots to land the aircraft safely on the designated runway. The application of the proposed controller under the assumption that no information about the aircraft's damage is available, coupled with automatic landing using the ILS is, in the author's opinion, probably the most realistic and rigorously tested controller used in FTC studies on the ELAL flight 1862 incident.

Chapter 10

Conclusions and Future Work

10.1 Conclusions

Chapter 4 has highlighted the benefits and abilities of sliding mode controllers to achieve FTC without requiring FDI. The application of a novel SMC controller on a high fidelity model of a B747 aircraft shows that the proposed scheme can handle actuator faults without requiring controller reconfiguration. The gain associated with the nonlinear component of the SMC controller is allowed to be adaptively increased when there is unexpected deviation of the switching variable from its nominal condition. This deviation and its size has been used in a sense to ‘measure’ the level of actuator performance degradation and triggers an increase in gain – depending on the severity of the fault. A predefined maximum gain has been used to declare a total failure of the actuator and to initiate a switch to the backup control surface. Another major contribution in this chapter, apart from the use of adaptive gains, is the use of LMIs to design the sliding surface in order to minimize the effect of the occurrence of a failure to the primary actuator before a change over to the redundant one.

Chapter 5 has focussed on one of the aspects of fault tolerance which has generally received less attention in the literature – sensor fault tolerant control. This chapter has implemented a recently developed robust fault estimation scheme based on a SMC observer. The contribution of this chapter is that the fault estimation capability of the SMC observer has been used to achieve sensor fault tolerant control using the high fidelity nonlinear model of the B747. This is probably the most challenging and realistic scenario this fault reconstruction scheme has been tested on. Another contribution is a rigorous analysis of the closed-loop stability of the system when driven by the fault estimate.

Chapter 6 described one of the major breakthroughs in terms of the subsequent work and chapters in this thesis, and leads to the ultimate implementation of an SMC FTC scheme on the SIMONA flight simulator in Chapter 7 and 9. Motivated by the challenge to cope with emergency situations such as the ELAL 1862 scenario, and building on ideas given in Chapter 4, the combination of sliding mode control with control allocation has provided a way for SMC to gain access to redundant actuators. This idea has shed some light in terms of solving one of the drawbacks of SMC; from FTC perspective – namely its inability to directly handle total actuator failures. The combination of SMC and CA has been shown to have great potential

for FTC. This new combination paves the way for a simple, yet effective way of redistributing control signals to the healthy actuators when failures occur. The control allocation idea used in this chapter is also quite different to other control allocation schemes in the literature. The control allocation strategy proposed in this chapter is based on the health level (or effectiveness level) of the actuators. Information about the actuator effectiveness is supplied by a sliding mode fault reconstruction algorithm. A rigorous stability analysis has been performed. The nonlinear gain required to maintain sliding for the combined SMC and CA scheme (which is lacking in the current literature) has also been provided in this chapter. In the event of a fault or failure or combination of both, the designed sliding surface is guaranteed to be stable if it satisfies certain conditions given in Proposition 3 in Chapter 6. This design procedure is simple as it uses existing sliding surface design methods which guarantee stability for the nominal no fault condition. The work described in the chapter shows stability guarantees can be ‘extended’ to fault or failure cases when the conditions in Proposition 3 are satisfied. The procedure for designing the sliding surface for the nominal no fault condition and checking for extended stability for the fault or failure case, is well suited for aircraft systems.

Chapter 7 describes the implementation of the proposed schemes from Chapter 6 on a 6-DOF motion flight simulator called SIMONA based at Delft University of Technology. The controller has been designed for both the longitudinal and lateral (with directional) axes. The results from this chapter show that the proposed SMC controller has the ability to run in realtime and without any chattering problem. The controller was tested on single actuator failure scenarios such as jams with offset, and runaway/hardover failures on primary control surfaces such as the elevators, ailerons and rudders, as well as the horizontal stabilizer.

Chapter 8 provides an alternative FTC tracking framework using a combination of model reference SMC and CA. This is based on the inherent ability and flexibility of using model reference tracking for FTC. The model reference framework is free from integrator windup which could occur during a fault/failure. Chapter 8 also includes adaptive schemes. A similar adaptive gain to the one discussed in Chapter 4 has been considered and analyzed in terms of the combination of SMC, CA and model reference. Chapter 8 also analyzes and tests typical fixed control allocation structures with equal distribution of the control signal. This fixed control allocation structure is different from the online control allocation which is proposed in Chapters 6 and 7 which is based on the ‘health’ level of the actuator. The fixed CA structures considered in Chapter 8 remove the dependency of the controller from any FDI scheme to estimate or declare that a total failure has occurred. This independence of the SMC controller from any FDI, and the fact that controller reconfiguration is not required, even in the event of actuator failures, is one of the major benefits of SMC. The proposed SMC schemes can directly handle faults and total failures of actuators without requiring any FDI or controller reconfiguration.

Chapter 9 describes the results associated with one of the major objectives of the work in this thesis: to be able to create a controller capable of landing the crippled ELAL flight 1862 aircraft which lost two engines and suffered from high drag and loss of lift due to damage on the leading edge of the right wing. The actual ELAL 1862 aircraft crashed in Bijlmermeer, Amsterdam when preparing for landing. The results in Chapter 9 represent the successful implementation of an FTC SMC controller in real time on the SIMONA 6-DOF flight simulator obtained from the controller evaluation campaign during the final workshop of GARTEUR AG16. The controller

was evaluated by pilots with experience of flying B747, B767, A330 and Citation II aircraft. The controller used in Chapter 9 for the ELAL 1862 scenario evaluation, is based on the model reference scheme proposed in Chapter 8. The idea of using the fixed and equal control allocation scheme (which does not use the health condition of the actuators) replicates the condition faced by the crew of ELAL 1862 who remained unaware of the loss of the two engines, and the extent of the damage it caused on the wing resulting in the loss of several control surfaces due to the loss of hydraulic systems 3 and 4. The results show that the proposed controller significantly reduced the workload of the pilot in such an emergency situation compared to the classical controller. The aircraft is also shown to be able to land using a typical ILS landing procedure which guides the aircraft to the runway without requiring further input from the pilot, thus allowing the pilot to take higher level decisions and monitor the performance of the controller.

10.2 Future work

In Chapter 5, some theoretical analysis of the effect of the fault estimation schemes on the performance of the controller has been discussed. Future work should include development of a sliding surface design method which takes into account the effect of imperfect sensor fault reconstruction. Ideally this would allow the controller to reject the effect of imperfections in the fault reconstruction.

Another avenue which can be explored is the inclusion of uncertainty in the analysis and design of the sliding mode control allocation schemes presented in Chapters 6 and 8. The inclusion of uncertainty can represent the effect of jams or runaway actuators, or changes of operating condition, or damage to the airframe after a failure. The inclusion of uncertainty will be challenging in terms of providing proofs of stability and for the design of the sliding surface. Different and alternative design strategies are required in order to obtain a sliding surface design which is robust and can reject the effect of this uncertainty.

Chapter 6 is based on the analysis of ‘extended’ stability of the nominal sliding surface design in the event of faults or failures by ensuring the conditions given in Proposition 3 are satisfied. Even though the sliding surface design is simple due to the use of ‘classical’ sliding surface design ideas, a more ‘sleek’ way of design would be to include the requirements of Proposition 3 ‘inside’ the design process.

Other potential future work is to look into a full nonlinear SMC controller for the aircraft. This is motivated by the fact that the aircraft operating condition is ever changing even without fault or failures. The use of a nonlinear control method such as dynamic inversion uses knowledge of the aircraft model and aerodynamics to cope with changes in operating condition. A full nonlinear control strategy will also remove the dependency and requirement of designing multiple linear controllers and scheduling them throughout the operating condition. The use of SMC within a full nonlinear controller, together with CA, seems to be promising for the purpose of creating a flight controller that not only can handle changes in operating conditions, but also faults, failures and airframe damage.

Nomenclature and Abbreviations

Nomenclature

$\ \cdot\ $	Euclidean norm (vectors) or induced spectral norm (matrices)
α, β	angle of attack and sideslip angle (rad)
$\bar{\lambda}(\cdot), \underline{\lambda}(\cdot)$	largest and smallest eigenvalues
$\nu(t)$	virtual control input and pseudo control
ϕ, θ, ψ	roll, pitch and yaw angle (rad)
\mathbb{R}, \mathbb{R}_+	field of real numbers and the set of strictly positive real numbers
s	Laplace variable
$\mathcal{N}(A)$	null space of the matrix A
$\mathcal{R}(A)$	range space of the matrix A
h_e, x_e, y_e	geometric earth position along the z (altitude), x and y axis (m)
p, q, r	roll, pitch and yaw rate (rad/sec)
V_{tas}	true air speed (m/s)
<i>Subscripts</i>	
<i>lat</i>	lateral axis
<i>long</i>	longitudinal axis
<i>max</i>	maximum

Abbreviations

<i>air, ail, aor, aol</i>	inner right, inner left, outer right and outer left ailerons
<i>cmd</i>	command signal
<i>EPR</i>	Engine Pressure Ratio
<i>ru, rl</i>	upper and lower rudders
<i>sp</i>	spoiler
V_{mca}	air minimum control speed
6-DOF	6 Degree of Freedom
ATC	Air Traffic Controller (airport control tower)
CA	Control Allocation
CFIT	Controlled Flight Into Terrain
CG	Centre of Gravity
DFDR	Digital Flight Data Recorder

DI	Dynamic Inversion
DME	Distance Measuring Equipment
FBW	Fly By Wire
FDI	Fault Detection and Isolation
FPA	flight Path Angle
FTC	Fault Tolerant Control
GARTEUR	Group for Aeronautical Research and Technology in Europe
GS	Glide Slope
IAS	Indicated Airspeed
ILS	Instrument Landing System
IMM	Interactive Multiple Model
KIAS	Indicated Air Speed in Knots
KLM	Royal Dutch Airlines
LMI	Linear Matrix Inequality
LOC	Localizer Capture
LPV	Linear Parameter Varying
LTI/LTV	Linear Time Invariant/Variant
MAC	Mean Aerodynamic Chord
MCT	Maximum Continuous Thrust
MMST	Multiple Model Switching and Tuning
MPC	Model Predictive Control
MRAC	Model Reference Adaptive Control
NLR	National Aerospace Laboratory, the Netherlands
PIM	Pseudo Inverse Method
ROV	Remote Operating Vehicle
s.p.d.	symmetric positive definite
SIMONA	Simulation, Motion and Navigation (6-DOF flight simulator in Delft University of Technology, the Netherlands)
SMC	Sliding Mode Control
TAS	True Airspeed
VOR	VHF Omni-directional Radio Range

Author's Biography

Halim Alwi was born in Klang, Malaysia. After completing his secondary school education in the Royal Military College, Kuala Lumpur, Malaysia in 1995, he studied at the University of Leicester (England) and graduated in 2000 with a B.Eng. (Hons) degree in Mechanical Engineering. From 2000 to 2004 he was an engineer at The New Straits Times Press, Malaysia where he was involved in the installation and commissioning of a new automated system for the mailroom, as well as overseeing maintenance of mailroom machines. In 2004 he moved back to the University of Leicester as a Ph.D. student under an EPSRC grant, and was awarded a Ph.D. in 2008. He is currently working as a Research Associate with the Control & Instrumentation Research Group at the Department of Engineering, University of Leicester.

List of publications

Conference publication:

1. H. Alwi and C. Edwards. Fault Tolerant Control of a Civil Aircraft Using a Sliding Mode Based Scheme. *44th IEEE Conference on Decision and Control*, 2005.
2. H. Alwi and C. Edwards. Robust Sensor Fault Estimation for Fault Tolerant Control of a Civil Aircraft Using Sliding Modes. *American Control Conference*, 2006.
3. H. Alwi and C. Edwards. Fault tolerant control of a civil aircraft using sliding modes. *6th IFAC Symposium on Fault Detection and Safety of Technical Process*, 2006.
4. H. Alwi and C. Edwards. Sliding mode FTC with on-line control allocation. *45th IEEE Conference on Decision and Control*, 2006.
5. H. Alwi and C. Edwards. Application of Fault Tolerant Control Using Sliding Modes With On-line Control Allocation on a Large Civil Aircraft. *16th IEEE Conference on Control Applications*, 2007.
6. H. Alwi and C. Edwards. Model Reference Sliding Mode FTC with On-line Control Allocation. *46th IEEE Conference on Decision and Control*, 2007.
7. H. Alwi and C. Edwards, O. Stroosma and J.A. Mulder, SIMONA Flight Simulator Implementation of a Fault Tolerant Sliding Mode Scheme with On-line Control Allocation, *American Control Conference*, 2008.
8. H. Alwi, C. Edwards and C.P. Tan. Sliding Mode Estimation Schemes for Unstable Systems Subject to Incipient Sensor Faults, *American Control Conference*, 2008.
9. H. Alwi, C. Edwards, O. Stroosma and J.A. Mulder. Piloted Sliding Mode FTC Simulator Evaluation for the ELAL Flight 1862 Incident, *AIAA Guidance, Navigation, and Control Conference*, 2008.

Journal publication:

1. H. Alwi and C. Edwards. Fault detection and fault-tolerant control of a civil aircraft using a sliding-mode-based scheme. *IEEE Transactions on Control Systems Technology*, 16(3):499-510, 2008.
2. H. Alwi and C. Edwards. Fault Tolerant Control Using Sliding Modes With on-line Control Allocation. Accepted in *Automatica*.
3. H. Alwi, C. Edwards, O. Stroosma and J.A. Mulder. On the Implementation of a Fault Tolerant Sliding Mode Scheme with Control Allocation on the SIMONA Research Flight Simulator, accepted in *AIAA journal of Guidance Control and Dynamics*.

Bibliography

- [1] . *Reliability, Availability, and Maintainability Dictionary*. ASQC Quality press, 1988.
- [2] . El al flight 1862, aircraft accident report 92-11. Technical report, Netherlands Aviation Safety Board, Hoofddorp, 1994.
- [3] . Uncontrolled descent and collision with terrain, USAIR flight 427, Boeing 737-300, N513AU, near Aliquippa, Pennsylvania September 8, 1994. Aircraft Accident Report NTSB/AAR-99-01, National Transportation Safety Board, 1994.
- [4] . Civil aviation safety data. Technical report, Civil Aviation Authority of the Netherlands (CAA-NL), 2003.
- [5] . In-flight upset; 240km NW Perth, WA; Boeing Co 777-200, 9M-MRG. Aviation Safety Investigation Report - Final 200503722, Australian Transport Safety Bureau, 2005.
- [6] . The transportation safety board of Canada issues safety recommendations to improve rudder inspections on Airbus aircraft. Communiqués TSB # A04/2006 A05F0047, Transportation Safety Board of Canada, 2006.
- [7] H. Alwi and C. Edwards. Fault tolerant control of a civil aircraft using a sliding mode based scheme. In *44th IEEE Conference on Decision and Control*, 2005.
- [8] H. Alwi and C. Edwards. Fault tolerant control of a large civil aircraft using a sliding mode based scheme. In *Proceedings of the IFAC Symposium SAFEPROCESS '06, Beijing*, 2006.
- [9] H. Alwi and C. Edwards. Robust sensor fault estimation for tolerant control of a civil aircraft using sliding modes. In *Silver Anniversary American Control Conference*, 2006.
- [10] H. Alwi and C. Edwards. Sliding mode FTC with on-line control allocation. In *45th IEEE Conference on Decision and Control*, 2006.
- [11] H. Alwi and C. Edwards. Application of fault tolerant control using sliding modes with on-line control allocation on a large civil aircraft. In *16th IEEE Conference on Control Applications*, 2007.
- [12] H. Alwi and C. Edwards. Model-reference sliding mode FTC with on-line control allocation. In *46th IEEE Conference on Decision and Control*, 2007.

- [13] H. Alwi and C. Edwards. Fault detection and fault-tolerant control of a civil aircraft using a sliding-mode-based scheme. *IEEE Transactions on Control Systems Technology*, 16(3):499–510, 2008.
- [14] H. Alwi, C. Edwards, O. Stroosma, and J.A. Mulder. Piloted sliding mode FTC simulator evaluation for the ELAL Flight 1862 incident. In *AIAA Guidance, Navigation, and Control Conference*, 2008.
- [15] H. Alwi, C. Edwards, O. Stroosma, and J.A. Mulder. SIMONA flight simulator implementation of a fault tolerant sliding mode scheme with control allocation. In *American Control Conference*, 2008.
- [16] Y.H. An. A design of fault tolerant flight control systems for sensor and actuator failures using on-line learning neural networks. Ph.D thesis, West Virginia University, 1998.
- [17] M.D. Anand, T. Selvaraj, S. Kumanan, and J. Janarthanan. A hybrid fuzzy logic artificial neural network algorithm-based fault detection and isolation for industrial robot manipulators. *International Journal of Manufacturing Research*, 2(3):279–302, 2007.
- [18] B.D.O. Anderson and J.B. Moore. *Optimal Control: Linear Quadratic Methods*. Prentice Hall International Edition, 1989.
- [19] J. Aravena, K. Zhou, X. R. Li, and F. Chowdhury. Fault tolerant safe flight controller bank. In *Proceedings of the IFAC Symposium SAFEPROCESS '06, Beijing*, 2006.
- [20] K. J. Åström and T. Hagglund. *PID Controllers: Theory, Design and Tuning*. Instrument Society of America, 1995.
- [21] K.J. Åström and B. Wittenmark. *Computer controlled systems : theory and design*. Prentice-Hall, Englewood Cliffs, N.J, 1984.
- [22] K.J. Åström and B. Wittenmark. *Adaptive Control*. Addison-Wesley, Reading MA., 1989.
- [23] G.J. Balas. Linear, parameter-varying control and its application to a turbofan engine. *International Journal of Robust and Nonlinear Control*, 12:763–796, 2002.
- [24] A. Balestrino, G. DeMaria, and A.S.I. Zinober. Nonlinear adaptive model-following control. *Automatica*, 20:559–568, 1984.
- [25] G. Bartolini and A. Ferrara. Real-time output derivative estimation by means of higher order sliding modes. In *Proceedings of the IMAC Multiconference CESA '98, Tunisia*, 1998.
- [26] R. E. Beck. *Application of Control Allocation Methods to Linear Systems with Four or More Objectives*. PhD thesis, Virginia Polytechnic Institute and State University, Blacksburg, Virginia, 2002.
- [27] M. Blanke, M. Kinnaert, J. Lunze, and M. Staroswiecki. *Diagnosis and Fault-Tolerant Control*. Springer, 2nd edition, 2006.
- [28] M. Blanke, M. Staroswiecki, and N.E. Wu. Concepts and methods in fault-tolerant control. In *Proceedings of the American Control Conference, Arlington*, pages 2606–2020, 2001.

- [29] C.D. Bocaniala and V. Palade. *Computational Intelligence Methodologies in Fault Diagnosis: Review and State of the Art*. Springer, 2006.
- [30] J. Bokor and G. Balas. Detection filter design for LPV systems - a geometric approach. *Automatica*, 40:511–518, 2004.
- [31] K.A. Bordignon and W.C. Durham. Closed-form solutions to constrained control allocation problem. *Journal of Guidance, Control, and Dynamics*, 18(5):1000–1007, 1995.
- [32] J. D. Bošković and R. K. Mehra. *Fault Diagnosis and Fault Tolerance for Mechatronic Systems: Recent Advances*, chapter Failure Detection, Identification and Reconfiguration in Flight Control. Springer-Verlag, 2002.
- [33] J.D. Bošković and R.K. Mehra. A multiple model-based reconfigurable flight control system design. In *Proceedings of the 37th IEEE Conference on Decision and Control*, pages 4503–8, 1998.
- [34] J.D. Bošković and R.K. Mehra. Control allocation in overactuated aircraft under position and rate limiting. In *Proceedings of the American Control Conference*, pages 791–796, 2002.
- [35] S.P. Boyd, L. El Ghaoui, E. Feron, and V. Balakrishnan. *Linear Matrix Inequalities in Systems and Control Theory*. SIAM: Philadelphia, 1994.
- [36] D. Brière, C. Favre, and P. Traverse. A family of fault-tolerant systems: electrical flight controls, from Airbus A320/330/340 to future military transport aircraft. *Microprocessors and Microsystems*, pages 75–82, 1995.
- [37] D. Brière and P. Traverse. Airbus A320/A330/A340 electrical flight controls: A family of fault-tolerant systems. *Digest of Papers FTCS-23 The Twenty-Third International Symposium on Fault-Tolerant Computing*, pages 616–623, 1993.
- [38] A. E. Bryson. *Control of spacecraft and aircraft*. Princeton University Press, 1994.
- [39] J. Buffington. Tailless aircraft control allocation. In *AIAA Guidance, Navigation and Control*, pages 737–747, 1997.
- [40] J. Buffington, P. Chandler, and M. Pachter. On-line system identification for aircraft with distributed control effectors. *International Journal of Robust and Nonlinear Control*, 9:1033–1049, 1999.
- [41] J.M. Buffington and D.F. Enns. Lyapunov stability analysis of daisy chain control allocation. *Journal of Guidance, Control, and Dynamics*, 19:1226–30, 1996.
- [42] F. W. Burcham, C. G. Fullertron, and T. A. Maine. Manual manipulation of engine throttles for emergency flight control. Technical Report NASA/TM-2004-212045, NASA, 2004.
- [43] F. W. Burcham, T. A. Maine, J. Kaneshinge, and J. Bull. Simulator evaluation of simplified propulsion-only emergency flight control system on transport aircraft. Technical Report NASA/TM-1999-206578, NASA, 1999.

- [44] F.W. Burcham, J. Burken, T.A. Maine, and J. Bull. Emergency flight control using only engine thrust and lateral center-of-gravity offset: A first look. Technical Memorandum NASA/TM-4789, NASA, 1997.
- [45] F.W. Burcham, T.A. Maine, J. Burken, and J. Bull. Using engine thrust for emergency flight control: MD-11 and B-747 results. Technical Memorandum NASA/TM-1998-206552, NASA, 1998.
- [46] J. Burken, J.W. Burcham, A.M. Trindel, J. Feather, S. Goldthorpe, and J.A. Kahler. Flight test of propulsion-based emergency control system on the MD-11 airplane with emphasis on the lateral axis. Technical Report NASA/TM-4746, NASA, 1996.
- [47] F. Caccavale and L. Villani. *Fault Diagnosis and Fault Tolerance for Mechatronic Systems: Recent Advances*. Springer, 2003.
- [48] P.J. Campo, M. Morari, and C.N. Nett. Multivariable anti-windup and bumpless-transfer. In *Proceedings of the American Control Conference*, pages 1706–1711, 1989.
- [49] J. Cattarius and D.J. Inman. Experimental verification of intelligent fault detection in rotor blades. *International Journal of Systems Science*, 31(11):1375–1379, 2000.
- [50] J. Chen and R.J. Patton. *Robust Model-Based Fault Diagnosis for Dynamic Systems*. Kluwer Academic Publishers, 1999.
- [51] W. Chen and J. Jiang. Fault-tolerant control against stuck actuator faults. *IEE Proc.-Control theory and applications*, 152:138–146, 2005.
- [52] H.H. Choi. A new method for variable structure control system design: a Linear Matrix Inequality approach. *Automatica*, 33:2089–2092, 1997.
- [53] Q.P. Chu, J.A. Mulder, and J.K. Sridhar. Decomposition of aircraft state and parameter estimation problems. In *System Identification (SYSID '94). A Postprint Volume from the IFAC Symposium*, 1995.
- [54] S.C.C. Chung and C.L. Lin. A transformed Lure problem for sliding mode control and chattering reduction. *IEEE Transactions on Automatic Control*, 44:563–568, 1999.
- [55] M.L. Corradini, G. Orlando, and G. Parlangeli. A fault tolerant sliding mode controller for accommodating actuator failures. In *44th IEEE Conference on Decision and Control*, 2005.
- [56] J. P. V. S. Cunha, R.R. Costa, and L. Hsu. Cooperative actuators for fault tolerant model-reference sliding mode control. In *IEEE International Symposium on Industrial Electronics, 2003*, 2003.
- [57] J. P. V. S. Cunha, L. Hsu, R. R. Costa, and F. Lizarralde. Output-feedback model-reference sliding mode control of uncertain multivariable systems. *IEEE Transactions on Automatic Control*, 48:2245–2250, 2003.

- [58] J.B. Davidson, F.J. Lallman, and W.T. Bundick. Real-time adaptive control allocation applied to a high performance aircraft. In *5th SIAM Conference on Control & Its Application*, 2001.
- [59] C. Dong-Gyun and K. Jong-Hwan. Pitch autopilot design using model-following adaptive sliding mode control. *Journal of Guidance, Control, and Dynamics*, 25:826–829, 2002.
- [60] C.M. Dorling and A.S.I. Zinober. Two approaches to hyperplane design in multivariable variable structure control systems. *International Journal of Control*, 44:65–82, 1986.
- [61] C.M. Dorling and A.S.I. Zinober. Robust hyperplane design in multivariable variable structure control systems. *International Journal of Control*, 48:2043–2054, 1988.
- [62] G.A. Dumont and M. Huzmezan. Concepts, methods and techniques in adaptive control. In *Proceedings of the American Control Conference*, pages 1137–1150, 2002.
- [63] W.C. Durham. Constrained control allocation. *Journal of Guidance, Control, and Dynamics*, 16:717–25, 1993.
- [64] R. L. Eberhardt and D. G. Ward. Indirect adaptive flight control system interactions. *International Journal of Robust and Nonlinear Control*, 9:1013–1031, 1999.
- [65] C. Edwards. A practical method for the design of sliding mode controllers using linear matrix inequalities. *Automatica*, pages 1761–1769, 2004.
- [66] C. Edwards and I. Postlethwaite. Anti-windup and bumpless-transfer schemes. Department of Engineering Report 96-5-Feb, Leicester University, 1996.
- [67] C. Edwards and S.K. Spurgeon. *Sliding Mode Control: Theory and Applications*. Taylor & Francis, 1998.
- [68] C. Edwards, S.K. Spurgeon, and R.J. Patton. Sliding mode observers for fault detection. *Automatica*, 36:541–553, 2000.
- [69] O.M.E. El-Ghezawi, S.A. Billings, and A.S.I. Zinober. Variable-structure systems and system zeros. *Proceedings of the IEE, Part D*, 130:1–5, 1983.
- [70] D. Enns. Control allocation approaches. In *AIAA Guidance, Navigation and Control*, pages 98–108, 1998.
- [71] J. Farineau. Lateral electric flight control laws of a civil aircraft based upon eigenstructure assignment technique. In *Guidance, Navigation and Control Conference, Boston, MA*, 1989.
- [72] E.J. Field, T.R. Pinney, M.M (René) van Paassen, and O. Stroosma R.A. Rivers. Effects of implementation variations on the results of piloted simulator handling qualities evaluations. In *AIAA Modeling and Simulation Technologies Conference and Exhibit*, 2004.
- [73] J.R. Fisher. Aircraft control using nonlinear dynamic inversion in conjunction with adaptive robust control. Master of Science Thesis, Texas A&M University, 2004.

- [74] T. Floquet, J.P. Barbot, W. Perruquetti, and M. Djemai. On the robust fault detection via sliding mode disturbance observer. *International Journal of Control*, 77:622–629, 2004.
- [75] L. Forssell and U. Nilsson. ADMIRE, the aero-data model in a research environment version 4.0, model description. Technical report, Swedish Defence Agency (FOI), 2005.
- [76] W.F. De Gaay Fortman, M.M. Van Paassen, M. Mulder, A.C. In 't Veld, and J.-P. Clarke. Implementing time-based spacing for decelerating approaches. *Journal of Aircraft*, 44:106–118, 2007.
- [77] P.M. Frank and X. Ding. Frequency domain approach to optimally robust residual generation and evaluation for model-based fault diagnosis. *Automatica*, 30:789–804, 1994.
- [78] G.F. Franklin, J.D. Powell, and A. Emami-Naeini. *Feedback Control of Dynamic Systems*. Prentice Hall International Edition, 4th Edition, 2002.
- [79] L. Fridman and A. Levant. Higher order sliding modes. In W. Perruquetti and J.P. Barbot, editors, *Sliding Mode Control in Engineering*, pages 53–96. Marcel Dekker, New York, 2002.
- [80] S. Ganguli, A. Marcos, and G.J. Balas. Reconfigurable LPV control design for Boeing 747-100/200 longitudinal axis. In *American Control Conference*, pages 3612–3617, 2002.
- [81] Z. Gao and P.J. Antsaklis. Stability of the pseudo-inverse method for reconfigurable control. *International Journal of Control*, 53(3):717–729, 1991.
- [82] J. Garcia-Velo and B.K. Walker. Aerodynamic parameter estimation for high-performance aircraft using extended Kalman filtering. *Journal of Guidance, Control, and Dynamics*, 20:1257–9, 1997.
- [83] J. Georgie and J. Valasek. Evaluation of longitudinal desired dynamics for dynamic-inversion controlled generic re-entry vehicles. *Journal of Guidance, Control, and Dynamics*, 26:811–819, 2003.
- [84] D. Gero. *Aviation disasters : the world's major civil airliner crashes since 1950*. Sparkford : Patrick Stephens, 2006.
- [85] M. Gopinathan, J.D. Bošković, R.K. Mehra, and C. Rago. A multiple model predictive scheme for fault-tolerant flight control design. In *Proceedings of the 37th IEEE Conference on Decision and Control*, pages 1376–81, 1998.
- [86] B. Gouverneur, J.A. (Bob) Mulder, M.M (René) van Paassen, and O. Stroosma. Optimization of the SIMONA research simulator's motion filter settings for handling qualities experiments. In *AIAA Modeling and Simulation Technologies Conference and Exhibit*, 2003.
- [87] M. Gunnarsson. Parameter estimation for fault diagnosis of an automotive engine using extended Kalman filters. Master Thesis, Linköpings University, 2001.

- [88] R. Hallouzi, V. Verdult, R. Babuska, and M. Verhaegen. Fault detection and identification of actuator faults using linear parameter varying models. In *Preprints of the IFAC World Congress*, 2005.
- [89] R. Hallouzi, M. Verhaegen, R. Babuška, and S. Kanev. Model weight and state estimation for multiple model systems applied to fault detection and identification. In *Symposium Modelling, Identification and Signal Processing (SYSID 2006) Identification and System Parameter Estimation*, 2006.
- [90] R. Hallouzi, M. Verhaegen, and S. Kanev. Model weight estimation for FDI using convex fault models. In *Proceedings of the IFAC Symposium SAFEPROCESS '06, Beijing*, 2006.
- [91] C. Hanke. The simulation of a large jet transport aircraft. Volume I: Mathematical model. Technical Report CR-1756, NASA and the Boeing company, 1971.
- [92] C. Hanke and D. Nordwall. The simulation of a jumbo jet transport aircraft. Volume II: Modelling data. Technical Report CR-114494/D6-30643-VOL2, NASA and The Boeing Company, 1970.
- [93] M. Harefors and D.G. Bates. Integrated propulsion-based flight control system design for a civil transport aircraft. In *Proceedings of the 2002 IEEE International Conference on Control Applications*, pages 132–7, 2002.
- [94] O. Härkegård. *Backstepping and Control Allocation with Applications to Flight Control*. PhD thesis, Division of Automatic Control, Department of Electrical Engineering Linköping University, Sweden, 2003.
- [95] O. Härkegård and S. T. Glad. Resolving actuator redundancy - optimal control vs. control allocation. *Automatica*, 41:137–144, 2005.
- [96] H.M Heerspink, W.R. Berkouwer, O. Stroosma, M.M van Paassen, M. Mulder, and J.A. Mulder. Evaluation of vestibular thresholds for motion detection in the SIMONA research simulator. In *AIAA Modeling and Simulation Technologies Conference*, 2005.
- [97] F.J.J. Hermans and M.B. Zarrop. Sliding mode observers for robust sensor monitoring. In *Proceedings of the 13th IFAC World Congress*, pages 211–216, 1996.
- [98] R.A. Hess and S.R. Wells. Sliding mode control applied to reconfigurable flight control design. *Journal of Guidance, Control and Dynamics*, 26:452–462, 2003.
- [99] R.A. Horn and C.R. Johnson. *Matrix Analysis*. Cambridge University Press, 1990.
- [100] M. Hou and R.P. Patton. An LMI approach to $\mathcal{H}_-/\mathcal{H}_\infty$ fault detection observers. In *Proceedings of the UKACC International Conference on Control, Exeter, UK*, pages 305–310, 1996.
- [101] R. R. Huber and B. McCulloch. Self-repairing flight control system. *Society of Automotive Engineers Technical Paper, Series 841552*, pages 1–20, 1984.

- [102] M. Huzmezan and J. Maciejowski. Reconfigurable flight control methods and related issues – a survey. Technical report prepared for the DERA under the research agreement no. ASF/3455, University of Cambridge, 1997.
- [103] M. Idan, M. Johnson, and A.J. Calise. Intelligent aerodynamic/propulsion flight control for flight safety: A nonlinear adaptive approach. In *Proceedings of the American Control Conference*, pages 2918–2923, 2001.
- [104] R. Isermann. Process fault detection based on modelling and estimation methods. *Automatica*, 20:387–404, 1984.
- [105] R. Isermann. Model-based fault-detection and diagnosis - status and applications. *Annual Reviews in Control*, 29:71–85, 2005.
- [106] R. Isermann. *An Introduction from Fault Detection to Fault Tolerance*. Springer, 2006.
- [107] R. Isermann and P. Balle. Trends in the application of model-based fault detection and diagnosis of technical processes. *Control Engineering Practice*, 5:709–719, 1997.
- [108] D. Ito, J. Georgie, J. Vasalek, and D.T. Ward. Re-entry vehicle flight control design guidelines: dynamic inversion. Technical Report NASA/TP-2002-210771, NASA, 2002.
- [109] D. Ito, J. Vasalek, and D.T. Ward. Robust dynamic inversion controller design and analysis for the X-38. In *AIAA Guidance, Navigation and Control conference and exhibit*, 2001.
- [110] B. Jiang and F.N. Chowdhury. Fault estimation and accommodation for linear MIMO discrete-time systems. *IEEE Transactions on Control Systems Technology*, 13:493–9, 2005.
- [111] B. Jiang, M. Staroswiecki, and V. Cocquempot. Fault estimation in nonlinear uncertain systems using robust sliding-mode observers. *IEE Proceedings: Control Theory & Applications*, 151:29–37, 2004.
- [112] J. Jiang and Y. Zhang. Accepting performance degradation in fault-tolerant control system design. *IEEE Transactions on Control Systems Technology*, 14:284–92, 2006.
- [113] Jr. J.J. Deyst, J.V. Harrison, E. Gai, and K.C. Daly. Fault detection, identification and reconfiguration for spacecraft systems. *Journal of the Astronautical Sciences*, 29:113–26, 1981.
- [114] C.N. Jones. Reconfigurable flight control: First year report. Technical report, Cambridge University Engineering Department, 2005.
- [115] D.A. Joosten, T.J.J. van den Boom, and T.J.J. Lombaerts. Effective control allocation in fault-tolerant flight control using feedback linearization and model predictive control. In *European Control Conference*, 2007.
- [116] D. Juricic, O. Moseler, and A. Rakar. Model-based condition monitoring of an actuator system driven by a brushless dc motor. *Control Engineering Practice*, 9:545–554, 2001.
- [117] R. E. Kalman and R. S. Bucy. A new approach to linear filtering and prediction problems. *Transaction of the ASME—Journal of Basic Engineering*, 83:95–108, 1961.

- [118] R.E. Kalman. A new approach to linear filtering and prediction problems. *Transaction of the ASME—Journal of Basic Engineering*, 82(Series D):35–45, 1960.
- [119] S. Kanev and M. Verhaegen. A bank of reconfigurable LQG controllers for linear systems subjected to failures. In *Proceedings of the 39th IEEE Conference on Decision and Control*, pages 3684–9, 2000.
- [120] S. Kanev and M. Verhaegen. Controller reconfiguration for non-linear systems. *Control Engineering Practice*, 8:1223–35, 2000.
- [121] J.Y. Keller and M. Darouach. Optimal two-stage Kalman filter in the presence of random bias. *Automatica*, 33:1745–8, 1997.
- [122] J.Y. Keller and M. Darouach. Two-stage Kalman estimator with unknown exogenous inputs. *Automatica*, 35:339–342, 1999.
- [123] H.K. Khalil. *Nonlinear Systems*. Prentice Hall, Englewood Cliffs NJ., 1992.
- [124] Y.W. Kim, G. Rizzoni, and V. Utkin. Automotive engine diagnosis and control via nonlinear estimation. *IEEE Control Systems Magazine*, 18:884–99, 1998.
- [125] Y.W. Kim, G. Rizzoni, and V. Utkin. Developing a fault tolerant power train system by integrating the design of control and diagnostics. *International Journal of Robust and Nonlinear Control*, 11:1095–1114, 2001.
- [126] L. Kleeman. Understanding and applying Kalman filtering. In *Proceedings of the Second Workshop on Perceptive Systems*, 1996.
- [127] T. Kobayashi and D.L. Simon. Application of a bank of Kalman filters for aircraft engine fault diagnostics. Technical report NASA/TM—2003-212526, NASA, 2003.
- [128] T. Kobayashi and D.L. Simon. Evaluation of an enhanced bank of Kalman filters for in-flight aircraft engine sensor fault diagnostics. *Journal of Engineering for Gas Turbines and Power*, 127:497–504, 2005.
- [129] J. Korbicz, J.M. Koscielny, Z. Kowalczyk, and W. Cholewa. *Fault diagnosis: Models, Artificial Intelligence, Applications*. Springer, 2004.
- [130] M. Kowal and J. Korbicz. Robust fault detection using neuro-fuzzy networks. In *Preprints of the IFAC World Congress*, 2005.
- [131] W.H. Kwon, P.S. Kim, and P.G. Park. A receding horizon Kalman fir filter for linear continuous-time systems. *IEEE Transactions on Automatic Control*, 44:2115–20, 1999.
- [132] T.M. Lam, M. Mulder, M.M. Van Paassen, and J.A. Mulder. Comparison of control and display augmentation for perspective flight-path displays. *Journal of Guidance, Control, and Dynamics*, 29:564–578, 2006.
- [133] I.D. Landau. *Adaptive Control: The Model Reference Approach*. Marcel Dekker, New York, 1979.

- [134] D.J. Leith and W.E. Leithead. Survey of gain-scheduling analysis and design. *International Journal of Control*, 73:1001–1025, 2000.
- [135] R. Li and Jon H. Olson. Fault detection and diagnosis in a closed-loop nonlinear distillation process. application of extended Kalman filters. *Industrial & Engineering Chemistry Research*, 30:898–908, 1991.
- [136] G. Liu. Control of robots manipulators with consideration of actuators degradation and failures. In *IEEE Int. Conf. on Robotics and Automation*, pages 2256–2571, 2001.
- [137] G. P. Liu and R. J. Patton. *Eigenstructure Assignment for Control System Design*. John Wiley & Sons, 1998.
- [138] T.J.J. Lombaerts, Q.P. Chu, J.A. Mulder, and D.A. Joosten. Real time damaged aircraft model identification for reconfiguring flight control. In *AIAA Atmospheric Flight Mechanics Conference and Exhibit*, 2007.
- [139] J.M. Maciejowski. *Multivariable feedback design*. Addison-Wesley, 1989.
- [140] J.M. Maciejowski. *Predictive Control with Constraints*. Prentice Hall, 2002.
- [141] J.M. Maciejowski and C.N. Jones. MPC fault-tolerant control case study: flight 1862. In *Proceedings of the IFAC Symposium SAFEPROCESS '03, Washington*, 2003.
- [142] J.F. Magni, S. Bennani, and J. Terlouw. *Robust flight control: a design challenge*. Springer-Verlag, 1997.
- [143] M. Mahmoud, J. Jiang, and Y. Zhang. *Active Fault Tolerant Control Systems Stochastic Analysis and Synthesis*. Springer, 2003.
- [144] R.E. Maine and K.W. Iliff. Formulation of a practical algorithm for parameter estimation with process and measurement noise. In *Identification and System Parameter Estimation 1982. Proceedings of the Sixth IFAC Symposium, 1983*, 1983.
- [145] R.E. Maine and K.W. Iliff. Agardograph 300 flight test technique series – volume 3 on identification of dynamic systems – applications to aircraft. part 1: The output error approach. Technical report AGARD-AG-300 Vol.3 Part 1, NATO, 1986.
- [146] A. Marcos. A linear parameter varying model of the BOEING 747–100/200 longitudinal motion. Master of science thesis, University of Minnesota, 2001.
- [147] A. Marcos and G.J. Balas. A Boeing 747–100/200 aircraft fault tolerant and diagnostic benchmark. Technical Report AEM–UoM–2003–1, Department of Aerospace and Engineering Mechanics, University of Minnesota, 2003.
- [148] A. Marcos and G.J. Balas. A robust integrated controller/diagnosis aircraft application. *International Journal of Robust and Nonlinear Control*, 15:531–551, 2005.
- [149] A. Marcos, S. Ganguli, and G.J. Balas. An application of H_∞ fault detection and isolation to a transport aircraft. *Control Engineering Practice*, 13:105–119, 2005.

- [150] Peter S. Maybeck. *Stochastic models, estimation, and control*, volume 141 of *Mathematics in Science and Engineering*. 1979.
- [151] D. McLean and S. Aslam-Mir. Reconfigurable flight control systems. In *International Conference on Control '91 (Conf. Publ. No.332)*, pages 234–42, 1991.
- [152] M.H. Smaili. Flight data reconstruction and simulation of EL AL Flight 1862. Graduation Report, Delft University of Technology, 1997.
- [153] L. Mirea and R.J. Patton. Component fault diagnosis using wavelet neural networks with local recurrent structure. In *Proceedings of the IFAC Symposium SAFEPROCESS '06, Beijing*, pages 91–96, 2006.
- [154] L. Mirea and R.J. Patton. A new dynamic neuro-fuzzy system applied to fault diagnosis of an evaporation station. In *Proceedings of the IFAC Symposium SAFEPROCESS '06, Beijing*, pages 253–258, 2006.
- [155] S.K. Mudge and R.J. Patton. Variable structure control laws for aircraft manoeuvres. In *Proceedings of the IEE Conference Control '88*, pages 564–568, 1988.
- [156] J.A. Mulder, Q.P. Chu, J.K. Sridhar, J.H. Breeman, and M. Laban. Non-linear aircraft flight path reconstruction review and new advances. *Progress in Aerospace Sciences*, 35:673–726, 1999.
- [157] J.A. Mulder, J.K. Sridhar, and J.H. Breeman. Agardograph 300 flight test technique series – volume 3 on identification of dynamic systems – applications to aircraft. part 2: Nonlinear analysis and manoeuvre design. Technical report AGARD-AG-300 Vol.3 Part 2, NATO, 1994.
- [158] M. Mulder, A.R. Veldhuijzen, M.M. Van Paassen, and J.A. Mulder. Integrating fly-by-wire controls with perspective flight-path displays. *Journal of Guidance, Control, and Dynamics*, 28:1263–74, 2005.
- [159] K.S. Narendra and J. Balakrishnan. Adaptive control using multiple models. *IEEE Transactions on Automatic Control*, 42:171–87, 1997.
- [160] K.S. Narendra, O.A. Driollet, M. Feiler, and K. George. Adaptive control using multiple models. *International Journal of Adaptive Control and Signal Processing*, 17:87–102, 2003.
- [161] L. Ni and C.R. Fuller. Control reconfiguration based on hierarchical fault detection and identification for unmanned underwater vehicle. *Journal of vibration and control*, 9:753–748, 2003.
- [162] Joao Oliveira, Q.P. Chu, J.A. Mulder, H.M.N.K Balini, and W.G.M. Vos. Multi-input design for aerodynamic parameter estimation. In *AIAA Guidance, Navigation, and Control Conference*, 2005.
- [163] E. Omerdic and D. Toal. Control allocation of over-actuated thruster-propelled underwater vehicles. In *1st Workshop on Networked Control System and Fault Tolerant Control*, 2005.

- [164] M.W. Oppenheimer and D.B. Doman. Control allocation for overactuated systems. Technical report AFRL-VA-WP-TP-2006-321, Air Force Research Laboratory, 2006.
- [165] A.R. Valente Pais, M. Mulder, M.M. Van Paassen, M. Wentink, and E. Groen. Modeling human perceptual thresholds in self-motion perception. In *AIAA Modeling and Simulation Technologies Conference*, 2006.
- [166] R.J. Patton. Fault tolerant control: the 1997 situation. In *Proceedings of the IFAC Symposium - SAFEPROCESS '97*, pages 1035 – 1055, 1997.
- [167] R.J. Patton and J. Chen. A review of parity space approaches to fault diagnosis for aerospace systems. *Journal of Guidance Control and Dynamics*, 17:278–285, 1994.
- [168] R.J. Patton, J. Chen, and H. Benkhedda. A study on neuro-fuzzy systems for fault diagnosis. *International Journal of Systems Science*, 31(11):1441–1448, 2000.
- [169] R.J. Patton and J. Korbicz. Advances in computational intelligence for fault diagnosis systems. *Special issue of International Journal of Applied Mathematics and Computer Science*, 9(3), 1999.
- [170] R.J. Patton, F.J. Uppal, and C.J. Lopez-Toribio. Soft computing approaches to fault diagnosis for dynamic systems: A survey. In *Proceedings of the IFAC Symposium SAFE-PROCESS '00, Budapest*, pages 298–311, 2000.
- [171] M.M. Polycarpou and A.T. Vemuri. Learning methodology for failure detection and accommodation. *IEEE Control System Magazine*, 15(3):16–24, 1995.
- [172] J.L. De Prins, F.K.M. Schippers, M. Mulder, M.M. Van Paassen, A.C. In 't Veld, and J.-P. Clarke. Enhanced self-spacing algorithm for three-degree decelerating approaches. *Journal of Guidance, Control, and Dynamics*, 30:576–90, 2007.
- [173] V. Puig, M. Witczak, F. Nejjari, J. Quevedo, and J. Korbicz. A GMDH neural network-based approach to passive robust fault detection using a constraint satisfaction backward test. *Engineering Applications of Artificial Intelligence*, 20(7):886–897, 2007.
- [174] C. Rago, R. Prasanth, R.K. Mehra, and R. Fortenbaugh. Failure detection and identification and fault tolerant control using the IMM-KF with applications to the Eagle-Eye UAV. In *Proceedings of the 37th IEEE Conference on Decision and Control*, pages 4208–13, 1998.
- [175] W.C. Reigelsperger, K.D. Hammett, and S.S. Banda. Robust control law design for lateral-directional modes of an F-16/MATV using μ -synthesis and dynamic inversion. *International Journal of Robust and Nonlinear Control*, 7:777–795, 1997.
- [176] M. Rodrigues, D. Theilliol, S. Aberkane, and D. Sauter. Fault tolerant control design for polytopic LPV systems. *International Journal of Applied Mathematics and Computer Science*, 17:27–37, 2007.
- [177] H.H. Rosenbrock. *State Space and Multivariable Theory*. New York: Wiley, 1970.

- [178] R. Routledge. *Discoveries and inventions of the nineteenth century: With numerous illustrations*. London : Routledge, 1876.
- [179] E.P. Ryan and M. Corless. Ultimate boundedness and asymptotic stability of a class of uncertain dynamical systems via continuous and discontinuous control. *IMA Journal of Mathematical Control and Information*, 1:223–242, 1984.
- [180] J. M. M. Sánchez and J. Rodellar. *Adaptive Predictive Control : From the Concepts to Plant Optimization*. Prentice Hall, 1996.
- [181] D. Shin, G. Moon, and Y. Kim. Design of reconfigurable flight control system using adaptive sliding mode control: actuator fault. *Proceedings of the Institution of Mechanical Engineers, Part G (Journal of Aerospace Engineering)*, 219:321–328, 2005.
- [182] J. Shin and C.M Belcastro. Performance analysis on fault tolerant control system. *IEEE Transactions on Control Systems Technology*, 14:920–925, 2006.
- [183] J. Shin, N.E. Wu, and C. Belcastro. Adaptive linear parameter varying control synthesis for actuator failure. *Journal of Guidance, Control, and Dynamics*, 27:787–794, 2004.
- [184] Y. Shtessel, J. Buffington, and S. Banda. Multiple time scale flight control using reconfigurable sliding modes. *AIAA Journal on Guidance, Control, and Dynamics*, 22:873–883, 1999.
- [185] Y. Shtessel, J. Buffington, and S. Banda. Tailless aircraft flight control using multiple time scale re-configurable sliding modes. *IEEE Transactions on Control Systems Technology*, 10:288–296, 2002.
- [186] S. Skogestad and I. Postlethwaite. *Multivariable Feedback Control: Analysis and Design*. J.Wiley, 1996.
- [187] J.J.E. Slotine and W. Li. *Applied Nonlinear Control*. Prentice Hall, Englewood Cliffs NJ., 1991.
- [188] M. H. Smaili and J. A. Mulder. Flight data reconstruction and simulation of the 1992 Amsterdam Bijlmermeer airplane accident. In *AIAA Modeling and Simulation Technologies Conference*, 2000.
- [189] M.H Smaili. Flightlab 747: Benchmark for advance flight control engineering. Technical report, Technical University Delft, the Netherlands, 1999.
- [190] M.H. Smaili, J. Breeman, T.J.J. Lombaerts, and D.A. Joosten. A simulation benchmark for integrated fault tolerant flight control evaluation. In *AIAA Modeling and Simulation Technologies Conference and Exhibit*, 2006.
- [191] S. A. Snell, D. F. Enns, and W. L. Garrard Jr. Nonlinear inversion flight control for a supermaneuverable aircraft. *Journal of Guidance, Control, and Dynamics*, 15:976–984, 1992.
- [192] H.W. Sorenson. *Kalman filtering : theory and application*. IEEE Press, 1985.

- [193] L. Spirkovska, D. L. Iverson, S. Poll, and A. Pryor. Inductive learning approaches for improving pilot awareness of aircraft faults. Technical report, NASA, 2005.
- [194] S.K. Spurgeon and R.J. Patton. Robust variable structure control of model reference systems. *Proceedings of the IEE - Part D*, 137:341–348, 1990.
- [195] R.F. Stengel. *Flight dynamics*. Princeton University Press, 2004.
- [196] G. W. Stewart. On scaled projections and pseudoinverses. *Linear Algebra and Its Applications*, 112:189–193, 1989.
- [197] O. Stroosma, M.M van Paassen, and M. Mulder. Using the SIMONA research simulator for human-machine interaction research. In *AIAA Modeling and Simulation Technologies Conference*, 2003.
- [198] I. Szaszi, S. Ganguli, A. Marcos, G.J. Balas, and J. Bokor. Application of FDI to a nonlinear Boeing-747 aircraft. In *Mediterranean Conference on Control and Automation*, 2002.
- [199] I. Szaszi, A. Marcos, G. J. Balas, and J. Bokor. Linear parameter-varying detection filter design for a Boeing 747-100/200 aircraft. *Journal of Guidance, Control, and Dynamics*, 28:461–470, 2005.
- [200] C.P. Tan. Sliding mode observers for fault detection and isolation. Ph.D thesis, University of Leicester, 2002.
- [201] C.P. Tan and C. Edwards. Sliding mode observers for detection and reconstruction of sensor faults. *Automatica*, pages 1815–1821, 2002.
- [202] C.P. Tan and C. Edwards. Sliding mode observers for robust detection and reconstruction of actuator and sensor faults. *International Journal of Robust and Nonlinear Control*, 13:443–463, 2003.
- [203] M.D. Tandale and J. Valasek. Issues on integration of fault diagnosis and reconfigurable control in active fault-tolerant control systems. In *Proceedings of the 2005 American Control Conference*, 2005.
- [204] M.D. Tandale and J. Valasek. Fault-tolerant structured adaptive model inversion control. *Journal of Guidance, Control, and Dynamics*, 29:635–642, 2006.
- [205] G. Tao, S. M. Joshi, and X. Ma. Adaptive state feedback and tracking control of systems with actuator failures. *IEEE Transactions On Automatic Control*, 46(1):78–95, 2001.
- [206] C. Tourne, D.B. Landrum, Y. Shtessel, and C.W. Hawk. Ramjet-powered re-usable vehicle control by sliding modes. *Journal of guidance, control and dynamics*, 21(3):409–415, 1998.
- [207] C. Tubb and E. Omerdic. Improves technical report fd 001(n), fault detection and handling. Technical Report FD 001(n), University of Wales College, Newport, October 8, 2001.

- [208] T. Tucker. *Touchdown: the development of propulsion controlled aircraft at NASA Dryden*. Monographs in Aerospace History, 1999.
- [209] F.J. Uppal, R.J. Patton, and M. Witczak. A neuro-fuzzy multiple-model observer approach to robust fault diagnosis based on the DAMADICS benchmark problem. *Control Engineering Practice*, 14:699–717, 2006.
- [210] V.I. Utkin. *Sliding Modes in Control Optimization*. Springer-Verlag, Berlin, 1992.
- [211] V.I. Utkin and K.-K.D. Young. Methods for constructing discontinuity planes in multi-dimensional variable structure systems. *Automation and Remote Control*, 39:1466–1470, 1978.
- [212] C.A.A.M. van der Linden. DASMAT: Delft University aircraft simulation model and analysis tool. Technical Report LR-781, Technical University of Delft, the Netherlands, 1996.
- [213] C.A.A.M. van der Linden, J.K. Sridhar, and J.A. Mulder. Multi-input design for aerodynamic parameter estimation. In *Proceedings of the American Control Conference*, 1995.
- [214] T.K. Vetter, S.R. Wells, and R.A. Hess. Designing for damage-robust flight control design using sliding mode techniques. *Proceedings of the Institution of Mechanical Engineers, Part G: Journal of Aerospace Engineering*, 217:245–261, 2003.
- [215] F.J. Vormer, M. Mulder, M.M. Van Paassen, and J.A. Mulder. Optimization of flexible approach trajectories using a genetic algorithm. *Journal of Aircraft*, 43:941–52, 2006.
- [216] B.L. Walcott and S.H. Žak. State observation of nonlinear uncertain dynamical systems. *IEEE Transaction on Automatic Control*, 32:166–170, 1987.
- [217] B.L. Walcott and S.H. Žak. Combined observer-controller synthesis for uncertain dynamical systems with applications. *IEEE Transactions on Systems, Man and Cybernetics*, 18:88–104, 1988.
- [218] G. Welch and G. Bishop. An introduction to the Kalman filter. Technical report TR 95-041, University of North Carolina, 2006.
- [219] S.R. Wells and R.A. Hess. Multi-input/multi-output sliding mode control for a tailless fighter aircraft. *Journal of Guidance, Control and Dynamics*, 26:463–473, 2003.
- [220] G. Wheeler, C. Su, and Y. Stepanenko. Sliding mode controller with improved adaptation laws for the upper bounds on the norm of uncertainties. *Automatica*, 34:1657–1661, 1998.
- [221] J. Wiig and H. Noura. Flight stage normalization of HUMS indicators. In *Annual Forum Proceedings - AHS International, v I, AHS International 62nd Annual Forum - Vertical Flight: Leading through Innovation - Proceedings*, 2006.
- [222] J. Wiig, H. Noura, D. Brun-Picard, and J.C. Anifrani. Trend analysis of helicopter condition monitoring indicators. In *American Control Conference*, 2006.
- [223] J. Wiig, H. Noura, D. Brun-Picard, and J.-R. Derain. Trend-based transmission system diagnosis. In *Proceedings of the 45th IEEE Conference on Decision and Control*, 2006.

- [224] M. Witczak. Advances in model-based fault diagnosis with evolutionary algorithms and neural networks. *International Journal of Applied Mathematics and Computer Science*, 16(1):85–99, 2006.
- [225] F. Wu. A generalized LPV system analysis and control synthesis framework. *International Journal Control*, 74:745–759, 2001.
- [226] N.E. Wu, Y. Zhang, and K. Zhou. Control effectiveness estimation using an adaptive Kalman estimator. In *Proceedings of the 1998 IEEE International Symposium on Intelligent Control (ISIC) held jointly with IEEE International Symposium on Computational Intelligence in Robotics and Automation (CIRA) Intelligent Systems and Semiotics (ISAS)*, pages 181–6, 1998.
- [227] N.E. Wu, Y. Zhang, and K. Zhou. Detection, estimation, and accommodation of loss of control effectiveness. *International Journal of Adaptive Control and Signal Processing*, 14:775–95, 2000.
- [228] J.X. Xu, Q.W. Jia, and T.H. Lee. On the design of a nonlinear adaptive variable structure derivative estimator. *IEEE Transactions on Automatic Control*, 45:1028–1033, 2000.
- [229] H. Yang and M. Saif. Fault detection in a class of nonlinear systems via adaptive sliding observer. In *Proceedings of the IEEE International Conference on Systems, Man and Cybernetics*, pages 2199–2204, 1995.
- [230] Z. Yang, M. Blanke, and M. Verhaegen. Robust control mixer method for reconfigurable control design using model matching. *IET Control Theory and Applications*, 1:349–357, 2007.
- [231] B. Yao. Adaptive robust control of nonlinear systems with applications to control of mechanical systems. Ph.D thesis, University of California at Berkeley, 1996.
- [232] K.-K.D. Young. Asymptotic stability of model reference systems with variable structure control. *IEEE Transactions on Automatic Control*, AC-22:279–281, 1977.
- [233] K.-K.D. Young. Design of variable structure model-following control systems. *IEEE Transactions on Automatic Control*, 23:1079–1085, 1978.
- [234] K.-K.D. Young and S.V. Drakunov. Sliding mode control with chattering reduction. In *Proceedings of the IEEE VSC and Lyapunov Workshop*, pages 188–190, 1992.
- [235] D.L. Yu and J.B. Gomm. Implementation of neural network predictive control to a multivariable chemical reactor. *Control Engineering Practice*, 11(11):1315–1323, 2003.
- [236] P.M.T. Zaal, F.M. Nieuwenhuizen, and M. Mulder and M.M. Van Paassen. Perception of visual and motion cues during control of self-motion in optic flow environments. In *AIAA Modeling and Simulation Technologies Conference*, 2006.
- [237] Y. Zhang and J. Jiang. Design of integrated fault detection, diagnosis and reconfigurable control systems. In *Proceedings of the IEEE Conference on Decision and Control*, pages 3587–3592, 1999.

- [238] Y. Zhang and J. Jiang. Integrated active fault-tolerant control using IMM approach. *IEEE Transactions on Aerospace and Electronic Systems*, 37:1221–1235, 2001.
- [239] Y. Zhang and J. Jiang. Bibliographical review on reconfigurable fault tolerant control systems. In *Proceedings of the IFAC Symposium SAFEPROCESS '03, Washington*, pages 265–276, 2003.
- [240] Y. Zhang and J. Jiang. Fault tolerant control system design with explicit consideration of performance degradation. *IEEE Transactions on Aerospace and Electronic Systems*, 39:838–848, 2003.
- [241] Y. Zhang and J. Jiang. Issues on integration of fault diagnosis and reconfigurable control in active fault-tolerant control systems. In *Proceedings of the IFAC Symposium SAFE-PROCESS '06, Beijing*, 2006.
- [242] Y. M. Zhang and J. Jiang. Active fault-tolerant control system against partial actuator failures. *IEE Proceedings: Control Theory & Applications*, 149:95–104, 2002.
- [243] K. Zhou, J.C. Doyle, and K. Glover. *Robust and Optimal Control*. Prentice Hall, New Jersey, 1996.
- [244] K. Zhou, P.K. Rachinayani, N. Liu, Z. Ren, and J. Aravna. Fault diagnosis and reconfigurable control for flight control systems with actuator failures. In *43rd IEEE Conference on Decision and Control, Bahamas*, 2004.
- [245] A.S.I. Zinober. Properties of adaptive discontinuous model-following control systems. In *Proceedings of the 4th IMA International Conference on Control Theory*, pages 337–346, 1984.
- [246] A.S.I. Zinober, O.M.E. El-Ghezawi, and S.A. Billings. Multivariable variable-structure adaptive model-following control systems. *Proceedings of the IEE, Part D*, 129:6–12, 1982.